THE COLLISIONAL BEHAVIOUR OF Mg, Ca AND Sr $[nsnp(^3P_J)]$
FOLLOWING EXCITATION WITH A PULSED DYE-LASER

BY

JOSE SCHIFINO

PEMBROKE COLLEGE

CAMBRIDGE

A thesis submitted for the Degree of Doctor of Philosophy
in the University of Cambridge.

November 1983

PREFACE

The work described in this thesis was carried out between October 1980 and October 1983 in the Department of Physical Chemistry, under the supervision of Dr. David Husain, entirely by the author, unless otherwise acknowledged in the text.

This thesis is the result of my own work and includes nothing which is outcome of work done in collaboration. I further state that no part of this thesis has already been or is being concurrently submitted for any other degree, diploma or other qualification.

José Schifino

ACKNOWLEDGEMENTS

CONTENTS

LIST OF PHOTOGRAPHS

All photographs are presented after chapter 2.

Photograph I: General view of the apparatus for the kinetic study of group IIA elements in the ^3P_J states, generated by pulsed dye-laser excitation and monitored by time-resolved forbidden emission $(^3P_1 \rightarrow {}^1S_0)$, using boxcar integration.

Photograph II: Quartz reactor employed in the kinetic study of $Mg(3\,^3P_J)$, indicating the water-cooled windows.

Photograph III: View of the inside of the furnace indicating the heating coils and the port holes for entry of the laser beam and exit of the spectroscopic signal.

Photograph IV: Quartz reactor employed in the kinetic study of $Mg(3\,^3P_J)$, placed inside the furnace.

Photograph V: Front view of the vacuum system for dye-laser excitation studies, indicating the main line, the gas handling system, pressure measuring devices and bulb with magnetic stirrer for mixture preparation.

Photograph VI: Back view of the vacuum system employed in the dye-laser excitation studies of the group IIA elements, including the diffusion pump and the flow system.

Photograph VII: Detection system employed in the kinetic study of group IIA elements showing the monochromator attached to the photomultiplier tube and placed in front of the exit window of the quartz reactor.

Photograph VIII: Electronic units employed in the dye-laser studies including the current-to-voltage converter, the boxcar integrator, the XY-recorder and the oscilloscopes for visual display.

1. INTRODUCTION

The study of the collisional behaviour of atoms in specific electronic states, particularly electronically excited atoms, is an area that has developed in recent years from both the experimental and fundamental view points. The availability of tunable lasers, as excitation sources, providing large numbers of photons in bandwidths comparable to the Doppler width of an electronic transition may certainly be regarded as a major contribution to the development of this field. Experiments on the collisional behaviour of electronically excited atoms have grown in detail and sophistication alongside with the development of new experimental techniques. The present thesis is concerned with the study of the collisional behaviour of group IIA elements, Mg, Ca and Sr, in their excited ^3P_J states, using pulsed dye-laser excitation and time-resolved emission from a forbidden transition.

The study of fluorescence quenching of strongly-allowed emitting atomic states, following excitation and using the radiative lifetime as an "internal clock", through the agency of a Stern-Volmer plot, is well established.[1] In the present thesis such studies will not be dealt with other than to indicate their existence.

Recent years have seen a large development of the direct investigation of excited states arising from the overall electronic structure of the ground state configuration. This is an area that has been extensively reviewed.[2-9] One experimental reason for the development of such an area arises from the optical metastability of the atomic state, once generated. The lifetime of the atomic state is dominated by collisional removal, including energy transfer and chemical reaction, and this brings the state readily within the time-range of modern electronics and data handling apparatus in order to carry out kinetic measurements in "real-time" rather than using the "internal clock" in the steady mode experiments of the Stern-Volmer type. The fact that many laser systems either in use or in development involve electronically excited states of metal atoms, and the

1

great interest in knowing the mechanisms by which these excited states are collisionally deactivated, constitute a practical reason for the research in metal atom quenching. Another fundamental objective is to investigate in further detail the general relationship between electronic structure and reactivity.

The collisional behaviour of electronically excited atoms has been reviewed in recent years by Husain[6] including reference to the group IIA elements where there was an emphasis on the reactivity of the heavier ground state species. The collisional quenching of electronically excited metal atoms has been the subject of a recent review by Breckenridge and Umemoto.[9] These authors present the extensive body of rate data now available and discuss the quenching mechanism of electronically excited metal atoms by several collision partners. For fundamental and practical reasons, this is an area undergoing continual change. However, detailed studies on the ^3P_J levels of the group IIA atoms, leading to absolute collisional rate data have been both very limited in scope and in experiments employed themselves.

In the present work the collisional behaviour of the ^3P_J states of Mg, Ca and Sr is described in the presence of a wide range of collision partners. The practical objective of this study is to assist our understanding of spontaneous emission, diffusion and quenching, of the group IIA elements, including chemical reaction and energy transfer.

The $[nsnp(^3P_J)]$ states of Mg, Ca and Sr constitute the lowest lying electronically excited states of these atoms above the $[ns^2(^1S_0)]$ ground states. The energies expressed in cm^{-1} for these states are given in table (1.1).[10]

TABLE 1.1

Energy of the $[nsnp(^3P_J)]$ states for Mg, Ca and Sr in cm^{-1}
(1 cm^{-1} = 1.2398 x 10^{-4} eV)

	$Mg(3^3P_J)$	$Ca(4^3P_J)$	$Sr(5^3P_J)$
J = 0	21,851	15,158	14,318
J = 1	21,870	15,210	14,504
J = 2	21,911	15,316	14,899

In the case of the heaviest member of the series, the $Ba[6s5d(^3D_{1,2,3})]$ manifold is lower in energy than the states of the $Ba(6s6p)$ manifold and hence, the $^3D_{1,2,3}$ states become the long-lived species of interest. The study of the collisional behaviour of Ba is beyond the scope of the present series of investigations.

The energy level structures for Mg, Ca and Sr are quite similar. The relevant electronic states in the case of magnesium are shown in figure (1.1). The present work will be concerned with the transition connecting the ^3P_J state to the ground $^1S_0$ state ($\lambda = 457.1$ nm for Mg). The investigations that have been reported so far have employed mainly the transitions connecting the ^3P_J states to the upper $^3S_1$ state, especially the $^3P_1 \to {}^3S_1$ transition at $\lambda = 517.3$ nm for Mg.

The relatively short life of the $^3P_1$ state as compared to the $^3P_2$ and $^3P_0$ states of the ^3P_J manifold makes this state and the transitions associated with it the most important from the experimental point of view. These ^3P_J states form a triplet manifold which decay to the ground state by a forbidden ($^3P_1 \to {}^1S_0$) transition. The two remaining components of the triplet act as reservoir states which are equilibrated to the $^3P_1$ state but show no appreciable radiative decay. Nevertheless, the role of these reservoir states in the mean radiative lifetime of the $^3P_1$ state has to be taken into account as will be discussed later.

The experiments performed in this investigation on these particular atomic states have in common the following aspects;

1- The production of metal atoms in a flow system using a heat pipe. The flow system is equivalent to a static system for the purpose of the atomic decay. In other words, the residence time of the flowing gas in the reaction vessel is much bigger than the atomic decay itself (see later).

2- Repetitive dye-laser excitation to the ^3P_J levels from the $^1S_0$ ground states by firing the laser at a frequency of 10 Hz and tuning to the wavelength corresponding to the transition under consideration.
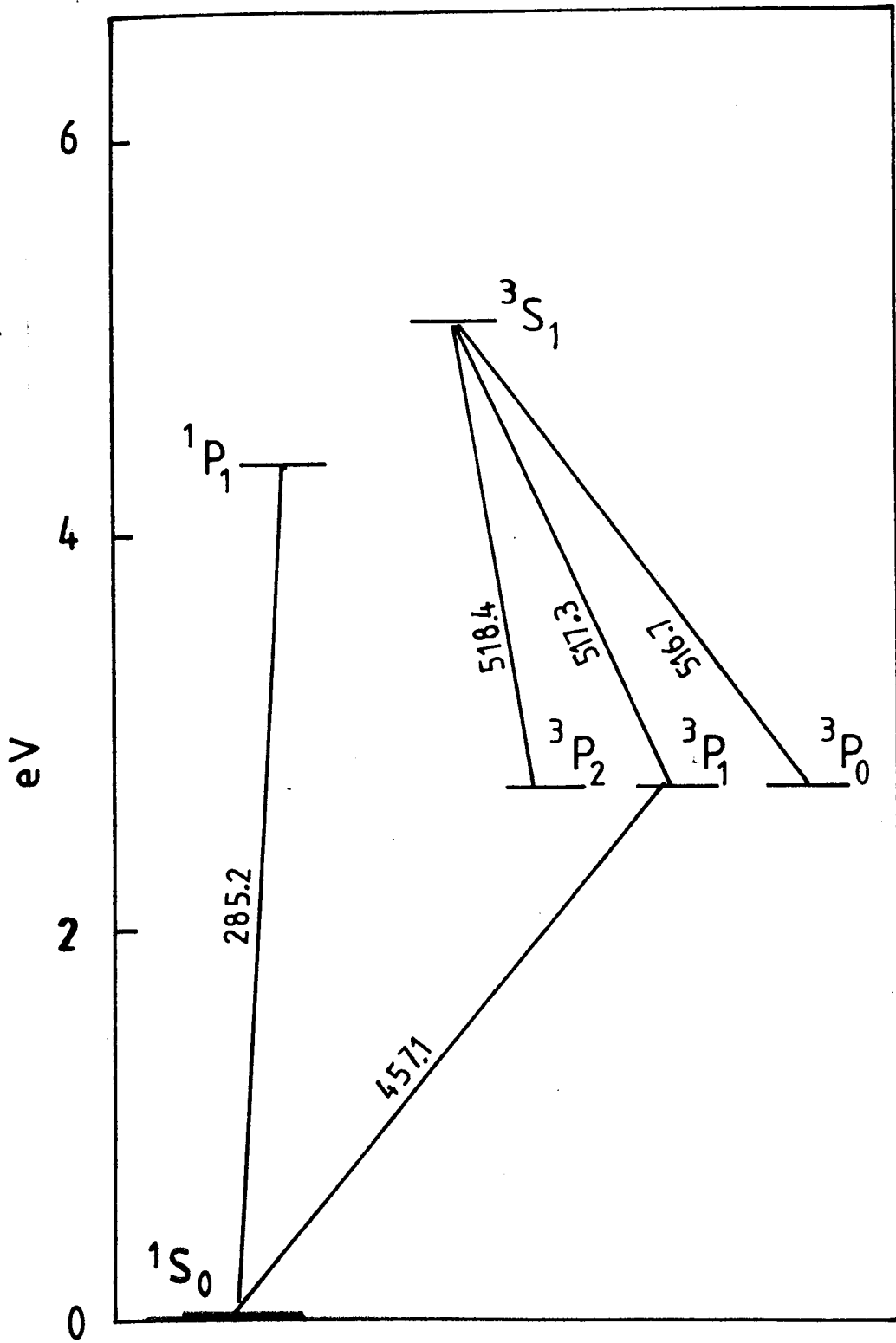
Figure 1.1 —   Energy level structure for Mg

3- Averaging of the particular signal used to monitor the ^3P_J state generated by pulsed dye-laser excitation.

The first two steps are inherent to the actual nature of the experiments described in the present work. The production of atoms of the group IIA elements in the vapour phase by using heat pipes has been extensively discussed in the literature.[11] The use of a dye-laser to excite alkaline earth elements is becoming a very well known technique. The detection of the optically metastable states produced by pulsed dye-laser excitation may be made by several techniques, the choice depending very much on the mean radiative lifetime of the transition to be used for the envisaged kinetic investigation.

Among the alternatives for the experiments that will be described in this work, we may consider;

1- Time-resolved resonance fluorescence: By photoelectric current measurement of electric dipole allowed fluorescence signals following further excitation with a resonance source. In theory, at least, time-resolved resonance fluorescence using an allowed atomic transition to a higher lying state could be used to monitor the kinetics of an optically metastable state. The resonance fluorescence signal, after passing either through a monochromator or an interference filter may be transformed into an electric current by means of a photomultiplier tube. The amplified signal may be fed into a boxcar integrator and displayed in a XY-chart recorder for kinetic analysis, or using a signal averager for analysis of the complete decay trace. Inspection of standard compilations[12] indicates conveniently placed strong atomic resonance transitions for the $^3P_{0,1,2}$ levels of Mg and Sr. For Ca, by contrast, conveniently situated and relatively strong transitions are those for the $^3P_1$ and $^3P_2$ levels, respectively;

$$Ca[5s(^3S_1) \longrightarrow 4s4p(^3P_1)] \qquad at \qquad \lambda = 612.2 \ nm$$

$$Ca[5s(^3S_1) \longrightarrow 4s4p(^3P_2)] \qquad at \qquad \lambda = 616.2 \ nm$$

This type of measurement, although not employed in the present work, may be thought as a convenient alternative in cases where forbidden emission

measurements of the type ($^3P_1 \rightarrow {}^1S_0$) are excessively complicated by scattered light from the laser source at the same wavelength. The forbidden emission measurements (see later) are resonance measurements in that the laser excitation and emission used to detect the decay of the atomic states are at same wavelength and, of course, both connect with the ground state. Time-resolved resonance fluorescence (and time-resolved resonance absorption), as conventionally described, are resonance measurements entirely with respect to the spectroscopic source. We may point out that the scattered light from the laser is certainly far more intense than that from a spectroscopic source, which makes the resonance fluorescence technique an alternative to the time-resolved emission method. The former technique would have been employed in the present investigation if the gating system had not been able to overcome the laser scattered light (see later).

2- Time-resolved resonance line absorption: In this case, a resonance spectroscopic lamp is used to further excite atoms previously excited by the laser, but unlike the method that has just been described, the attenuation of the resonance source is employed to monitor the kinetics of the excited atoms. In this procedure the scattered light does not interfere significantly with the measurements, provided a monochromator is used to isolate the light from the spectroscopic lamp which is being used as a probe.

3- Time-resolved forbidden emission: The forbidden transitions ($^3P_J \rightarrow {}^1S_0$) for Mg, Ca and Sr are sufficiently strong to permit detection of the ^3P_J states by direct emission, which is quite convenient for the proposed experiments, given that the effect of scattered light from the laser can be overcome. The literature indicates the following values for the mean radiative lifetimes for these forbidden transitions;

TABLE 1.2

Mean radiative lifetimes and Einstein coefficients for the
$^3P_1 \to {}^1S_0$ transitions

Atom	τ_e/s	A_{nm}/s^{-1}	Reference
Mg	2.2×10^{-3}	4.5×10^2	13
Ca	1.4×10^{-4}	7.2×10^3	12
Sr	1.5×10^{-5}	6.7×10^4	12

The values of the Einstein coefficients make it quite evident that the forbidden transitions are strong enough to permit detection of the ^3P_J states by direct emission. The Einstein coefficients for these transiti$\,$ns may be contrasted with an allowed transition for an atomic emission where A_{nm} is of the order of 10^8 s^{-1}. On the other hand, for a highly forbidden emission like the one used in the study of $O(2^1D_2)$ generated by the laser pulsed irradiation of ozone,[14]

$$O[(2^1D_2) \to O(2^3P_2)] \qquad A_{nm} = 6.9 \times 10^{-3} \text{ s}^{-1}$$

the extremely weak emission involves extensive signal averaging as the number of quanta detected in any experiment is very small.

Because the transition under consideration has an Einstein coefficient, A_{nm}, much smaller than a fully allowed transition, but bigger than many forbidden transitions, we may say that it is sufficiently allowed to be pumped by the dye-laser and forbidden enough so that the excited states have mean radiative lifetimes that can be monitored in real time using modern electronics. The advantages in using the direct forbidden emission are evident from the simplicity of such a measurement dispensing with the spectroscopic lamp and the complications associated with it.

Whilst the present thesis is concerned with the collisional behaviour of the low lying electronically excited states of the group IIA elements, Mg, Ca and Sr [nsnp(^3P_J)], the body of work described here can be regarded within the broader framework of excited atom chemistry in general. This a rapidly developing area and it is clearly beyond the scope of the present work to review this fully.

The largest body of unified rate data for the collisional behaviour of electronically excited states has been generated in recent years for the elements in groups IV - VII.

C, Si, Ge, Sn, Pb (np^2) $(^3P_{0,1,2}$ $^1D_2$ $^1S_0)$

N, P, As, Sb, Bi (np^3) $(^4S_{3/2}$ $^2D_{3/2,5/2}$ $^2P_{1/2,2/3})$

O, S, Se, Te, (np^4) $(^3P_{2,1,0}$ $^1D_2$ $^1S_0)$

F, Cl, Br, I, (np^5) $(^2P_{3/2,1/2})$

The rate data for these atomic states have been extensively reviewed as indicated hitherto.[2-9] Further, Golde[15a] has reviewed rate data for the collisional behaviour of electronically excited noble gas atoms. The fundamental structure for considering rate data for atom-molecule collisions is governed by the magnitude and scope of the rate data available. In principle, a given rate constant is ideally considered in terms of the detailed construction of a potential energy surface and the dynamics on that surface.[16] However, calculation of a realistic surface is far from easy and many approximations have to be made. The massive body of rate data for all these electronically excited atoms, many of which are heavy, and the large range of collision partners, requires some simplified approach in order to consider the data as a whole. The approach used in recent years by Donovan and Husain[2] is to employ the symmetry of the potential surfaces involved on collision through the agency of correlation diagrams. This approach, using the method described by Shuler[17] was applied by Donovan and Husain[2] in the construction of correlation diagrams in C_s symmetry for light atom-molecule collisions on the basis of a weak spin-orbit coupling approximation. These authors[2] have employed such diagrams to discuss the difference in the collisional behaviour of a given atom or molecule in different electronic states, and this approach is now, in fact, being used in bibliographical compilations of rate data.[18] For the heavy elements, where the Russel-Saunders LS coupling breaks down, Husain[6] has described the method of $J\Omega$ coupling for atom-molecule collisions. This is a far more complex approach and the available pathways, given the loss of the spin selection rule, are less restrictive and more numerous. The various considerations of the potential

energy surfaces for atom-molecule collisions will have practical applications in particular systems. Its reference here is to provide the overall framework against which the rate data for the group IIA elements will be eventually discussed, in the next chapters.

Murrel[109b] has, for example, indicated that potential energy surfaces may be employed in this context. Recent reviews of the collision partners of electronically excited atoms include those of Callear[109a], Donovan and Gillespie[8], Klots and Setser[7] and Clyne and Curran[15b], the latter including the chemistry of the electronically excited halogen atoms $(^2P_{1/2})$. However, the main review for the present work is that of Breckenridge and Umemoto[9], who have covered the group IIA elements in great detail. This review, of 1982, is a modern and complete summary of the work on Mg, Ca and $Sr(^3P_J)$ to that date. Notwithstanding this, as will become evident in this thesis, a large body of work, in which the present investigation may be included, has been carried out since then.

The studies that have been published so far on the collisional behaviour of Mg, Ca and Sr, deal with the mean radiative lifetime of the $^3P_1$ states and collisional removal of these states by added quenching gases. It is proposed to measure the mean radiative lifetime, to study the quenching by a wider range of collision partners and, whenever possible, to make studies on the diffusion coefficients of these excited species in the noble gases.

Before embarking in the discussion of the present work, a brief bibliographical review in this particular area is presented. The brief review that follows is not claimed to be complete, and it is here presented in order to place this work in context. The works that will be mentioned constitute the framework to be used later (chapters 3, 4 and 5) in the discussion of the experimental results of this investigation.

The measurement of the mean radiative lifetime of $Mg(3^3P_1)$ has received attention from both theoretical and experimental viewpoints. Several workers[19-23] have calculated the lifetime of this excited state and Wright et al.,[13] using pulsed dye-laser excitation and atomic absorption spectroscopy, made an experimental determination of the mentioned

lifetime. The static system employed by these workers made use of the $(^3P_1 \rightarrow ^3S_1)$ transition to monitor the $^3P_1$ state population. Quenching by H_2 and N_2 is mentioned only as contaminants and the collisional quenching constants for these two gases were not quantified.

Furcinitti et al.,[24] using the same technique that has just been described have made new measurements on the mean radiative lifetime of $Mg(3^3P_1)$ in He and Ne buffer gas, extrapolating the decays to infinite noble gas pressure. The effect of quenching by the walls, associated with diffusion, was noted but no quenching has been ascribed to the noble gas atoms.

Blickensderfer et al.,[25] also using a static system, pulsed dye-laser excitation and atomic absorption spectroscopy, have studied quenching of $Mg(^3P_J)$ by a limited number of collisional partners. Experiments were conducted with 300 Torr of He buffer gas and quenching cross sections have been reported for various collisional partners.

Quenching of $Mg(3^3P_J)$, $Ca(4^3P_J)$ and $Sr(5^3P_J)$ by N_2O and O_2 was observed by Benard et al.[26] studying the production of this metastable species in low pressure flames. These authors[26] discuss the mechanism of production of the ^3P_J states and energy transfer to a passive species like CO (electronic to diatomic vibrational energy transfer) and active species like N_2O where highly exothermic chemical reaction takes place.

As opposed to the static systems that have been mentioned so far, flow systems with production of $Mg(3^3P_J)$ by low and high current discharges have also been used. Taieb and Broida,[27] have produced $Mg(3^3P_J)$ in a low current discharge and quenching was studied using the afterglow method. Quenching constants have been presented and the reaction of $Mg(3^3P_J)$ with N_2O and O_2 was confirmed by photoluminescence of the B-X MgO system. Benard et al.,[28] using the same technique, employed a high current discharge for the production of the excited species and studied the energy transfer from $Mg(3^3P_J)$ to $Ca(4^1S_0)$ atoms.

Atomic beams of Mg, Ca and Sr, excited to the ^3P_J states, have been used by Kowalski[29] in the determination of the total attenuation cross sections for the reaction of these excited states with Cl_2 molecules. The

experimental values have been compared with the theoretical ones, calculated on the basis of the "harpoon model" and a good agreement was found.

The quenching of $Mg(3^3P_J)$ by H_2 has been recently studied by Breckenridge and Nikolai,[30] using emission from the forbidden $(^3P_1 \rightarrow {}^1S_0)$ transition following excitation by a pulsed dye-laser in a static system. These authors have demonstrated the temperature dependence of such a reaction and the change from a physical to a chemical exit channel control. The same reaction has been object of theoretical studies by Adams et al.,[31] who carried out calculations on relevant portions of the potential surface of the first triplet state of MgH_2. The resulting ab initio calculations have been used in a further study by Breckenridge and Stewart[32] on the temperature dependence of the quenching of $Mg(3^3P_J)$ by H_2 and D_2. The experimental technique was the same employed before by Breckenridge[30] and the isotopic effect reported is in accord with the results of the present work (see later).

Reactions of $Mg(3^3P_J)$ with the halogens F_2 and Cl_2, and the reaction of $Ca(4^3P_J)$ with Cl_2 have been studied by Kowalski and Menzinger[33] who have measured cross sections for beam attenuation, chemiionization $MX^+({}^1\Sigma_g^+)$ and chemiluminescence from $MX(A^2\Pi)$.

The reaction of $Mg(3^3P_J)$ with N_2O has recently received attention by a number of workers.[34-36,38] Dagdigian[34] has investigated the reaction of $Mg(3^3P_J)$ with O_2 and N_2O under single collision condition using the laser fluorescence technique for the determination of electronic states of the product MgO. The reaction dynamics were discussed in terms of C_s symmetry. The study was complemented by Cox and Dagdigian[35] who investigated the reactions of $Sr(5^3P_J)$ and $Mg(3^3P_J)$ with N_2O. The results are discussed and compared with previous work on $Ca(4^3P_J)$.[36] Bourguignon et al.,[37] using the same technique have studied the reactivity of $Mg(3^3P_J)$ and $Mg(3^1P_1)$ with N_2O and have shown that both excited states react with N_2O whereas the ground state $Mg(3^1S_0)$ does not. This result is confirmed by Yarkony[38] who performed ab initio self-consistent-field calculations on the lowest singlet $({}^1A')$ and triplet $(^3A')$ potential energy surfaces of the reaction

$$Mg + N_2O({}^1\Sigma^+) \rightarrow MgO + N_2({}^1\Sigma_g^+)$$

10
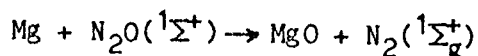
This author[38] compares the above mentioned reaction with the analogous Ca + N_2O system where $Ca(^1S_0)$ is reactive, unlike $Mg(^1S_0)$.

The investigations on the collisional behaviour of $Ca(4^3P_J)$ have been more restricted than those on $Mg(3^3P_J)$, although, more recently a number of studies have been published on this subject.

McIlrath[39], appear to have been the first to monitor $Ca(4^3P_J)$ in the time-resolved mode using atomic absorption spectroscopy with a photographic plate following pulsed dye-laser excitation of calcium vapour, but this was not exploited as a general tool for the determination of fundamental rate data apart from relaxation measurements within the $Ca(4^3P_J)$ manifold.[40]

Despite the routine use of dye-laser excitation to generate $Ca(4^3P_J)$, time-resolved spectroscopic studies have not been extensively used to determine collisional rate data with added gases. Malins et al.[41-43] have employed modulated dye-laser excitation coupled with phase sensitive detection and Stern-Volmer analyses to study the collisional quenching of $Ca(4^3P_J)$ by various gases including the noble gases, and by Mg, Ca and Sr in the ground $(^1S_0)$ states. Whitkop and Wiesenfeld[44] have employed time-resolved atomic absorption following dye-laser excitation to study quenching of $Ca(4^3P_J)$ by $Ba(6^1S_0)$. Atomic beam studies of $Ca(4^3P_J)$, generated by low voltage discharges through calcium vapour, have mainly been used for detailed investigations of chemiluminescence cross sections for reactions with Cl_2 and HCl,[29,33,45,47] and N_2O,[34,36] as well as for laser induced fluorescence measurements on CaO following reaction of $Ca(4^3P_J)$ with O_2 and CO_2.[48] The studies of the $Ca(4^3P_1 \rightarrow 4^1S_0)$ emission from low pressure flames catalysed by N_2O + CO with calcium additives have not led to absolute rate data for $Ca(4^3P_J)$.[26,49,50]

The study of $Sr(^3P_J)$, perhaps because of the experimental difficulties, as we shall see later, has been extremely limited. Solarz et al.[51] have studied the reaction of $Sr(^3P_1)$ with HF and HCl in a beam gas arrangement employing laser induced fluorescence detection. Phase sensitive detection of pulsed dye-laser excitation has been employed by Malins et al.[42] to study energy transfer from $Ca(4^3P_J)$ to $Sr(5^1S_0)$ and quenching of the

resulting $Sr(5^3P_J)$ by the noble gases. Apart from this study, no quenching rate data appear to be available for $Sr(5^3P_J)$.

In the present chapter the nature and the objectives of this investigation have been established. The experimental techniques have been mentioned and a bibliographical review on the collisional behaviour of Mg, Ca and $Sr[nsnp(^3P_J)]$ has been presented in order to allow experimental results to be discussed later. In chapter 2 the experimental technique used in this work will be discussed, special attention being given to the study on $Mg(3^3P_J)$. Modifications to the experimental technique, required for the studies on $Ca(4^3P_J)$ and $Sr(5^3P_J)$ are discussed in chapter 4 and 5, respectively. Chapter 3 is dedicated to the investigations on $Mg(3^3P_J)$, including the radiative lifetime, diffusion in noble gases and collisional quenching. The experimental results are presented and discussed where appropriate. Chapter 4 and 5 present the analogous studies on $Ca(4^3P_J)$ and $Sr(5^3P_J)$, respectively. Chapter 6 is dedicated to the conclusions resulting from the present investigation on the collisional behaviour of Mg, Ca and $Sr[nsnp(^3P_J)]$.

2. TIME-RESOLVED EMISSION EXPERIMENTS

The objective of this chapter is to outline the experimental procedure which has been used for the present thesis. Although three different elements of the group IIA have been studied, namely, Mg, Ca and Sr, the experimental procedure, if not identical, is quite similar. In order to avoid unnecessary repetition, the experimental set up will be described here in general terms. Those modifications concerning apparatus and experimental procedure that were necessary for a particular element studied will be dealt with in the appropriate chapter.

Broadly speaking, the system employed for the study of the collisional behaviour of Mg, Ca and $Sr[nsnp(^3P_J)]$ can be divided into three major parts; production of the excited species, gas handling and detection of the fluorescence signal. This division is here made just for the sake of clarity, as the system works as a whole integrated apparatus. The three parts above mentioned will be considered in great detail and it is proposed to conclude this chapter by describing the reagents employed in the experiment as well as the purification processes, when that was the case.

2.1 Production of the excited species

The excited species required for these experiments are $Mg(3^3P_J)$, $Ca(4^3P_J)$ or $Sr(5^3P_J)$ depending upon the particular element of group IIA being studied. The ^3P_J excited atoms are produced by optically pumping the ground state $^1S_0$ atoms kept in the vapour phase inside a reaction vessel. Light at the wavelength required for the transition $^1S_0 \rightarrow ^3P_1$ is derived from a tunable laser-pumped dye-laser. Basically, a metallic sample of the element to be studied is placed in the reaction vessel that will be described later. The vessel is brought to a temperature sufficiently high for the vapour pressure to have a reasonable value for the experiment (ca. 0.1 Torr). By keeping the temperature constant, one hopes to achieve an

atomic density in the vapour phase which is near to that of the equilibrium vapour pressure. The nature of the experiment does not normally require the knowledge of the initial atomic density, provided it can be maintained constant for each individual experiment.

The reaction vessel, where the production of the excited ^3P_J atoms takes place is placed inside an electrical furnace specially built to contain the vessel and to keep it at the required temperature. The temperature was monitored by a thermocouple placed inside the furnace and near to the central body of the reaction vessel. The potential drop across the thermocouple was read in a millivoltmeter (Cambridge Instruments Co. Ltd.). The cold junction of the thermocouple was kept at room temperature, which can reasonably be assumed constant throughout any particular experiment. The furnace has four heating elements and the temperature control is achieved by using a Variac transformer, which allows a temperature setting of ± 5 K.

The tunable dye-laser used in this work (J.K. Lasers, model DLPY4 2000 YAG) was pumped by means of a Nd-YAG primary laser. The Nd-YAG pumping laser has a fundamental wavelength of λ = 1064 nm (E = 450 mJ; pulse width ca. 20 ns) and frequency doubled by a DCDA crystal allows a vertically polarised beam at λ = 532 nm (E = 150 mJ) to be generated. By using a third harmonic generator (KD*P crystal) the fundamental and the second harmonic beams can be combined to produce a horizontally polarised beam at λ = 355 nm (E = 90 mJ). The laser can be operated at frequencies varying from 1 Hz to 20 Hz and has been used throughout this work at 10 Hz, since this is the frequency that gives the best performance for the particular Nd-YAG laser used. The possibility of choice of the primary laser wavelength output enables a great number of dyes to be efficiently pumped and increases the tunability of the dye-laser. In the study of the collisional behaviour of group IIA elements, where ^3P_J excited states had to be produced by pumping the $^1S_0$ ground states, the following combinations of pumping beams and dyes were used.

TABLE 2.1

Atom	Pumping beam	Dye	Wavelength
Mg	355 nm	Coumarin 460	457.1 nm
Ca	532 nm	Cresyl Violet 670	657.3 nm
Sr	532 nm	Nile Blue 690	689.3 nm

Details of concentration of the dye solution and output of the dye-laser are given in the relevant chapters. The dye-laser (J.K. Lasers, System 2000) was designed to be pumped by the harmonic output of a solid state laser like the Nd-YAG. The laser has suitable mirrors for use when pumping by a 532 nm or 355 nm source. Two dye cells are provided; one to be used as an oscillator and the other one as an amplifier. The output energy depends on the energy of the pumping beam ($E = 150$ mJ at 532 nm; $E = 90$ mJ at 355 nm) and on the conversion achieved for a particular dye (ca. 10% for the dyes employed in the present work). The primary Nd-YAG laser and the pulsed dye-laser are shown in photograph I, which is a general view of the apparatus employed in this investigation.

A couple of aluminium coated mirrors were used to direct the beam to the furnace window. A considerable loss of energy occurs during this beam steering, especially at low wavelengths ($\lambda = 457$ nm for instance) but, on the other hand, great flexibility is achieved by using mirrors and the energy reaching the excitation zone is enough for the desired production of ^3P_J excited species in the required concentrations.

Two kinds of reactors have been employed in the present work and although they were made of different materials [quartz for the study of $Mg(3^3P_J)$ as opposed to stainless steel for $Ca(4^3P_J)$ and $Sr(5^3P_J)$] the design remained basically the same. Previous workers have used reactors made of quartz lined with tantalum foil[13,24,25,52] or stainless steel[30,32,43] with slightly different designs. Stainless steel has been preferred for the higher temperatures required in the study of $Ca(4^3P_J)$ since this element has the lowest vapour pressure[53] of the three under consideration. On the other hand, the higher reactivity of strontium makes the stainless steel more desirable than quartz, because the latter is attacked at temperatures higher than 670 K.

The quartz reactor, initially employed for the study of $Mg(3^3P_J)$ is shown diagramatically in figure (2.1). As stated previously, it was constructed of quartz with optical Pyrex windows, sealed by means of O-rings, orthogonally placed for the entrance of the dye-laser excitation beam on the one hand and for the exit of the time-resolved emission signal on the other. Pyrex was preferred to quartz as a material for the optical windows because of its low reactivity towards the group IIA elements. The transmission of Pyrex, even for the lowest wavelength employed ($\lambda = 457.1$ nm for the study of Mg) is high enough to justify its choice. The vapour of the metallic element was introduced into the reactor by means of a slow flow of a noble gas, including, where necessary, a further added quenching gas, over the heated metal in a side arm within the furnace maintained at an appropriate temperature thermoelectrically measured. Gas flow through the reactor was achieved by means of a further pair of side arms, with pre-heating tape at the entrance of the reactor flow in order to maintain a sensibly constant temperature for that part of the reactor which lies within the furnace. The entrance and exit optical Pyrex windows were external to the furnace and were water-cooled using a flow system contained by means of O-rings within brass fittings.

The effective size of the reactor is not, of course, the physical size of the quartz container but is of complex geometry, determined by the area of the input dye-laser excitation beam and the light gathering power of the small monochromator (see later), employing slits of finite width and height. Simple considerations of heat transfer for the gas within the effective reactor volume show this to be at the elevated temperature required even though the entrance and exit windows are cooled. This arrangement is particularly facilitated using the slow flow system, kinetically equivalent to a static system, as mentioned earlier. By the same token, the attack of the inner quartz surface (by magnesium in this case) of the reactor with the furnace is of no consequence. The reaction volume is effectively a small region within the overall reactor volume as indicated; the quality of the fluorescence signals being determined by the state of cooled entrance and the exit windows which were found to be totally unaffected by the metallic vapours that had fully condensed at the outlet edge of the furnace wall. It was therefore found, in contrast to previous dye-laser excitation studies on magnesium vapour, necessary to

16

WATER OUTLET

GAS FLOW

PRE-HEATER

QUARTZ REACTION VESSEL

Mg

OVEN

TO MONOCHROMATOR

HEATING ELEMENT

PUMP

WATER COOLING

WATER OUTLET
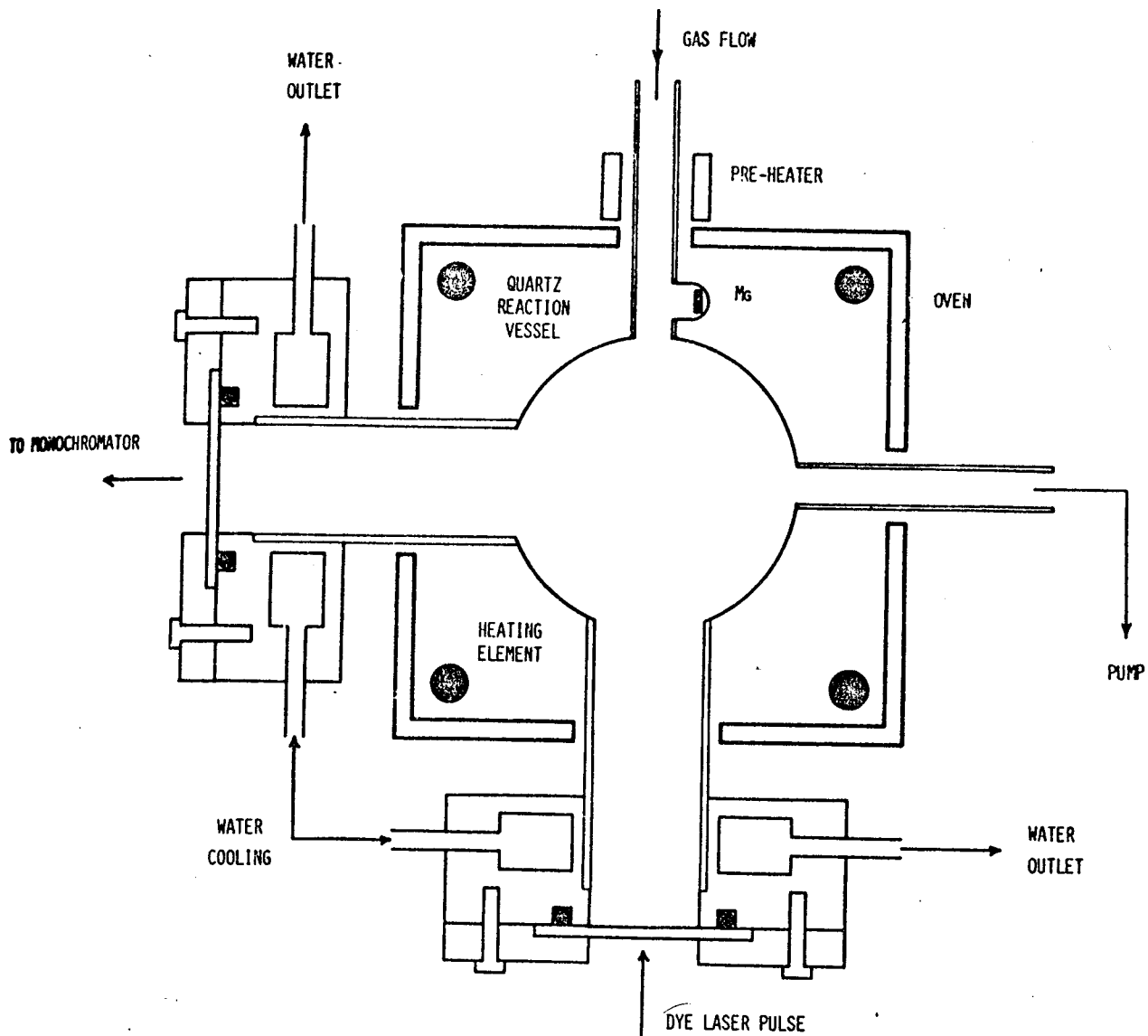
DYE LASER PULSE

Figure 2.1

Detailed diagram of the reaction vessel employed for the kinetic study of $Mg(3^3P_J)$ by time-resolved atomic emission following pulsed dye laser excitation of $Mg(3s^2(^1S_0)) \longrightarrow Mg(3s3p(^3P_1))$ ($\lambda = 457.1$ nm.)

use neither a stainless steel reactor[30,32,43] nor tantalum foil within the quartz reactor,[13,24,25,52] even though deposition of magnesium took place on the quartz. Finally, we may emphasise the need only for reproducible metallic vapour densities within the reactor during sampling of the emission, following the series of laser pulses from which is extracted a decay curve for the ^3P_J excited species exhibiting first-order kinetics. An absolute atomic density commensurate with the equilibrium vapour pressure, for a given temperature, is not necessary, although the density should be close to this in view of the proximity of the side-arm containing the metallic sample to the reactor volume and the slow flow employed. Only in the special case of quenching by $Sr(5^3P_J)$ by ground state $Sr(5^1S_0)$ was it necessary to estimate the absolute atomic concentration (see later).

Photograph II shows the quartz reactor employed in the kinetic study of $Mg(3^3P_J)$, photograph III shows the interior of the furnace with its four heating elements and photograph IV is a view of the quartz reactor placed inside the furnace.

2.2 Gas handling system

The purpose of the gas handling system is to allow gas mixtures of known composition to be flown through the reaction vessel. The gas handling system must also provide facilities for preparation of gas mixtures and eventually purification of gases to be used in the experiments. To that purpose a vacuum line was specially built for the experiments described in the present work. Details of the vacuum line are shown in photographs V and VI. The vacuum line was constructed in Pyrex glass and it is a conventional line capable of holding a vacuum of ca. 10^{-5} Torr, with the addition of the flow system which will be described in some detail later. The vacuum was achieved by the combination of a primary rotary pump (Metrovac, GDR1, Associated Electrical Ind. Ltd.) and an oil diffusion pump (Edwards 203B). For the flow system itself, another rotary pump (NGN, model PD/2), connected to the reactor gas outlet, was employed. Pressure in several points of the line was measured by two spiral gauges, a Bourdon gauge, two aneroid gauges and a capacitance manometer [MKS, 221A,

Chell Instruments Ltd, 0 - 100 Torr, (1 Torr = 133 N.m^{-2})] which was also used to control the pressure in the flow system. A Pirani (Genevac PGH3) and a Penning type gauge (Edwards, model 6) were used to measure the vacuum achieved.

The flow system is represented diagramatically in figure (2.2). It consists of two 10 litre bulbs; one to contain a buffer gas such as helium and the other containing a mixture of the buffer and the quenching gas. By taking known amounts of gas from these bulbs, mixtures of varying concentration of the quenching gas at constant total pressure can be prepared. The final concentration may be varied from zero (pure buffer gas) up to the quenching gas concentration in the relevant bulb. The importance of keeping a constant total pressure is related to the diffusion component of the first-order decay constant under consideration and will be dealt with later. Apart from these two bulbs B1 and B2 [(see figure (2.2)] three needle valves N1, N2 and N3 were provided to control the composition of the gas mixture flowing through the reaction vessel. The needle valves control the admission of gas to the flow line FL, leading to the reaction vessel RV and pumped by the flow pump FP through the needle valve N4. The needle valve N4 controls the flow through the reaction vessel and once it has been adjusted it should be kept unchanged throughout the experiments. The pressure in the flow line FL was measured by means of the same capacitance gauge MKS, mentioned earlier. Flow calibrations are necessary before a flow of known concentration and constant total pressure can be set up. Flow calibrations were made by diverting the flowing gas to a 10 litre bulb B3 and measuring the pressure variation as a function of time. The pressure in the bulb B3 as a function of time was measured by the baratron MKS gauge for differing pressures of helium in the flow line FL. The calibration is prepared as a linear relationship between the logarithm of the flow rate (log f) and the logarithm of the pressure (log p). Thus, we may write

$$\log f = a.\log p + b \qquad (2.1)$$

Hence, once a calibration curve has been built and the values of a and b are known, one can readily calculate the flow rate for a particular pressure of gas in the flow line FL. On the other hand, if we have a flow
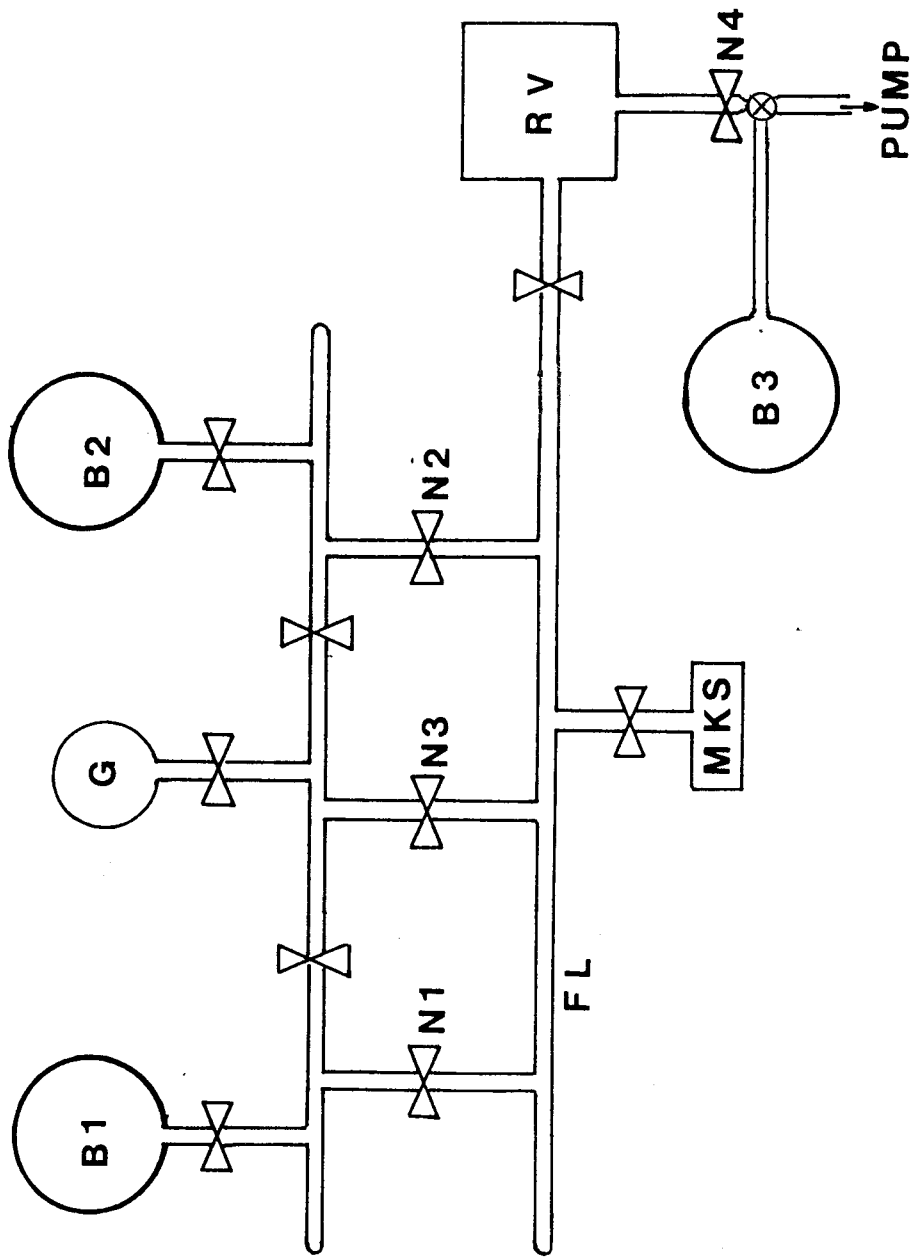
Figure 2.2 - Diagram of the flow system employed in the time-resolved emission experiments.

rate f_1 from the bulb B1 and a flow rate f_2 from the bulb B2, we may write for the total flow rate

$$f = f_1 + f_2 \qquad (2.2)$$

The flow rate, f, will be the flow rate corresponding to the total pressure p. The flow rates f_1 and f_2 are determined by the required concentration of the quenching gas, using the relation;

$$p_i = [f_i/(f_1 + f_2)]p \qquad (2.3)$$

where p represents the total pressure $(p_1 + p_2)$ in the case of a two component system. Knowing the flow rates f_1 and f_2, it is possible to calculate the pressures p_1 and p_2 required, by making use of equation (2.1). The needle valve N1 can be used to set up a flow rate f_1 corresponding to the pressure p_1. The same procedure, with the needle valve N2, is used to set up a flow rate f_2 at pressure p_2. By allowing gas to flow through the needle valves N1 and N2, simultaneously, a flow rate $f = f_1 + f_2$ is achieved and the final pressure should be p, according to equation (2.1). Thus, although the final pressure is not the sum of the individual pressures p_1 and p_2, its value can be calculated by means of equation (2.1) and (2.2) and a flow of varying concentration of quenching gas at constant total pressure can be set up in this way.

2.3 Detection of the fluorescence signal

Figure (2.3) shows a block diagram of the apparatus for the kinetic study of the ^3P_J states of group IIA elements, following excitation by pulsed dye-laser and monitored by time-resolved emission from a forbidden transition.

Following rapid optical pumping to the $^3P_1$ state, the slower time-resolved emission back to the $3s^2(^1S_0)$ state is then used to monitor the decay of the electronically excited magnesium atom, for example, and to separate the various first-order kinetic contributions arising from the spontaneous emission itself, diffusion and collisional quenching. So intense is the time-resolved emission that optical isolation can conveniently be effected by means of a small monochromator (Minichrom,

FLOW SYSTEM

f_1 f_2

OVEN +
REACTION
VESSEL

PUMP

MIRROR

MONOCHROMATOR

PHOTOMULTIPLIER
POWER SUPPLY

PHOTOMULTIPLIER

PHOTOMULTIPLIER
GATING CIRCUIT

DYE LASER

OSCILLOSCOPE

CURRENT-TO-VOLTAGE
CONVERTER

MONOSTABLE
PULSE
GENERATOR

XY RECORDER

BOXCAR
INTEGRATOR

LASER
CONTROL UNIT

ND - YAG LASER
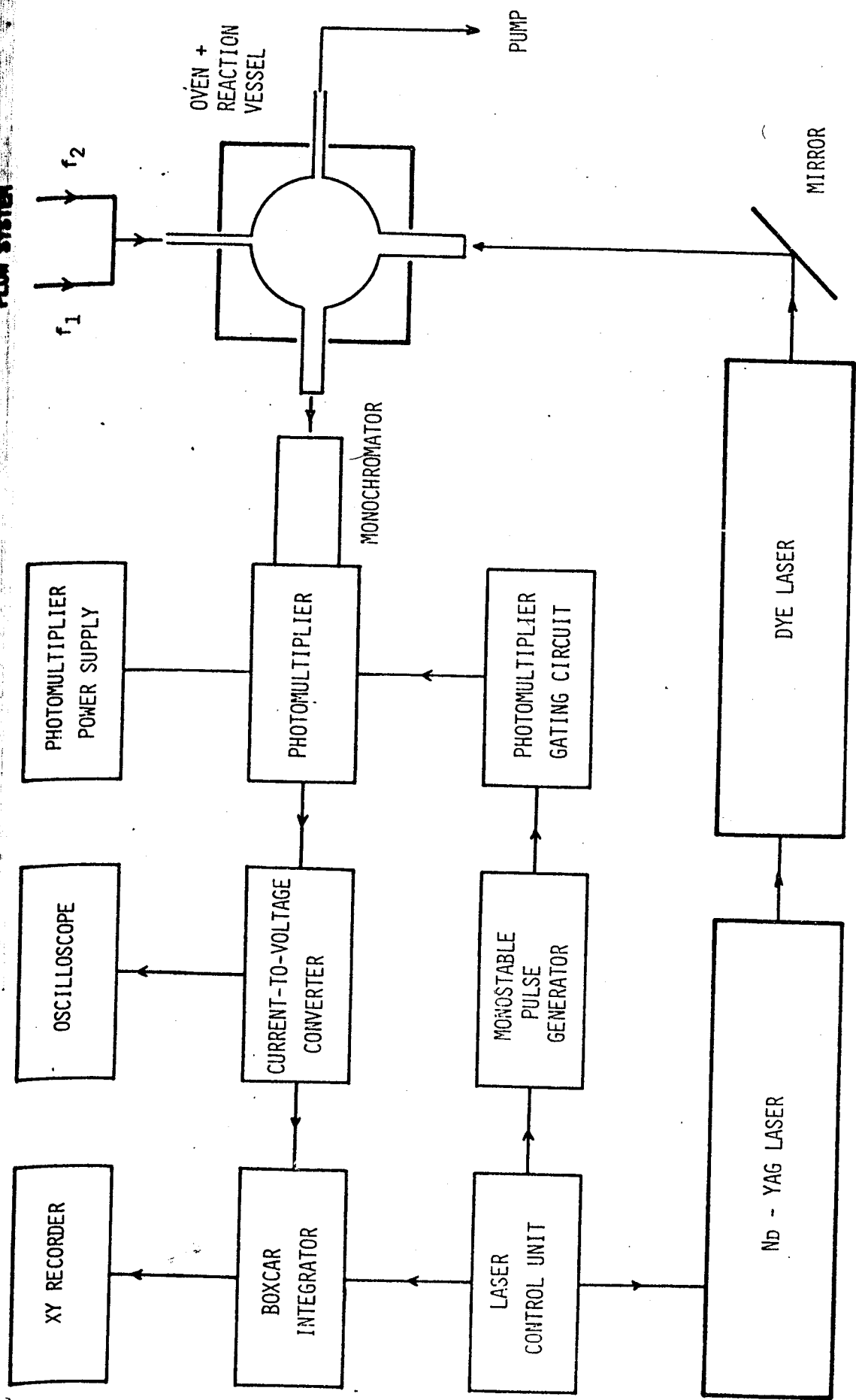
Figure 2.3

Block diagram of the apparatus for the kinetic study of $Mg(3^3P_J)$
by time-resolved atomic emission following pulsed dye laser excitation
of $Mg(3s^2(^1S_0)) \longrightarrow Mg(3s3p(^3P_1))$ (λ = 457.1 nm).

1-MC1-02, Fastie-Ebert mounting; f/4; focal length 74 mm; range 200-800 nm; grating 20 mm square; 1800 lines per mm; 6 nm per mm). The system employs fixed slits (150, 300 and 600 μ, 4 mm high), the present measurement using the larger slits and hence, dispensing with the grating resolution of the monochromator ($d\lambda/\lambda$ = 2.8 x 10^{-5}). Nevertheless, it was found that this means of optical separation dramatically reduces the effect of scattered light compared with that encountered with the interference filter that was initially employed. In fact, the small monochromator is effectively mounted on the photomultiplier housing, as opposed to the converse. This arrangement may be contrasted with that employing an interference filter as described by Breckenridge and Nicolai.[30] Photograph VII shows the monochromator attached to the photomultiplier tube and in front of the reactor window. Because the signal to be detected is at the same wavelength as the excitation source, scattered light becomes a major concern and has to be reduced as much as possible. The scattered light can be significantly reduced by means of a pre-trigger gating system associated with the photomultiplier tube E.M.I. 6256B. The pre-trigger gating system employed here is not a full gating arrangement with electron defocusing but rather a convenient system developed to be used with the photomultiplier tube already mentioned, as described in the work by Husain, Krause and Slater on $Sb(5^4S_{3/2})$.[54] The photomultiplier tube E.M.I. 6256B, although not specifically designed for gating, allows suitable access to the dynodes and a convenient gating efficiency can be achieved (i.e., attenuation of the photomultiplier signal by a factor of ca. 100 during gating). However, unlike the study mentioned before, the facilities in the laser system itself permit considerable simplification of the circuitry employed, with the elimination of both a trigger pulse generator and a delay circuit. The operation of the gating circuit in the present application may be summarised as follows. The repetition rate of the laser is set, by choice, in these measurements to 10 Hz. For each firing of the pair of flash lamps in the primary laser system used to store energy in the Nd-YAG rod, the laser control unit generates a pulse of magnitude ca. 8 V and of duration ca. 10 μs. The pulse is, of course, designed to initiate the Pockels cell driver in the Q-switched mode, but it may also be used to trigger a monostable pulse generator, powered by means of a 18 V d.c. stabilised power supply. The circuit employed here is a modification to

that described both hitherto[54] and as originally reported by Acuna et al,[55] but further developed to apply considerably longer pulses, of length up to 300 µs and of magnitude ca. 100 V across the 5th and 7th dynodes of the 13-dynode E.M.I. 6256B photomultiplier tube, which are accessible. Thus, the initial pulse generated in the primary laser, in conjunction with the monostable pulse generator, is used to switch off the photomultiplier tube for lengths of time to ca. 300 µs. Following energy storage in the Nd-YAG rod, the Pockels cell is switched on at an optimum fixed delay time for the instrument of ca. 180 µs after firing the flash lamps. Thus, the photomultiplier tube is switched on at t = (300 - 180) µs, in this instance, after firing the dye-laser itself. One must notice that the delay time for the Pockels cell drive (ca. 180 µs) cannot be changed without affecting the Nd-YAG laser performance and the only way to vary the "gating time" would be by modifying the pulse length in the monostable pulse generator. In the described set up, only one delay time could be used (120 µs) for gating because the monostable did not allow any other setting between 180 µs and 300 µs. In spite of this inflexibility, this was found to be a very efficient way of pre-trigger photomultiplier gating and eliminates the large scattered light signals. Further, the pulse used for initiating the photomultiplier gating circuitry is also used to trigger the boxcar integration system [figure (2.3)]. The gating system was subsequently modified for the experiments on $Sr(5^3P_J)$ as described in detail in chapter 5.

The photoelectric signal resulting from the E.M.I. 6256B photomultiplier tube was then amplified without distortion by means of a current-to-voltage converter[56] and fed to a boxcar integrator (Brookdeal Electronics, linear gate type 415, scan delay generator 423A) which had been triggered, as described, by means of the initial pulse generated on operation of the flash-lamp discharges in the primary laser system. The current-to-voltage converter used to amplify the transient photoelectric pulses employs a fast settling operational amplifier with a variable feedback capacitance and resistance, in order to preserve the inherent time response of the photomultiplier. Resistances may be varied in seven steps from 100 KΩ to 10 MΩ while capacitors may be selected in nine steps from 10 pF to 4700 pF. Exact values for each step are shown in the circuitry presented in the appendix. A typical setting that may be used is,

21

$R = 220$ KΩ and $C = 100$ pF, which gives a time constant of $RC/2 = 1.1 \times 10^{-5}$ s. The settings in the boxcar integrator are basically determined by the magnitude of the first-order kinetic constant resulting from the time-resolved emission. A constant gate (50 μs for Mg and Ca and 20 μs for Sr) was employed for all boxcar analyses and time bases of 1,2,5 and 10 ms, depending on the decay times of the ^3P_J states under the various experimental conditions. Most experiments employed a time base of 2 ms and a "reading time" of 200 s. Thus, a decay curve using a pulse-laser repetition rate of 10 Hz, was constructed by taking 50 μs samples from 2000 pulses. The use of a boxcar integrator is, on the one hand a wastage of information since one is throwing away about 98% of the data, but on the other hand it has the advantage of being much less sensitive to spurious trigger than a signal averaging system. Individual emission pulses which were sampled to construct an overall decay were monitored oscilloscopically (Tektronix Storage Oscilloscope 564B) purely for the purpose of visual display and not for kinetic analysis as in the previous investigations involving dye-laser excitation of Mg(3^3P_J).[13,25,30] The output of the boxcar integrator was finally fed to an XY-recorder (Bryans Ltd) for kinetic analysis.

Photograph VIII shows part of the electronics used in the present work, including the current-to-voltage converter, the boxcar integrator, the XY-recorder, the p.m. power supply and the oscilloscope. The gating system is not shown in this photograph.

2.4 Materials

The following materials have been used in the present work. The stated purity of each material is given whenever supplied by the manufacturer. Purification processes, when employed, are indicated. The materials used in the present investigation may be subdivided in three groups; a) metals of the group IIA; b) dyes for the dye-laser and; c) quenching gases and vapours.

2.4.1 Metals of the group IIA

Magnesium: (Johnson, Matthey and Co. Ltd., "Spectroscopically standardised rod", "H.S." Brand; purity greater than 99.98%; main impurities: Fe, 0.013%; Mn, 0.0023%; Pb, 0.0013%.

Calcium: granulated (East Anglia Chemicals)

Strontium: purum (Fluka A.G., Buchs S.G.), purity greater than 99%

2.4.2 Dyes for the dye-laser

Coumarin 460: (Exciton Chemical Co. Inc.)

Cresyl Violet 670: perchlorate, (Exciton Chemical Co. Inc.)

Nile Blue 690: perchlorate, (Exciton Chemical Co. Inc.)

2.4.3 Gases and vapours

Gas purity is a particularly serious consideration in studies of diffusion in the noble gases and in the associated measurement of the mean radiative lifetime of group IIA elements from extrapolating decay measurements on the electronically excited atom to infinite pressure of these gases. The kinetic contribution of the diffusional removal of the ^3P_J states is relatively small and variations of this diffusional component with typical noble gas pressures employed in this type of investigation are also small. On the other hand, collisional quenching by O_2 as an impurity is relatively efficient[27] $k[Mg(3^3P_J) + O_2] = 3.0 \times 10^{-11}$ $cm^3 molecule^{-1} s^{-1}$ (room temperature) and its absolute effect may become large at high total pressure. Hence, special note is taken of molecular oxygen as an impurity in these studies, particularly for the noble gases.

The following gases and vapours have been used in the present work. Unless otherwise stated, gases have been used directly from their cylinders.

Helium: Matheson "Gold Label", stated purity 99.999%; major impurities: Ne, 8 ppm; N_2, 5 ppm; H_2O, 15 ppm and O_2, 6 ppm.

Neon: B.O.C. Research Grade, stated purity 99.999%; major impurities: He, 5 ppm; O_2, N_2, H_2, hydrocarbons and H_2O, 1 ppm each.

Argon: B.O.C. Research Grade, stated purity 99.999%; main impurities: N_2, 5 ppm; H_2O, 2 ppm, H_2, CO_2 and hydrocarbons, 1 ppm each. [A number of experiments were also carried out with "zero grade Argon" (B.O.C.), purified by means of a B.O.C. Rare Gas Purification Unit Mark 3. This procedure, coupled with the use of a compressor, in fact, yielded a sample with an O_2 impurity of 50 ± 10 ppm as measured mass spectrometrically.]

Krypton: B.O.C. Research Grade, stated purity 99.99%; main impurities: Xe < 50 ppm, N_2 < 25 ppm, O_2, CO_2, H_2 and hydrocarbons < 5 ppm each.

Xenon: B.O.C. Research Grade, stated purity 99.993%; main impurities: Kr, 50 ppm; N_2, 20 ppm; O_2, CO_2, 5 ppm each; Ar, hydrocarbons, H_2O, 2 ppm each; H_2, 1 ppm.

Nitrogen: B.O.C. Research Grade; stated purity 99.994%; main impurities: Ar, 50 ppm, O_2, Ne, and H_2O, 2 ppm each.

Hydrogen: B.O.C. Research Grade, stated purity 99.96%; main impurities: N_2 400 ppm, hydrocarbons, 20 ppm; O_2, CO_2 and H_2O, 2 ppm each.

Methane: B.O.C. Research Grade, stated purity 99.9925%; main impurities: N_2, 50 ppm; hydrocarbons, 20 ppm; H_2, O_2, CO_2 and H_2O, 2 ppm each.

Carbon Monoxide: B.O.C. Research Grade, stated purity 99.96%; main impurities; N_2 40 ppm; hydrocarbons 20 ppm; O_2, CO_2 and H_2O, 2 ppm each.

Carbon Dioxide: B.O.C. Research Grade, stated purity 99.999%; main impurities; N_2 5 ppm; H_2O 2 ppm; H_2, O_2, CO and hydrocarbons, 1 ppm each.

Carbon Tetrafluoride: B.O.C., Freon 14; stated purity 99.97%; main impurities, H_2O 10 ppm; CO 0.2%, air 1.0%, organic impurities 0.3%, free acidity as HCl 0.1 ppm.

Nitrous oxide: B.O.C. Research Grade, stated purity 99.997%; main impurities; N_2 20 ppm; CO_2 10 ppm; nitrogen oxides 5 ppm; O_2 and H_2O 2 ppm each.

Deuterium: Matheson, C.P. grade, stated purity 99.7%.

Nitric Oxide: Matheson, C.P. grade; stated purity 99.0%; purified by several freeze-pump-thaw cycles followed by distillation from a dry-ice-acetone slush to liquid nitrogen temperature (-196 oC)

Ammonia: Matheson, C.P. grade; stated purity 99.96%; purified by several freeze-pump-thaw cycles.

Ethylene: Matheson, technical grade; stated purity 99.6%; purified by several freeze-pump-thaw cycles.

Acetylene: Matheson, technical grade; stated purity 99.0%, purified by several freeze-pump-thaw cycles.

Benzene: B.D.H. Analar, purified by several freeze-pump-thaw cycles followed by fractional distillation from room temperature to liquid nitrogen temperature (-196 oC).

Photograph I: General view of the apparatus for the kinetic study of group IIA elements in the ^3P_J states, generated by pulsed dye-laser excitation and monitored by time-resolved forbidden emission $(^3P_1 \rightarrow {}^1S_0)$, using boxcar integration.

Photograph II: Quartz reactor employed in the kinetic study of $Mg(3^3P_J)$, indicating the water-cooled windows.

Photograph III: View of the inside of the furnace indicating the heating coils and the port holes for entry of the laser beam and exit of the spectroscopic signal.

Photograph IV: Quartz reactor employed in the kinetic study of $Mg(3^3P_J)$, placed inside the furnace.

Photograph V: Front view of the vacuum system for dye-laser excitation studies, indicating the main line, the gas handling system, pressure measuring devices and bulb with magnetic stirrer for mixture preparation.

Photograph VI: Back view of the vacuum system employed in the dye-laser
excitation studies of the group IIA elements, including the diffusion pump
and the flow system.

Photograph VII: Detection system employed in the kinetic study of group IIA elements showing the monochromator attached to the photomultiplier tube and placed in front of the exit window of the quartz reactor.

Photograph VIII: Electronic units employed in the dye-laser studies including the current-to-voltage converter, the boxcar integrator, the XY-recorder and the oscilloscopes for visual display.

This chapter deals with a range of properties of the electronically excited magnesium atom, namely, the mean radiative lifetime, diffusion in noble gases and collisional quenching. The general considerations have applicability to the three lower ^3P_J states of Mg, Ca and Sr. In this particular chapter, the investigations and results for the behaviour of Mg(3^3P_J) are considered in detail. Reference will further be made to this work later when describing the experiments carried out on calcium (chapter 4) and strontium (chapter 5).

Among the three group IIA elements to be studied, magnesium was chosen as the first atomic state to be investigated for a number of reasons. The transition $^3P_1 \rightarrow {}^1S_0$ for magnesium exhibits an Einstein coefficient smaller than those for the analogous transitions of calcium and strontium. In other words, one can expect a longer observed mean radiative lifetime for magnesium compared with calcium or strontium. Bearing in mind that scattered light is a major problem to be considered in these experiments, it is easier, in theory, to work with relatively long decay times. The amount of data available in the literature for Mg(3^3P_J) vastly exceeds the limited data for Ca(4^3P_J) and Sr(5^3P_J). This difference can be accounted for in part by the astrophysical interest for the emission lines of the metastable ^3P_J states of Mg, but also, as a consequence of the greater ease resulting from carrying out measurements in this larger time domain.

3.1 Mean radiative lifetime and diffusion in noble gases

The accuracy in the determination of the mean radiative lifetime (τ_e) of a forbidden transition derived from a first-order kinetic parameter, namely, the Einstein coefficient for spontaneous emission ($A_{nm} = 1/\tau_e$), measured in real time, is principally limited by the procedure in measuring a relatively small intercept of a plot obtained from a series of first-order decay measurements as a function of composition. This has been

illustrated hitherto, for example, in various measurements of

$$+_e[I(5^2P_{1/2}) \rightarrow I(5^2P_{3/2}) + h\nu \quad (\lambda = 1315 \text{ nm})]^{57-59}$$

and similar kinetic considerations apply in the present measurements on $Mg(3^3P_1)$ with the addition of a further factor. We need, first, to note that, from the viewpoint of emission, the $3s3p(^3P_0)$ and $3s3p(^3P_2)$ states are "reservoir" states within the ^3P_J manifold, following Wiese et al.[60] Hence, emission from either $Mg(3^3P_0)$ or $Mg(3^3P_2)$ (τ_e = 29 and 76 min, respectively[60]), populated via collisions of $Mg(3^3P_1)$ with the various gases present, subsequent to excitation to the $^3P_1$ state by means of the pulsed laser, can be neglected. Further, we may readily assume that, at pressures employed in the present investigations, the 3^3P_0, 3^3P_1 and 3^3P_2 spin-orbit components (E = 21851, 21870 and 21911 cm^{-1}, respectively[10]) are maintained in Boltzmann equilibrium through collisions during the kinetic measurements. This may be seen from empirical considerations of the number of collisions required to transfer such small amounts of electronic energy to translation[61] $[\Delta E(^3P_{0 \rightarrow 1})$ = 19 cm^{-1}, $\Delta E(^3P_{1 \rightarrow 2})$ = 41 cm^{-1}].[10] Thus, defining the standard equilibrium constants

$$Mg(3^3P_0) \rightleftharpoons Mg(3^3P_1) \qquad K_1 \qquad (3.1)$$

$$Mg(3^3P_1) \rightleftharpoons Mg(3^3P_2) \qquad K_2 \qquad (3.2)$$

and considering, for the moment, the removal of all states within the $Mg(3^3P_J)$ manifold by emission only from $Mg(3^3P_1)$ we may write the following kinetic scheme;

$$Mg(3^3P_0) \rightleftharpoons Mg(3^3P_1) \rightleftharpoons Mg(3^3P_2)$$

$$Mg(3^1S_0) + h\nu \qquad\qquad Mg(3^1S_0) + h\nu$$
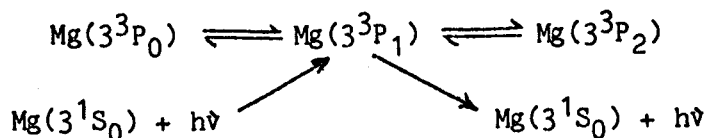
The differential equation for this system, reads;

$$-d\{[Mg(3^3P_0)] + [Mg(3^3P_1)] + [Mg(3^3P_2)]\}/dt = A_{nm}[Mg(3^3P_1)] \quad (3.3)$$

Using equations (3.1) and (3.2) we may write;

$$-d\{[Mg(3^3P_0)] + [K_1 Mg(3^3P_0)] + [K_2 K_1 Mg(3^3P_0)]\}/dt$$
$$= A_{nm}[K_1 Mg(3^3P_0)] \quad (3.4)$$

hence,

$$(1 + K_1 + K_2 K_1)\{-d[Mg(3^3P_0)]/dt\} = A_{nm}[K_1 Mg(3^3P_0)] \quad (3.5)$$

and rearranging (3.5) we arrive to;

$$-d\{\ln[Mg(3^3P_0)]\}/dt = A_{nm}/(1 + 1/K_1 + K_2) \qquad (3.6)$$

By the same token, it is easy to show that;

$$-d\{\ln[Mg(3^3P_1)]\}/dt = A_{nm}/(1 + 1/K_1 + K_2) = k'_{em} \qquad (3.7)$$

and,

$$-d\{\ln[Mg(3^3P_0)]\}/dt = A_{nm}/(1 + 1/K_1 + K_2) = k'_{em} \qquad (3.8)$$

At $T = 800$ K, which is the temperature used for the work on Mg, the equilibrium constants defined in equations (3.1) and (3.2) are;

$$K_1 = (g_1/g_0).\exp(-\Delta E_1/kT) \qquad (3.9)$$

and,

$$K_2 = (g_2/g_1).\exp(-\Delta E_2/kT) \qquad (3.10)$$

where g_0, g_1 and g_2 are the degeneracies of the 3^3P_0, 3^3P_1 and 3^3P_2 states respectively, namely 1, 3 and 5. Using the energy spacings between those states; $\Delta E_1 = \Delta E(3^3P_{0\rightarrow1}) = 19$ cm^{-1} and $\Delta E_2 = \Delta E(3^3P_{1\rightarrow2}) = 41$ cm^{-1} and considering that $kT = 555.9$ cm^{-1} ($T = 800$ K), we obtain;

$$K_1 = 3.\exp(-19/555.9) = 2.899$$

and,

$$K_2 = (5/3).\exp(-41/555.9) = 1.548$$

thus,

$$(1 + 1/K_1 + K_2) = 2.893$$

At infinite temperature this function becomes 3 and arises solely from the statistical weights in the 3^3P_J spin-orbit levels. In the present experiments, for $T = 800$ K, the first-order kinetic contribution to the decay of $Mg(3^3P_1)$ yields the mean radiative lifetime of $Mg(3^3P_1)$, (τ_e), via the relation

$$k'_{em} = 1/(2.893\tau_e) \qquad (3.11)$$

where k'_{em} has been defined in equations (3.7) and (3.8). Hence, emission is restricted to the 3^3P_1 state, but collisional removal by quenching gases

28

(Q) and diffusional removal (β), which is inversely proportional to the pressure, is ascribed to all states within the $Mg(3^3P_J)$ manifold. The rate parameters are assumed to be equal for each spin-orbit level in view of the similar nature of the electronic structure. Hence,

$$-d\{\ln[Mg(3^3P_1)]\}/dt = k' = k'_{em} + \beta + k_Q[Q] \quad (3.12)$$

Experimentally, the objective is thus to determine the overall first-order decay coefficient, k', as a function of composition and to separate the contributions to this quantity as given in equation (3.12).

It is assumed that $\beta(s^{-1})$ may be considered as arising from the long-time solution of the diffusion equation,[62,63] which for a cylinder takes the form;

$$\beta = (\pi^2/l^2 + 5.81/r^2)D_{12} \quad (3.13)$$

However, solving this equation requires the knowledge of boundary conditions of an uncertain geometry, not the physical magnitude of the reaction vessel but the effective geometry of the combination of the excitation area for the laser and the light-gathering power of the optical detection system. In these experiments, β will be allowed for empirically at a given fixed total pressure in the presence of varying quantities of added quenching gas. Hence, equation (3.12) yields on integration;

$$[Mg(3^3P_1)]_t = [Mg(3^3P_1)]_{t=0} \cdot \exp(-k't) \quad (3.14)$$

and the resonance fluorescence emission is then given by;

$$I_F = \phi A_{nm}[Mg(3^3P_1)]_t \quad (3.15)$$

where ϕ represents a factor which involves the light-gathering power of the optical detection system plus the sensitivity of the electronics.

Substituting in equation (3.15) the value of $[Mg(3^3P_1)]_t$ given by equation (3.14) we may write;

$$I_F = \phi A_{nm}[Mg(3^3P_1)]_{t=0} \cdot \exp(-k't) \quad (3.16)$$

Thus, the semi-logarithmic decay of I_F with time yields k'. The variation of k' with $[Q]$ at a fixed total pressure yields k_Q, the

second-order rate constant for collisional removal (see later).

Figure (3.1) shows examples of the XY-output for the variation of the emission (I_F) of the transition $Mg(3^3P_1 \longrightarrow 3^1S_0)$ (λ = 457.1 nm) following the pulsed dye-laser excitation of $Mg(3^1S_0)$ in helium buffer gas at two differing pressures. First-order kinetic plots of $\ln(I_F)$ as a function of time for these two decays are displayed in figure (3.2). From these plots, the first-order decay coefficient k' is obtained by a linear computerised least-square analysis. The first-order decay coefficient k', as one can see from equation (3.12), is the result of three different processes; spontaneous emission (A_{nm}), diffusion (β) and collisional quenching (k_Q).

If we consider that the diffusion term β is inversely proportional to the pressure, we may write;

$$k' = k'_{em} + \beta'/p + k_Q[Q] \qquad (3.17)$$

where β' is the pressure independent diffusion coefficient.

Equation (3.17) shows that measurements of k' for varying pressures of a noble gas, where no collisional quenching is involved (i.e. k_Q = 0), should exhibit a linear relationship between k' and $1/p(noble\ gas)$. The intercept of a plot k' vs. $1/p(noble\ gas)$ gives k'_{em} and the slope gives β' the relative diffusion coefficient of $Mg(3^3P_J)$ in the noble gas used in the experiment.

Figure (3.3) shows the linear variations of k' with $1/p_{He}$, indicating the variation of the diffusional contribution for $Mg(3^3P_J)$ in the helium buffer gas. A linear computerised least-square analysis yielded the slope, and specifically in this context, the intercept of the plot of $1/p_{He}$ = 0 with the appropriate error (1σ) (0.16 $\pm$ 0.0418 x 10^3 s^{-1}) which in turn, yielded τ_e = 2.1 $\pm$ 0.5 ms through equation (3.11). Plots for neon and argon, similar to that for helium are presented in figure (3.4) and yielded τ_e = 1.6 $\pm$ 1.0 and 1.9 $\pm$ 0.4 ms, respectively.

However, analyses of this type for the decay of $Mg(3^3P_1)$ in the gases krypton and xenon may not be carried out even though the diffusional contribution dominates the variation of k' with p_{Kr} and p_{Xe}. Despite inefficient quenching of the excited atom demonstrated by these noble
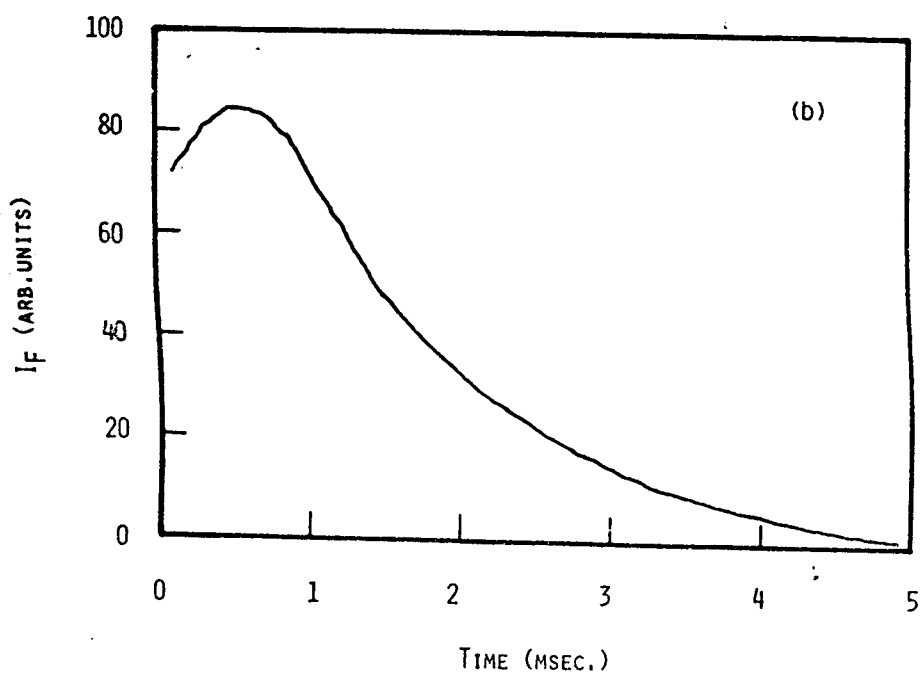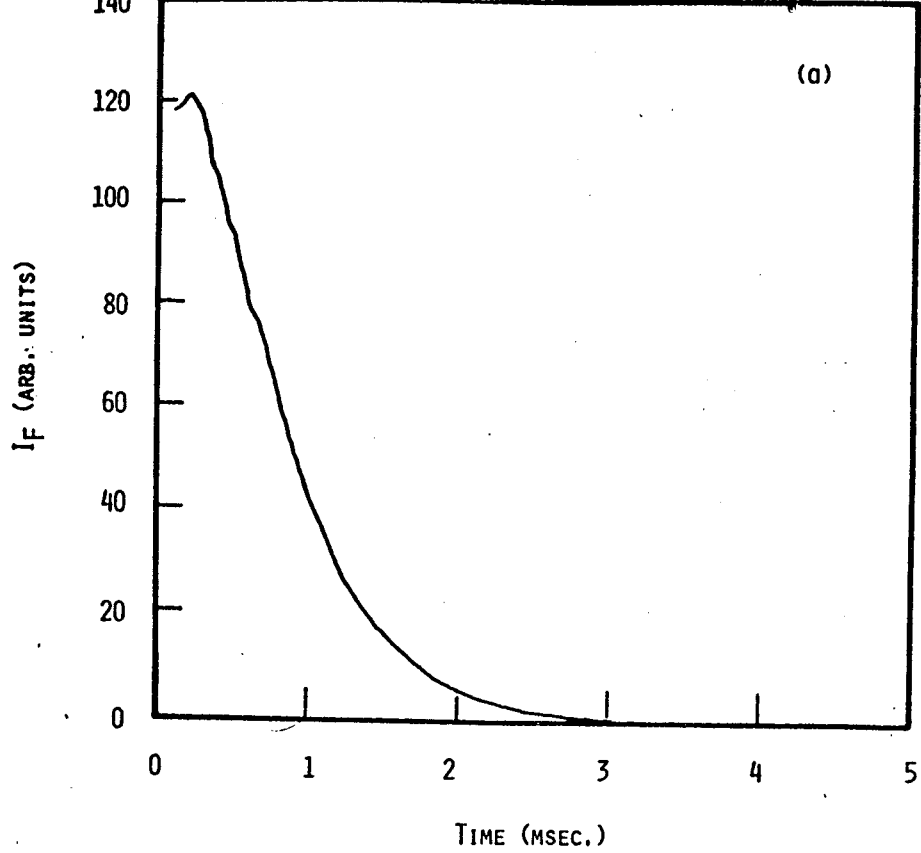
Figure **3.1**

Examples of the output of the XY recorder indicating the decay
of the time-resolved atomic emission (I_F) at λ = 457.1 nm
($Mg(3s3p(^3P_1))$ $\longrightarrow$ $Mg(3s^2(^1S_0))$ following pulsed dye laser excitation
of magnesium vapour to the 3^3P_1 state in the presence of helium.
(T = 800 K)

P_{He}(torr):   (a) 20;   (b) 50
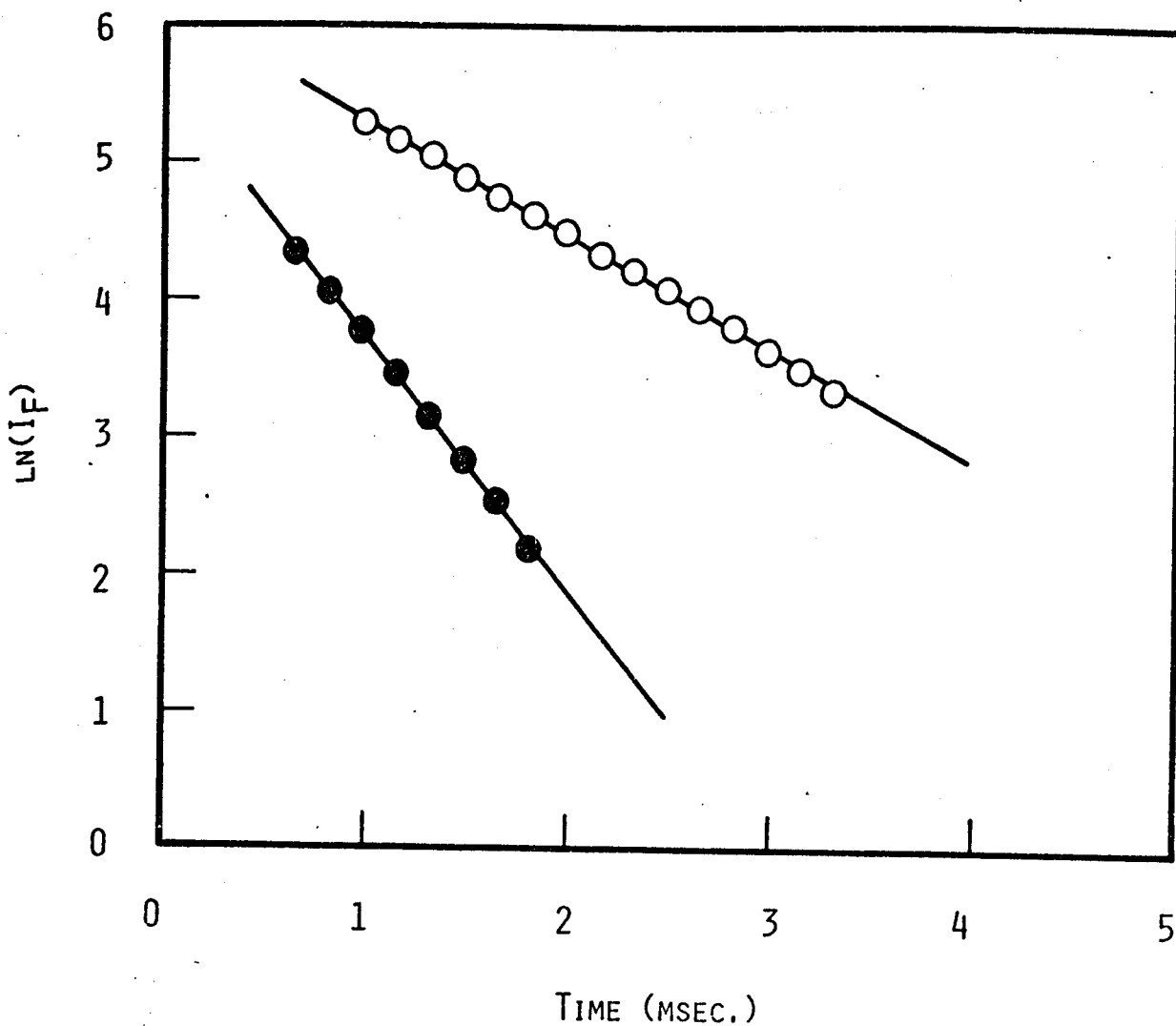
Figure 3.2

Examples of first-order kinetic plots for the decay of the time-resolved atomic emission $(\ln(I_F)$ vs. t) at $\lambda = 457.1$ nm $(Mg(3^3P_1) \longrightarrow Mg(3^1S_0))$ following pulsed dye laser excitation of magnesium vapour in the presence of helium. (T = 800 K).

p_{He}(torr): $\bigcirc$ 50; ⬤ 20
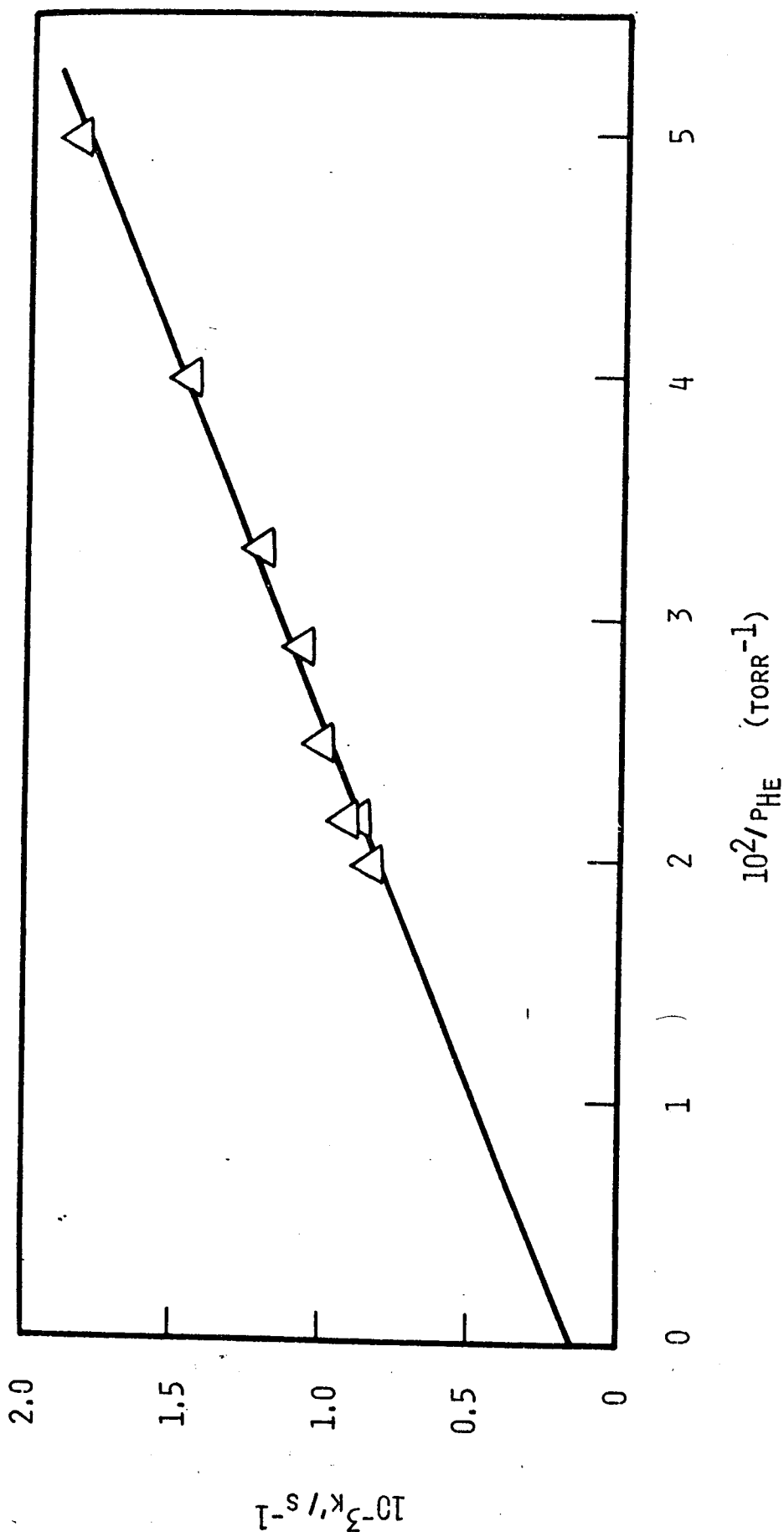
Figure **3.3**

Variation of the first-order rate coefficient (k') for the decay of $Mg(3^3P_J)$, following the generation of $Mg(3^3P_1)$ by pulsed dye laser excitation, with the reciprocal of the pressure of helium. (T = 800 K)

The vertical axis is labelled $10^{-3}k' / s^{-1}$ with values 0, 0.5, 1.0, 1.5, 2.0.

The horizontal axis is labelled $10^2/p_{HE}$ ($TORR^{-1}$) with values 0, 1, 2, 3, 4, 5.
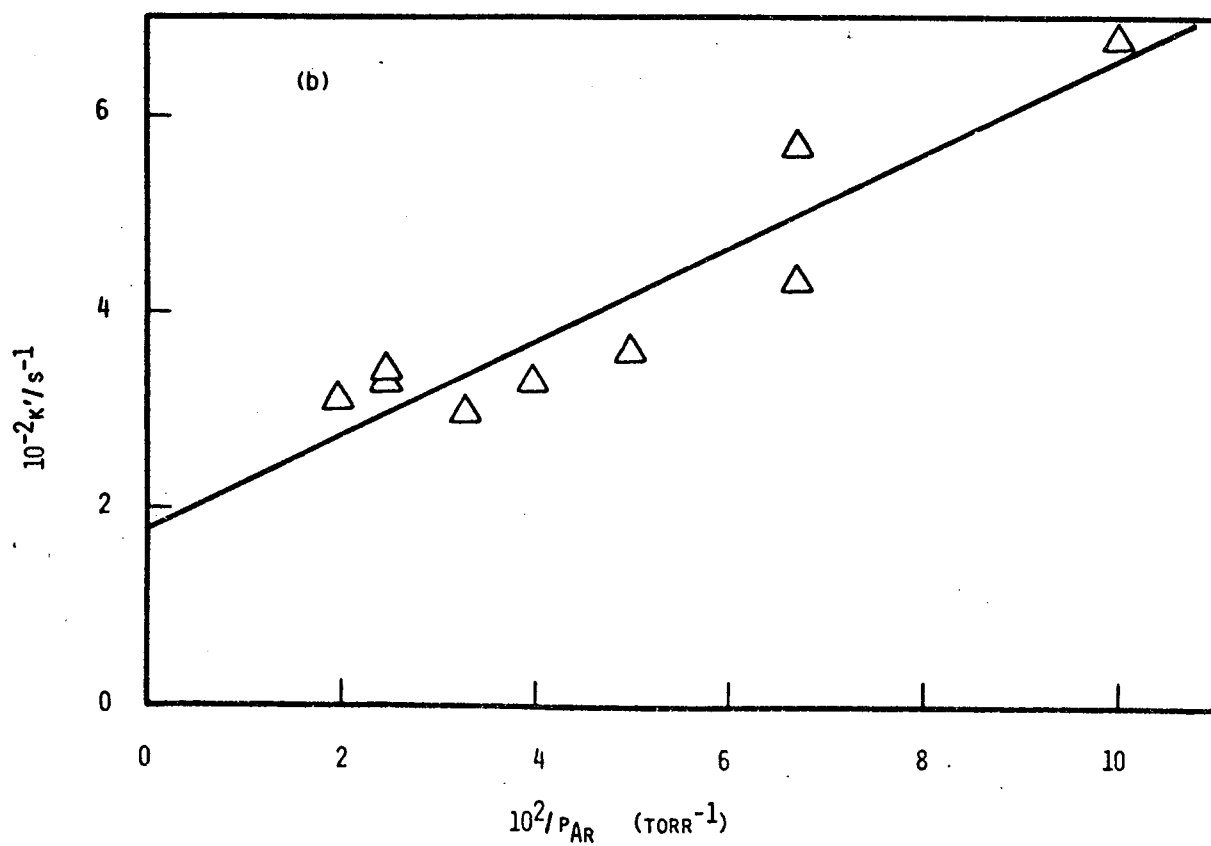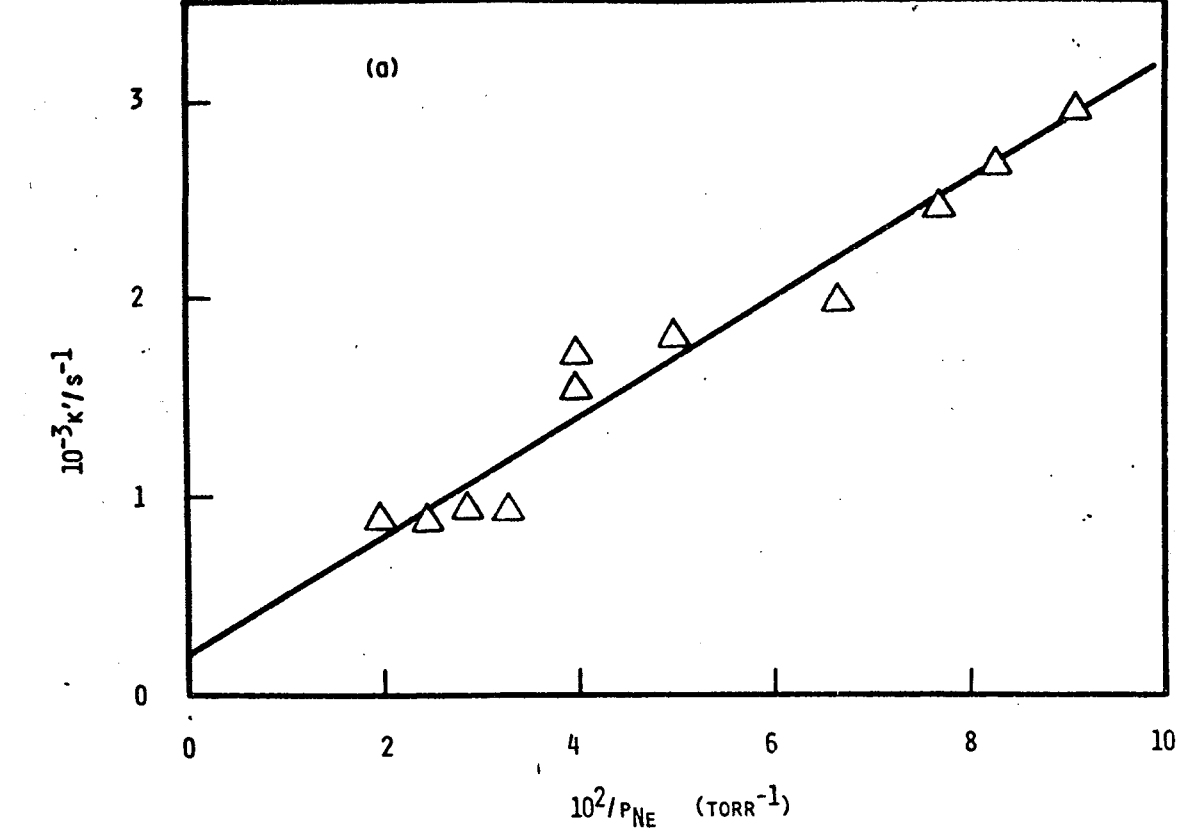
Figure **3.4**

Variation of the first-order rate coefficient (k') for the decay of Mg(3^3P_J),
following the generation of Mg(3^3P_1) by pulsed dye laser excitation,
with the reciprocal of the pressure of (a) neon and (b) argon.   (T = 800 K)
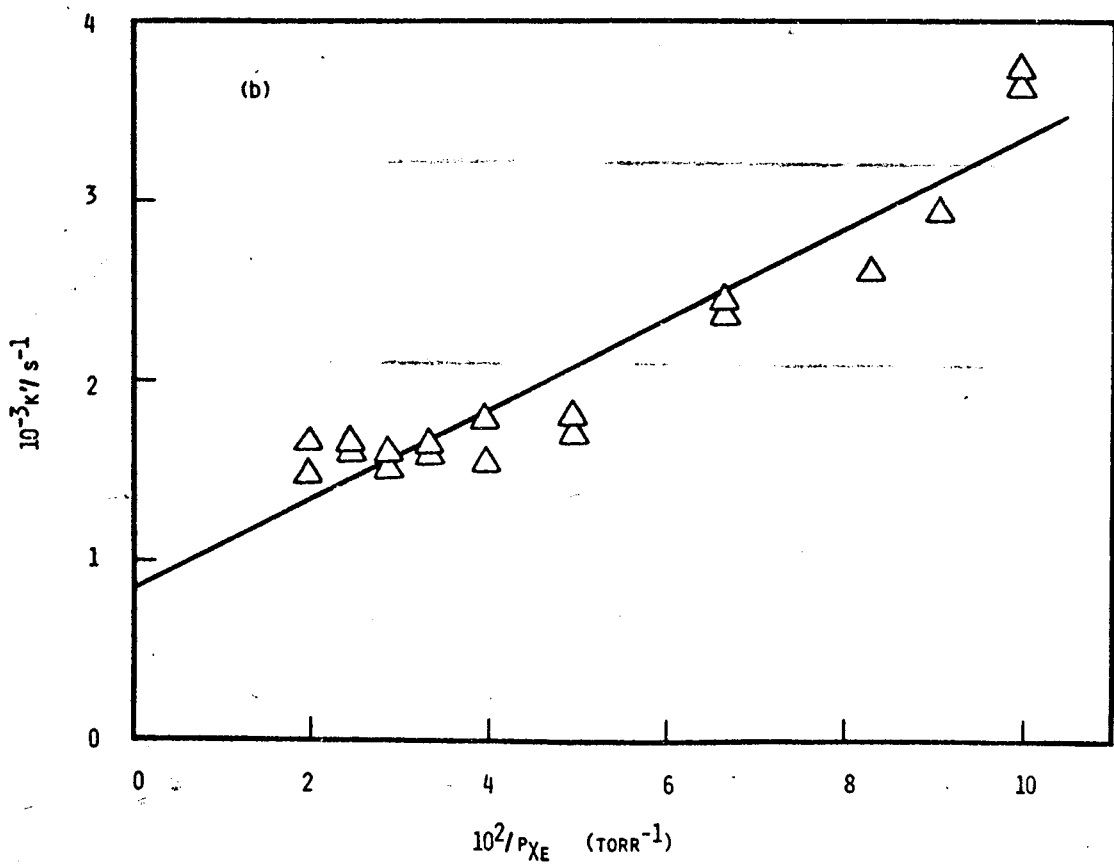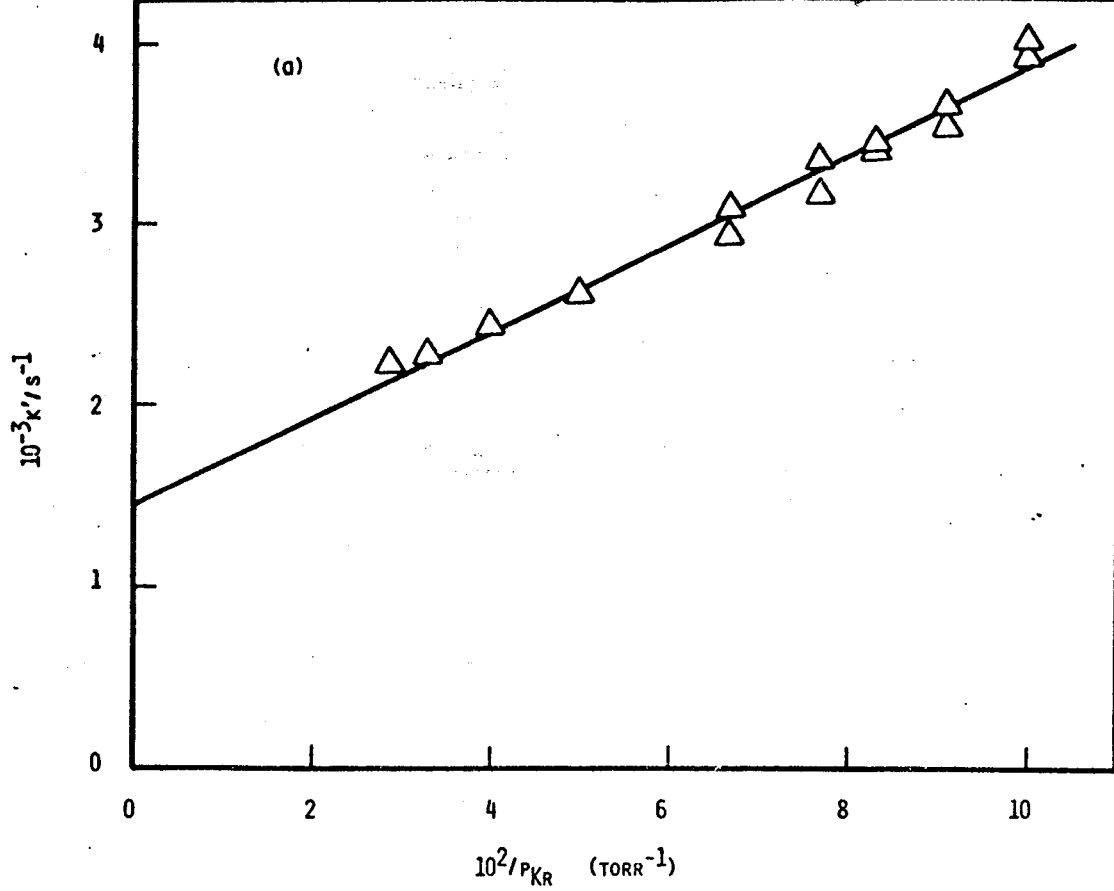
Figure 3.5

Variation of the first-order rate coefficient (k') for the decay of $Mg(3^3P_J)$, following the generation of $Mg(3^3P_1)$ by pulsed dye laser excitation, with the reciprocal of the pressure of (a) krypton and (b) xenon. (T = 800 K)

gases (ca. 10^{-5}, vide infra), this becomes kinetically significant at high pressures of the noble gases, the most observable effect of which is to yield intercepts at $1/p = 0$ for plots analogous to that of figure (3.3) which are too large in relation to k'_{em} [figure (3.5)]. For these two noble gases, the measurements of k' may be used to demonstrate consistency; (a) with the value of $\tau_e[Mg(3^3P_1)]$ derived from measurements on the lighter noble gases, (b) with sensible diffusional decay rates for $Mg(3^3P_J)$ in Kr and Xe and, (c) with collisional quenching efficiencies in accord with estimates reported hitherto for $Ca(4^3P_J)$[41] in the absence of the appropriate data for $Mg(3^3P_J)$. Thus, assuming a collisional quenching contribution by Kr and Xe, we may write the first-order decay coefficient for the decay of $Mg(3^3P_J)$ in those noble gases in the form;

$$k' = k'_{em} + \beta'/p + \alpha p \qquad (3.18)$$

in this case α represents the collisional quenching contributions by Kr and Xe. Hence;

$$(k' - k'_{em})/p = \alpha + \beta'/p^2 \qquad (3.19)$$

where k'_{em} is taken from the data derived for helium and α can be determined as the intercept of a plot $(k' - k'_{em})/p$ against $1/p^2$. Figure (3.6) shows the plots for the decay of $Mg(3^3P_1)$ in the form of equation (3.19) for krypton and xenon. The intercepts of the plots in figure (3.6) yield values of α(0.028 x 10^3 and 0.012 x 10^3 $s^{-1}Torr^{-1}$ for Kr and Xe, respectively) which may be used to estimate quenching data for these noble gases. In view of possible contributions by impurities, especially O_2, these data are presented as upper limits.

It may be readily shown that quenching of $Mg(3^3P_J)$ by krypton and xenon as indicated in the values of figure (3.6) is approximately ten times greater than that expected from the O_2 impurity levels, coupled with the previously reported quenching rate constants for that gas,[27] and substantiated in the present investigation (see later). Hence, it is found that $k_{Kr} \leq 2.3$ x 10^{-15} $cm^3molecule^{-1}s^{-1}$ and $k_{Xe} \leq 1.0$ X 10^{-15} $cm^3molecule^{-1}s^{-1}$ at 800 K. The only data with which these result may be compared are those reported by Malins and Benard[41] for $Ca(4^3P_J)$ at T = 923 - 1173 K. These authors report $k_{Kr} = 6.1$ x 10^{-15} $cm^3molecule^{-1}s^{-1}$ and $k_{Xe} = 6.7$ x 10^{-15} $cm^3molecule^{-1}s^{-1}$.
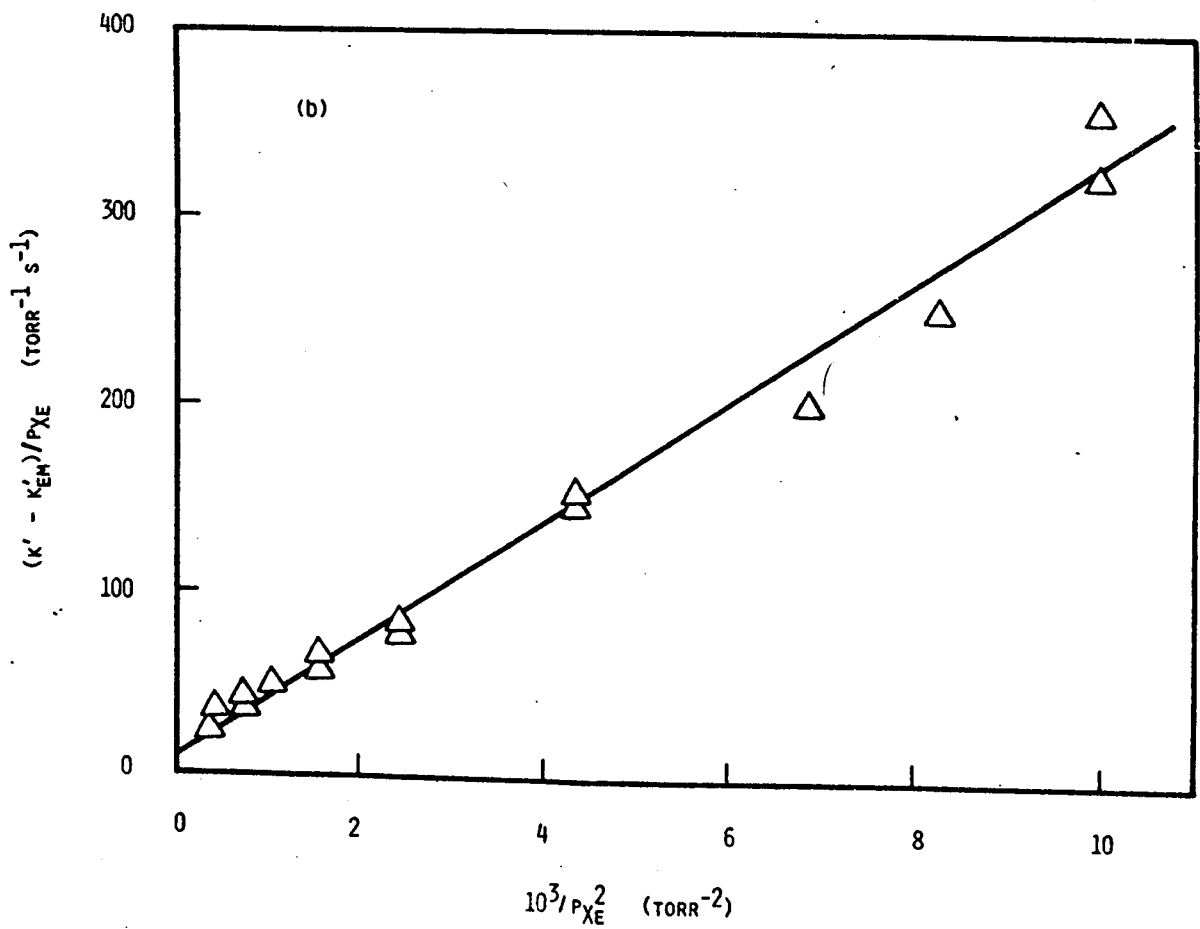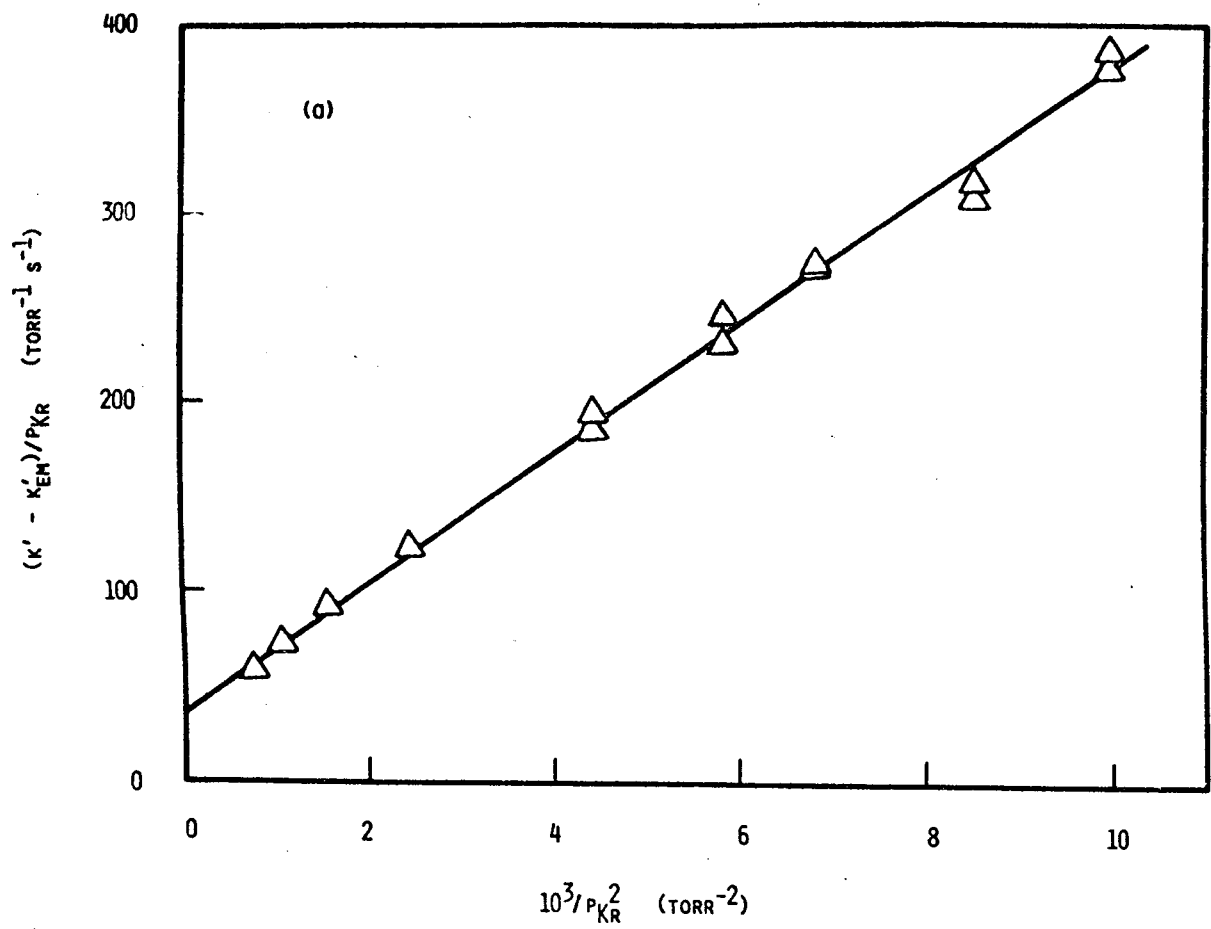
Figure 3.6

Plots of $(k' - k'_{em})/p$ versus $1/p^2$ for the first-order decay of $Mg(3^3P_J)$ in the presence of (a) krypton and (b) xenon. (T = 800 K)

The linearity in the slopes in figure (3.6) indicates the diffusional contribution via the term β'/p^2. This type of analysis is of general use and may be extended even to those cases where no quenching is expected by the noble gas. Thus, if we go back to the data for He, Ne and Ar, and plot $(k' - k'_{em})/p$ against $1/p^2$, the graphs showed in figure (3.7) will be obtained. These plots yield intercepts which pass through the origin within experimental error and which demonstrate no significant contribution to the removal of $Mg(3^3P_J)$ by collisional quenching.

Table (3.1) lists various values that have been obtained for the mean radiative lifetime of $Mg(3^3P_1)$ derived from both theory and experiment, including the results of the present investigation. Attention will be concentrated on measurements of τ_e derived from rate measurements on $Mg(3^3P_J)$ following pulsed dye-laser excitation.

TABLE 3.1

Mean Radiative Lifetime (τ_e) for $Mg(3^3P_1) \longrightarrow Mg(3^1S_0) + h\nu$

τ_e /ms	Reference
theory	
0.53	(23)
4.17	(22)
2.3	(60)
4.6	(21)
experiment	
5.3	(20)
4.0	(19)
1.9 ± 0.4	(64)
1.8 ± 0.2	(65)
2.2 ± 0.2	(13)
4.5 ± 0.5	(52)
3.8 ± 1.2	(72)
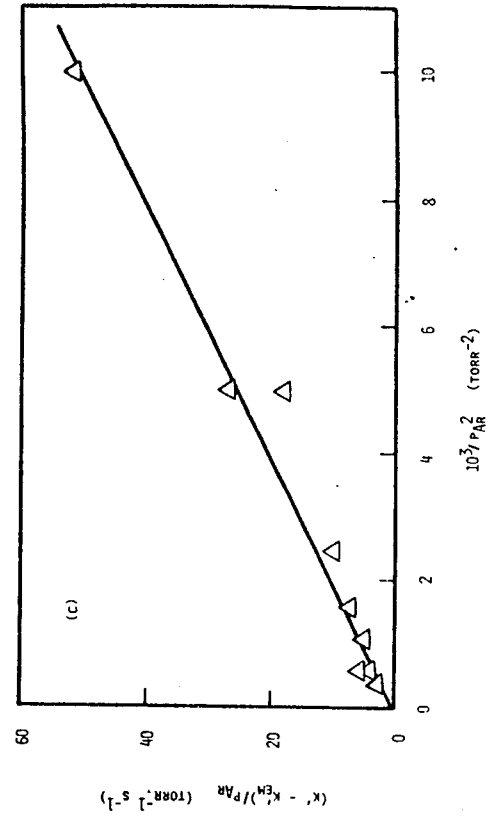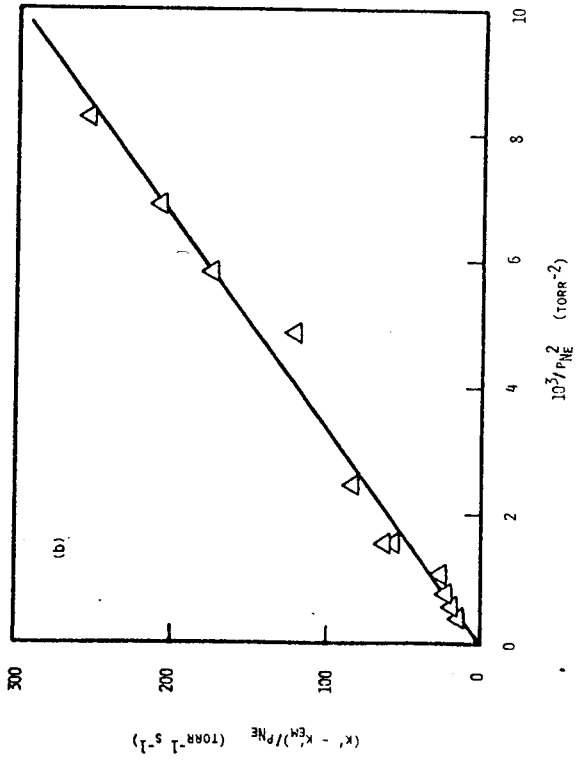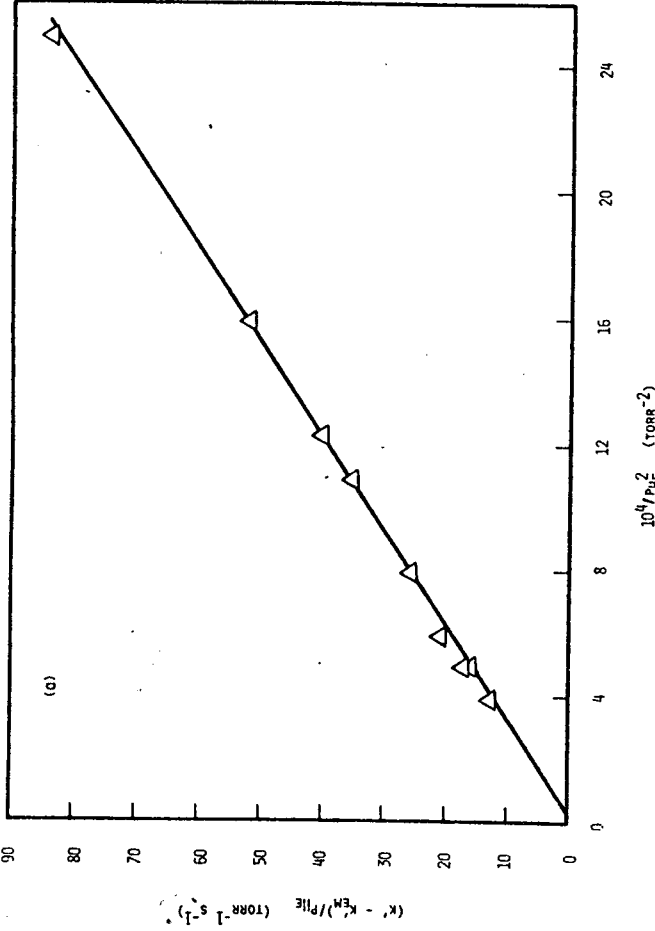
Figure 3.7

Plots of $(k' - k'_{em})/p$ versus $1/p^2$ for the first-order decay of $Mg(3^3P_J)$, in the presence of (a) helium, (b) neon and (c), argon. (T = 800 K)

TABLE 3.1 (continued)

τ_e /ms	Reference
2.1 ± 0.5	(this work), buffer gas He
1.6 ± 1.0	Ne
1.9 ± 0.4	Ar
(2.1 ± 0.5)	Kr
(2.1 ± 0.5)	Xe

We have seen that equation (3.12) clearly indicates that the measurement of $\tau_e[Mg(3^3P_1) \rightarrow Mg(3^1S_0) + h\nu]$ through determinations of the decay rates of the excited magnesium atom in fundamentally linked with measurements of β for diffusion and with those of collisional quenching, $k_Q[Q]$, where appropriate.

The initial measurements of Wright et al,[13] following dye-laser excitation simply considered the overall decay of $Mg(3^3P_J)$ in a buffer gas of neon in the range 50 - 400 Torr as due solely to removal by spontaneous emission of the excited atom with no contributions due to diffusion or to quenching by impurities. This yielded $\tau_e = 2.2 \pm 0.2$ ms[13] (see table 3.1). Later measurements of a similar nature[52] yielded $\tau_e = 4.5 \pm 0.5$ ms [table (3.1)] derived from the extrapolated value of the decay coefficient for the $Mg(3^3P_1)$ at infinite noble gas pressure. However, a linear plot of k' against $1/p$ was not constructed and hence, no systematic variation of the diffusion rate for $Mg(3^3P_J)$ in the noble gas was used to establish internal kinetic consistency for the various decays. The particular importance of quantifying the diffusional rate in the present type of investigation must be stressed, if k'_{em} is to be determined by extrapolation of k' to infinite pressure, as the error in the slope for a plot constructed on the basis of equation (3.12) is reflected and magnified in the error in the intercept. The present results for τ_e have been derived from the decay measurements on $Mg(3^3P_J)$ for a wide range of pressures in all the noble gases and with quantitative recognition of the diffusional removal of the excited atom, supporting the lower value of τ_e which is reported as $\tau_e = 2.1 \pm 0.5$ ms.

3.2 Diffusion of $Mg(3^3P_J)$ in noble gases

In the previous section, it has been clearly demonstrated that the decay of $Mg(3^3P_J)$ occurs as a result of three separate processes; spontaneous emission, diffusion and collisional quenching. Having examined the spontaneous emission and the associated mean radiative lifetime, attention may now be focussed on the diffusion component.

Whilst the diffusional removal of $Mg(3^3P_J)$ in the noble gases is clearly established, detailed measurements of the diffusion coefficients are prevented by the absence of information on the boundary conditions commensurate with the effective geometry of the reaction vessel. This is a particularly restrictive consideration in the present circumstances, as β is related to the reciprocal of the square of the appropriate geometrical dimensions, as seen through the long-time solution of the diffusion equation,[62,63] and where β will be sensitively influenced by the monochromator slit height and width. In fact, what is being considered in this particular geometry is the diffusion of the excited species out of the reaction zone determined by the laser beam and by the light-gathering power of the detection system. These factors must be kept as constant as possible, within the experimental limitations, in order that the relative diffusion coefficients may be compared. This may be contrasted where diffusional decay is determined by a geometry close to that of the cell itself if the emitted light at $\lambda = 457.1$ nm were collected through a large interference filter or if the $Mg(3^3P_1)$ were sampled through the whole reaction vessel by atomic resonance absorption spectroscopy, even if the light is finally focused into a monochromator slit. Thus, the present measurements may be used only to estimate relative values of the diffusion coefficients. The relative values of the diffusion coefficients obtained in the present investigation are shown in table (3.2). The values have been calculated from the slopes of plots in the form of equation (3.17) and (3.19), the value for He being taken as unity.

TABLE 3.2

Relative values of the diffusion coefficient, D_{12}, for $Mg(3^3P_J)$ in the noble gases.

Noble gas	D_{12} (relative)
He	1.00
Ne	0.90
Ar	0.32
Kr	1.04
Xe	0.96

The data for most of the noble gases yield diffusion coefficients of similar relative magnitudes, with the exception of that of argon. It is difficult to ascribe serious experimental limitations to the kinetic measurements themselves for this particular noble gas as the decay rates in argon are consistent with the correct value for $\tau_e[Mg(3^3P_1)]$ as derived from measurements in the other noble gases, and with the quenching rate datum for $Mg(3^3P_J)$ by O_2 (see later). In general, the diffusional removal of $Mg(3^3P_J)$ in the noble gases is clearly established and this constitutes an important component of the kinetic measurements from which there is extracted the mean radiative lifetime of $Mg(3^3P_1)$ via the measured Einstein coefficient for spontaneous emission.

We may finally consider quenching of $Mg(3^3P_J)$ by impurities within the context of diffusion. At high pressures of the noble gases (near $1/p = 0$), when the diffusional component is relatively small, quenching by low levels of gases characterised by high collisional efficiencies, (e.g. O_2[27]) becomes significant. The direct application of a plot of the type given in figure (3.3) for a sample of argon containing O_2 at 50 ± 10 ppm, implicitly neglecting the growth of the term $k_{O_2}[O_2](k_Q[Q])$ with p_{Ar}, yields an intercept and hence a value of k'_{em} which is too large, as expected [figure (3.8)]. However, plots in the form of equation (3.20) may be used to study quenching of $Mg(3^3P_J)$ by added gases. Normally, collisional quenching constants in pulsed experiments of this type are determined by measurement of the variation of k' with quenching gas concentration and at constant total pressure and hence with a constant
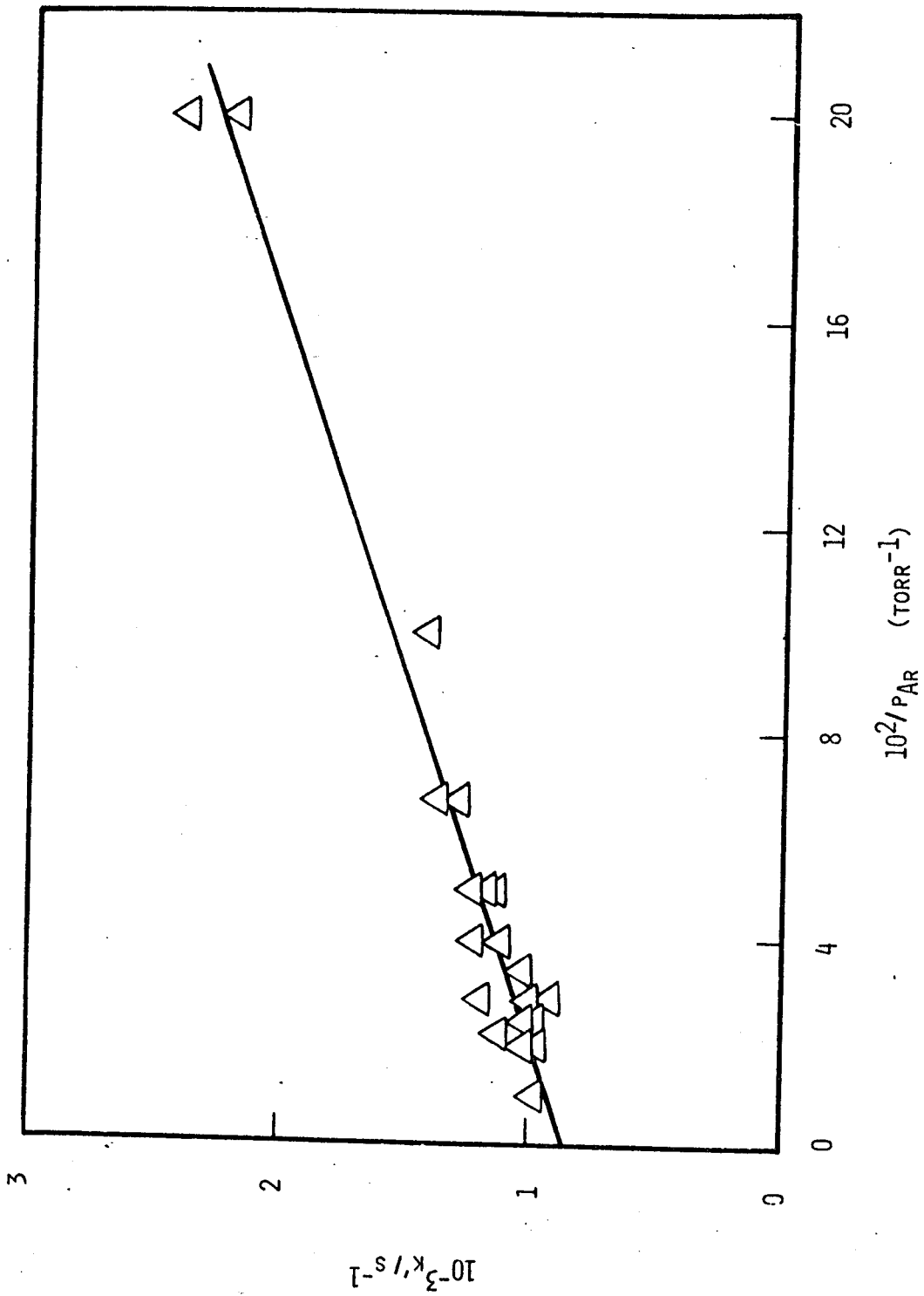
Figure **3.8**

Variation of the first-order rate coefficient (k′) for the decay of Mg(3^3P_J), following the generation of Mg(3^3P_1) by pulsed dye laser excitation, with the reciprocal of the pressure of argon containing molecular oxygen as a trace impurity (50 $\pm$ 10 ppm).   (T = 800 K)

contribution to removal by diffusion. This procedure will be employed and described in the following section. On the other hand, quenching rate constants may be determined using the variation of k' derived from decay measurements on different total pressures of a quenching-gas + buffer-gas mixture of defined relative composition (i.e. defined impurity level of O_2), provided the diffusional component is clearly recognised quantitatively. This is implicit in the use of equation (3.19). The resulting plot for the O_2 mixture is shown in figure (3.9). The intercept of this plot (0.02 ± 0.0002 x 10^3 $s^{-1}Torr^{-1}$), coupled with the O_2 analysis, [1] yields $k[Mg(3^3P_J) + O_2] = 3.3 \pm 0.8$ x 10^{-11} $cm^3molecule^{-1}s^{-1}$ (800 K). This can be compared with the result of Taieb and Broida[27] of $k[Mg(^3P_J) + O_2] = 3.0$ x 10^{-11} $cm^3molecule^{-1}s^{-1}$ (room temperature).

3.3 Collisional quenching of $Mg(3^3P_J)$

The experimental arrangement described in the previous sections has been applied to the study of the collisional quenching of $Mg(3^3P_J)$ by monitoring the decay of the time-resolved emission, (I_F) $(\lambda = 457.1$ nm), in the presence of varying low pressures of an added quenching gas, Q, and at a fixed total pressure. Hence, the first-order contribution to k' from spontaneous emission and from diffusion becomes constant in a series of experiments in which [Q] is varied by means of the flow system and thus, equation (3.19) becomes;

$$k' = K + k_Q[Q] \qquad (3.20)$$

where k_Q is the absolute second-order rate constant for collisional quenching by the added gas. Figure (3.10) shows examples of the logarithmic variation of I_F as a function of time for a series of experiments in which $[N_2]$ is varied at a fixed constant total pressure. In the present experiments the total pressure, i.e., the pressure of buffer-gas plus the quenching-gas, was kept at 30 Torr. The total pressure in the line is determined by the flow for a fixed opening of the exit needle valve (see earlier). The variation of the slopes of these plots.
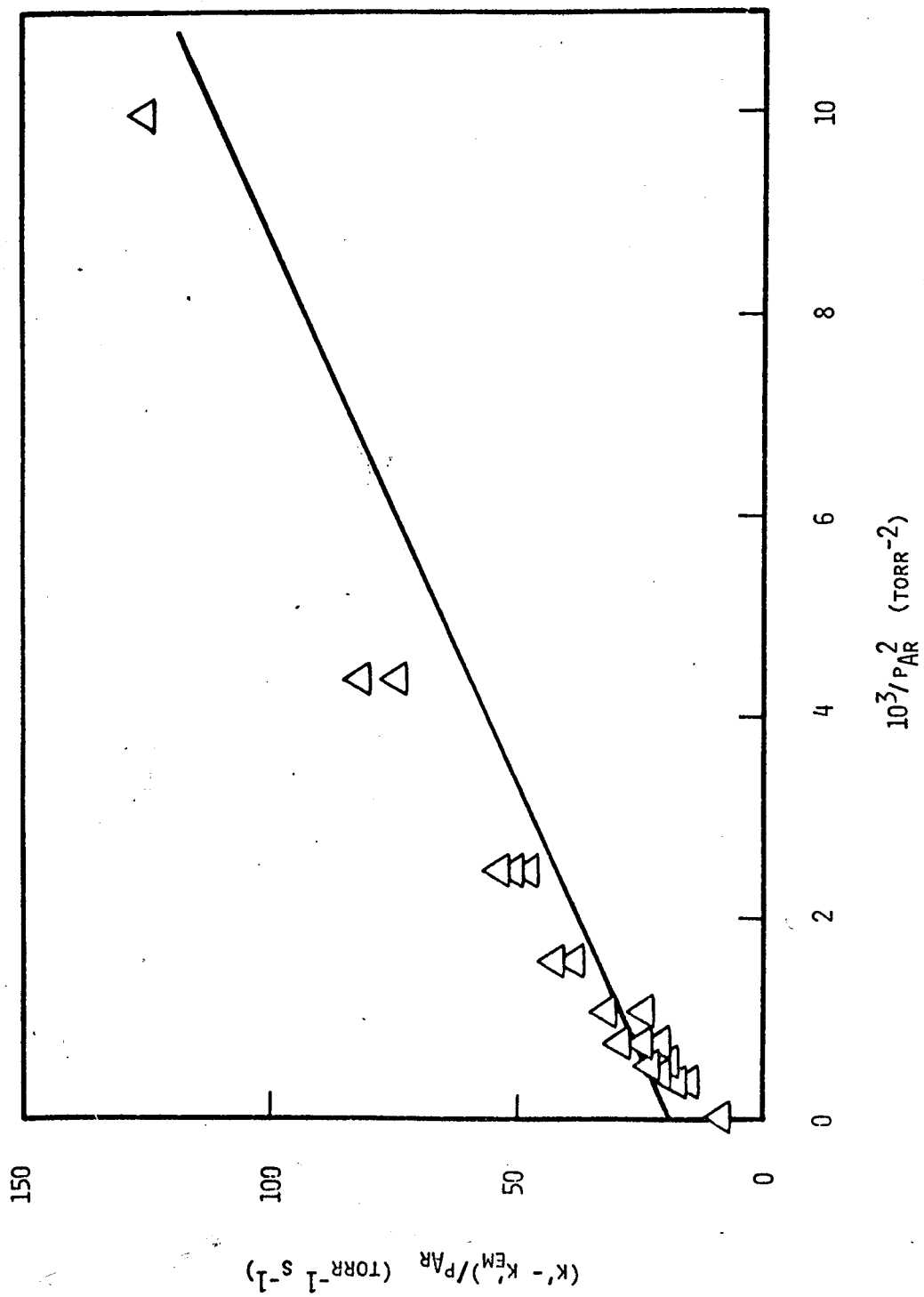
Figure **3.9**

Plot of $(k' - k'_{em})/p$ versus $1/p^2$ for the first-order decay of $Mg(3^3P_J)$, in the presence of argon containing molecular oxygen as a trace impurity $(50 \pm 10 \text{ ppm})$. $(T = 800 \text{ K})$
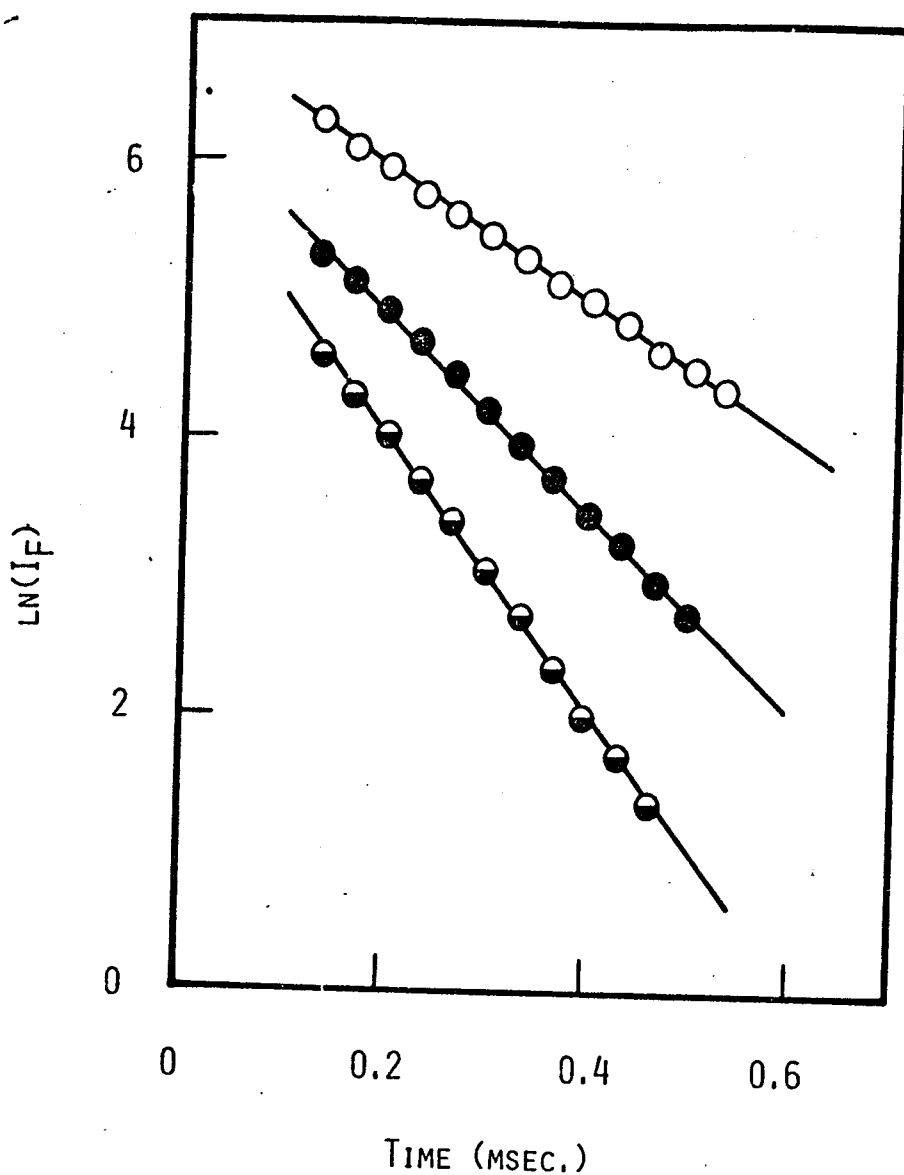
Figure **3.10**

Examples of pseudo first-order kinetic plots for the decay of $Mg(3^3P_J)$, derived from the time-resolved atomic emission ($\ln(I_F)$ vs. t) at $\lambda = 457.1$ nm $(Mg(3^3P_1) \longrightarrow Mg(3^1S_0))$ following the pulsed dye laser excitation of magnesium vapour in the presence of molecular nitrogen and helium buffer gas. (P_{total} with He $= 30$ torr, $T = 800$ K)

$10^{-16}[N_2]$/molecules cm^{-3}: $\bigcirc$ 0.72;   ● 1.27;   ● 1.81

(-k') with $[N_2]$ is shown in figure (3.11) for the series of measurements investigated here, together with a similar plot for CO as the quenching gas. Similar plots were obtained for the variation of k' with $[H_2]$ and $[CH_4]$ as presented in figure (3.12). Pressures of quenching gases were employed such that the helium buffer gas remained in sufficient excess to avoid significant departures from the He flow calibrations constructed for this noble gas. The excess of buffer gas is also important to prevent a temperature increase within the excitation zone.

This study of the absolute second-order rate constants for $Mg(3^3P_J)$ has been further extended to a range of added gases. Quenching by deuterium, as we shall see, demonstrates a considerable isotopic effect. Linear molecules with 18-electrons closed shell structures, like N_2O and CO_2 have been also investigated and the results are discussed later. The result obtained for CH_4 is compared with the one for another spherical molecule, CF_4, and finally a number of unsaturated hydrocarbons, namely, C_2H_2, C_2H_4 and C_6H_6 have been investigated.

Plots of k' against [Q] for the species above mentioned are shown in figures (3.13), (3.14), (3.15) and (3.16), the slopes of which give the second-order quenching constants listed in table (3.3).

TABLE 3.3

Absolute second-order rate constants (k_Q, $cm^3 molecule^{-1}s^{-1}$) for the collisional quenching of $Mg(3^3P_J)$ by added quenching gases, Q.

Q	k_Q	
H_2	$7.3 \pm 0.6 \times 10^{-13}$	(800 K)[a]
	6.7×10^{-13}	(800 K, calc.)[b]
	$9.1 \pm 1.0 \times 10^{-13}$	(873 K)[c]
	$1.1 \pm 0.5 \times 10^{-13}$	(room temp.)[d]
	$9.5 \pm 4.2 \times 10^{-13}$	(800 K, calc.)[e]
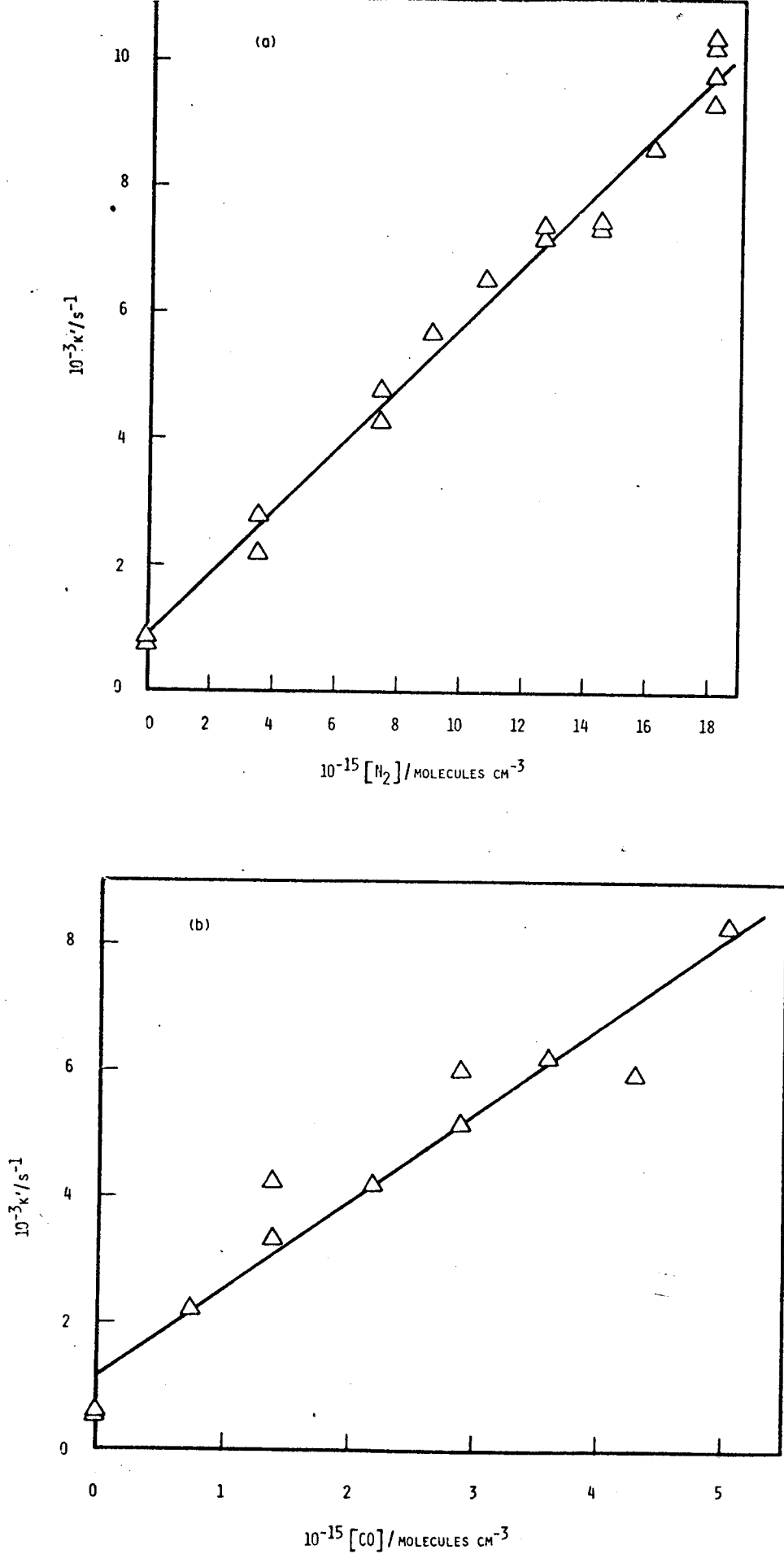
Figure **3.11**

Variation of the pseudo first-order rate coefficient (k')
for the decay of Mg(3^3P_J) in the presence of (a) N_2 and (b) CO.
(P_{total} with He = 30 torr,   T = 800 K)
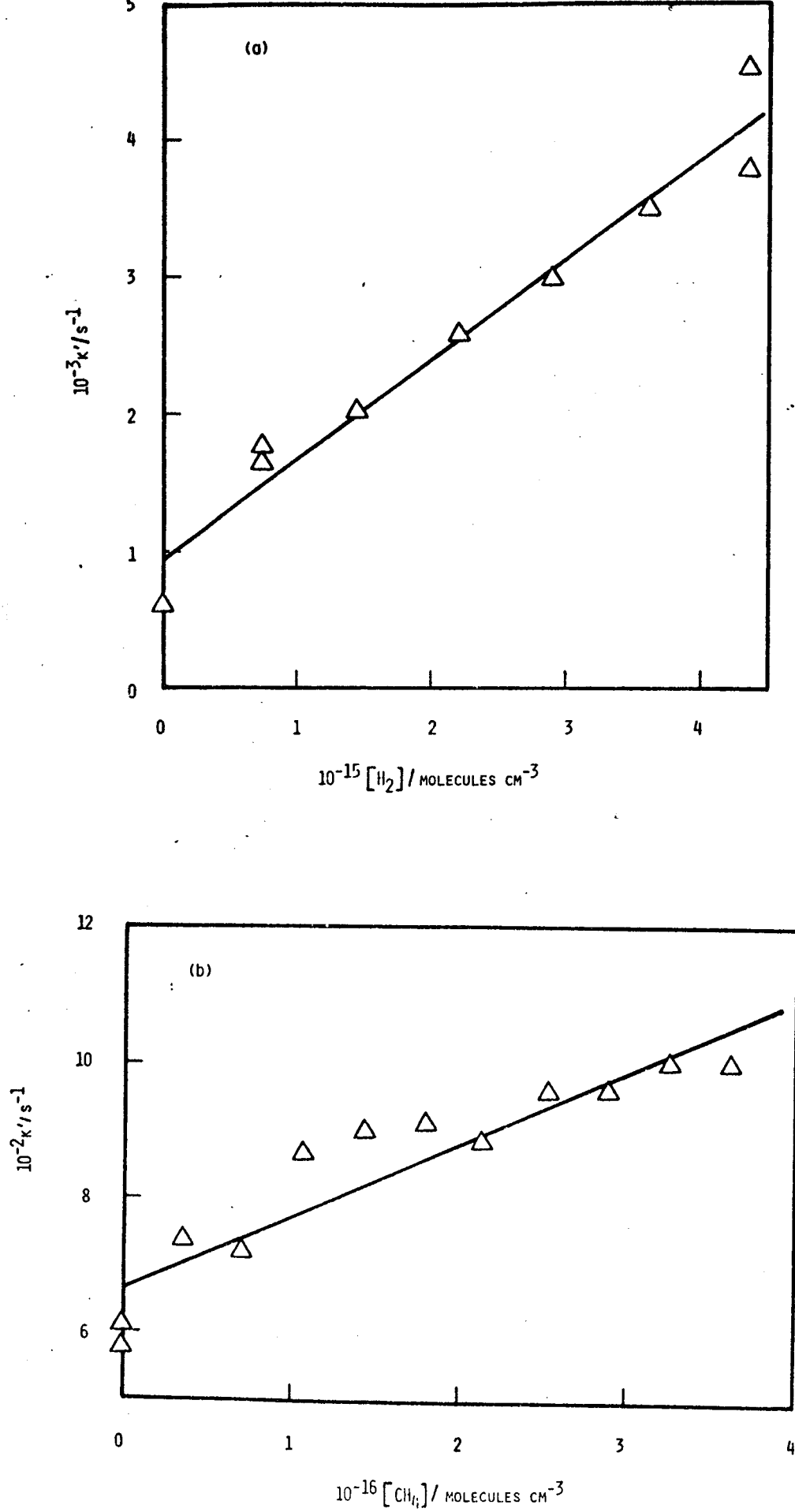
Figure 3.12

Variation of the pseudo first-order rate coefficient (k')
for the decay of Mg(3^3P_J) in the presence of (a) H_2 and (b) CH_4.
(p_{total} with He = 30 torr,   T = 800 K)
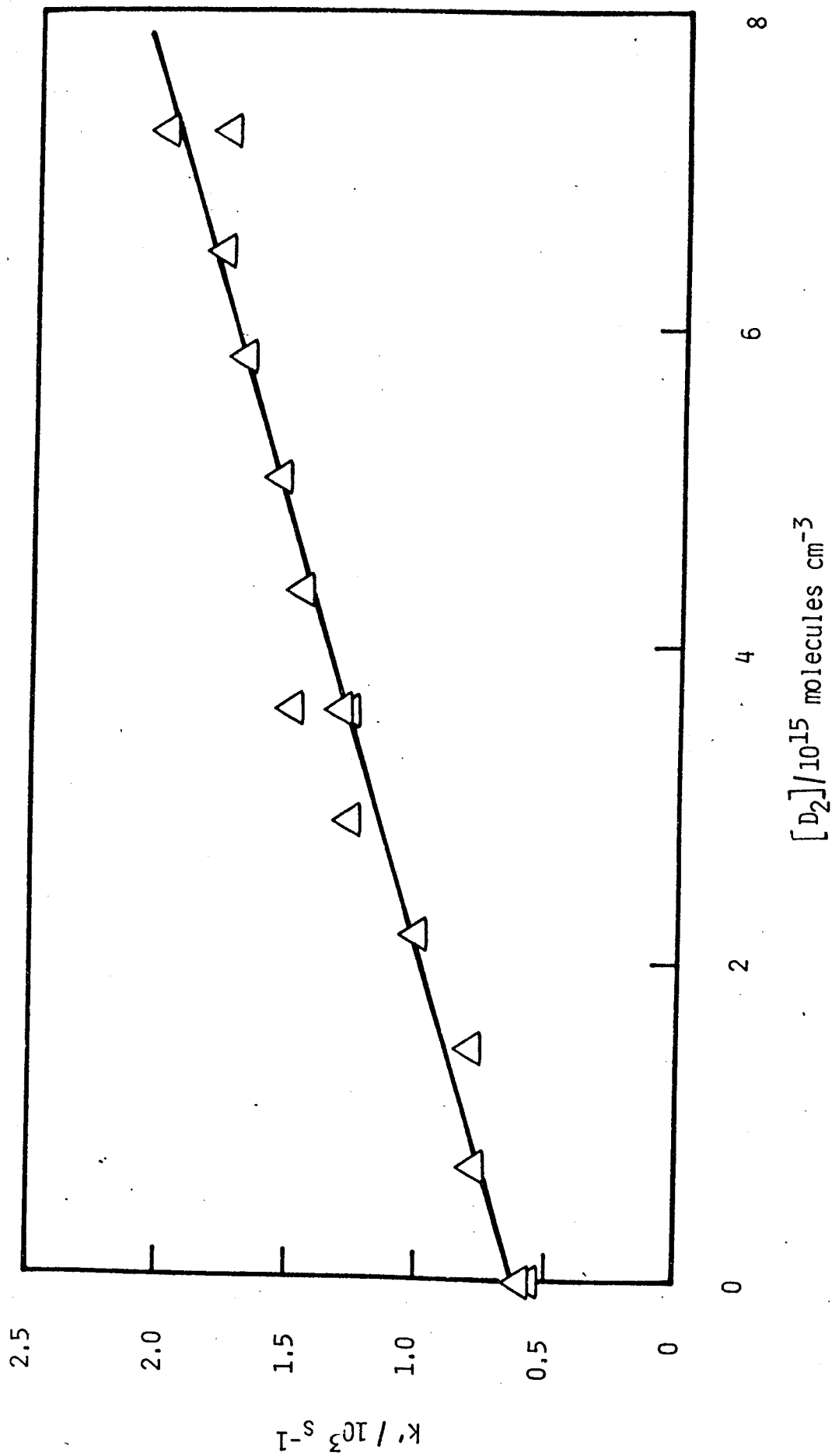
Figure **3.13**

Variation of the pseudo first-order rate coefficient (k') for the decay of $Mg(3^3P_J)$ in the presence of D_2. (p_{total} with He = 30 torr, T = 800 K).

Y-axis: $k' / 10^3 \ s^{-1}$

X-axis: $[D_2]/10^{15}$ molecules cm^{-3}

(a)

(b)
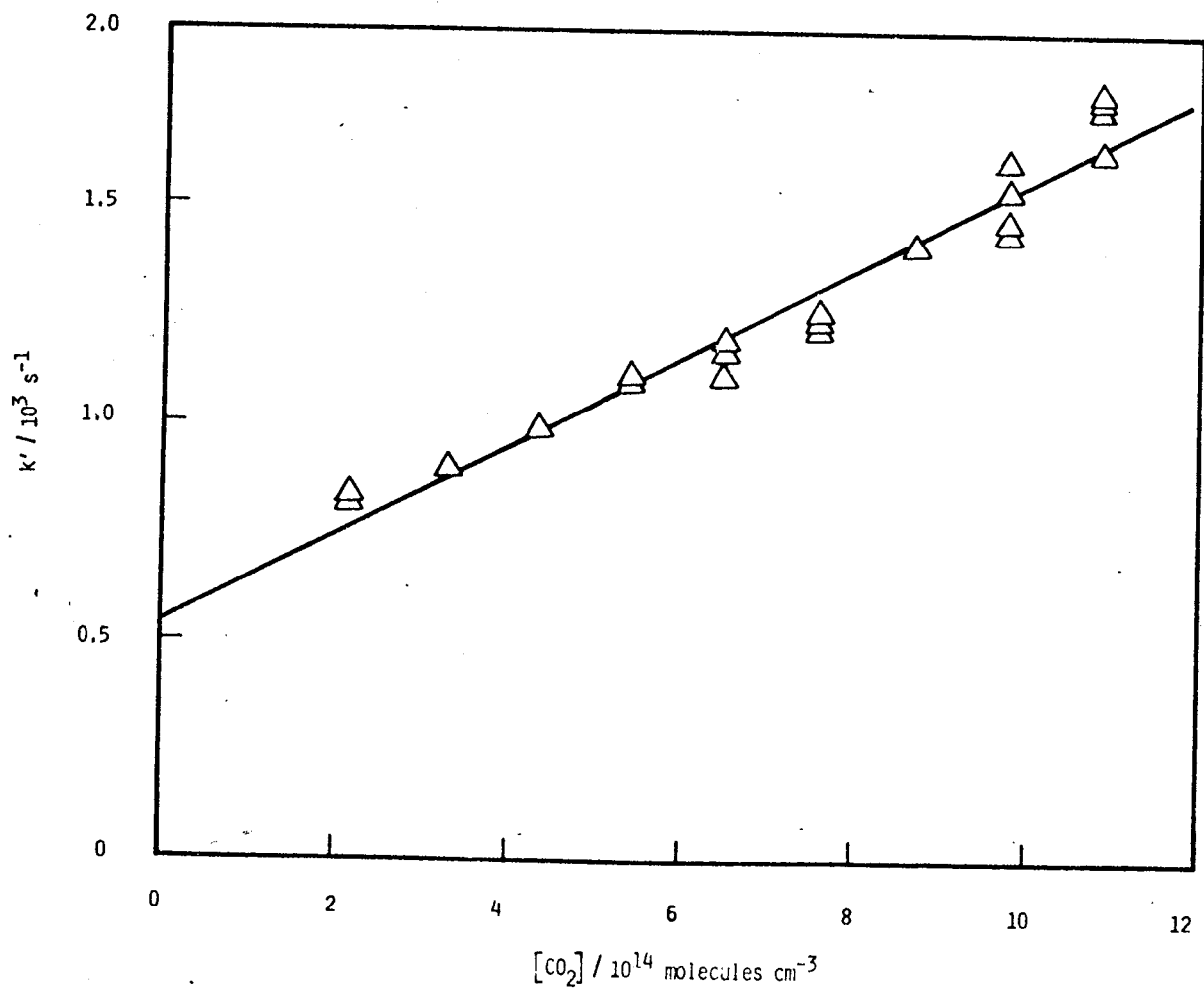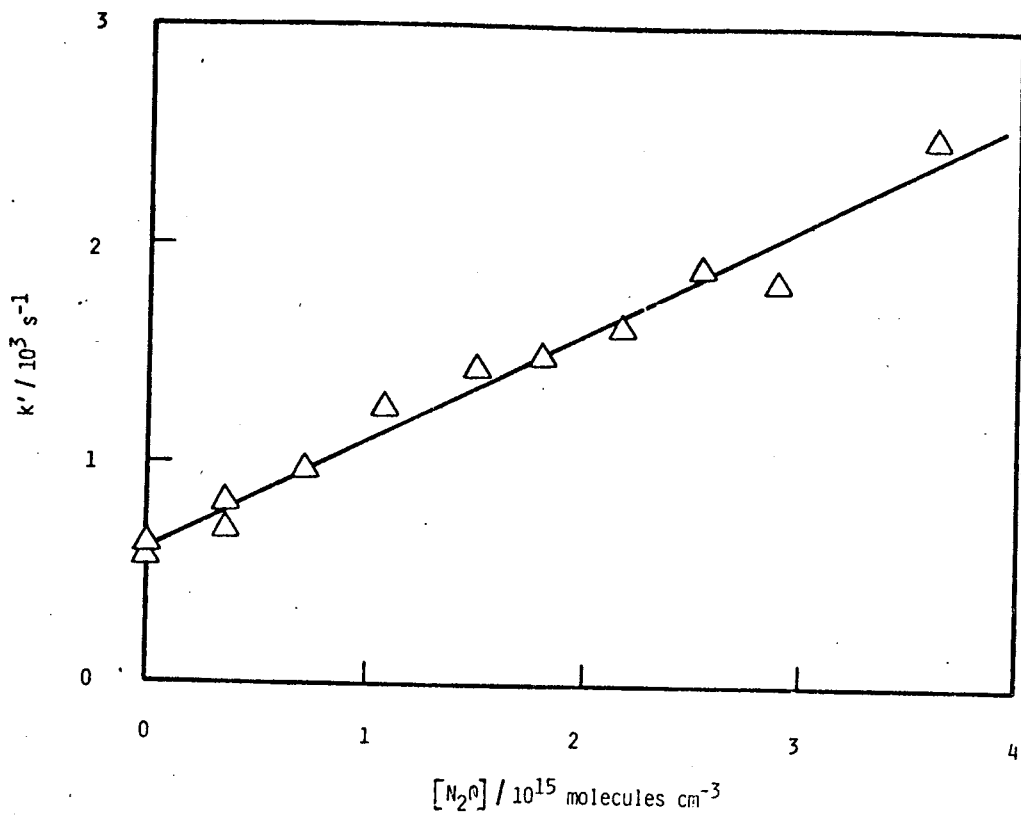
Figure **3.14**

Variation of the pseudo first-order rate coefficient (k') for the decay of $Mg(3^3P_J)$ in the presence of (a) N_2O and (b) CO_2. (P_{total} with He = 30 torr, T = 800 K)

(a)

(b)
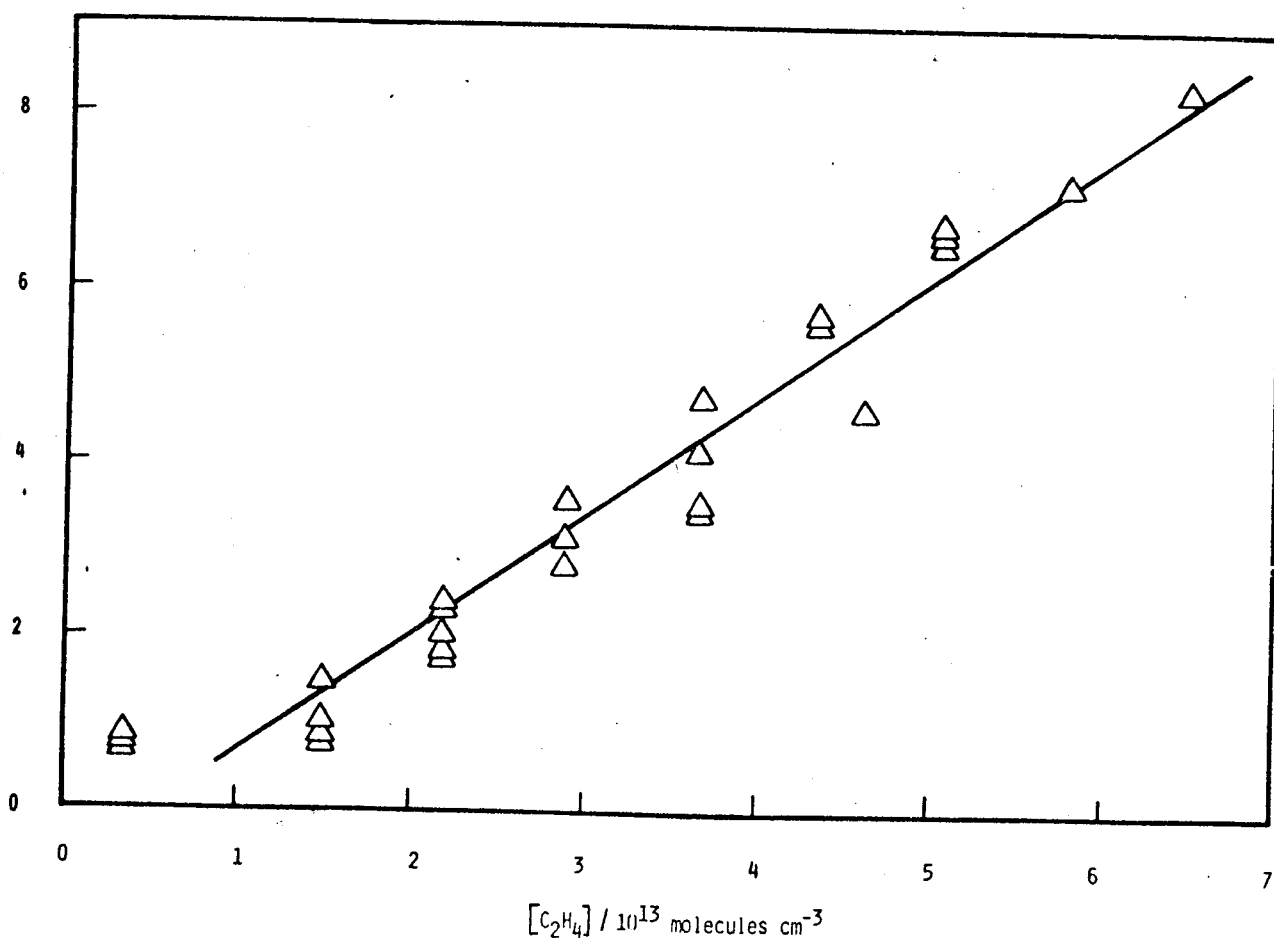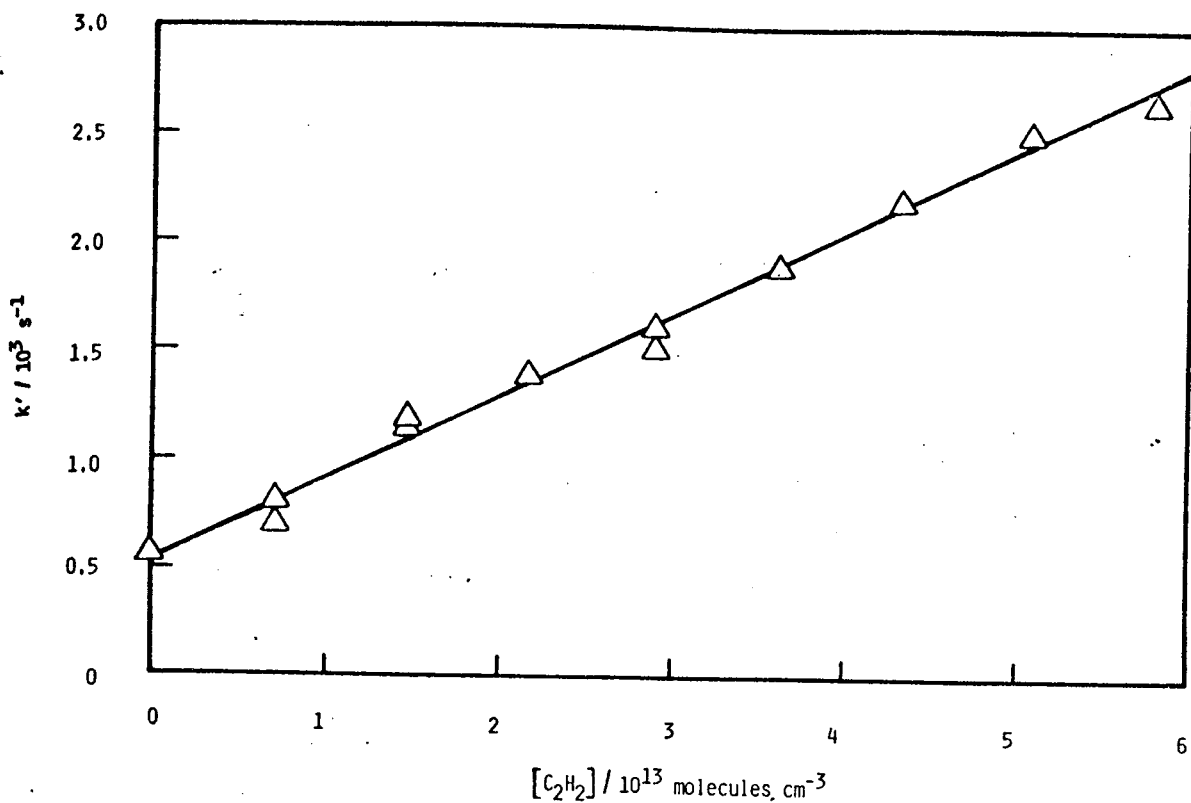
Figure **3.15**

Variation of the pseudo first-order rate coefficient (k') for the decay of Mg(3³P_J) in the presence of (a) C_2H_2 and (b) C_2H_4. (P_{total} with He = 30 torr, T = 800 K).

(a)

(b)
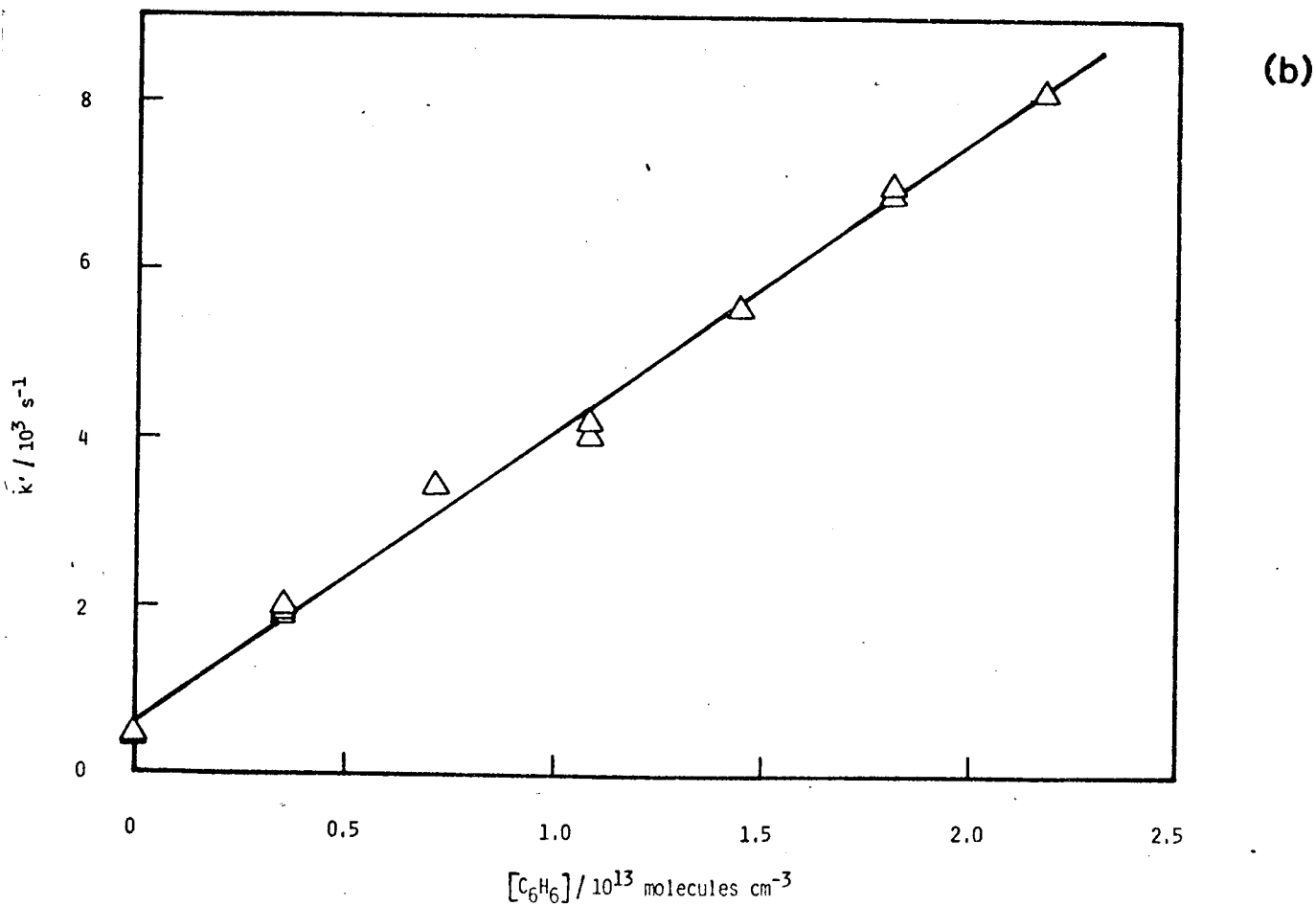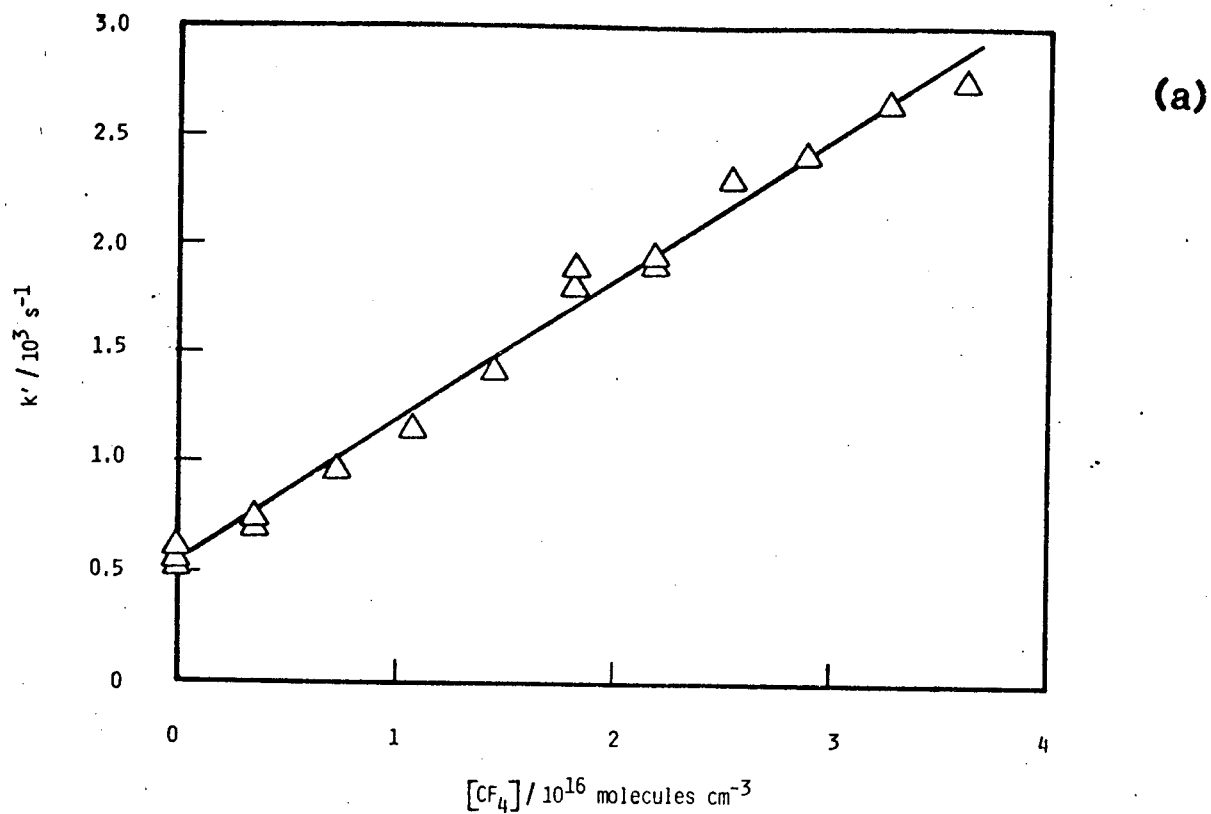
Figure **3.16**

Variation of the pseudo first-order rate coefficient (k') for the decay of Mg(3^3P_J) in the presence of (a) CF_4 and (b) C_6H_6. (P_{total} with He = 30 torr, T = 800 K)

TABLE 3.3 (continued)

Q	k_Q	
D_2	$1.9 \pm 0.1 \times 10^{-13}$	(800 K)[a]
	$3.5 \pm 1.7 \times 10^{-13}$	(800 K, calc.)[e]
N_2	$4.9 \pm 0.2 \times 10^{-13}$	(800 K)[a]
	$4.2 \pm 0.2 \times 10^{-13}$	(873 K)[c]
	$7.1 \pm 3.3 \times 10^{-13}$	(room temp.)[d]
O_2	$3.3 \pm 0.8 \times 10^{-11}$	(800 K)[a]
	$3.0 \pm 0.8 \times 10^{-11}$	(room temp.)[d]
CO	$1.4 \pm 0.1 \times 10^{-12}$	(800 K)[a]
	$1.0 \pm 0.1 \times 10^{-12}$	(873 K)[c]
	$2.0 \pm 0.7 \times 10^{-12}$	(room temp.)[d]
CO_2	$1.0 \pm 0.1 \times 10^{-12}$	(800 K)[a]
	1.20×10^{-11}	(room temp.)[d]
N_2O	$4.9 \pm 0.3 \times 10^{-13}$	(800 K)[a]
	2.45×10^{-11}	(room temp.)[d]
	$2.2 \pm 0.5 \times 10^{-12}$	(300 K)[f]
	2.1×10^{-10}	(900 K)[g]
CH_4	$1.1 \pm 0.2 \times 10^{-14}$	(800 K)[a]
	$2.8 \pm 0.1 \times 10^{-14}$	(873 K)[c]
CF_4	$6.5 \pm 0.2 \times 10^{-14}$	(800 K)[a]
C_2H_2	$3.8 \pm 0.2 \times 10^{-11}$	(800 K)[a]
	$3.0 \pm 1.7 \times 10^{-11}$	(room temp.)[d]
C_2H_4	$1.4 \pm 0.1 \times 10^{-10}$	(800 K)[a]
	$3.4 \pm 0.4 \times 10^{-11}$	(873 K)[c]
C_6H_6	$3.5 \pm 0.1 \times 10^{-10}$	(800 K)[a]
	$1.1 \pm 0.2 \times 10^{-10}$	(873 K)[c]
Kr	$\le 2.3 \times 10^{-15}$	(800 K)[a]
Xe	$\le 1.0 \times 10^{-15}$	(800 K)[a]

Notes to table (3.3)

(a) Dye-laser excitation + time-resolved forbidden emission (this work)

(b) Dye-laser excitation + time-resolved forbidden emission
    (single-shot mode, ref. 30)

(c) Dye-laser excitation + time-resolved atomic resonance
    absorption (ref. 25)

(d) Discharge flow + forbidden emission (ref. 27)

(e) Dye-laser excitation + time-resolved forbidden emission
    (single-shot mode, ref. 32)

(f) Discharge flow + forbidden emission (ref. 37)

(g) Chemiluminescence + single collision conditions (ref. 67)

Comparison of these results are made, where appropriate, with values of k_Q for $Mg(3^3P_J)$ obtained from measurements of forbidden emission on a flow discharge system,[27] time-resolved atomic resonance absorption following dye-laser excitation[25] and "single-shot mode" atomic resonance fluorescence also following dye-laser excitation.[30,32]

The results are generally in good agreement with measurements reported by Breckenridge et al.[25] resulting from dye-laser excitation coupled with time-resolved atomic resonance absorption monitoring as well as, for the datum with H_2, the more recent studies restricted to this molecule using time-resolved forbidden emission.[30] The results are also in good agreement with those reported by Taieb and Broida,[27] who monitored emission from a discharge-flow system.

In fundamental terms, quenching of $Mg(3^3P_J)$ by H_2 and D_2 merits the most detailed consideration of the collision partners studied in this investigation. The absolute values of the individual quenching constants for these two gases obtained both by the signal-averaging method of this study and that of Breckenridge and Stewart[32] using time-resolved forbidden emission in the "single-shot" mode following dye-laser excitation are in accord within the error limits. It is clear from visual inspection of the single-shot output observed routinely in the present studies, using standard oscilloscopic display, that there is a major improvement in signal quality when employing boxcar integration, as

expected. The present measurements have confirmed the significant isotope effect observed for the overall collisional removal of $Mg(3^3P_J)$ by H_2 and D_2 reported by Breckenridge and Stewart.[32] These authors reported $k_{H_2}/k_{D_2} = 2.7$ at 800 K compared with the value 3.8 obtained here, again the ratios agreeing within the error limits.

Neither the present measurements, nor those of Breckenridge and Stewart[32] have yielded the branching ratios for chemical reaction and energy transfer following collision between $Mg(3^3P_J)$ + H_2 and D_2, although Breckenridge and Nicolai[30] have detected $MgH(X^2\Sigma^+)$ by laser induced fluorescence in this chemical system. Breckenridge and Stewart[32] did fit their overall collisional quenching rate data for $Mg(3^3P_J)$ + H_2,D_2 to the form;

$$k = B + A.exp(-E/RT) \qquad (3.21)$$

ascribing the magnitude of the term B in each case to inefficient physical quenching and the temperature-dependent term to chemical reaction on the basis that the measured activation energies were in accord with reaction thermochemistries in both cases. The role of vibrational energy in these chemical reactions is yet to be resolved, both experimentally and theoretically. Whilst the observed activation energy (E) and the thermochemistry for the reaction between $Mg(3^3P_J)$ and H_2 are consistent with chemical reaction of the Boltzmann fraction of $H_2(v=1)$ proceeding with unit collisional efficiency, the rate data for $Mg(3^3P_J)$ + D_2 do not fit a similar model where $D_2(v=2)$ would be required if vibrational energy alone were the controlling factor. The gross features of the quenching data are in accord with ab initio calculations that have been carried out on the appropriate potential energy surfaces.[31,68] Breckenridge and Stewart[32] indicate that trajectory calculations using these surfaces are in progress and should yield more detailed information on the role of vibrational energy on chemical reaction for those systems.

The collisional behaviour of atoms in general with the molecules N_2O and CO_2 merits consideration together in view of their linear, 18 electrons, closed-shell structures. Correlation diagrams, especially for atomic reactions with such molecules, are of limited application as predictive instruments as they do not include activation energy barriers

for reaction, an aspect particularly important with these species where electron promotion from the closed shell will be reflected in the activation energy, even for exothermic O-atom abstraction process with N_2O[2,4-6] [$D(N_2-O)$ = 1.677 eV[69]]. Of course, these diagrams nevertheless indicate the relevant potential surfaces involved in reaction within the confines of the appropriate coupling case. Chemical reaction between $Mg(3^3P_J)$ + N_2O to yield ground state $MgO(X^1\Sigma^+)$ would be highly exothermic (ΔH = -4.56 eV, $D_0^0(MgO)$ = 3.53 eV[70]). Bourguignon et al.[37] have presented a correlation diagram connecting the states of Mg + N_2O and MgO + N_2 in C_s symmetry using the weak spin-orbit coupling approximation and have concluded that $Mg(3^3P_J)$ + N_2O only correlate with the low-lying $a^3\Pi$ state and a low-lying $b^3\Sigma^+$ state, a conclusion supported by laser-induced fluorescence measurements.[37] On the other hand, the quenching rate constant resulting from the present investigations for $Mg(3^3P_J)$ + N_2O is clearly found to be an order of magnitude slower than their result, which was derived from forbidden atomic emission on a flow discharge system[37] [table (3.3)], a result which is, in turn, an order of magnitude slower than that found by essentially the same method hitherto[27] [table (3.3)]. Whilst detailed in the range of observations reported, the system described by Bourguignon et al.[37] involving many secondary reactions, including $Mg(3^3P_J)$ + $Mg(3^3P_J)$ annihilation, and reactions of the resulting $Mg(3^1P)$ and various electronic states of MgO, is complex. Further, a rate as high as that privately communicated by Dagdigian[71] in ref. (37) for T = 900 K [table (3.3)] would mean that no fluorescence signal could be effectively observed for the present experimental conditions in figure (3.14), notwithstanding a further personal communication by Yarkony and Bauschlicher[72] in that paper of a small, not quantified, energy barrier in the $Mg(3^3P_J)$ + N_2O energy surface. Furthermore, the beam attenuation cross-sections reported by Dagdigian[71] are not consistent with the rates of formation of the various electronic states of MgO.[37] Similarly, in view of revision of the reported quenching rate constant of $Mg(3^3P_J)$ + N_2O by a factor of ca. 10 for the two groups of forbidden emission measurements on a flow discharge system,[27,37] a similar reduction in the value of the quenching rate constant for $Mg(3^3P_J)$ + CO_2 would bring the result into accord with the present measurements. We may reasonably conclude that the discharge system is complex[27,37] compared with the arrangement for optical

41

excitation of $Mg(3^3P_J)$ employed in the present measurements. Unfortunately, quenching of $Mg(3^3P_J)$ by N_2O and CO_2 have not been reported in other investigations wherein the atoms were generated by dye-laser beam excitation.

The rate constant for the overall collisional removal of $Mg(3^3P_J)$ by CH_4 obtained by the present method for T = 800 K [table (3.3)] is found to be marginally slower than that obtained hitherto using the single-shot mode for the higher temperature of 873 K.[66] This may arise from both the combination of technique and the overall energy barrier for the total collisional process. Whilst an upper limit of the chemical reaction rate constant for this endothermic process

$$Mg(3^3P_J) + CH_4 \longrightarrow MgH + CH_3 \qquad \Delta H = 0.336 \text{ eV}$$
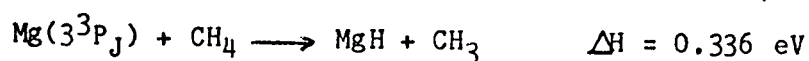
$[D^o_0(MgH) = 1.34 \text{ eV},[70], D(CH_3-H) = 4.406 \text{ eV}[69]]$ would be ca. 2×10^{-12} $cm^3molecule^{-1}s^{-1}$ at 800 K, overall removal appears to be dominated by physical quenching. Breckenridge and Umemoto[73] report a branching ratio for chemical reaction of < 0.01 from laser-induced fluorescence measurements on $MgH(X^2\Sigma^+)$ at what is presumably 426 °C (not 426 K)[73,74] from the quoted vapour pressure of magnesium that was employed (ca. 10^{-3} Torr). No data have been reported previously for the collisional removal of $Mg(3^3P_J)$ by CF_4 with which the present result can be compared [table (3.3)]. In this case, chemical reaction is thermochemically more favourable;

$$Mg(3^3P_J) + CF_4 \longrightarrow MgF + CF_3 \qquad \Delta H = -1.6 \text{ eV}$$
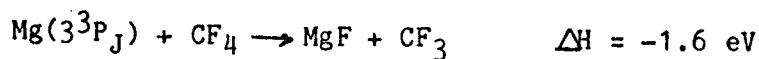
$[D^o_0(MgF) = 4.75 \text{ eV}[70]; D(CF_3-F) = 5.3 \text{ eV}[75]]$ and may play a greater role in the overall removal of the excited atom on collision.

Regarding the unsaturated hydrocarbons, the agreement between the result of the investigation of the quenching constant for C_2H_2 and that derived from the flow discharge technique[27] [table (3.3)] may be fortuitous in view of the complexities discussed for that method in the case of N_2O (see earlier). The use of an efficient quenching gas would not significantly reduce the effect of secondary processes[37] as experiments are generally performed by the control of pressures of added gases to yield decays of $Mg(3^3P_J)$ that are commensurate with the time-resolution of

a technique. The present measurements of rate constants for quenching by C_2H_4 and C_6H_6 yield values [table (3.3)] for these two gases that are approximately a factor of three greater than those derived from single-shot measurements using dye-laser excitation.[25] Certainly, for a vapour such as C_6H_6, where adsorption in the vacuum system is a standard problem, especially at low pressures, this effect should be significantly reduced in the present type of repetitive signal averaged technique which employs a flow system where losses of reactant vapour are effectively reduced, yielding higher quenching rates. Collisional removal of $Mg(3^3P_J)$ clearly proceeds at a rate approaching that of the collision number.

With final regard to this particular technique, it may be considered no accident that there is a sparsity of collisional rate data for the removal of $Mg(3^3P_J)$ by corrosive, oxidising gases, bearing in mind that magnesium vapour is generated from the solid at elevated temperatures. Surface oxidation, whilst trivial in concept, is significant in restricting the use of the present kinetic method. Thus, the rate of quenching by O_2 was determined by the present technique using low pressures of this gas and the measured decays of $Mg(3^3P_J)$ corrected for diffusional losses. The use of O_2 at significant pressures in the flow system in order to obtain quenching data for $Mg(3^3P_J)$ through conditions that permit equation (3.20) to be used simply results in the loss of the resonance fluorescence signal at $\lambda = 457.1$ nm. Quenching of $Mg(3^3P_J)$ by O_2 using the single-shot method has not, apparently, been reported,[30] presumably for this type of experimental reason. Similar limitations have been observed with the study of $Ca(4^3P_J)$ where $Ca(4^1S_0)$, in equilibrium with solid calcium at elevated temperatures, was optically excited using a dye-laser.[43]

4. KINETIC STUDY OF CALCIUM (4^3P_J)

In the previous chapter a range of time-resolved resonance fluorescence experiments on $Mg(3^3P_J)$ have been described. Proceeding with the investigation of the collisional behaviour of the group IIA elements in general, and following the natural order, the study of $Ca(4^3P_J)$ will now be considered. Although the same experimental technique that was used for atomic magnesium is to be employed for calcium, differences in chemical and physical properties between these two elements dictate some modifications that will be discussed briefly.

One significant change concerns the reactor. Quartz was abandoned in favour of stainless steel as the material for construction of the reaction vessel. The choice of stainless steel is due to the higher temperature required in the study of $Ca(4^3P_J)$; 1000 K as opposed to 800 K for $Mg(3^3P_J)$. The temperature increase is related to the relatively low vapour pressure of calcium compared with magnesium.[53] In order to achieve the same vapour density as the corresponding to magnesium at 800 K, calcium has to be maintained at 1000 K. the temperature in which calcium has a vapour pressure of ca. 0.2 Torr.[53] The higher temperature, allied with the higher reactivity of calcium compared with magnesium, precludes quartz being used in the reaction vessel.

The stainless steel reaction vessel used for the experiments on $Ca(4^3P_J)$, apart from slight modifications that will be mentioned, has a design that was essentially kept similar to the one successfully used with $Mg(3^3P_J)$. The use of stainless steel in kinetic studies on $Ca(4^3P_J)$ has normally been adopted by previous workers,[41,43] although Furcinitti et al.[24] have used a tantalum-lined cylindrical quartz reaction vessel for measurements at somewhat lower temperatures (ca. 800 K) with a sealed system.

The stainless steel reaction vessel was built with inlet and outlet Pyrex windows for the incident laser beam and the emergent resonance

fluorescence signal. The windows, situated externally to the oven, were sealed on to the system by means of O-rings and orthogonally placed with respect to each other. The steel arms leading to the windows were water-cooled by means of copper tubing wound around the arms. Heat transfer between the stainless steel and the copper was achieved by means of a graphite-containing cement ("Thermon" Heat Transfer Cement, Grade T63). Calcium was loaded into the reaction vessel by means of a special stainless steel spoon which could be introduced through the additional opening located in the gas inlet arm. The opening, sealed by a stainless steel cap and O-ring, allowed the calcium sample to be replaced by a fresh one, whenever necessary and without disturbing the geometry of the light detection system. This procedure proved to be necessary in order to overcome the effect of contamination of the calcium samples (see later) and the necessity of a fixed geometry in order to compare the values of the diffusion coefficients obtained. With the stainless steel reactor it was possible to dispense with the pre-heating tape used before for the quartz reactor (see chapter 3). When the central body of the reaction vessel was kept at T = 1000 K, the temperature used in the experiments with $Ca(4^3P_J)$, the gas inlet arm remained hot enough to pre-heat the flowing gas and guarantee an homogeneous temperature within the excitation zone.

The quantum efficiency (Q.E.) of the E.M.I. 6256B photomultiplier tube used in the studies on $Mg(3^3P_J)$ (chapter 3) is much lower at the longer wavelength employed for the studies on $Ca(4^3P_J)$, [Q.E.(λ = 657.3 nm) = ca. 0.2%] compared to that at λ = 457.1 nm (Q.E. = ca. 5.5%). However, the advantages of pre-trigger photomultiplier gating that have been described for using with this particular laser system, so critical in the necessary elimination of the massive scattered light signal, overweigh any increase in efficiency that would result from employing a p.m. tube with a sensitivity extended to longer wavelength (e.g., a standard "S20" response) but for which the relevant gating circuitry was not readily available, at the time the experiments on $Ca(4^3P_J)$ were carried out. Unlike the previous studies on $Mg(3^3P_J)$, the operating voltage used on the tube (p.m. power supply Brandenburg 415B, operating voltage = ca. 1100 V) was both greater in account of the lower quantum efficiency at the longer wavelength and the smaller signals obtained when studying $Ca(4^3P_J)$ at low pressure of

added inert gas. Quite apart from the kinetic effects on $Ca(4^3P_J)$ due to the pressure of the noble gas, the absolute magnitude of the fluorescence signal at $\lambda = 657.3$ nm decreased with decreasing pressure on account of line narrowing arising from the reduction in pressure broadening coupled with the relatively large finite bandwidth of the laser excitation source (ca. 0.1 cm^{-1}). Thus, the absolute yield of $Ca(4^3P_1)$ generated by excitation from the dye-laser decreases. This effect, as it will be seem later, is further noticed when the inert gas is changed, the signals for a given pressure with xenon being considerably greater due to the larger line broadening by this gas. These effects are readily observed in the quality of the "single-shot" traces, monitored routinely, oscilloscopically, purely for visual inspection, and emphasising the need for signal averaging.

The dye-laser, used for pulse excitation of calcium vapour at $\lambda = 657.3$ nm was pumped by the second harmonic ($\lambda = 532$ nm, E = ca. 150 mJ per pulse) of a Nd-YAG primary laser at a repetition rate of 10 Hz. Cresyl violet 670 (Exciton Chemical Co. Inc., U.S.A.) was employed as a 7×10^{-4} M solution in methanol to produce light at the required wavelength ($\lambda = 657.3$ nm; pulse length = ca. 15 - 20 ns; pulse width = 0.1 cm^{-1}; output = ca. 10 mJ per pulse).

The adjustments of the boxcar integrator were essentially the same as previously described for the experiments on $Mg(3^3P_J)$ (see earlier). Owing to the smaller mean radiative lifetime of $Ca(4^3P_J)$ as compared with $Mg(3^3P_J)$ the decays were registered in shorter time scales [usually 2 ms as opposed to 5 ms for $Mg(3^3P_J)$].

4.1 The mean radiative lifetime of $Ca(4^3P_J)$

The mean radiative lifetime for $Ca(4^3P_1) \longrightarrow Ca(4^1S_0)$ has been investigated by a variety of experimental methods, including absolute intensity measurements of various types,[12,76-78] interferometric measurements,[20,79,80] atomic beam techniques,[81,82] and time-resolved atomic resonance absorption following dye-laser excitation,[24,44] as well as being the object of theoretical calculations,[23,60,83,87]. These will be dealt

with, where appropriate, in detail, in the light of the results of the present series of studies yielding τ_e. McIlrath,[39] has monitored $Ca(4^3P_{0,1,2})$ in the time-resolved mode using atomic absorption spectroscopy with a photographic plate following pulsed dye-laser excitation of calcium vapour, but this was not exploited as a general tool for the determination of fundamental rate data apart from relaxation measurements within the $Ca(4^3P_J)$ manifold.[40]

The principal experimental objective in the determination of the mean radiative lifetime for $Ca(4^3P_J) \longrightarrow Ca(4^1S_0) + h\nu$ from time-resolved measurements on the electronically excited calcium atom is the quantified description of the removal of $Ca(4^3P_1)$, once generated, of both the Einstein coefficient which is one parameter representing the kinetic decay, and also the competing kinetic processes involved in the overall removal of the excited atom. These are normally collisional processes and, in the present system, diffusional processes as well. Two extremes for extrapolation procedures can be considered for measurements of A_{nm} under the present collision conditions. Both depend upon rapid collisional Boltzmann equilibration within the 4^3P_J manifold (4^3P_0, E = 15,158 cm^{-1}; 4^3P_1, E = 15,210 cm^{-1} and 4^3P_2, E = 15,316 cm^{-1})[10] during the actual decay measurements themselves, a justifiable assumption from empirical considerations of such energies to be transfered on collision for normal experimental conditions.[61] McIlrath and Carlsten[40] have observed that a Boltzmann equilibrium was established in the $Ca(4^3P_J)$ manifold within 40 ns subsequent to dye-laser excitation of $Ca(4^1S_0)$ to $Ca(4^3P_1)$ at p_{He} = 10 Torr. Hence, for the time scales employed in the present investigation, this equilibrium may be applied for all the conditions of pressure used in these measurements. Defining the standard equilibrium constants, as hitherto for magnesium [equation (3.1) and (3.2)];

$$Ca(4^3P_0) \rightleftharpoons Ca(4^3P_1) \qquad K_1 \qquad (4.1)$$

$$Ca(4^3P_1) \rightleftharpoons Ca(4^3P_2) \qquad K_2 \qquad (4.2)$$
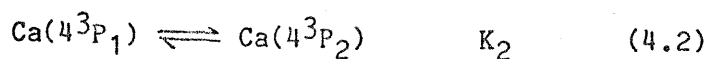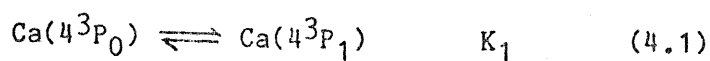
the rate equation for the decay of $Ca(4^3P_1)$ is entirely analogous to that presented previously for $Mg(3^3P_J)$ given the high optical metastability of the $Ca(4^3P_0)$ and $Ca(4^3P_2)$,[88] namely,

$$-d\{\ln[Ca(4^3P_0)]\}/dt = -d\{\ln[Ca(4^3P_1)]\}/dt = -d\{\ln[Ca(4^3P_2)]\}/dt$$

$$= k' \qquad (4.3)$$

and k' is defined as;

$$k' = A_{nm}/(1 + 1/K_1 + K_2) + \beta'/p + \Sigma k_Q[Q] \qquad (4.4)$$

where the symbols have their usual meaning as defined in chapter 3. Thus, A_{nm} may be determined experimentally through the use of kinetic equation (4.4) by two different procedures. Experimental conditions may be chosen through the use of inert gases which are characterised by low collisional quenching efficiencies for $Ca(4^3P_J)$[84] such that the term $\Sigma k_Q[Q]$ is negligible. Hence, A_{nm} may be obtained by extrapolation to infinite pressure of the noble gas from the linear plot of k' versus $1/p$ to $1/p = 0$. The rate constant k' may also be determined from extrapolation to infinite pressure directly from the plot of k' versus p(noble gas) as in the measurements of the decay of $Ca(4^3P_1)$ following pulsed dye-laser excitation using time-resolved resonance absorption spectroscopy as described by Furcinitti et al.[24] Alternatively, the term $\Sigma k_Q[Q]$ may be made dominant by the choice of experimental conditions, as in the study of the decay of $Ca(4^3P_J)$ following pulsed dye-laser excitation in the presence of $Ba(6^1S_0)$ and excess helium buffer gas as reported by Whitkop and Wiesenfeld.[44] The decay of $Ca(4^3P_J)$ is then monitored by time-resolved atomic resonance absorption and extrapolated to $[Ba(6^1S_0)] = 0$.[44]

The former alternative of extrapolation of k' to infinite pressure $(1/p = 0)$ through the diffusional component measured at relatively low pressure is chosen here. This procedure enjoys the advantage that the extrapolation may be made without employing significantly high pressures and the accompanying kinetic complexities arising from both physical quenching of $Ca(4^3P_J)$ by the noble gas itself and by impurities. These become important at high pressures, and will be considered quantitatively later. For the conditions of the present experiment with calcium, where $T = 1000$ K, equations (3.9) and (3.10) give $K_1 = 2.784$; $K_2 = 1.431$ and $(1 + 1/K_1 + K_2) = 2.794$. Hence, the objective in the present studies is to determine k' described by equation (4.4) in the region where β'/p is significant for this atomic state compared with the magnitude of A_{nm} and where, with the exception of xenon (see later), $\Sigma k_Q[Q]$ is not.

Figure (4.1) shows examples of the XY-output for the variation of the emission (I_F) at $\lambda = 657.3$ nm following dye-laser pulsed excitation of $Ca(4^1S_0)$ at this resonance wavelength in the presence of two different pressures of helium gas. There is clearly a significant decrease in the decay rate on increasing the noble gas pressure. This difference can be further seen in the first-order plots $[\ln(I_F)$ against time] constructed from such decays, as indicated for these two particular examples, in figure (4.2). The slopes of these plots yield k', the overall first-order decay coefficient for each composition. Figure (4.3a) shows the variation of k' with p_{He} and the effect of the diffusion component is noticed in the region of low pressures (below 10 Torr). Furcinitti et al.[24] have used the flat portion of such a curve to obtain a value of τ_e by plotting all the data on a single graph for Ne and Ar for pressures in the range ca. 20 - 500 Torr. All their measurements were carried out in the regime where no diffusional component was detected.[24] Figure (4.3b) shows the variation of k' against $1/p_{He}$. The intercept of the plot at $1/pHe = 0$, as we have seen before, yields $k'em$ which is defined by;

$$k'_{em} = A_{nm}/(1 + 1/K_1 + K_2) \qquad (4.5)$$

and hence, A_{nm} is derived from the limiting rate at infinite pressure of helium, using all the rate data and uncomplicated by impurity quenching at high pressures. The intercept of figure (4.3b) is found to be 954 ± 68 s^{-1} which, when combined with the value 2.794 for $(1 + 1/K_1 + K_2)$, yields $\tau_e = 0.376 \pm 0.027$ ms. Similar plots of k' versus $1/p$ for neon and argon are shown in figure (4.4), again yielding values of τ_e listed in table (4.1).

In contrast to the equivalent studies on $Mg(3^3P_J)$, it is only in the case of xenon that quenching of $Ca(4^3P_J)$ becomes significant whereas collisional removal by krypton is relatively inefficient. Figure (4.5) shows plots of k' versus $1/p$ for these gases. The plot for krypton is similar to those for the lighter gases, although the intercept is ca. 20% smaller than observed with helium, closer to that for neon [figure (4.5)] and yielding a comparable value for τ_e [table (4.1)]. It is seen that in the case of xenon there is little variation in the decay rate with pressure, the observations hence indicating an approximate balance between the increase in diffusion on decreasing the pressure accompanied by a decrease in the collisional quenching rate. We may therefore use the
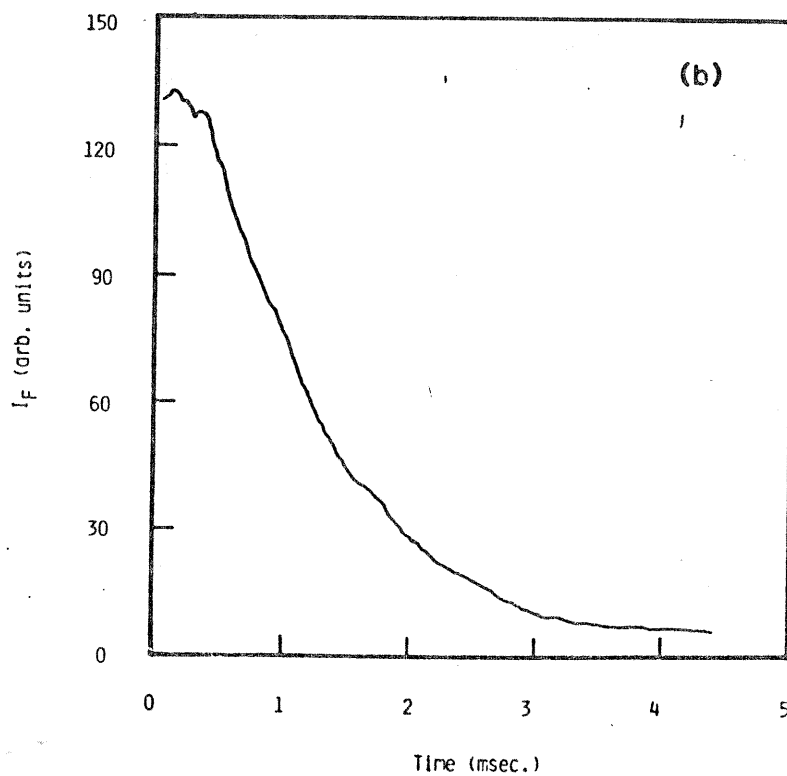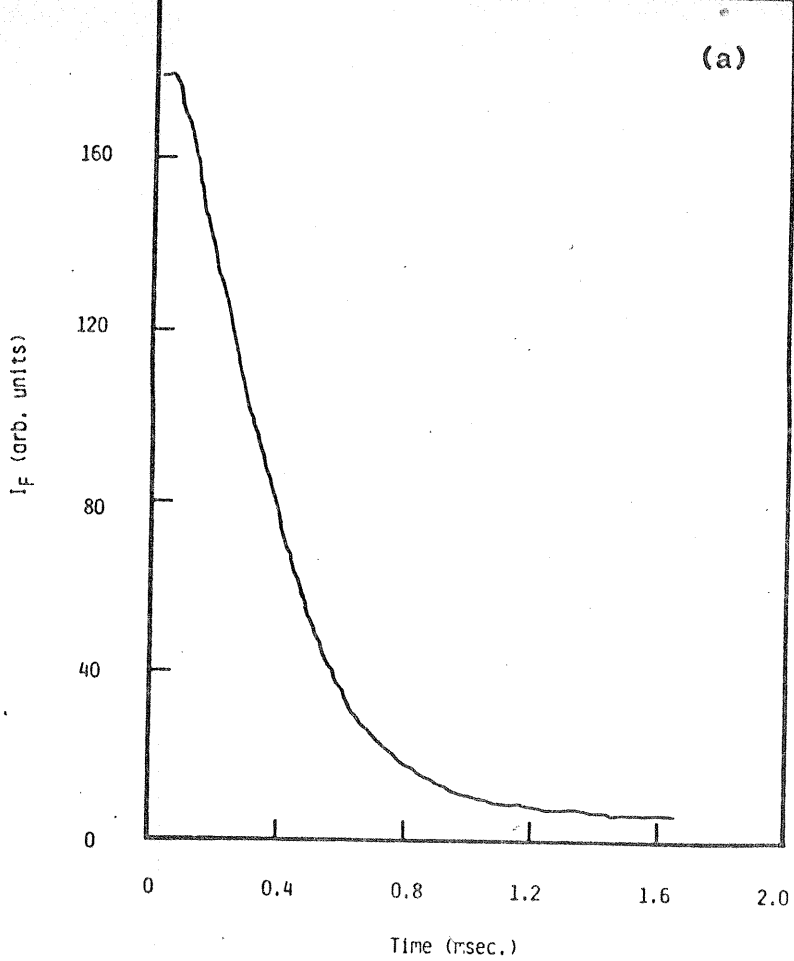
Figure 4.1

Examples of the output of the XY recorder indicating the decay of time-resolved atomic emission (I_F) at $\lambda = 657.3$ nm ($Ca(4s4p(^3P_1) \longrightarrow Ca(4s^2(^1S_0)))$) following pulsed dye-laser excitation of calcium vapour in the presence of helium. (T = 1000 K).

P_{He}(torr): (a) 3.0 ; (b) 30 .
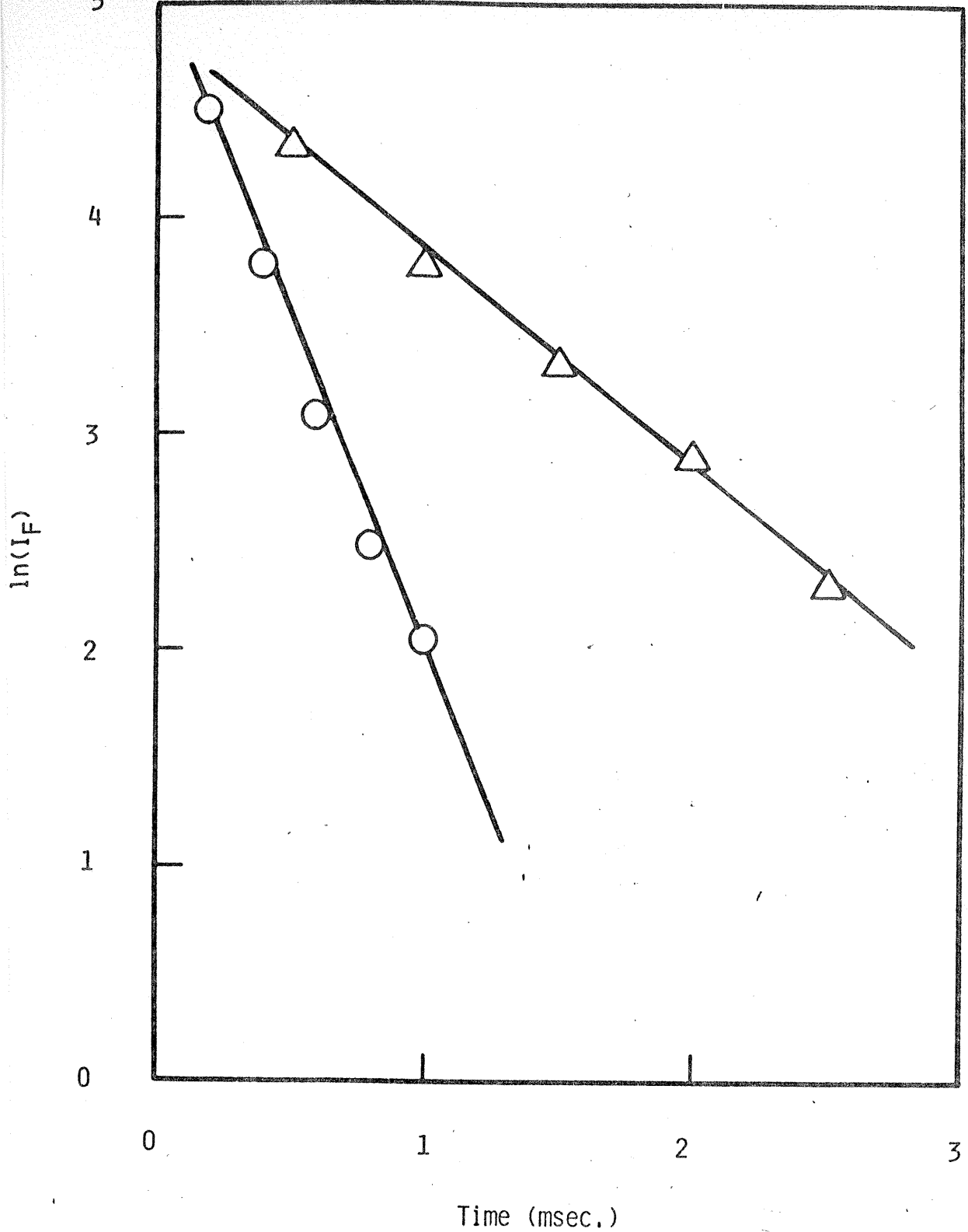
Figure **4.2**

Examples of first-order kinetic plots for the decay of the time-resolved atomic emission ($\ln(I_F)$ against t) at $\lambda = 657.3$ nm ($Ca(4^3P_1) \longrightarrow Ca(4^1S_0)$) following pulsed dye-laser excitation of calcium vapour in the presence of helium.   (T = 1000 K)

p_{He}(torr): ◯   3.0 ; △   30

(a)

(b)
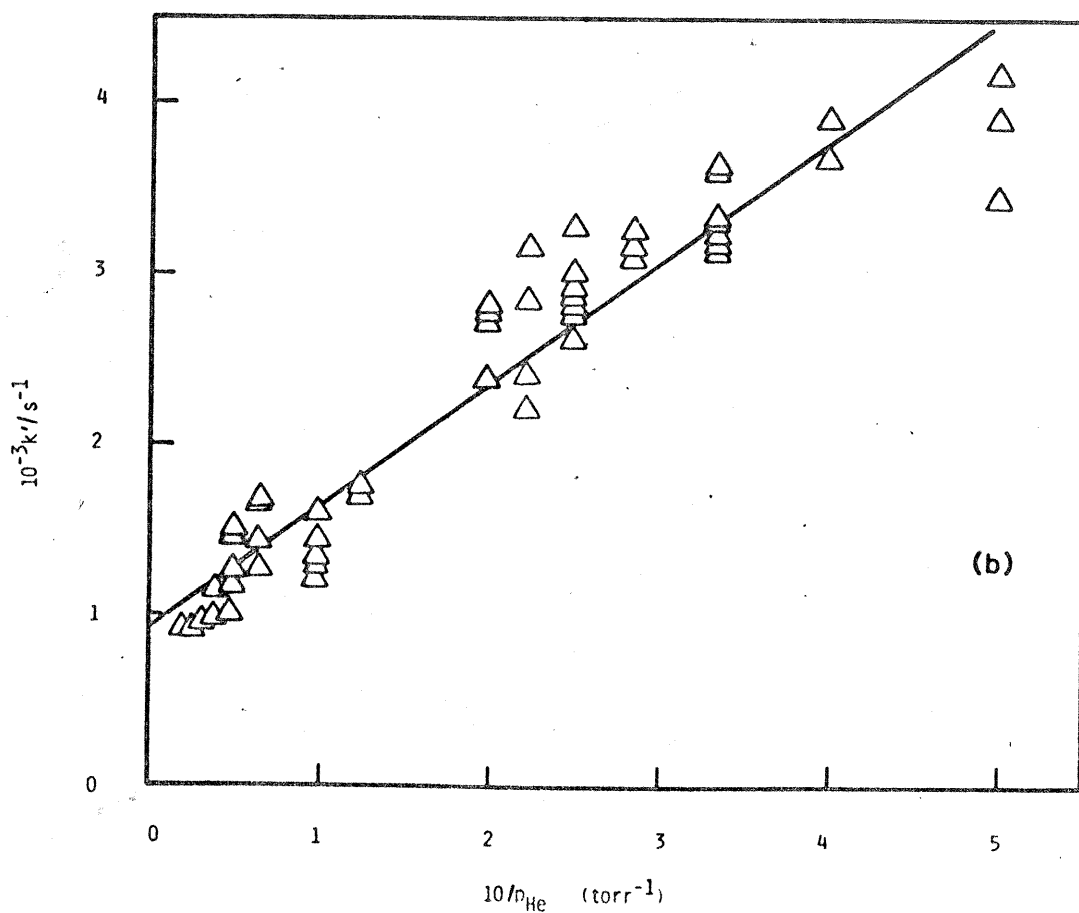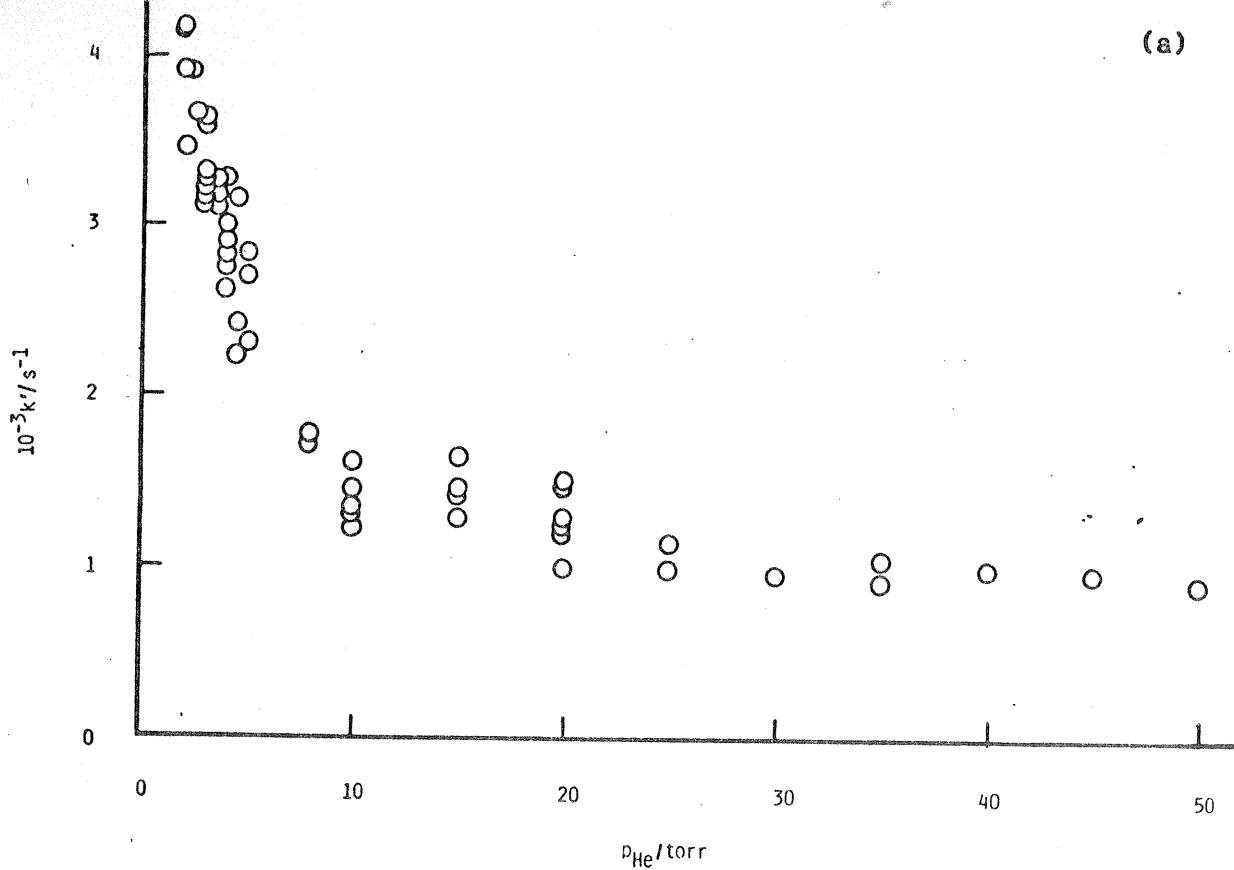
Figure 4.3

Variation of the first-order rate coefficient (k') for the decay of Ca(4^3P_J) in helium following the generation of Ca(4^3P_1) by pulsed dye-laser excitation. (T = 1000 K)

(a)   k' against p_{He} ;   (b)   k' against $1/p_{He}$.
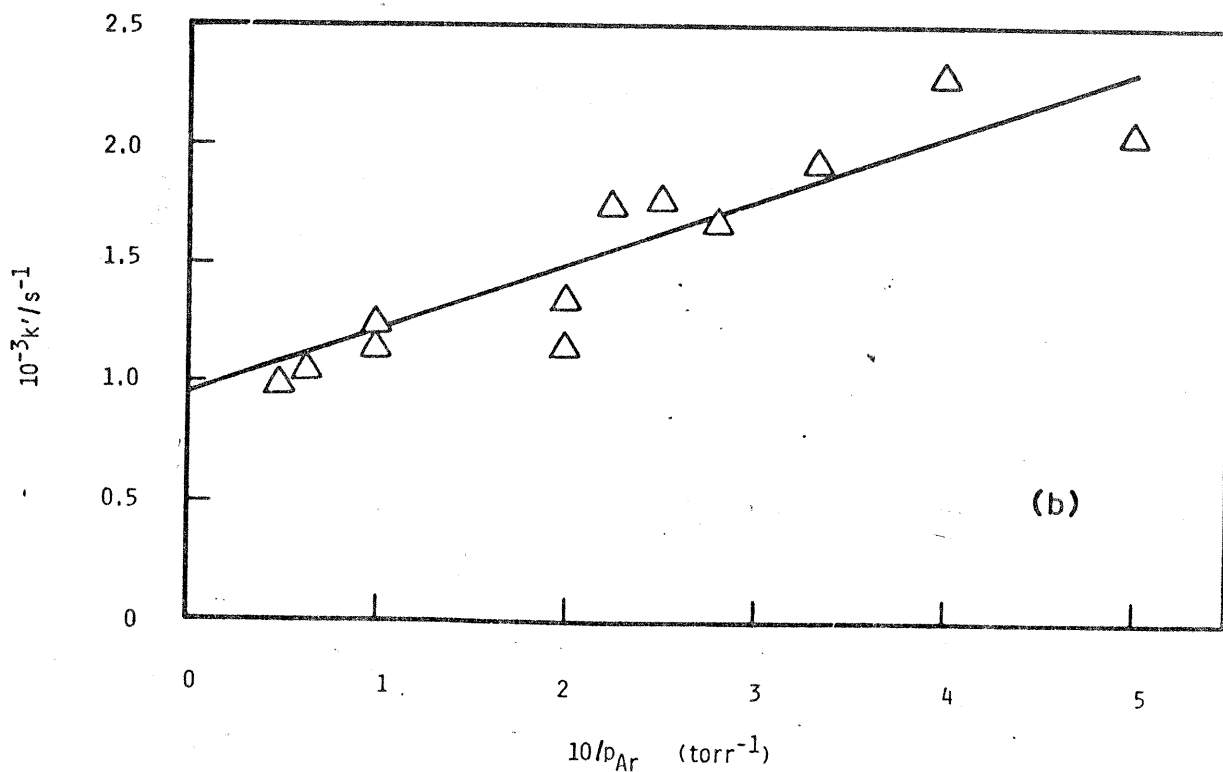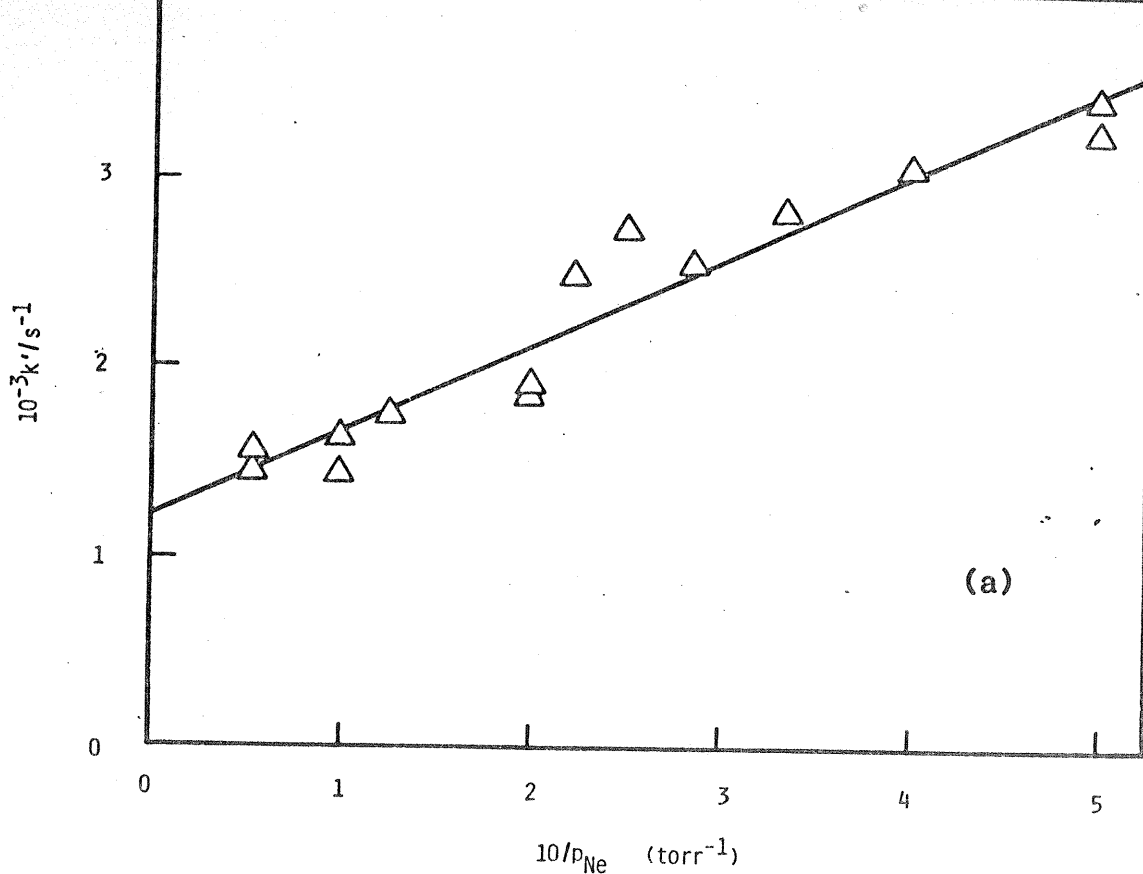
Figure **4.4**

Variation of the first-order rate coefficient (k') with the reciprocal of the pressure for the decay of $Ca(4^3P_J)$ in neon and argon following the generation of $Ca(4^3P_1)$ by pulsed dye-laser excitation. (T = 1000 K)

(a) Ne ;   (b) Ar
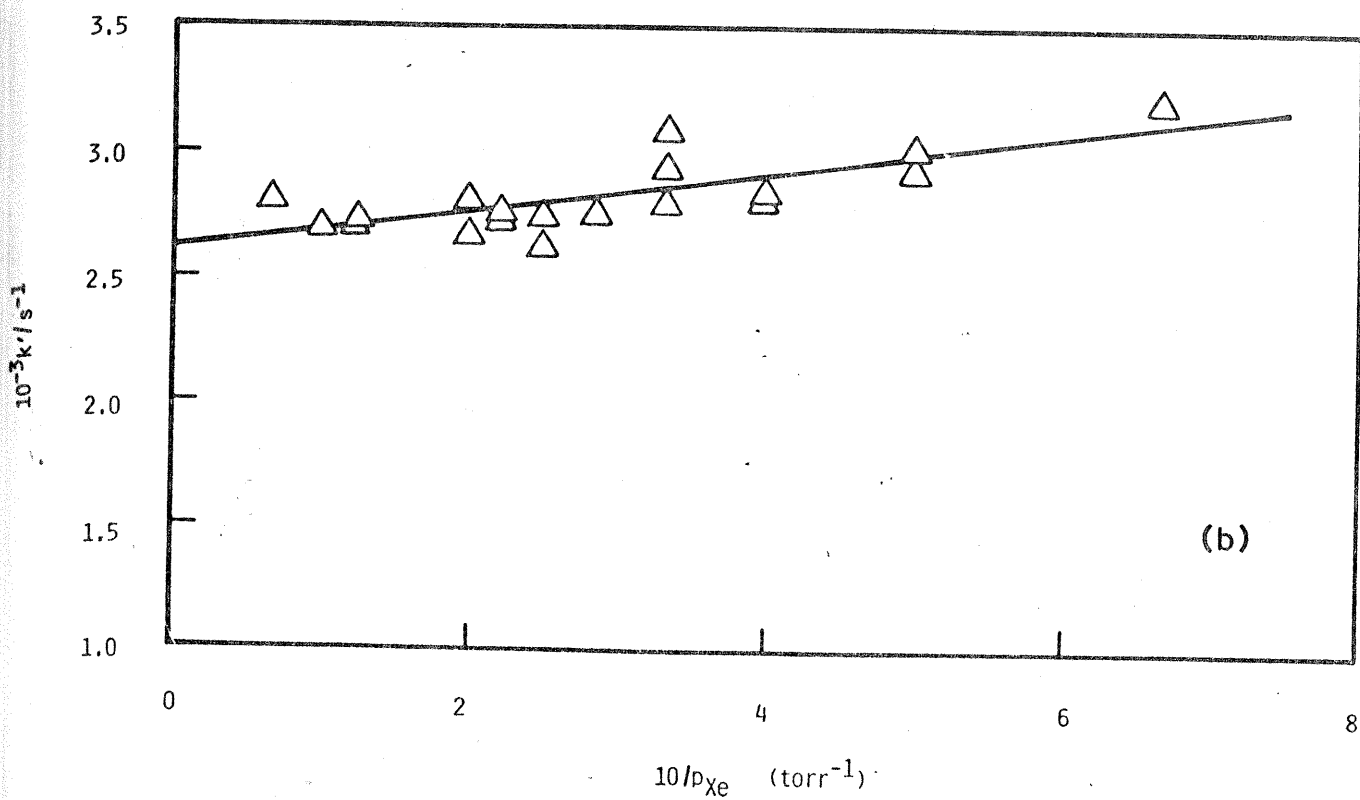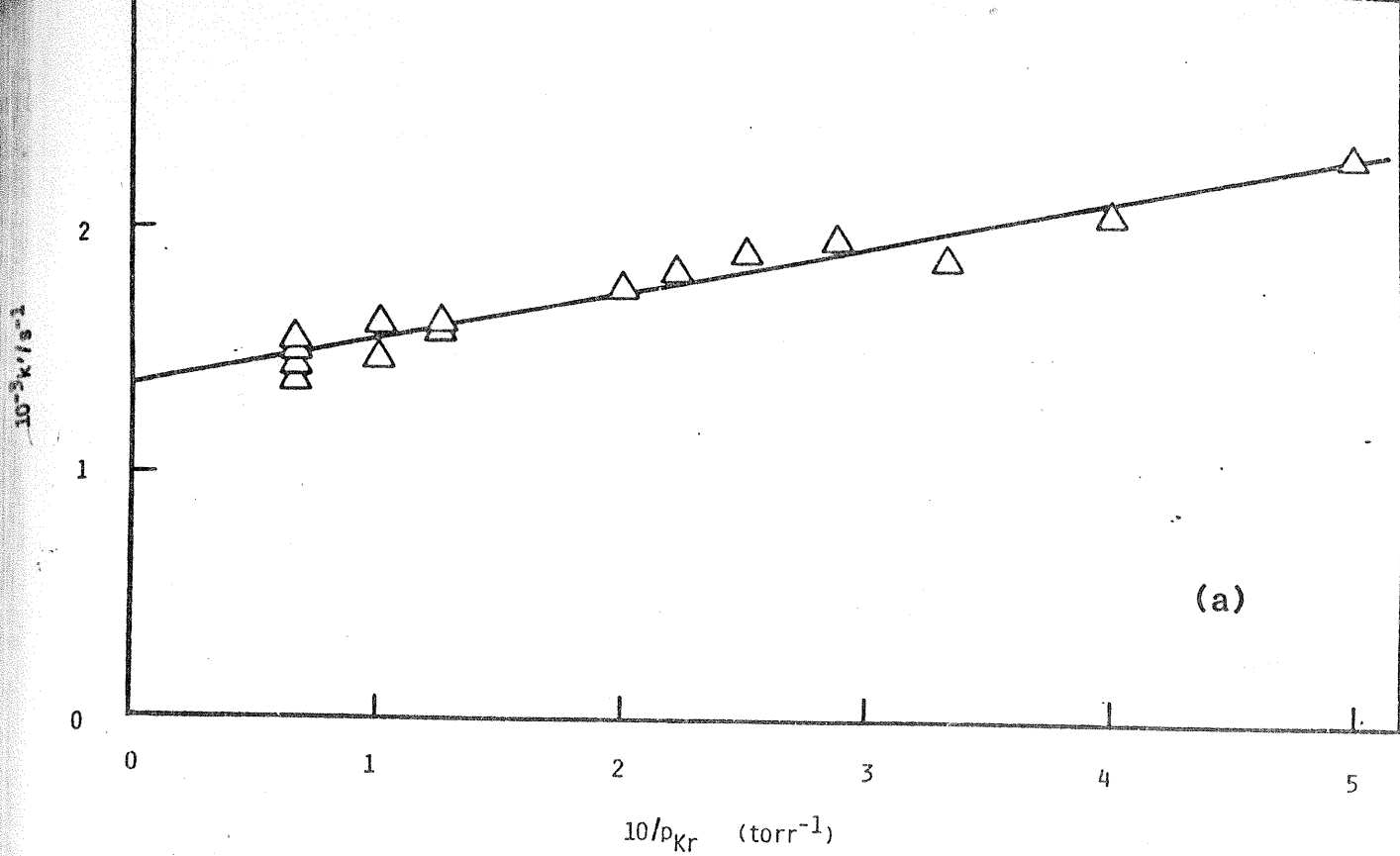
Figure 4.5

Variation of the first-order rate coefficient (k') with the reciprocal of the pressure for the decay of $Ca(4^3P_J)$ in krypton and xenon following the generation of $Ca(4^3P_1)$ by pulsed dye-laser excitation. (T = 1000 K)

(a) Kr ; (b) .Xe

measured values of k' for xenon and k'_{em} from the decay measurements for helium, for example, to determine the absolute collisional quenching constant for $Ca(4^3P_J)$ by Xe. Employing equation (3.19) as we did before in the studies on $Mg(3^3P_J)$ we may write for xenon;

$$(k' - k'_{em})/p_{Xe} = \alpha + \beta'/p_{Xe}^2 \qquad (4.6)$$

The meaning of β' which represents the diffusional loss of $Ca(4^3P_J)$ and its dependence on the boundary conditions have been discussed earlier (chapter 3). Figure (4.6) shows the plots both for xenon and also for krypton in view of the contrast with earlier work on $Mg(3^3P_J)$. The intercept for xenon was found to be $2.31 \pm 0.21 \times 10^2$ $Torr^{-1}s^{-1}$, yielding the quenching constant $k_{Xe} = 2.4 \pm 0.3 \times 10^{-14}$ $cm^3molecule^{-1}s^{-1}$ (1000 K). The intercept for krypton, using the same equation (4.6), is very small ($\alpha = 38 \pm 6$ $Torr^{-1}s^{-1}$) and, indeed, comparable to that for neon for the equivalent plot ($\alpha_{Ne} = 39 \pm 19$ $Torr^{-1}s^{-1}$) and, thus, lying within the error of passage through the origin. Similarly, the plot of argon yielded $\alpha_{Ar} = 8 \pm 17$ $Torr^{-1}s^{-1}$. Of course, the value for α_{He} may not be determined in this maner as the values for α are obtained using the value of k'_{em} for this particular gas. These results for α are thus used only to indicate upper limits for quenching by these three gases, namely, k_{Ne}, k_{Ar} and $k_{Kr} \leqslant$ 4×10^{-15} $cm^3molecule^{-1}s^{-1}$ in view of the error in the measurements of k'_{em} through the use of intercepts for these gases.

For the mean radiative lifetime, the average of the observed values are reported, including that used in the extraction of k_{Xe} as $\tau_e =$ 0.34 ± 0.02 ms (2σ). The values of τ_e for measurements in the different noble gases are compared in table (4.1) with those reported hitherto from a wide range of investigations.
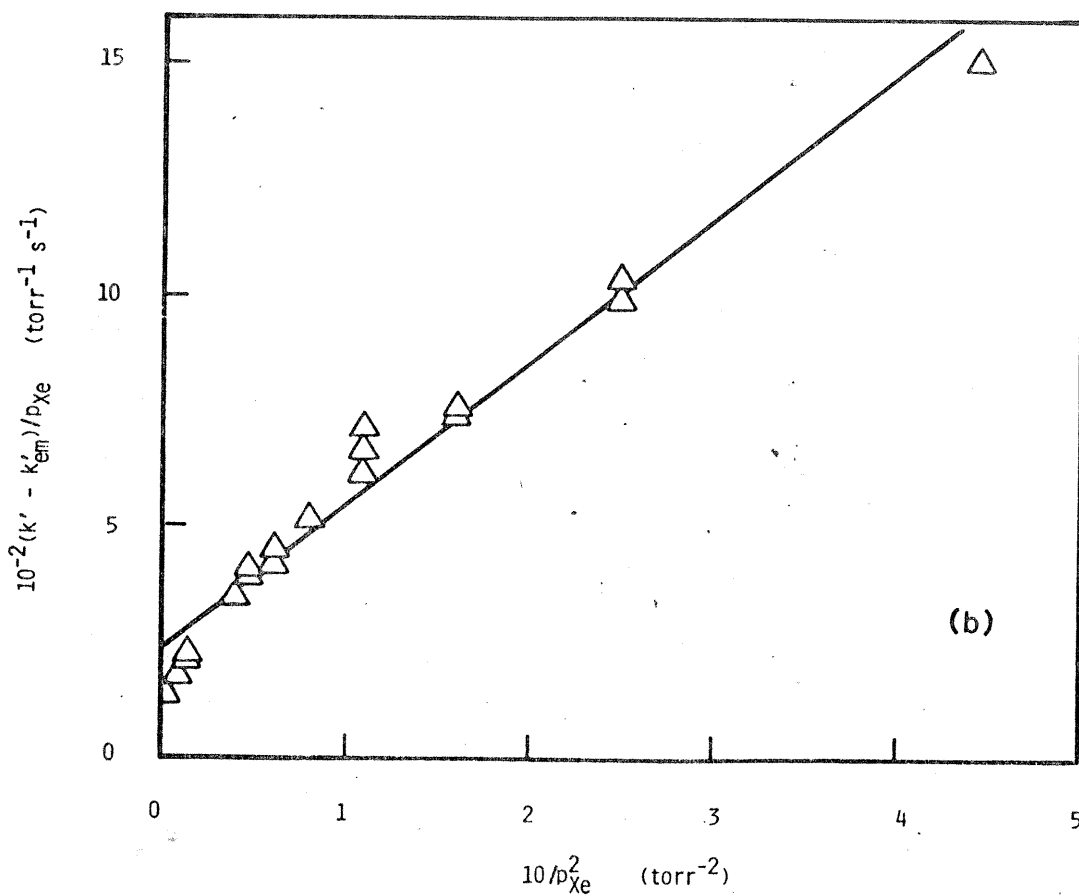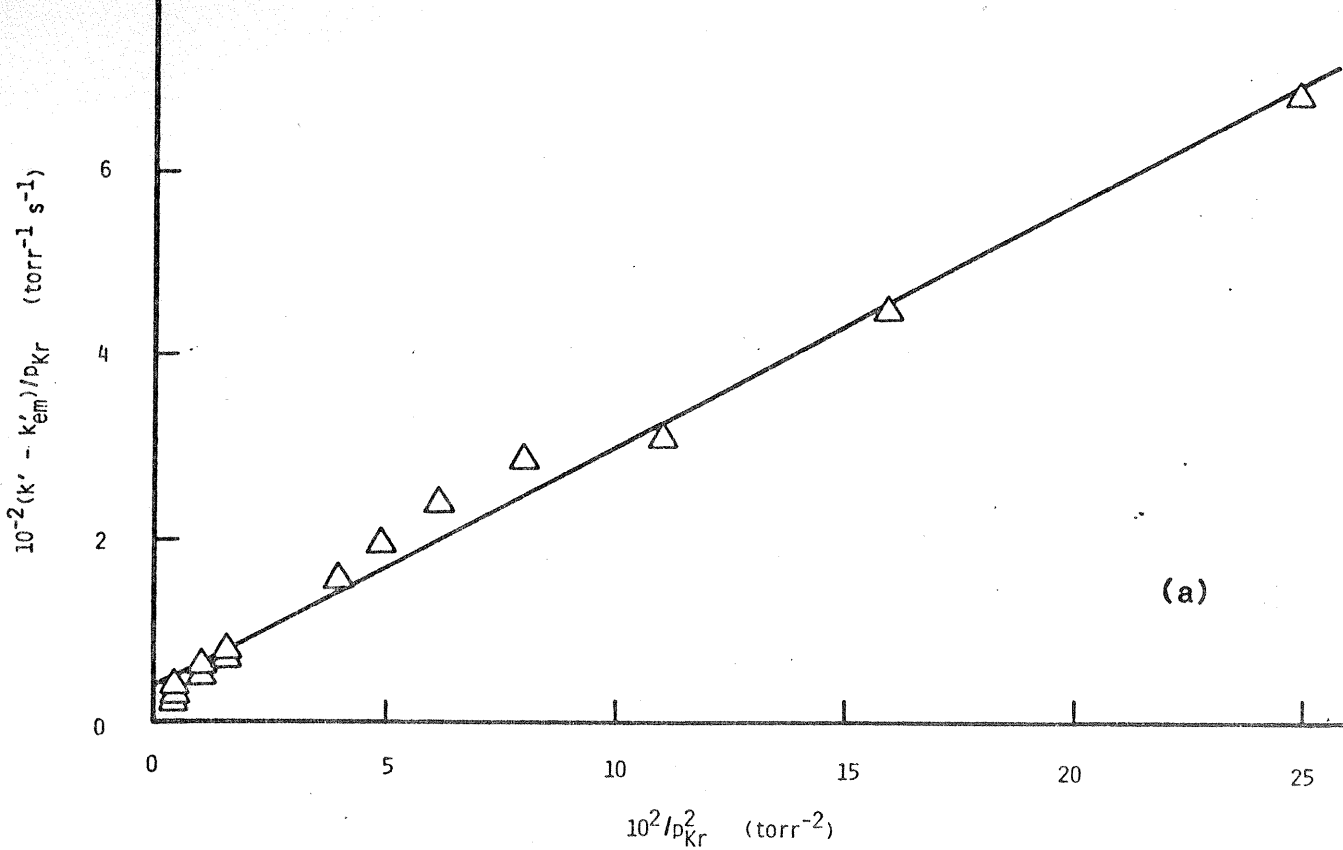
Figure **4.6**

Variation of the first-order rate coefficient (k') for the decay of $Ca(4^3P_J)$ in krypton and xenon following the generation of $Ca(4^3P_1)$ by pulsed dye-laser excitation.

(T = 1000 K; $(k' - k'_{em})/p$ against $1/p^2$)   (a) Kr ;   (b) Xe

TABLE 4.1

Mean radiative lifetime for $Ca(4^3P_1) \rightarrow Ca(4^1S_0) + h\nu$

τ_e /ms	Reference
0.32	(83)[a]
0.33	(84)[a]
0.22	(23)[a]
0.34	(85)[a]
0.26	(86)[a]
0.34	(87)[a]
0.38	(60)[b]
1.37	(76)[c]
0.52	(77)[d]
0.14	(12)[d]
0.53	(78)[d]
0.52	(20)[e]
0.38 ± 0.15	(79)[e]
0.44	(80)[e]
0.55 ± 0.04	(81)[f]
0.50 ± 0.04	(82)[f]
0.39 ± 0.04	(24)[g]
0.33 ± 0.03	(44)[g]
0.376 ± 0.027	(He buffer gas) (*)
0.294 ± 0.022	(Ne buffer gas) (*)
0.378 ± 0.031	(Ar buffer gas) (*)
0.264 ± 0.005	(Kr buffer gas) (*)
(0.376 ± 0.027)	(Xe buffer gas, He) (*)

(a) Theoretical

(b) Compilation

(c) Estimate from Fraunhoffer reversal

(d) Intensity measurements

(e) Hook method (interferometric)

(f) Atomic beam technique

(g) Dye-laser excitation + time-resolved atomic resonance absorption

(*) This work

The present set of measurements is in accord with the high pressure measurements of τ_e by Furcinitti et al.[24] and the intercept of k' for [Ba] = 0 reported by Whitkop and Wiesenfeld[44] in which $\Sigma k_Q[Q]$ was dominant [equation (4.4)]. Both of these earlier workers employed dye-laser excitation. The agreement with Furcinitti et al.[24] is particularly striking as the high pressure procedure imposes severe restrictions on gas purity. The quoted typical purities for He, Ne and Ar (table 14, p. 77, ref 24) are clearly in accord with their reported results. Atomic beams should offer an ideal route for the determination of τ_e for $Ca(4^3P_1)$ as collisional processes do not participate in the removal of the excited atom. Unfortunately, the beam experiments are so designed that the transit time of $Ca(4^3P_1)$ in the apparatus is comparable to the radiative decay time of the excited state; the kinetic analysis is complex and the resulting values of τ_e tend to be marginally high (0.55 ± 0.04 ms,[24] 0.50 ± 0.04 ms[44]) [table (4.1)].

The final set of experimental determinations of τ_e for $Ca(4^3P_1 \rightarrow 4^1S_0)$ that may be compared with the results of the present investigations are those derived from steady intensity measurements or line shapes via interferometry[12,20,76-80] [table (4.1)]. The accuracy in the determination of τ_e from intensity measurements is determined by various factors, particularly intensity calibrations. In many cases, this results from the use of relative intensity measurements using atomic lines of known intensity as internal calibrations. Such restrictions are significant in the case of the transition $Ca(4^3P_1) \rightarrow Ca(4^1S_0) + h\nu$ as the Einstein coefficient is approximately five orders of magnitude lower than that of an allowed transition with which it may be compared, and further, the assumption of a Boltzmann equilibrium density in the emitting state is critical to the analysis. These considerations account for the range of values of τ_e that have been reported by this type of method. The value reported by Corliss and Bozmann (τ_e = 0.14 ms)[12] is the lowest and indicates one end of the range, while that estimated by Fraunhoffer reversal (τ_e = 1.37 ms),[76] the other. Finally, we may note various theoretical calculations that have yielded values of τ_e, which are in good agreement with experiment [table (4.1)].

As with the previous studies on $Mg(3^3P_J)$ (chapter 3), the present measurements, carried out at a similar atomic density of calcium as calculated from detailed vapour pressure measurements and assessments,[88-90] yield mean radiative lifetimes for $Ca(4^3P_1)$ in general accord with those derived from a range of alternative techniques [table (4.1)]. Thus, the role of electronic to translational energy transfer for quenching of $Ca(4^3P_J)$ by the ground state $Ca(4^1S_0)$ cannot be significant in this system. It is difficult to assess the status of the measurements of k_{Ca} for this process reported by Malins and Benard[41] of 5.1×10^{-12} $cm^3 molecule^{-1} s^{-1}$, derived from phase shift measurements, as that technique yielded quenching rate constants for the noble gases which were incorrect by many orders of magnitude in some cases (see later). It is clear from the measurements of Furcinitti et al.[24] of $\tau_e[Ca(4^3P_1)]$, carried out in a sealed system where [Ca] would have reached the equilibrium density value, that the term $k_{Ca}[Ca]$ would have been negligible even in terms of the value of k_{Ca} reported by Malins and Benard[41] and [Ca] calculated for T = 520 $^\circ$C (793 K).[24,88,90]

Of course, in the present measurements, $[Ca(4^1S_0)]$ may well not reach the value of the equilibrium vapour pressure in the region of the reactor exposed to the laser beam. Notwithstanding calculated values of $k_{Ca}[Ca(4^1S_0)]$ the present measurements are in accord with those derived from a sealed system where the effect was clearly negligible.

4.2 Diffusion of $Ca(4^3P_J)$ in noble gases

The kinetic analysis leading to the determination of the mean radiative lifetime of $Ca(4^3P_1)$ from measurements on the decay of $Ca(4^3P_J)$ at relatively low pressures of noble gas shows that the rate process of diffusion and spontaneous emission are intimately linked. Before proceeding with quantitative consideration of diffusion itself, we may immediately contrast the present measurements on $Ca(4^3P_J)$ employing plots based on equations (4.4) and (4.6) with analogous measurements on $Mg(3^3P_J)$ that have been described in chapter 3. This is immediately apparent on considering the difference in the Einstein coefficient, A_{nm}, for;

$$Mg(3\,^3P_1) \longrightarrow Mg(3\,^1S_0) + h\nu \qquad (\lambda = 457.1 \text{ nm})$$

and

$$Ca(4\,^3P_1) \longrightarrow Ca(4\,^1S_0) + h\nu \qquad (\lambda = 657.3 \text{ nm})$$
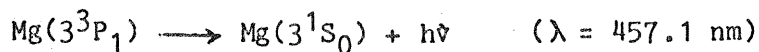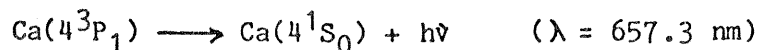
The data in table (3.1) and table (4.1) indicate that A_{nm} for the $Mg(3\,^3P_1)$ emission is approximately a factor of seven times smaller than that for $Ca(4\,^3P_1)$. Thus, the term β'/p only competes significantly with A_{nm} in the present studies at much lower pressures than in the equivalent study on $Mg(3\,^3P_J)$, notwithstanding some modifications in the design of the stainless steel reaction vessel, as described previously. The contribution of the term β'/p to the first-order decay in the present system occurs at pressures of noble gas of ca. 10 Torr. By contrast, Furcinitti et al.,[24] who studied the decay $Ca(4\,^3P_J)$ in the presence of Ne and Ar observed no significant variation between k' and the noble gas pressure. Pressures below 20 Torr were not investigated.[24] Further, the use of atomic resonance absorption on a cylindrical reaction vessel in those experiments[24] would require the use of even lower pressures before diffusional losses become significant compared with A_{nm} in the case of $Ca(4\,^3P_1)$. Thus, only by the use of low pressures and the limited light gathering power of a monochromator slit when using fluorescence can diffusion be studied in the present system.

As indicated in chapter 3, absolute diffusion coefficients cannot be determined by the present method in the absence of data for the boundary conditions of the diffusion equation. However, we may, as for $Mg(3\,^3P_J)$, use the plots given in figures (4.3b), (4.4), (4.5a) and (4.6b) to quote relative values of D_{12} for $Ca(4\,^3P_J)$ which are presented in table (4.2).

TABLE 4.2

Relative diffusion coefficients (D_{12}) for $Ca(4\,^3P_J)$
in the noble gases

Noble gas	D_{12}
He	1.00
Ne	0.69
Ar	0.35
Kr	0.34
Xe	0.46

The principal difference with the earlier relative measurements of $D_{12}[Mg(3^3P_J)$, noble gases] (chapter 3) is the relatively greater diffusional rate for $Ca(4^3P_J)$ in He compared to the other noble gases. The value for xenon also reflects the greater weighting given to measurements at low pressure through the use of equation (4.6) compared with equation (4.4).

4.3 Collisional quenching of $Ca(4^3P_J)$

The present measurements on the study of diffusion of $Ca(4^3P_J)$ in the noble gases and of the mean radiative lifetime (τ_e) have led to collisional rate data for quenching of $Ca(4^3P_J)$ in those noble gases which are presented in table (4.3). Thus, xenon exhibits a measurable deactivation rate but the data for the remaining gases indicate negligible quenching efficiency. Hence, these results are in disagreement with Malins and Benard[41] who report a monotonic variation of $k_{He} = 2.13 \times 10^{-15}$ to $k_{Xe} = 6.7 \times 10^{-15}$ cm^{3}molecule^{-1}s^{-1} across the noble gases and discuss the results in fundamental terms. The upper limits described in the present work for Ne, Ar and Kr arise from the errors in the measurements using standard electronics and pressures conventionally employed in flow systems. The comparable magnitudes between the upper limits reported here and the actual rate constants reported by Malins and Benard[41] is fortuitous. The most striking disagreement concerns the lighter gases, and this can be seen further from the high pressure measurement of Furcinitti et al.[24] For the gases argon and neon, Furcinitti[91] fitted the high pressure data (in the notation of the present work) to the form;

$$k' = a + bp \qquad (4.7)$$

where b would be the second-order quenching constant. This yielded b = ca. 10^{-4} Torr^{-1}s^{-1}.[91] As a rate constant, this yields $k_{Ne} \cong k_{Ar} \cong 8 \times 10^{-21}$ cm^{3}molecule^{-1}s^{-1}, approximately six orders of magnitude lower than values reported by Malins and Benard.[41] Thus, within experimental error, all the values of k' for the conditions of Furcinitti's measurements across the whole pressure range were of magnitude 916 s^{-1} and could be attributed to decay solely by spontaneous emission. If, for example, one uses the value of Malins and Benard[41] for $k_{Ar} = 4.8 \times 10^{-15}$ cm^{3}molecule^{-1}s^{-1}, for the

highest pressure of argon (or neon) used by Furcinitti of 500 Torr, $k' = k'_{em} + k_{Ar}[Ar] = $ ca. 3×10^4 s^{-1} at 520 °C (793 K). For the lighter noble gases at least, the data of Malins and Benard[41] require serious reconsideration.

The determination of absolute rate data for the removal of electronically excited calcium atoms, $Ca[4s4p(^3P_J)]$, by added gases constitutes a significant aspect of the general development of our understanding of the relationship between collisional behaviour and electronic structure[2,6,7] and its application to group IIA elements in particular.[9]

The collisional quenching of $Ca(4^3P_J)$ by added gases was studied in a manner similar to that employed hitherto for the study of $Mg(3^3P_J)$ (chapter 3), namely, by carrying out decay measurements at a constant total pressure at which first-order removal by diffusion and spontaneous emission are constant in a series of kinetic runs in which the concentration of the quenching gas [Q] is varied. Hence, we may write;

$$k' = K + k_Q[Q] \qquad (4.8)$$

where k_Q is the absolute second-order quenching rate constant. Notwithstanding the apparently straight-forward nature of such an experimental approach, its use in the measurement of absolute rate constants for collisional quenching of $Ca(4^3P_J)$ has been very limited indeed, in marked contrast to $Mg(3^3P_J)$.[25,30,32]

Apart from the present work, it would appear that the only other quantitative measurements of this type, leading to absolute quenching rate data for $Ca(4^3P_J)$ are, firstly that of Whitkop and Wiesenfeld[44] who employed time-resolved atomic resonance absorption spectroscopy to determine the absolute rate constant for the removal of $Ca(4^3P_J)$ by $Ba(6^1S_0)$. Secondly, a similar method to that employed by Whitkop and Wiesenfeld[44] is described by Furcinitti[91] who reports quenching rate data for $Ca(4^3P_J)$ by H_2 and N_2, and from whose thesis upper limits for quenching rate constants by neon and argon may be derived. These time-resolved studies may be contrasted with the use of phase-sensitive detection coupled with Stern-Volmer analysis following modulated dye-laser

excitation to determine collisional rate data for $Ca(4^3P_J)$.[41-43] The interpretation of the measured phase shifts is model dependent and, certainly, in the case of the noble gases,[41] has led to quenching rate data for $Ca(4^3P_J)$ which are often too high (see earlier). The study of $Ca(4^3P_J)$ in atomic beams has yielded detailed measurements on chemiluminescence cross sections for reactions with the molecules Cl_2, HCl and N_2O.[29,33,45,46,67,92] Laser-induced fluorescence measurements on CaO have been employed to determine cross sections for reactions of $Ca(4^3P_J)$ with O_2 and CO_2 in atomic beams.[48] Whilst various measurements and mechanistic interpretations have been ascribed to the emission

$$Ca(4^3P_1) \longrightarrow Ca(4^1S_0) + h\nu \qquad (\lambda = 657.3 \text{ nm})$$
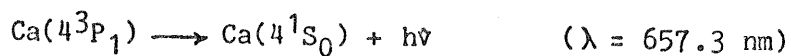
in low pressure flames with calcium additives and catalysed by $N_2O + CO$ mixtures, absolute rate data for $Ca(4^3P_J)$ have not been reported.[26,49,50] In this work, the collisional quenching of $Ca(4^3P_J)$ by a wide range of added gases following pulsed dye-laser excitation of $Ca(4^1S_0)$ is investigated. It is clear, from previous studies reported in the literature and from the present investigation that the main limitation in the measurement of collisional quenching arises from the effects of surface poisoning of the solid calcium from which the $Ca(4^1S_0)$ is derived, by the added gases at elevated temperatures. Reduction in the fluorescence signal was observed with added gases, particularly N_2, as also observed hitherto by Nicks et al.[43] This is overcome sufficiently in the present measurements which employ time-resolved forbidden emission at $\lambda = 657.3$ nm in a slow flow system, kinetically equivalent to a static system. The use of repetitive pulsing on a flow system and the regular change of the solid calcium sample has permitted rate data to be determined.

Figure (4.7) gives examples of first-order kinetic plots for the decay of $Ca(4^3P_J)$ in the presence of nitrogen. Figure (4.8) shows the plot of k' against $[N_2]$ constructed from the slopes of plots of the type given in figure (4.7), yielding the absolute second-order rate constant for collisional quenching by this molecule of $k_{N_2} = 8.9 \pm 0.9 \times 10^{-13}$ $cm^3molecule^{-1}s^{-1}$ (1000 K). This may be compared with the value of $k_{N_2} = 1.80 \pm 0.39 \times 10^{-13}$ $cm^3molecule^{-1}s^{-1}$ (793 K) derived from time-resolved atomic resonance absorption spectroscopy following dye-laser excitation.[91] That work was not subsequently published further, perhaps
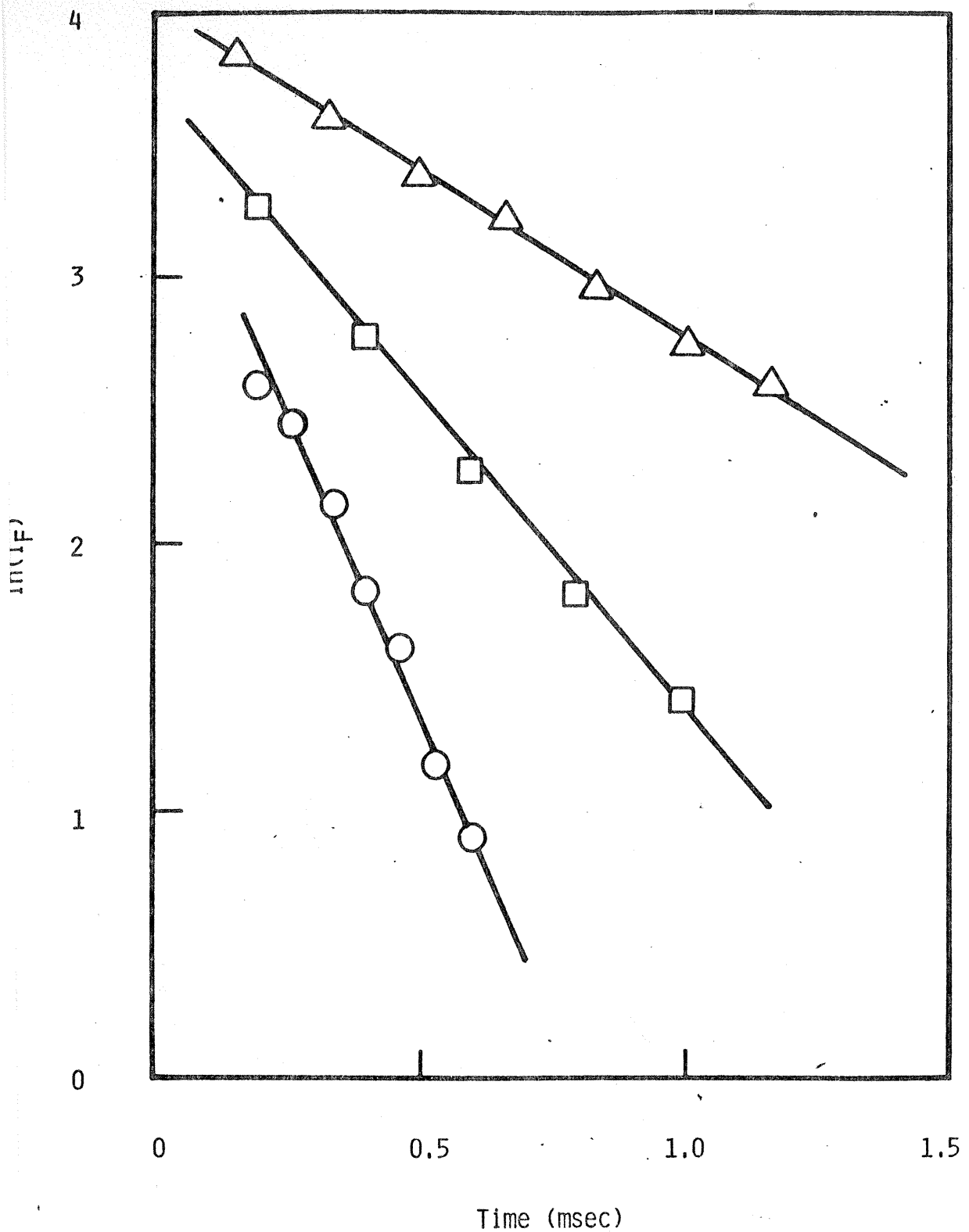
Figure 4.7

Examples of first-order kinetic plots for the decay of the time-resolved atomic emission ($\ln(I_F)$ against t) at $\lambda = 657.3$ nm ($Ca(4^3P_1) \longrightarrow Ca(4^1S_0)$) following pulsed dye-laser excitation of calcium vapour in the presence of nitrogen. (p_{total} with He $= 30$ torr, $T = 1000$ K)

$[N_2] / 10^{15}$ molecules cm^{-3} : $\triangle$ 0.0 ; $\square$ 0.87 ; $\bigcirc$ 2.9

Figure 4.8

Variation of the pseudo first-order rate coefficient (k') for the decay of $Ca(4^3P_J)$ in the presence of nitrogen. (p_{total} with He = 30 torr, T = 1000 K)

for similar reasons of experimental difficulty. Nicks et al.[43] report a value of k_{N_2} = 5.1 x 10^{-13} $cm^3molecule^{-1}s^{-1}$ (ca. 1073 K), with no quoted error, using phase shift measurements. Whilst the agreement within ca. 20% between the result for H_2 using the phase shift technique and that resulting from time-resolved atomic resonance absorption[91] was noted[43] (see later), this disagreement for N_2, by ca. a factor of three, was not, possibly also on account of the experimental difficulties which are particularly significant for this gas. Nicks et al[43] report that the atomic density of calcium rapidly drops to a level which results in a reduction of the signal in their system which becomes too low for measurements when employing N_2. This is attributed to poisoning of the surface of the metallic calcium. Similar effects with nitrogen were observed in this system. Figure (4.7) results from a series of kinetic experiments in which the metallic sample was changed a number of times. Hence, the highest concentration of N_2 employed in these measurements was not determined by the magnitude of the decay constant due to quenching of $Ca(4^3P_J)$ by N_2 but by the loss of signal due to surface poisoning.

Figure (4.9) shows the variation of k' for the decay of $Ca(4^3P_J)$ in the presence of H_2 and D_2, respectively. These plots yield k_{H_2} = 6.0 ± 0.6 x 10^{-14} $cm^3molecule^{-1}s^{-1}$ (1000 K, 1σ), lower than values observed by previous workers [k_{H_2} = 3.4 x 10^{-13} $cm^3molecule^{-1}s^{-1}$ (800 °C)[43]; k_{H_2} = 2.26 ± 0.15 x 10^{-13} $cm^3molecule^{-1}s^{-1}$ (793 K)[91]] although these various measurements have been carried out at different temperatures, and k_{D_2} = 2.7 ± 0.3 x 10^{-14} $cm^3molecule^{-1}s^{-1}$ (1000 K, 1σ) [table (4.3)], a result which has not been reported hitherto. This yields an isotope effect of k_{H_2}/k_{D_2} = 2.2 which can be compared with the analogous ratio for $Mg(3^3P_J)$ of 3.8 reported previously in this work (chapter 3) and that of 2.7 reported by Breckenridge and Stewart.[32] These authors[32] have demonstrated that the kinetic isotope ratio for this type of overall removal process is critically dependent on the role of vibrational energy. This clearly requires more detailed investigation, including the study of CaH and CaD by laser induced fluorescence in order to determine the branching ratio between chemical reaction and energy transfer, at elevated temperatures where vibrational energy in the colliding molecule becomes more important.
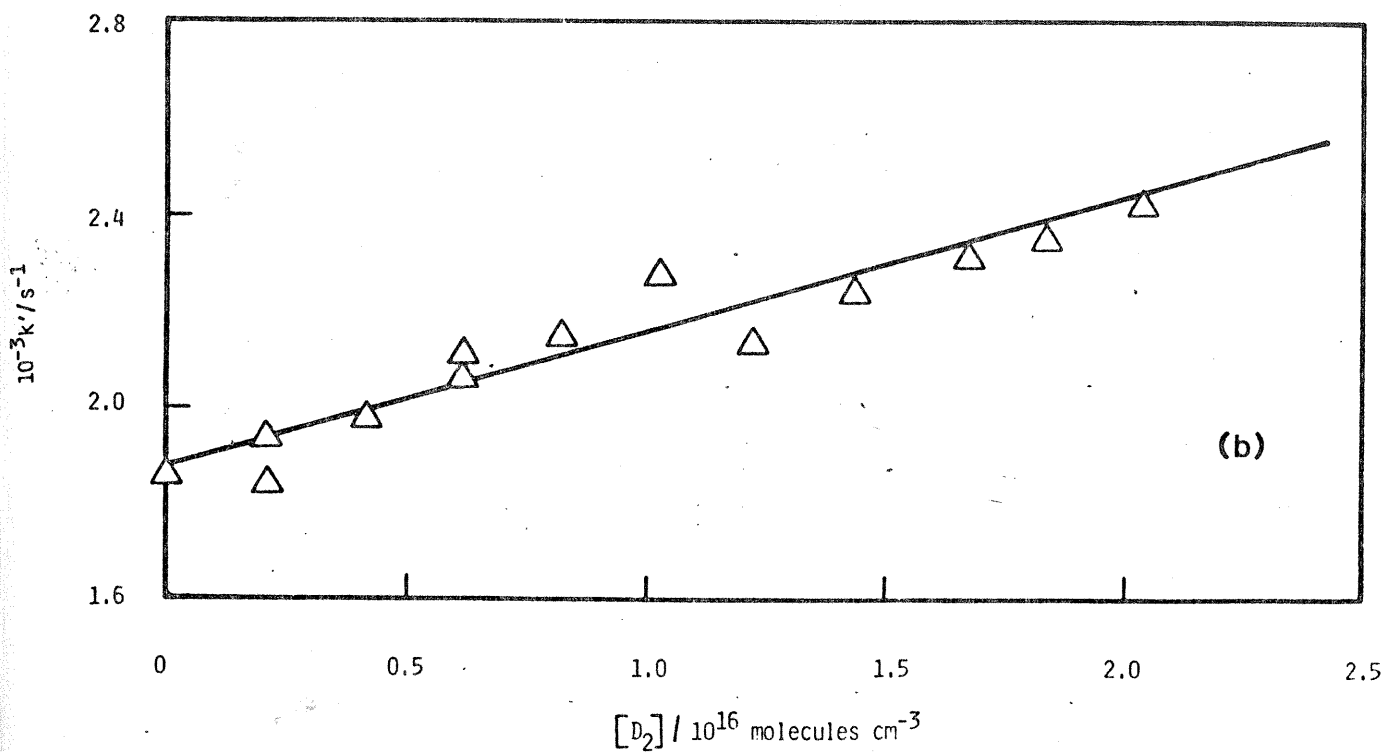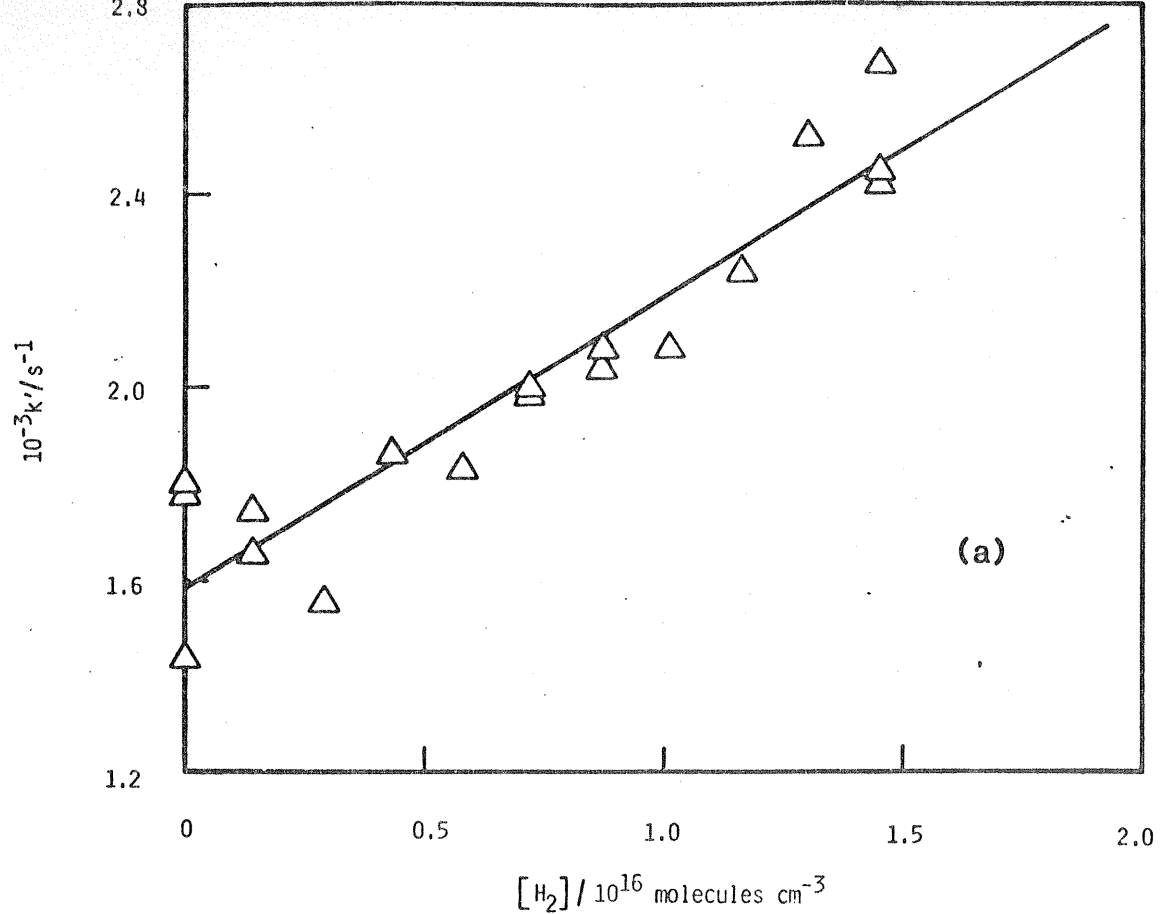
Figure **4.9**

Variation of the pseudo first-order rate coefficient (k') for the decay of Ca(4³P$_J$) in the presence of hydrogen and deuterium.   (p_{total} with the He = 30 torr, T = 1000 K)

(a)   H$_2$;   (b)   D$_2$

Figure (4.10) shows the variation of k' with [CO] and [NO], respectively. The slope of Figure (4.10a) thus yields the absolute second-order rate constant for the collisional removal of $Ca(4^3P_J)$, 1.885 eV above the 4^1S_0 ground state,[10] by CO [table (4.3)]. Figure (4.10b) gives the analogous plot for the other diatomic quenching molecule studied in this investigation, namely, NO. For these two gases, and, indeed, for all the quenching gases studied in this investigation with the single exception of benzene (see later), the sample of solid calcium had to be changed a number of times in order to construct a given plot of k' against [Q]. Inspection on removal of each sample clearly shows the effect of surface reaction. The value of k' for the blank ([Q] = 0) was checked for each change of calcium sample. However, the absolute intensity of the fluorescence signal in the presence of added gases was significantly reduced by surface poisoning and this is the principal cause of the larger scatter in plots of the type shown in Figure (4.10) compared with the analogous plots for $Mg(3^3P_J)$ presented previously (chapter 3) using the present technique. It is this reduction in the absolute magnitude of $I_F(\lambda = 657.3$ nm) rather than the size of the effective time constant of the overall decay of $Ca(4^3P_J)$ (1/k') that determines the largest value of [Q] that may be employed in a kinetic series yielding a plot of k' against [Q].

Figure (4.11) shows the relevant plots of k' against [Q] for the triatomic molecules CO_2 and N_2O. These linear, 18-electron molecules with closed shell structures are of broad fundamental interest in atomic reactions in general[2,4-6] and will be considered later in further detail in the light of orbital correlations and data derived from atomic beam studies. Figure (4.12) shows the results of the investigations with the saturated molecules NH_3, CH_4 and CF_4 and figure (4.13), the results for the unsaturated molecules C_2H_2, C_2H_4 and C_6H_6. In terms of experimental quality of plots of the type based on equation (4.8), that for benzene was found to be the best in these studies [figure (4.13c)]. There was no loss of signal due to surface poisoning and figure (4.13c) was obtained from a single sample of solid calcium. Further, the measured decay rates for $Ca(4^3P_J)$ at the higher concentrations of C_6H_6 clearly show that limitations in construction of the plots k' versus [Q] do not arise from restrictions based on the value of k' but on the reduction in the magnitude

59
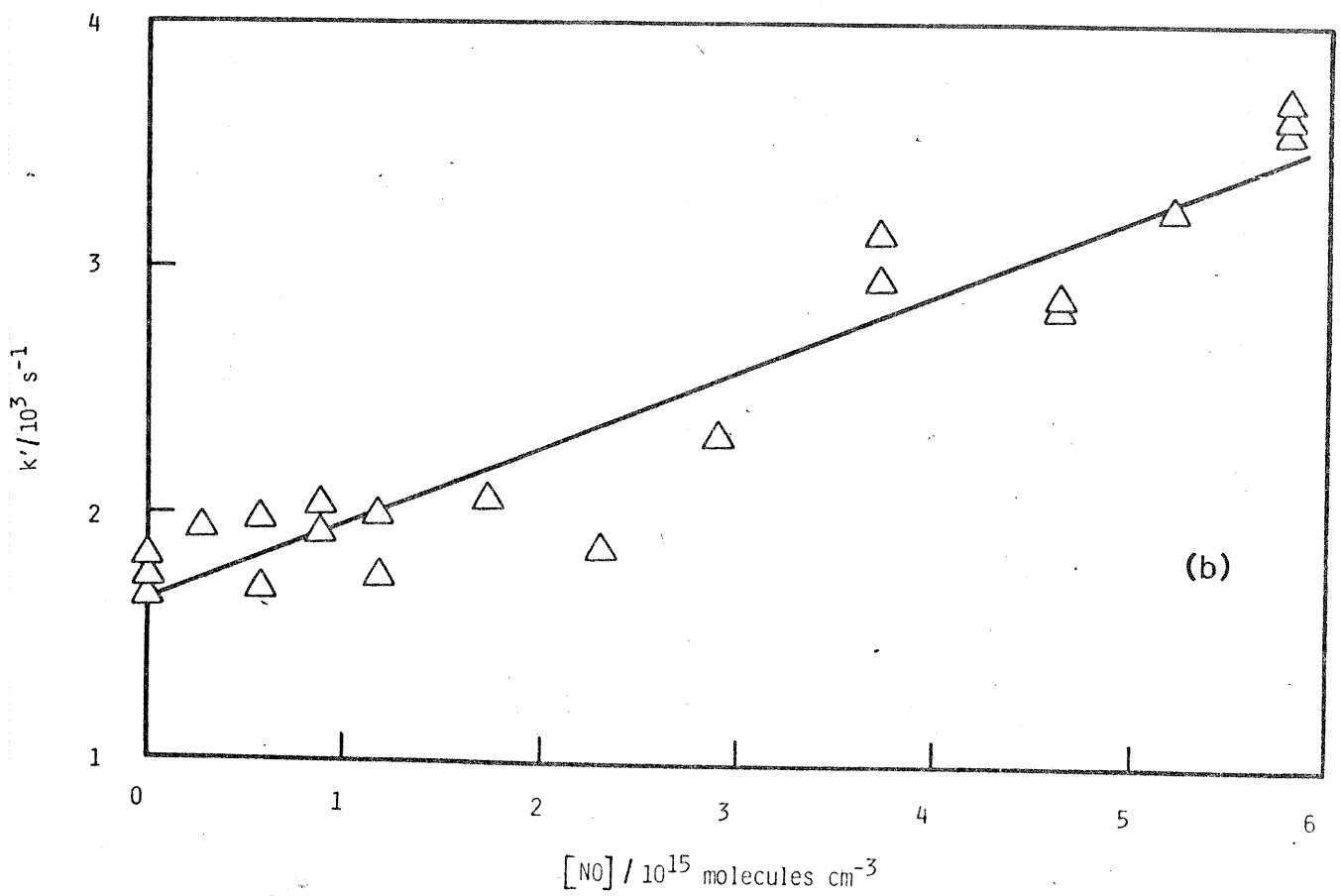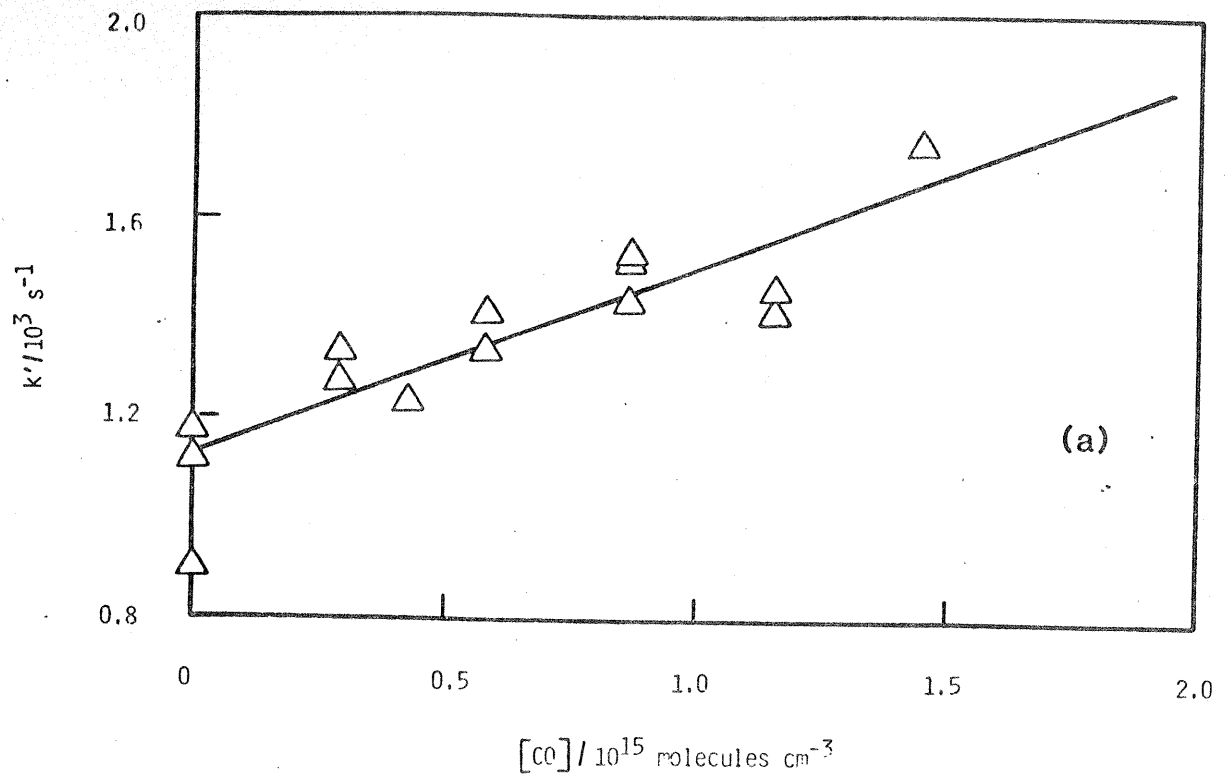
Figure **4.10**

Variation of the pseudo first-order rate coefficient (k') for the decay of $Ca(4^3P_J)$ in the presence of (a) CO and (b) NO. $(p_{total}$ with He $= 30$ torr, T $= 1000$ K)
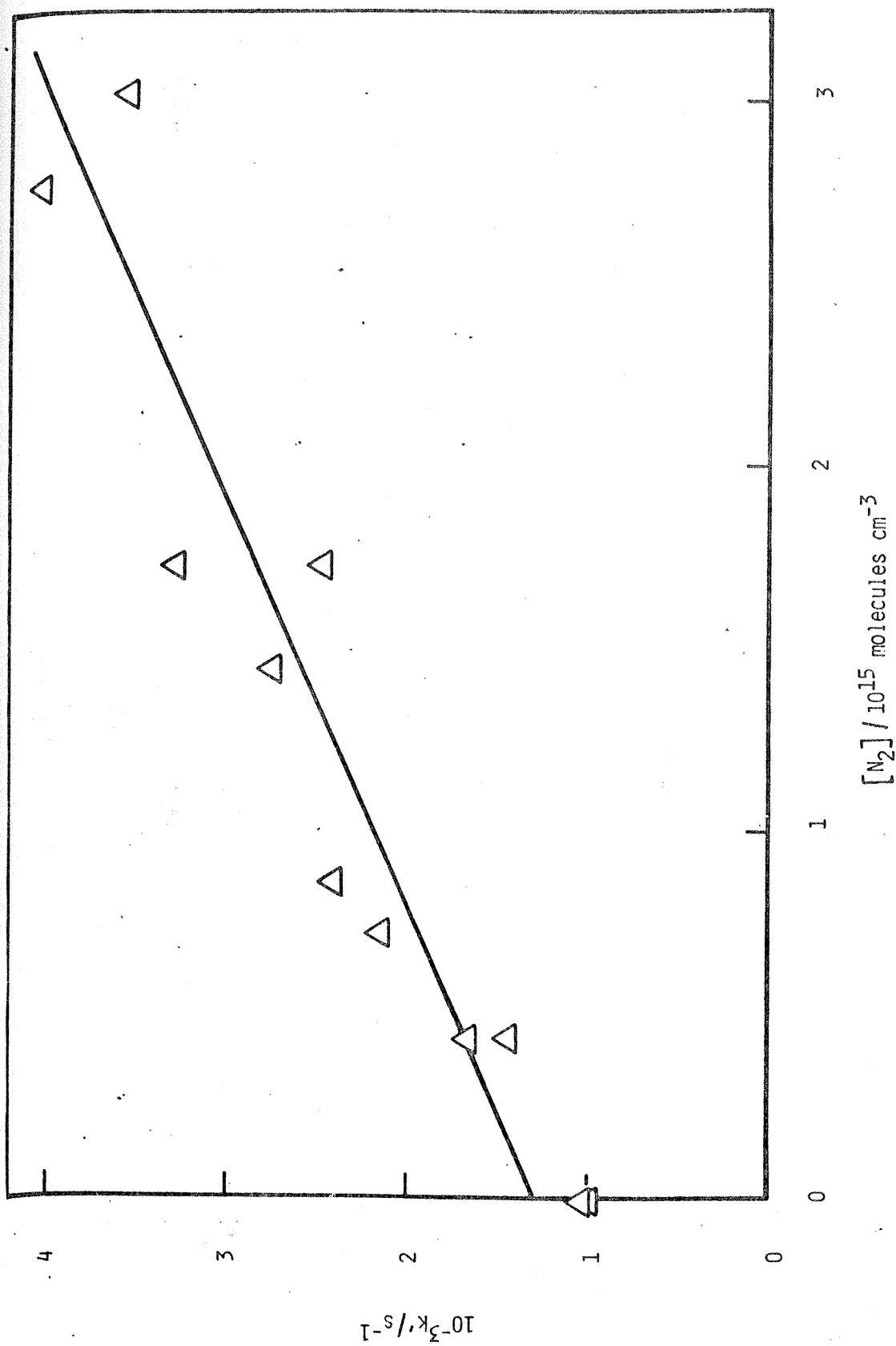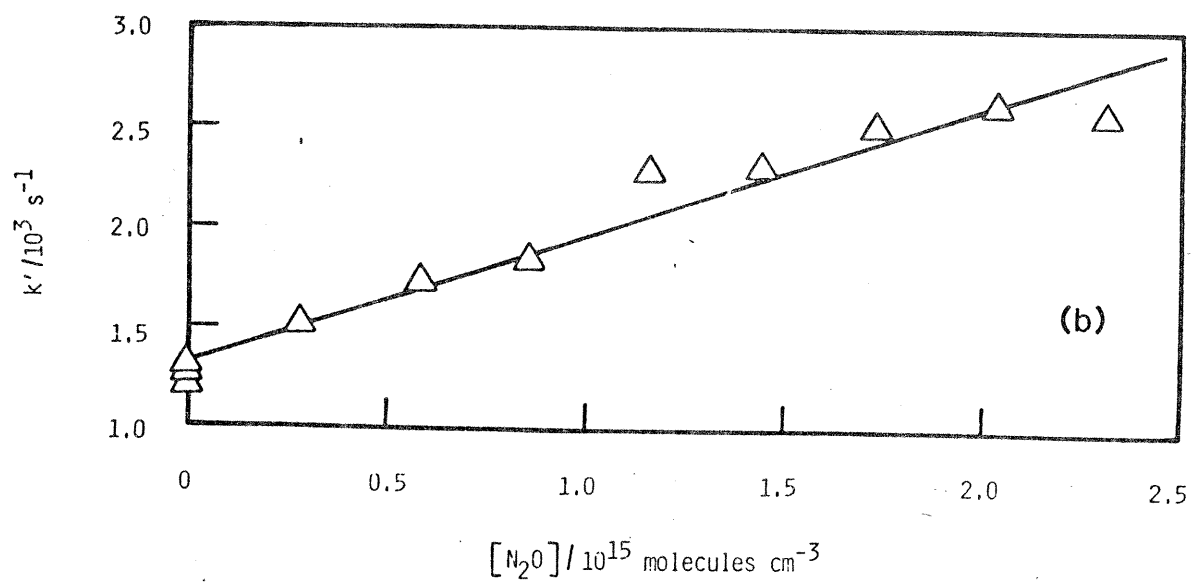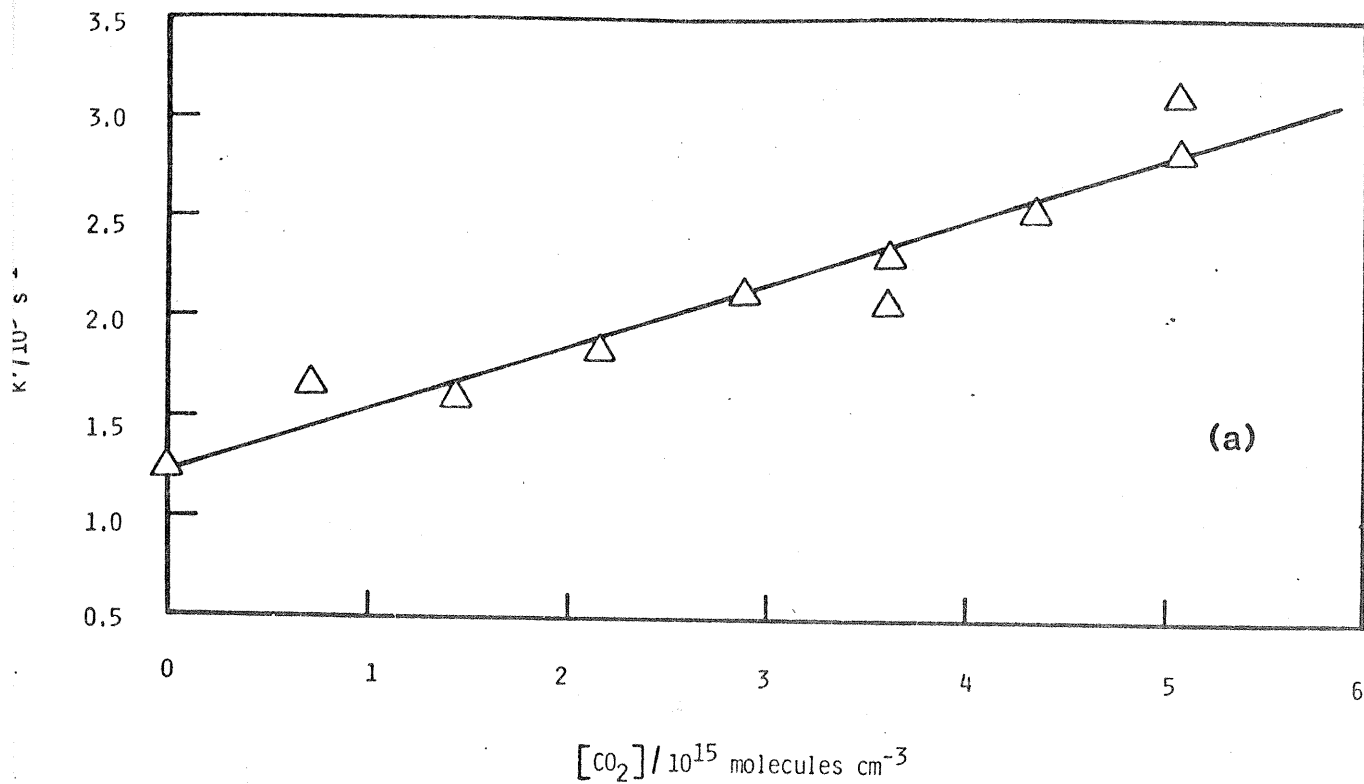
Figure 4.11

Variation of the pseudo first-order rate coefficient (k') for the decay of $Ca(4^3P_J)$ in the presence of (a) CO_2 and (b) N_2O. ($P_{total\ with\ He}$ = 30 torr, T = 1000 K)
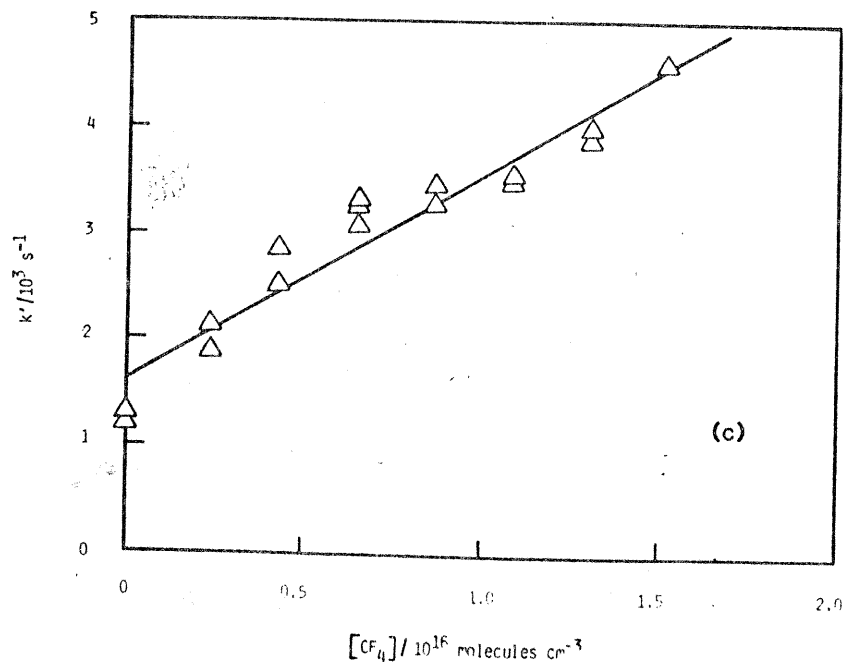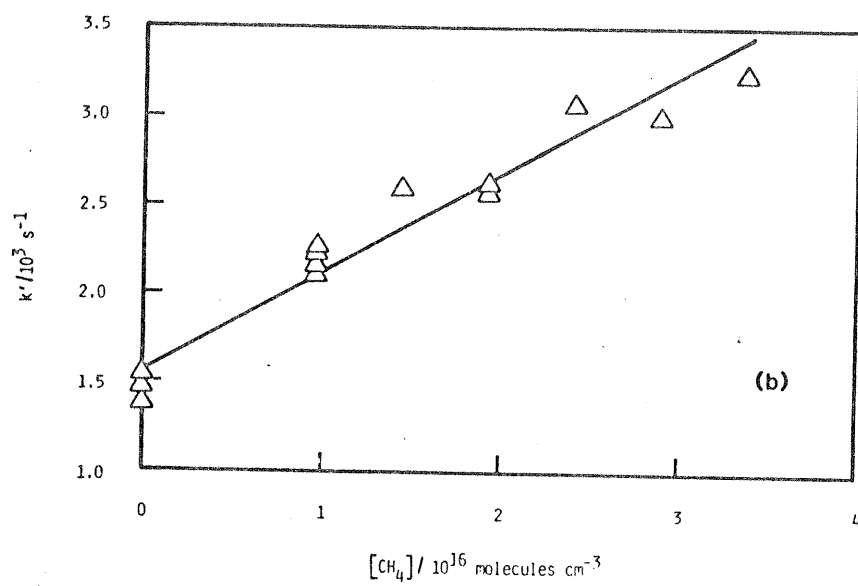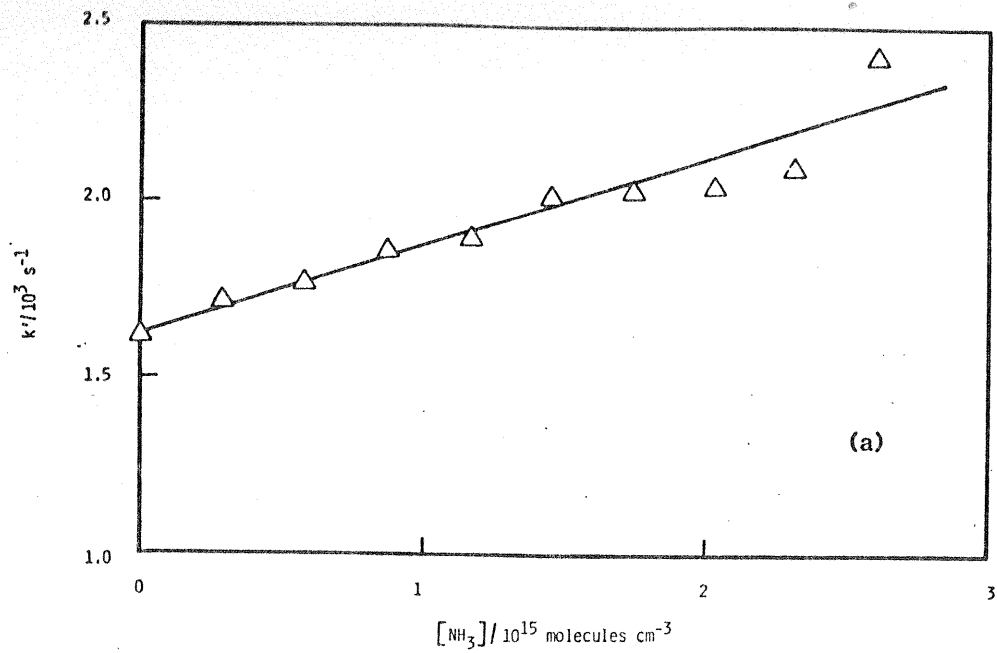
Figure 4.12

Variation of the pseudo first-order rate coefficient (k') for the decay of Ca(4^3P_J) in the presence of (a) NH_3, (b) CH_4 and (c) CF_4. (P_{total} with He = 30 torr, T = 1000 K)
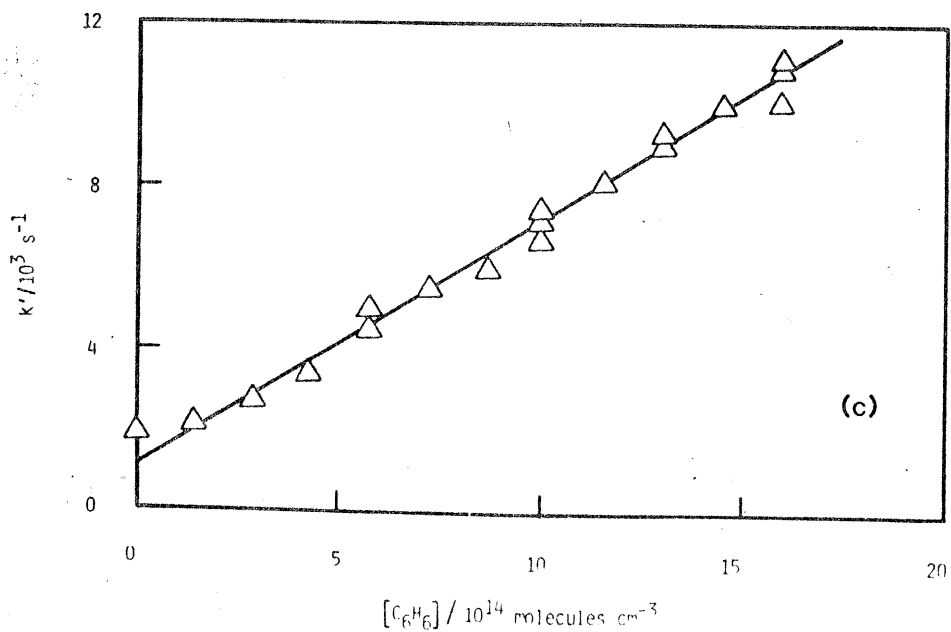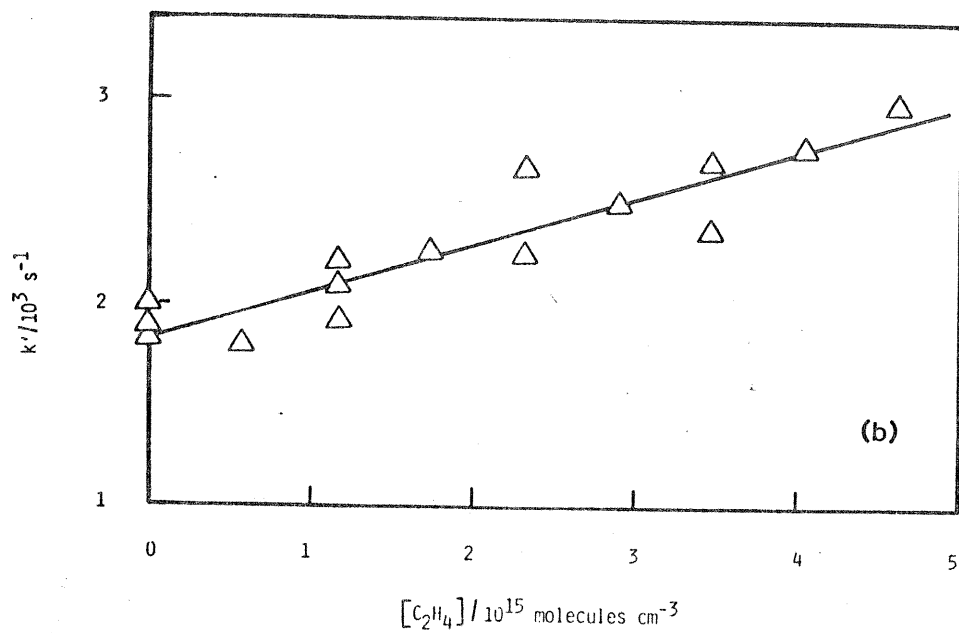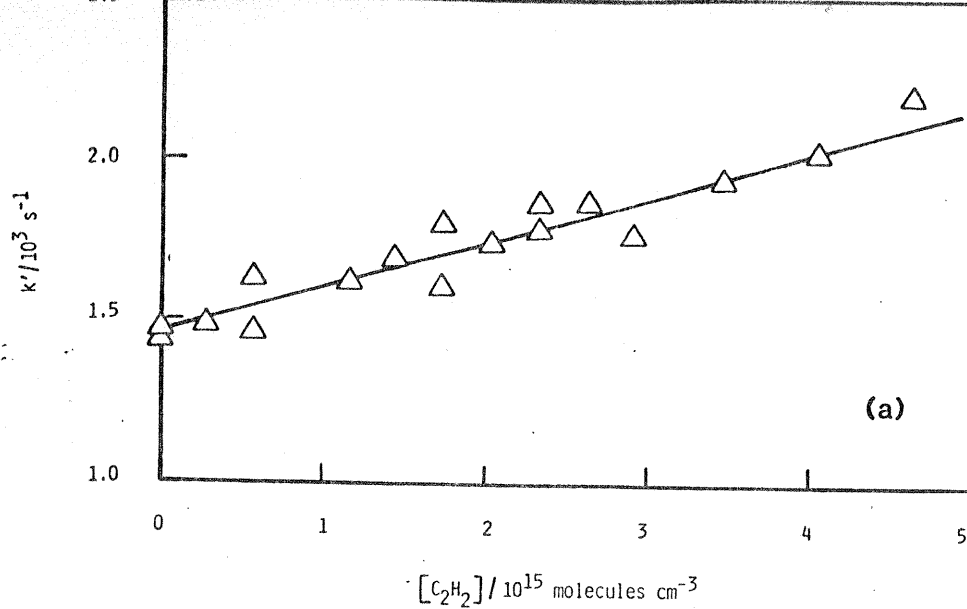
Figure **4.13**

Variation of the pseudo first-order rate coefficient (k') for the decay of Ca(4^3P_J) in the presence of (a) C_2H_2, (b) C_2H_4 and (c) C_6H_6. (P_{total} with He = 30 torr, T = 1000 K)

of the absolute signal of I_F. Notwithstanding these limitations, these experiments clearly show that the present method can be used to determine absolute rate constant for the collisional quenching of $Ca(4^3P_J)$ by a wide range of collision partners. These values of k_Q, derived from slopes of the plots given in figures (4.10) to (4.13), are presented in table (4.3) together with data, where available, from other investigations.

TABLE 4.3

Absolute second-order rate constants (k_Q, $cm^3 molecule^{-1} s^{-1}$) for the collisional quenching of $Ca(4^3P_J)$, generated by dye-laser excitation, by added quenching gases, Q.

Q	k_Q		Ref.
He	$\leq 4 \times 10^{-15}$	(1000 K)	(*)[a]
	2.13×10^{-15}	(ca. 1050 K)	(41)[b]
Ne	$\leq 4 \times 10^{-15}$	(1000 K)	(*)[a]
	2.23×10^{-15}	(ca. 1000 K)	(41)[b]
	$\sim 8 \times 10^{-21}$	(793 K)	(91)[c]
Ar	$\leq 4 \times 10^{-15}$	(1000 K)	(*)[a]
	4.8×10^{-15}	(ca. 1050 K)	(41)[b]
	$\sim 8 \times 10^{-21}$	(793 K)	(91)[c]
Kr	$\leq 4 \times 10^{-15}$	(1000 K)	(*)[a]
	6.11×10^{-15}	(ca. 1050 K)	(91)[b]
Xe	$2.4 \pm 0.3 \times 10^{-14}$	(1000 K)	(*)[a]
	6.70×10^{-15}	(ca. 1050 K)	(41)[b]
H_2	$6.0 \pm 0.6 \times 10^{-14}$	(1000 K)	(*)[a]
	$2.26 \pm 0.15 \times 10^{-13}$	(793 K)	(91)[c]
	3.4×10^{-13}	(1073 K)	(43)b

TABLE 4.3 (continued)

Q	k_Q		Ref.
D_2	$2.7 \pm 0.3 \times 10^{-14}$	(1000 K)	(*)[a]
N_2	$8.9 \pm 0.9 \times 10^{-13}$	(1000 K)	(*)[a]
	$1.8 \pm 0.39 \times 10^{-13}$	(793 K)	(91)[c]
	5.1×10^{-13}	(1073 K)	(43)[b]
CO	$3.7 \pm 0.5 \times 10^{-13}$	(1000 K)	(*)[a]
	3.2×10^{-13}	(1073 K)	(43)b
NO	$3.2 \pm 0.3 \times 10^{-13}$	(1000 K)	(*)[a]
CO_2	$3.1 \pm 0.3 \times 10^{-13}$	(1000 K)	(*)[a]
	1.5×10^{-13}	(1073 K)	(43)[b]
N_2O	$6.5 \pm 0.5 \times 10^{-13}$	(1000 K)	(*)[a]
NH_3	$2.5 \pm 0.3 \times 10^{-13}$	(1000 K)	(*)[a]
CH_4	$5.4 \pm 0.4 \times 10^{-13}$	(1000 K)	(*)[a]
	3.1×10^{-14}	(1073 K)	(43)[b]
CF_4	$1.9 \pm 0.2 \times 10^{-13}$	(1000 K)	(*)[a]
C_2H_2	$1.4 \pm 0.2 \times 10^{-13}$	(1000 K)	(*)[a]
C_2H_4	$2.3 \pm 0.3 \times 10^{-13}$	(1000 K)	(*)[a]
C_6H_6	$6.0 \pm 0.2 \times 10^{-12}$	(1000 K)	(*)[a]

a – Pulsed dye-laser excitation + time-resolved atomic resonance fluorescence

b – Modulated dye-laser excitation + Phase shift measurements

c – Dye-laser excitation + time-resolved atomic resonance absorption spectroscopy

(*) This work

The absolute rate constants for the collisional quenching of $Ca(4^3P_J)$, by the noble gases, H_2, D_2 and N_2 have already been considered in detail,

although comparison with analogous data for $Mg(3^3P_J)$ has not been made apart from reference to data for the noble gases. Thus, for $Mg(3^3P_J)$, the gases Kr and Xe exhibit measurable quenching rates whereas only xenon of the noble gases demonstrates a measurable efficiency for collisional quenching of $Ca(4^3P_J)$. In broad comparative terms, quenching of $Ca(4^3P_J)$ by H_2 and D_2 proceed at rates approximately one tenth of those for the analogous processes with $Mg(3^3P_J)$ [table (3.3)] whilst, for N_2, the deactivation rates are similar for both electronically excited atoms [Table (4.3)]. For the data on $Ca(4^3P_J)$ derived in the present investigation, that for CO [table (4.3)] is in agreement with the quenching rate constant obtained from phase shift measurements[43] though, in view of the difficulty in interpreting such phase shifts, it is not clear if one can conclude whether this agreement is fortuitous or not. The disagreement with the data for the noble gases resulting from phase shift measurements[41] has been discussed in detail. It is found, further, that, as with those gases, the present technique yields a lower value for k_{CH_4} [see later, table (4.3)].[43] For NO, and the remaining collision partners studied here, there are no rate data for $Ca(4^3P_J)$ with which the present results may be compared, neither does it appear that a quenching constant for $Mg(3^3P_J)$ + NO has been reported. The observed quenching efficiency for the removal of $Ca(4^3P_J)$ by NO [table (4.3)] presumably reflects the strong chemical interaction between these two species, a property observed in the kinetic behaviour describing collisions between other metal atoms in ^3P states [e.g. $Pb(6^3P_0, 6^3P_1, 6^3P_2)$;[93,94] $Sn(5^3P_0, 5^3P_1, 5^3P_2)$[95,96]].

The collisional quenching of $Ca(4^3P_J)$ by the triatomic molecules CO_2 and N_2O is described in a detail similar to that given previously for $Mg(3^3P_J)$ (2.71 eV) following analogous considerations of orbital symmetry and the effect of the 18 electrons closed shell structures of these molecules on atomic abstraction reactions in general.[3-6] Firstly, we may note the comparable magnitudes of the quenching rates constants for $Ca(4^3P_J)$ [table (4.3)] and for $Mg(3^3P_J)$ + N_2O {$k[Mg(3^3P_J) + N_2O]$ = $4.9 \pm 0.3 \times 10^{-13}$ $cm^3 molecule^{-1}s^{-1}$, (800 K)}, obtained by a similar technique as described here. O-atom abstraction is highly exothermic for the electronically excited calcium atom;

$$Ca(4^3P_J) + N_2O \longrightarrow CaO + N_2 \qquad \Delta H = -4.97 \text{ eV}$$

62
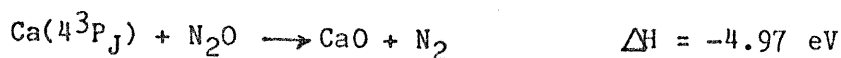
[$D(N_2-O) = 1.677$ eV;[69] $D_0^O(CaO(X^1\Sigma^+) \gtrsim 4.76 \pm 0.15$ eV[70]] and hence a set of electronically excited states of CaO are energetically accessible. Irvin and Dagdigian[92] have studied the chemiluminescence from the reaction of $Ca(4^3P_J) + N_2O$ under single collision conditions. Emission from the electronic states of CaO arising from the reaction of $Ca(4^1D_2)$ generated in the low voltage discharge from which the atoms are derived is relatively small and corrections from this contribution can readily be made. The emission resulting from the collision of $Ca(4^3P_J) + N_2O$ arises from a group of states of CaO in the region of 3.5 eV ($C^1\Sigma^+$, $^{3,1}\Sigma^-$, $D^1\Delta$, $d^3\Delta$, $^3\Sigma^+$, $B^1\Pi$ and $^3\Pi$) to the low lying $A^1\Pi$ and $a^3\Pi$ states. The emission is further complicated by the role of highly rotationally excited emitting molecules overlain by continuous emission. Clearly, the system is too complex for the large number of pathways to chemical products, including $CaO(X^1\Sigma^+)$ and also to physical quenching, to be characterised quantitatively at this stage. What is clear is that these observations are not in accord with the correlations based on C_s symmetry using the weak spin orbit coupling approximation,[17,92] the correlation diagram for which is given by Irvin and Dagdigian.[92] Quenching of $Ca(4^3P_J)$ by CO_2 [table (4.3)], marginally more efficient than reported from phase shift measurements,[43] is found to be a factor of approximately three times slower than that for $Mg(3^3P_J)$ {$k[Mg(3^3P_J) + CO_2] = 1.0 \pm 0.1 \times 10^{-12}$ $cm^3 molecule^{-1}s^{-1}$ (800 K)}. The thermochemistry indicates that only the low lying $a^3\Pi$ (1.03 eV)[70] and $A^1\Pi$ (1.045 eV)[70] states are accessible on reaction;

$$Ca(4^3P_J) + CO_2 \longrightarrow CaO + CO \qquad \Delta H = -1.19 \text{ eV}$$
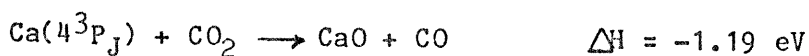
[$D(CO-O) = 5.453$ eV[69]]. Pasternack and Dagdigian,[48] who argue for a thermochemistry of -1.38 eV for the reaction, have monitored these two low lying states as well as the ground state of CaO by laser-induced fluorescence, in the single-collision condition and report that for the processes;

$$Ca(4^3P_J) + CO_2 \quad
\begin{array}{c}
\overset{k_1}{\nearrow} \quad CaO(a^3\Pi,\ A^1\Pi) + CO(X^1\Sigma^+) \\
\underset{k_2}{\searrow} \quad CaO(X^1\Sigma^+) + CO(X^1\Sigma^+)
\end{array}$$
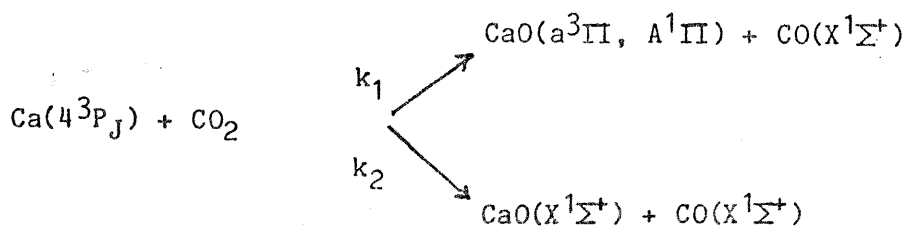
$k_1/k_2 = 0.3$ to within a factor of two. The part played by physical quenching is also clearly of interest here. As with N_2O, it is apparent that the weak spin orbit coupling approximation breaks down in the production of singlet states of CaO.

For the larger polyatomic molecules, we may only note general comparisons with analogous data for $Mg(3^3P_J)$ and with thermochemistry. Quenching of $Mg(3^3P_J)$ by NH_3 has not been reported. H-atom abstraction from NH_3 by $Ca(4^3P_J)$ would be endothermic [$D(NH_3) = 4.38$ eV;[69] $\Delta H = +0.795$ eV] hence removal must proceed via physical quenching. The quenching rate [table (4.1)] is of similar magnitude to those reported for $Hg(6^3P_0)$ and $Cd(5^3P_{0,1})$ by this molecule.[9] The collisional removal of $Ca(4^3P_J)$ by CH_4 and CF_4 are characterised by absolute rate constants [table (4.1)] which are significantly greater than those for $Mg(3^3P_J)$ for no obvious reason apart from the quantity of energy to be transfered on collision. H-atom abstraction by $Ca(4^3P_J)$ for the former would be highly endothermic whereas F-atom abstraction for the latter, highly exothermic $\{D(CH_4) = 4.406$ eV;[69] $D(CF_4) = 5.3$ eV;[75] $D_0^o[CaH(X^2\Sigma)] \leq 1.70$ eV;[70] $D_0^o CaF(^2\Sigma^+) = 5.48$ eV[70]$\}$. By contrast, quenching of $Ca(4^3P_J)$ by the unsaturated molecules C_2H_2, C_2H_4 and C_6H_6 proceeds at rates which are at least a factor of ca. 100 slower than the analogous processes for $Mg(3^3P_J)$. Detailed discussion of individual quenching processes by these unsaturated molecules is too speculative to be fruitful. Clearly, the scatter in the rate data for $Ca(4^3P_J)$ is considerably larger than that for the analogous study with $Mg(3^3P_J)$ though not for C_6H_6 [figure (4.13c)], for experimental reasons indicated above. However, the orders of magnitude differences for the unsaturated molecules lie well outside the range due to scatter. It is clear that the study of absolute rate constants for the collisional quenching of $Ca(4^3P_J)$ by corrosive, oxidising gases will need to be carried out by an alternative procedure to that of a flow of the reactant gas over a heated metal.

5. KINETIC STUDY OF STRONTIUM ($5\,^3P_J$)

The investigation on $Sr(5\,^3P_J)$, using experimental techniques similar to those described in the preceding chapters for $Mg[3s3p(^3P_J)]$ and $Ca[4s4p(^3P_J)]$, respectively 2.71 and 1.883 eV above their $ns^2(^1S_0)$ ground states, presents some further features that deserve a brief consideration. Firstly, the forbidden transition $Sr(^3P_1 \rightarrow\ ^1S_0)$ is much more allowed than the corresponding transitions for Mg and Ca, which may easily be seen by comparison of the Einstein coefficients, A_{nm}. As a consequence, the production of the ^3P_J states by optically pumping the ground $^1S_0$ state should be easier than it was in the previous studies of magnesium and calcium. On the other hand, a bigger Einstein coefficient implies a shorter mean radiative lifetime. The energy spacings in the ^3P_J manifold are bigger than those for Mg and Ca, which might result in a non-Boltzmann equilibrium following optical excitation. Further, there will be a greater breakdown in the weak spin-orbit coupling assumption, and the corresponding effect on collisional behaviour as seen through symmetry arguments. For effective optical pumping of the ground $^1S_0$ state of strontium to the $^3P_1$ excited state, the dye-laser must operate at $\lambda =$ 689.3 nm, which is achieved by pumping the dye (Nile Blue 690) with the second harmonic of the Nd-YAG primary laser ($\lambda =$ 532 nm). The dye was employed as a solution 4×10^{-4} M in methanol, since this is the concentration which renders the maximum laser output. The output energy at $\lambda =$ 689.3 nm was ca. 5 mJ per pulse (pulse length = ca. 20 ns; pulse width = ca. 0.1 cm^{-1}; repetition rate = 10 Hz).

The use of the long wavelength fluorescence transition at $\lambda =$ 689.3 nm to monitor $Sr(5\,^3P_1)$ subsequent to dye-laser excitation at the same wavelength requires special attention to the elimination of scattered light. This primarily arises from the need to employ a photomultiplier with a long wavelength "S20" response (p.m. tube E.M.I. 9797B; operating voltage = 750 V; Brandenburg power supply 415R, 0 - 2.2 kV) and the short decay times over which the fluorescence is monitored. The principle of initiating the gating system of a photomultiplier tube using the initial

pulse generated in the primary laser in order to apply a voltage across a pair of dynodes, and so switch on the gate for length t, follows that described in the previous chapters. By employing the delay between the process of energy storage in the neodymium-YAG rod and the operation of the Pockels cell 180 μs subsequent to this, the p.m. tube is switched on at a time $(t - 180 \mu s)$ following the dye-laser pulse. The practice, however, of using fixed "gate times" in a circuit of the type originally reported by Acuna et al.[55] for the p.m. tube E.M.I. 6256B and subsequently employed in this type of measurement for $t = 300 \mu s$, is clearly not ideal when fluorescence needs to be measured in the range 50 - 200 μs, quite apart from the construction of a circuit appropriate to the "S20" tube. In this particular application, a circuit has been employed which permits fine tuning of the gate length in order to minimise the value of $(t - 180 \mu s)$ for the operating conditions of this system. [1] The essence of the circuit is based upon a CMOS 4001B NOR logic chip connected as a monostable. The circuit includes seven switched timing ranges each with fine tuning effected by means of a helipot, permitting continuous tuning over the range 8 - 720 μs. The procedure for "gating off" the photomultiplier is to employ a high voltage switch (BF 259 transistor) to short the D4, D5 and D6 dynodes of this eleven stage p.m. tube for the time, t. The minimum gate length $(t - 180 \mu s)$ should be a function of the "rise time" of the p.m. tube (ca. 2 ns). In practice, it is determined by light collection of the optical system. Thus, using a set of circular baffles in the outlet arm of the stainless steel reactor yielding greater physical elimination of scattered light, a gate time of $(t - 180 \mu s) = $ ca. 1 μs can readily be achieved. This is, of course, at the expense of the magnitude of the fluorescence signal. It was found preferable to increase the light gathering power of the detection system by the elimination of this baffle system, requiring a gate time of $(t - 180 \mu s) = $ ca. 5 μs but permitting monitoring of the exponentially decaying fluorescence signal at much longer times.

---

[1] Mr. J. Guttridge and his colleagues of the electronics workshop of the Department of Physical Chemistry are deeply thanked for the design and construction of this circuit.

The vapour pressure of strontium is high enough for the work to be carried out about the same temperature as that employed for magnesium. Actually, the experiments on $Sr(5^3P_J)$ were carried out at T = 950 K, which correspond to a strontium vapour pressure of 0.3 Torr.

By contrast with earlier studies, (Chapters 3 and 4), fluorescence measurements were made across a convenient temperature range (ca. 850 - 1000 K) over which the concentration of ground state strontium atoms varies by a factor of ca. 100.[88,89] This was carried out in order to investigate the role of radiation trapping in this system and also the quenching of $Sr(5^3P_J)$ by $Sr(5^1S_0)$. The lowest temperature employed was simply determined by the magnitude of the fluorescence signal that could be monitored with the present experimental arrangement. This is, of course, much higher than the temperature range employed in the sealed system by Havey et al. (643 - 733 K).[97]

The boxcar integrator, taking into account the relatively shorter mean radiative lifetime of $Sr(5^3P_J)$ was adjusted so that a gate of 10 μs was scanned through the signal in a reading time of 100 s.

Unlike the various measurements that have been described on $Mg(3^3P_J)$ and $Ca(4^3P_J)$ resulting from monitoring of the emission $^3P_1 \longrightarrow {}^1S_0 + h\nu$ in the time-resolved mode following dye-laser excitation (see previous chapters), the only analogous study that has been described for $Sr(5^3P_J)$, appears to be a measurement of the mean radiative lifetime reported by Havey et al.[97] The rate constants that have been reported by Malins et al.[42] for the collisional quenching of $Sr(5^3P_J)$ by the noble gases were, in fact, derived from phase shift measurements following dye laser excitation of $Ca(4^1S_0)$ to $Ca(4^3P_1)$ and subsequent energy transfer from $Ca(4^3P_J)$ to $Sr(5^1S_0)$. These measurements were not, of course, carried out in "real-time". Detailed investigations of collisional processes undergone by $Sr(5^3P_J)$ with added molecules have primarily been carried out using chemiluminescence from electronically excited product molecules in molecular beams.[29,35,51,98,99] Atomic emission from $Sr(5^3P_1)$ has been detected from flames containing strontium with added N_2O + CO and has been considered from a mechanistic viewpoint.[26,100]

The present investigation describes a study of the atomic emission, $Sr(5\,^3P_1) \rightarrow Sr(5\,^1S_0) + h\nu$ at $\lambda = 689.3$ nm in the time–domain following direct pulsed dye–laser excitation of $Sr(5\,^1S_0)$. These studies, as stated earlier, involved particular modification to the detection system employed previously on account of the much shorter mean radiative lifetime (τ_e) of $Sr(5\,^3P_1)$. Time–resolved emission at $\lambda = 689.3$ nm in the "single–shot mode" following pulsed dye–laser excitation on a static system and employing oscilloscopic monitoring has been used by Havey et al. to measure $\tau_e[Sr(5\,^3P_1)]$.[97] Various other techniques have been employed to measure $\tau_e[Sr(5\,^3P_1)]$ including steady emission intensity measurements,[12,20,101] the "hook" interferometric technique,[80] double resonance methods[102-104] and atomic beam studies employing a modulated discharge,[105] The resulting values vary by about a factor of ten (see later). The mean radiative lifetime of $Sr(5\,^3P_1) \rightarrow Sr(5\,^1S_0) + h\nu$ at $\lambda = 689.3$ nm has also been the subject of theoretical calculations.[23,87] In the present investigations, time–resolved emission has been investigated in all the noble gases and at different temperatures, primarily to study the effect of radiation trapping, which is significant in this system, and also the collisional quenching of $Sr(5\,^3P_J)$ by $Sr(5\,^1S_0)$. This is found to be negligible as is collisional quenching by all the noble gases, and only upper limits for the rate constants may be assigned. This latter aspect may be contrasted with the collisional quenching of $Mg(3\,^3P_J)$ and $Ca(4\,^3P_J)$ by the heavier noble gases.

Figure (5.1) shows typical examples of the XY-output for the variation of the fluorescence intensity (I_F) at $\lambda = 689.3$ nm with time $[Sr(5\,^3P_1) \rightarrow Sr(5\,^1S_0) + h\nu]$ following dye-laser excitation of strontium vapour in helium at two different temperatures (900 and 950 K). These decays may be contrasted immediately with analogous measurements on $Mg(3\,^3P_J)$ and $Ca(4\,^3P_J)$ where typical decay times were, respectively, 5 and 2 ms. First-order kinetic plots $[\ln(I_F)$ against $t]$ may readily be constructed from decay traces of the type shown in Figure (5.1) and these are shown in Figure (5.2) for the experimental conditions of the former. The negative of the slopes of these first-order plots then yield the
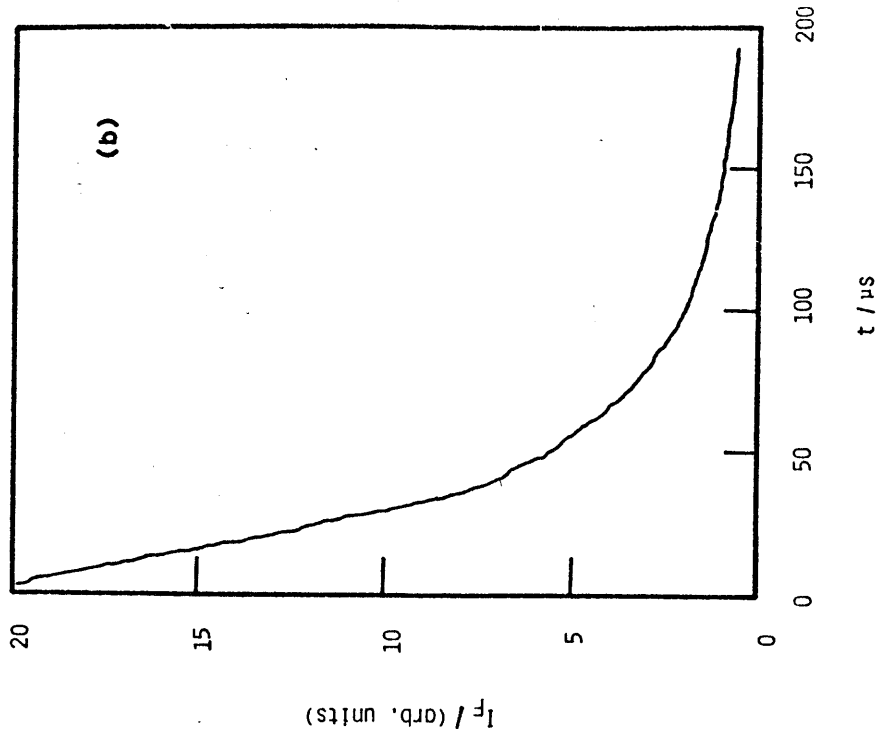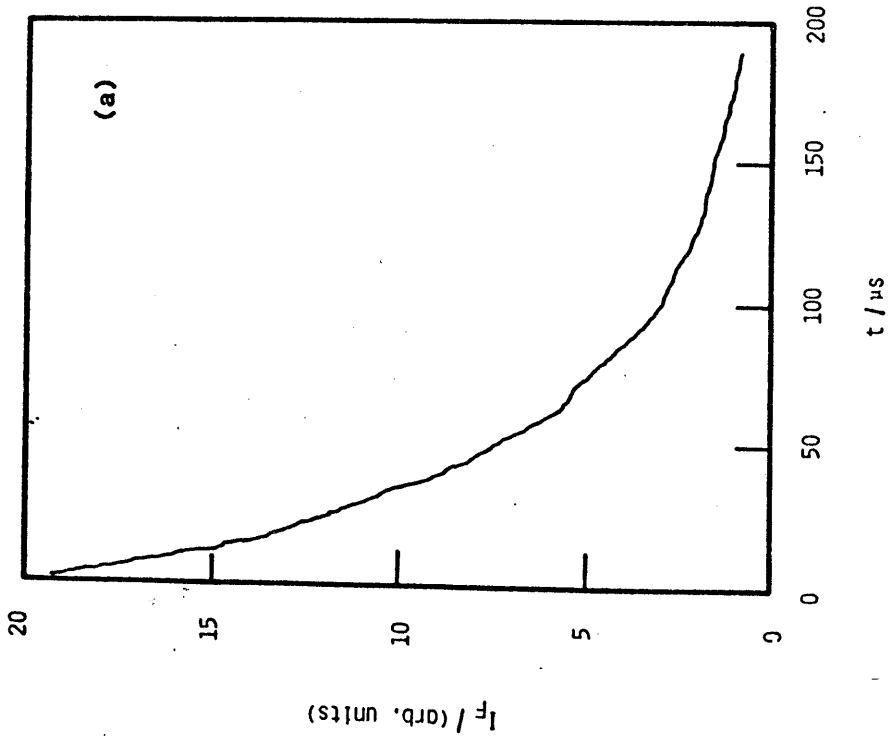
Figure **5.1**

Examples of the output of the XY recorder indicating the decay of the time-resolved atomic emission (I_F) at λ = 689.3 nm (Sr(5s5p($^3P_1$)) $\longrightarrow$ Sr(5s^2($^1S_0$))) following pulsed dye-laser excitation of strontium vapour to the 5^3P_1 state in the presence of helium. (p_{He} = 30 torr)

(a) T = 950 K ; (b) T = 900 K.
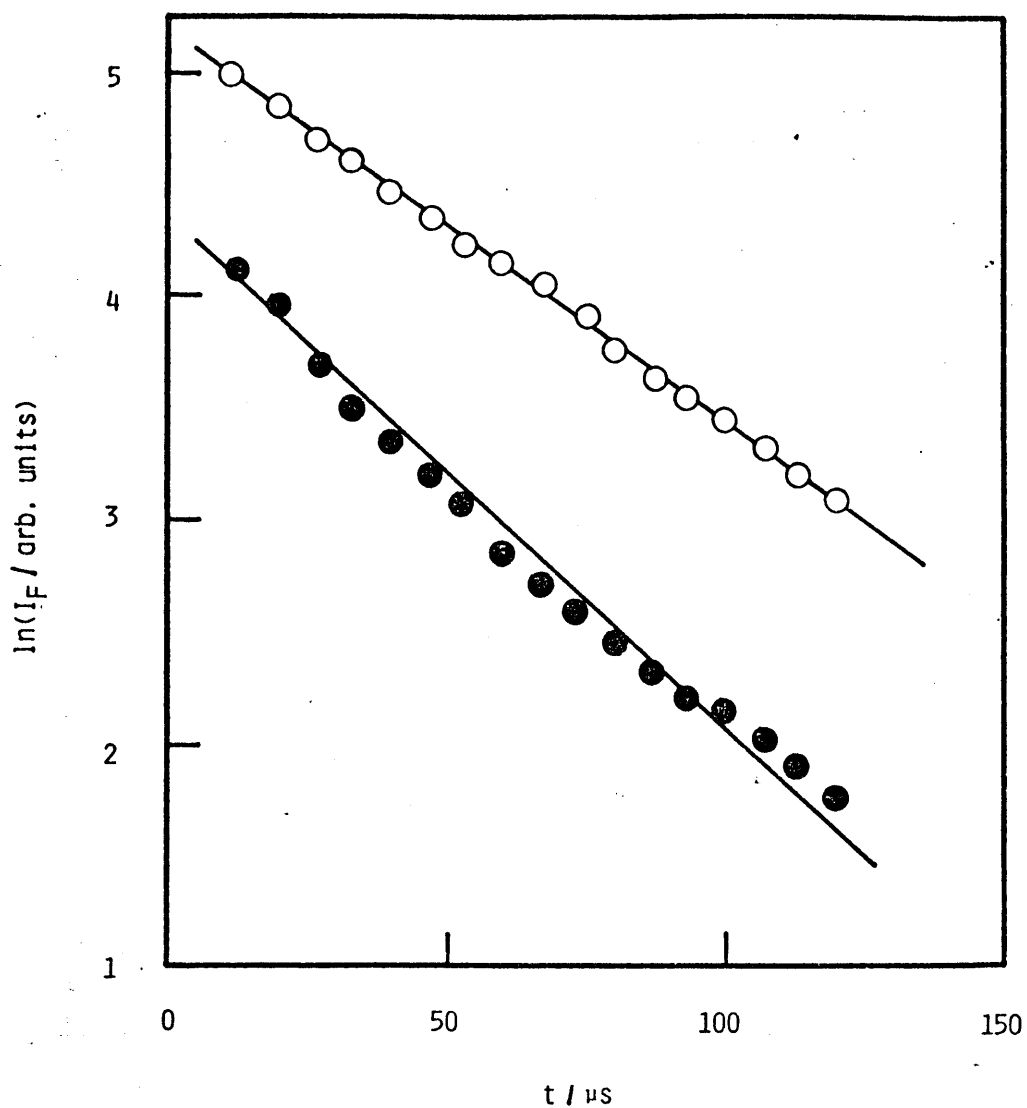
Figure **5.2**

Examples of first-order kinetic plots for the decay of the time-resolved atomic emission $(\ln(I_F)$ against t) at $\lambda = 689.3$ nm $(Sr(5^3P_1) \longrightarrow Sr(5^1S_0))$ following pulsed dye-laser excitation of strontium vapour in the presence of helium. $(p_{He} = 30$ torr$)$

○   T = 950 K ;   ●   T = 900 K.

overall first-order decay coefficient (k') for $Sr(5^3P_J)$. Following the procedure of the previous investigations for $Mg(3^3P_J)$ and $Ca(4^3P_J)$, we may write:

$$-d\{\ln[Sr(5^3P_0)]\}/dt = -d\{\ln[Sr(5^3P_1)]\}/dt = -d\{\ln[Sr(5^3P_2)]\}/dt$$

$$= k' = A_{nm}/(1 + 1/K_1 + K_2) + \beta'/p_M + \Sigma k_Q[Q] \quad (5.1)$$

The 5^3P_0 and 5^3P_2 states, as in the case of Mg and Ca (see chapters 3 and 4), are highly optically metastable with respect to the 5^1S_0 ground state and are so called "reservoir" states, spontaneous emission from them being neglected.[9,60] By empirical considerations[61] of the energy to be transfered on collision (5^3P_0, E = 14318; 5^3P_1, E = 14504; 5^3P_2, E = 14899 cm^{-1})[10] and by analogy with the direct observations of McIlrath and Carlsten[40] who reported the establishment of Boltzmann equilibration in $Ca(4^3P_J)$ under comparable conditions (p_{He} = 10 Torr) within 40 ns, Boltzmann equilibrium is assumed to be maintained within $Sr(5^3P_J)$ during decay measurements recorded here. The appropriate equilibrium constants connecting the spin orbit components are characterised in the usual manner:

$$Sr(5^3P_0) \rightleftharpoons Sr(5^3P_1) \qquad K_1$$

$$Sr(5^3P_1) \rightleftharpoons Sr(5^3P_2) \qquad K_2$$
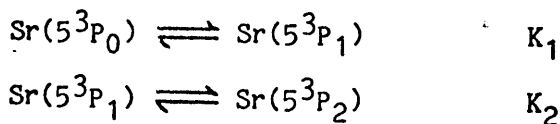
and A_{nm} ($= 1/\tau_e$) is the Einstein coefficient for the $5^3P_1 \rightarrow 5^1S_0$ transition, the only state involving emission. Apart from emission, kinetic parameters are thus ascribed to the Boltzmannised $Sr(5^3P_J)$.

Unlike the investigations described for $Mg(3^3P_J)$ and $Ca(4^3P_J)$, the diffusional term, β'/p_M in equation (5.1), is barely detectable in these measurements. In view of the reciprocal relationship of this term with pressure, it was shown that the contribution to diffusional loss of $Ca(4^3P_J)$ had to be detected at lower pressures than in similar experiments on $Mg(3^3P_J)$ on account of the greater dominance of A_{nm} for $Ca(4^3P_1) \rightarrow Ca(4^1S_0)$ + hν compared to the analogous emission for $Mg(3^3P_1)$. It has also been shown that the approximation of the use of the "long-time solution" of the diffusion equation[62,63] leads to a value of β' in equation (5.1) consistent with the slit dimensions of the monochromator in experiments of the present type. The term β' will consequently be larger than either would be the case for resonance absorption measurements or resonance fluorescence measurements using an interference filter.

Nevertheless, the term A_{nm} here [eqn. (5.1)] is totally dominant in the absence of significant collisional quenching, $\Sigma k_Q[Q]$. This is the case with all the noble gases in the present study.

Figure (5.3a) shows that the first-order decay coefficient (k') is essentially constant over the pressure range of helium employed and hence the loss of $Sr(5^3P_J)$ may be totally attributed to emission from $Sr(5^3P_1)$, namely:

$$k'_{em} = A_{nm}/(1 + 1/K_1 + K_2) \qquad (5.2)$$

Figure (5.3b) shows the data of figure (5.3a) plotted in the form of k' against $1/p_{He}$ to investigate the decay of $Sr(5^3P_J)$ according to the form:

$$k' = k'_{em} + \beta'/p_{He} \qquad (5.3)$$

Whilst a positive slope is just detectable and leads to a value of comparable with those observed in the cases of $Mg(3^3P_J)$ and $Ca(4^3P_J)$, the first term in equation (5.3) is so dominant on account of the large Einstein coefficient, A_{nm}, that the decay in helium (and the other noble gases, see later) is taken to be described by equation (5.2).

At first sight, the mean value of k'_{em} in figure (5.3a) ($k'_{em} = 2.0 \pm 0.2 \times 10^4 \ s^{-1}$, 1σ) coupled with the value of $F(900 \ K) = (1 + 1/K_1 + K_2) = 2.335$ yields $A_{nm} = 4.67 \pm 0.5 \times 10^4 \ s^{-1}$. However, measurements in all the noble gases, M, at $T = 950 \ K$ [figure (5.4)] yield, consistently, lower values of k'_{em} which are in sensible accord within the errors (1σ):

Noble gas	k'_{em} (950 K)/$10^4 \ s^{-1}$
He	1.74 ± 0.07
Ne	1.54 ± 0.09
Ar	1.45 ± 0.10
Kr	1.49 ± 0.14
Xe	1.47 ± 0.08

Radiation trapping is clearly playing a role in this system. This might appear surprising as the true value of A_{nm} for the forbidden transition $Sr(5^3P_1) \rightarrow Sr(5^1S_0) + h\nu$ is approximately 2×10^3 times smaller than that for an electric-dipole allowed atomic transition. Various radiation trapping calculations, using the diffusion theory of radiation for a
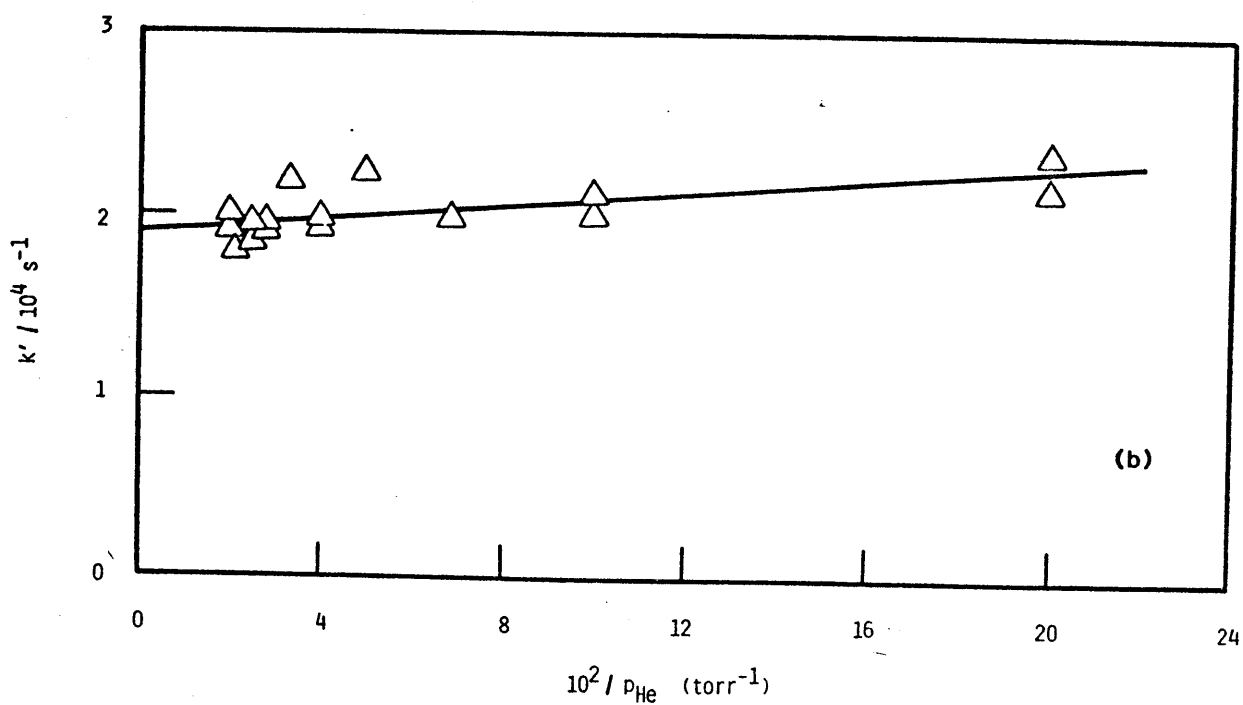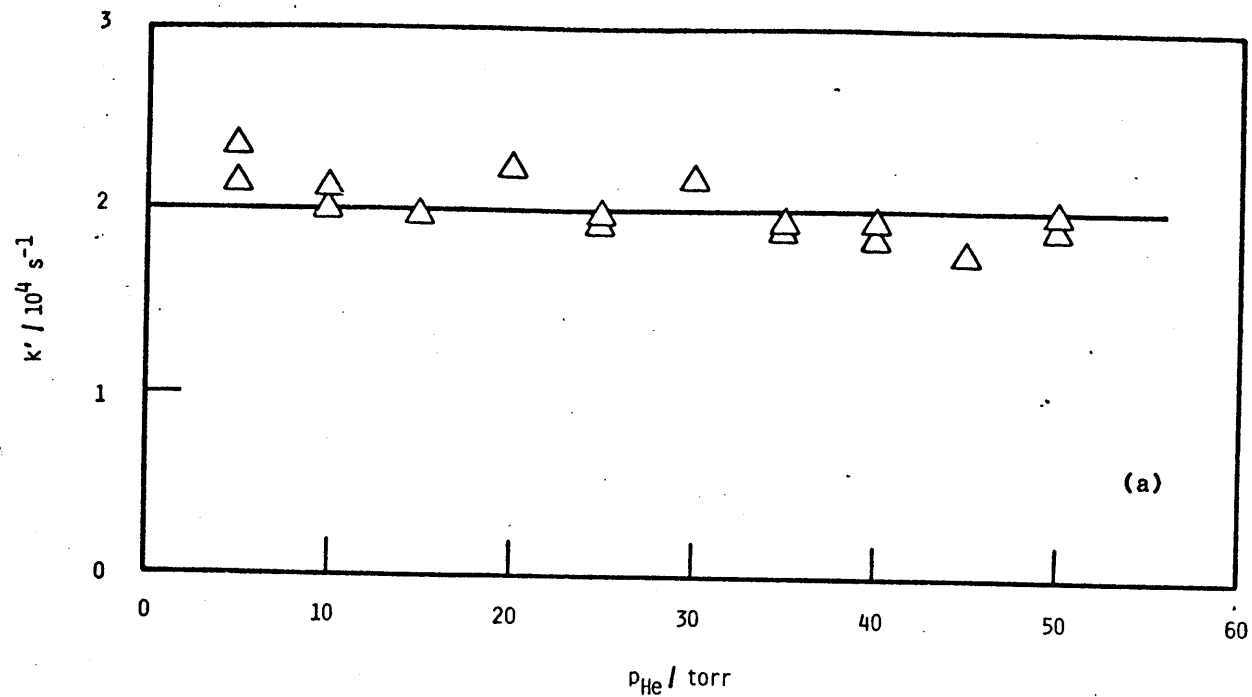
Figure 5.3

Variation of the first-order rate coefficient (k') for the decay of $Sr(5^3P_J)$, following the generation of $Sr(5^3P_1)$ by pulsed dye-laser excitation, in the presence of helium. (T = 900 K)

(a) k' versus p_{He} ;   **(b)** k' versus $1/p_{He}$
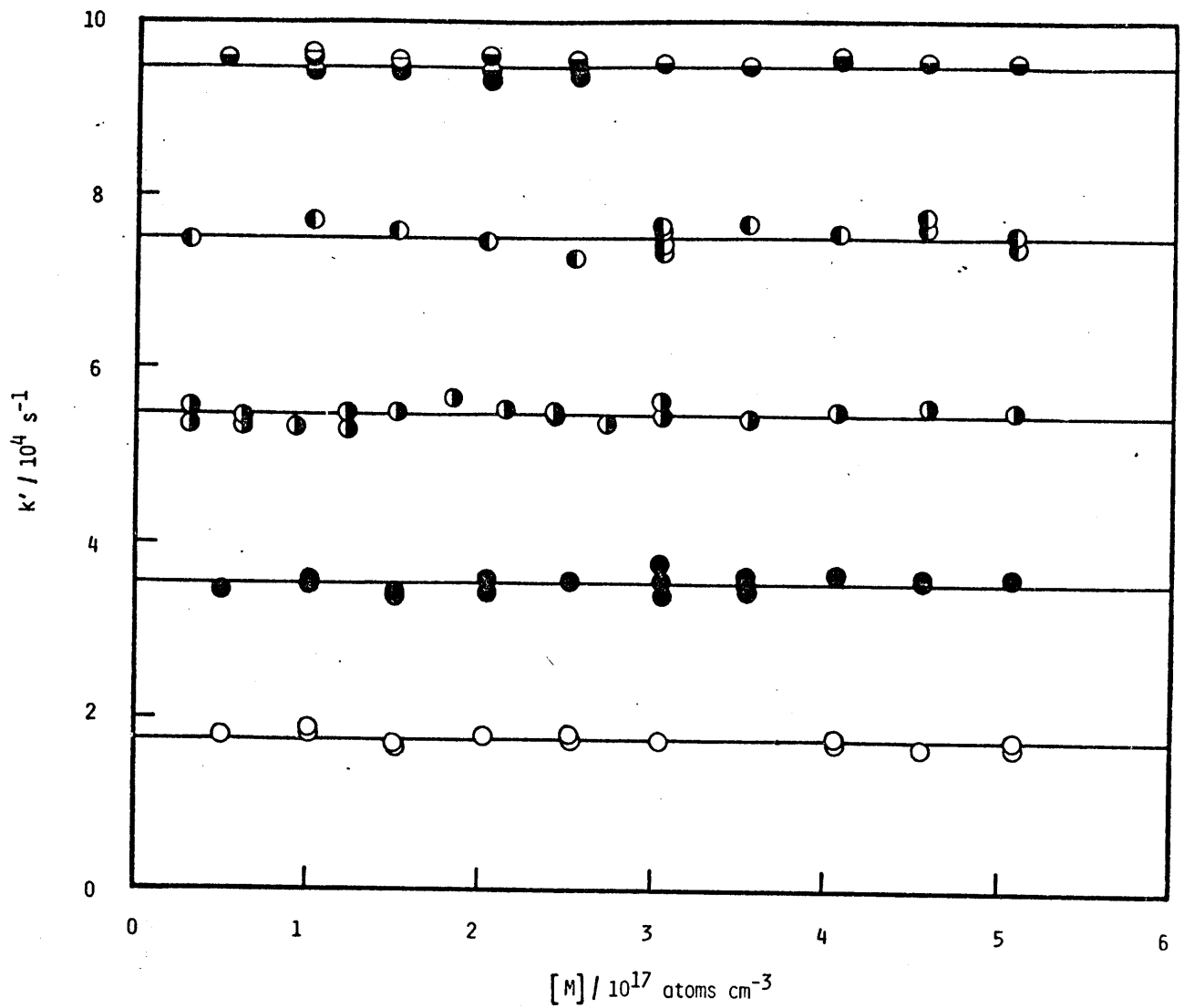
Figure **5.4**

Variation of the first-order rate coefficient (k') for the decay of $Sr(5^3P_J)$, following the generation of $Sr(5^3P_1)$ by pulsed dye-laser excitation, in the presence of the noble gases at T = 950 K.

○ He ; ● Ne (k' + 2 x 10⁴ s⁻¹) ; ◐ Ar (k' + 4 x 10⁴ s⁻¹) ;

◑ Kr (k' + 6 x 10⁴ s⁻¹) ; ⊖ Xe (k' + 8 x 10⁴ s⁻¹)

number of electric-dipole allowed atomic transitions, have been described by Husain and co-workers[54,106-108]. Typical ratios for the effective to true radiative lifetimes $(\tau^*/\tau_e = A_{nm}/A^*_{nm})$ were found to lie in the range 4 to 5 for atomic densities in the region of 10^{12} atom.cm^{-3}. In the present case, atomic densities greater by ca. four orders of magnitude are being employed and the effect of radiation trapping is of the order of 30% in terms of the value of A_{nm} or τ_e. Radiation trapping was therefore investigated in some detail in the case of helium buffer gas.

Figure (5.5) shows the variation of k' for emission as a function of the atomic density of $Sr(5^1S_0)$ derived from measurements in the temperature range 850 - 1000 K over which $[Sr(5^1S_0)]$ was varied by a factor of ca. 100.[88,89] The extrapolation procedure may be simplified by employing a mean value of F = 2.34 in the range 850 - 1000 K as this function does not vary greatly over this temperature range [F(850, 900, 950, 1000 K) = 2.31, 2.34, 2.36, 2.38, respectively] and most fluorescence decay measurements are carried out in the region of T = 900 - 950 K. Furthermore, in fact, one only requires an extrapolation to an atomic density of strontium where radiation trapping is negligible. Figure (5.5) shows this extrapolation (O), yielding $A_{nm} = 4.98 \pm 0.10 \times 10^4 s^{-1}$ and $\tau_e = 20.1 \pm 0.4$ μs.

The above value of τ_e may be employed together with the values of k' in figure (5.4) and F(950 K) to note the magnitude of radiation trapping in this system through the ratio τ^*/τ_e resulting from the atomic density of $Sr(5^1S_0)$ at 950 K:

Noble Gas	τ^*/τ_e
He	1.21 ± 0.06
Ne	1.37 ± 0.11
Ar	1.46 ± 0.11
Kr	1.42 ± 0.16
Xe	1.44 ± 0.15

Table (5.1) shows the present result for $\tau_e[5^3P_1 \rightarrow 5^1S_0 + h\nu$ (λ = 689.3 nm)] and the range of values derived from previous investigations. Of the various comments that may be made of these data, one immediately notes the large value of τ_e derived from the use of modulated atomic beams.[105]
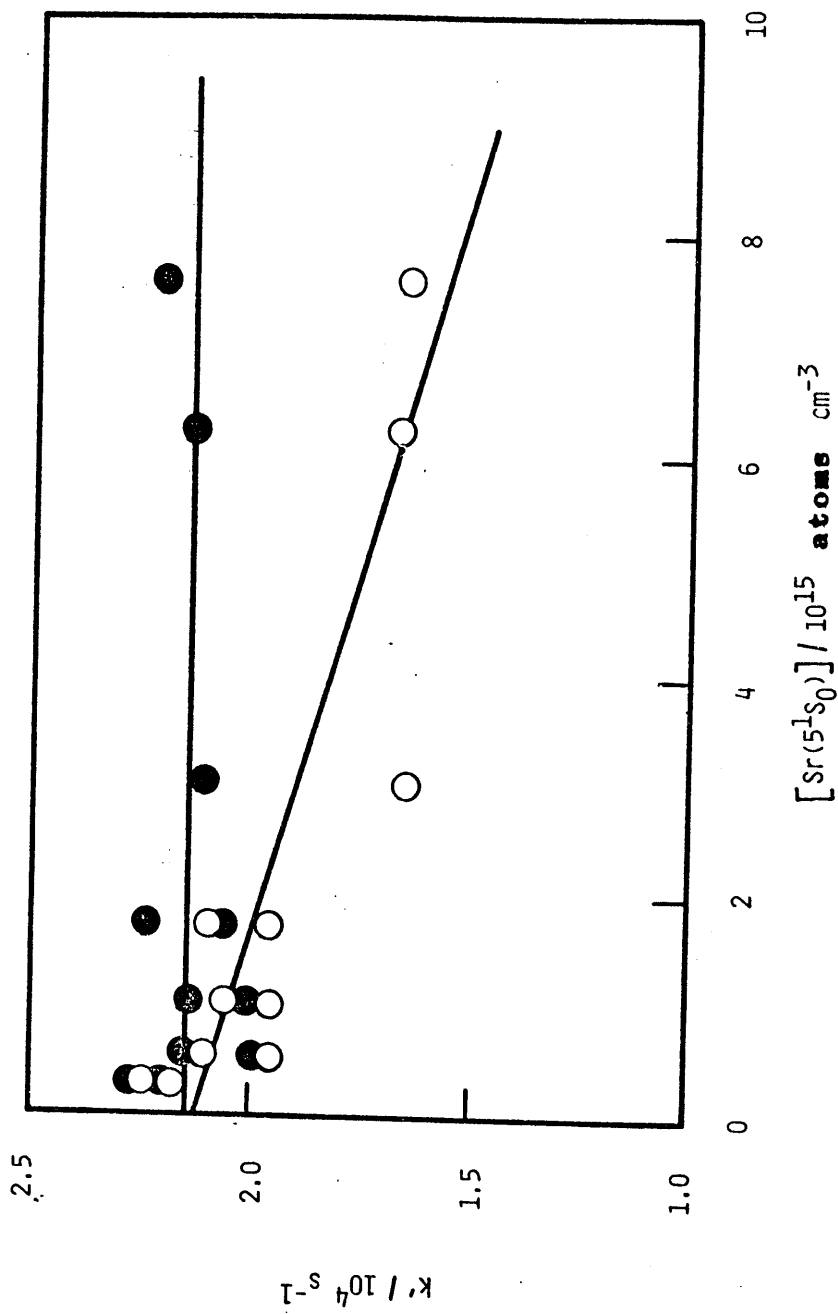
Figure **5.5**

Variation of the first-order rate coefficient (k') for the decay of $Sr(5^3P_J)$, following the generation of $Sr(5^3P_1)$ by pulsed dye-laser excitation, with the concentration of ground state atomic strontium, $Sr(5^1S_0)$.

○ Rate data indicating the effect of radiation trapping at $\lambda = 689.3$ nm
($Sr(5s5p(^3P_1)) \longrightarrow Sr(5s^2(^1S_0) + h\nu$)

● Rate data corrected for radiation trapping

TABLE 5.1

Mean Radiative Lifetime (τ_e) for $Sr(5^3P_1) \longrightarrow Sr(5^1S_0) + h\nu$

($\lambda = 689.3$ nm)

$\tau_e/\mu s$	Ref.
19.9	(87)[a]
14.5	(23)[a]
18	(20)[b]
16.4	(101)[b]
15	(12)[b]
25	(80)[c]
21	(102,103)[d]
6.4	(104)[d]
74	(105)[e]
21 ± 1	(97)[f]
20.1 ± 0.4	(*)[g]

a. Theoretical

b. Intensity measurements

c. "Hook method" (Interferometric)

d. Double resonance measurements

e. Atomic beam technique

f. Dye-laser excitation + time-resolved atomic fluorescence (Single-shot).

g. (*) This work. Dye-laser excitation + time-resolved atomic fluorescence (Signal averaging).

Similar behaviour was observed in the case of $\tau_e[Ca(4^3P_1) \rightarrow Ca(4^1S_0)]$[81,82] and appears to result from complexities in the analysis arising from separating the time-dependence of the spontaneous emission and the transit time through the beam apparatus. Larger values of τ_e obtained by experimental methods [Table (5.1)] other than from beams are prone to some

radiation trapping at suitable atomic densities. Clearly, the present signal-averaged result is in excellent agreement with the single-shot measurements of Havey et al.[97] [Table (5.1)] carried out at temperatures and densities of Sr where there was no significant radiation trapping. Especially striking is the agreement resulting from the correction due to radiation trapping, and the demonstration of radiation trapping itself in the time-domain for this forbidden transition. Finally, the excellent agreement between experiment [Table (5.1)] and theory[87] may be noted.

5.2 Collisional quenching of $Sr(5^3P_J)$

The only rate data reported hitherto for the collisional quenching of $Sr(5^3P_J)$ are those described by Malins et al.[42] derived from the phase shift technique for the noble gases and for $Ca(4^1S_0)$. That particular system[42] is more complex than the arrangement described by Malins and Benard[41] for the study of $Ca(4^3P_J)$ itself in that not only is the interpretation model-dependent, but that the experimental arrangement required indirect generation of $Sr(5^3P_J)$ by electronic energy transfer from $Ca(4^3P_J)$ following the generation of $Ca(4^3P_1)$ by dye-laser excitation. Thus, Malins et al.[42] report an absolute second-order rate constant for the near resonance ($\Delta H = +0.085$ eV) electronic energy exchange process:

$$Sr(5^3P_J) + Ca(4^1S_0) \longrightarrow Sr(5^1S_0) + Ca(4^3P_J)$$
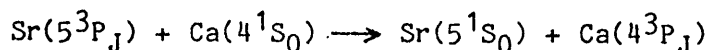
of $k = 1.1 \times 10^{-11}$ $cm^3 molecule^{-1}s^{-1}$ (T = 900 - 1000 K). These authors also report a set of rate constants for the quenching of $Sr(5^3P_J)$ by the noble gases which is given in table (5.2). The present measurements only yielded upper limits for quenching of $Sr(5^3P_J)$ by these collisional partners estimated from the scatter in the data (2σ) in figure (5.4) together with the range of noble gas concentrations employed [table (5.2)].

TABLE 5.2

Absolute second-order rate constants for the collisional quenching
of $Sr(5^3P_J)$ by the noble gases (k_Q, $cm^3atom^{-1}s^{-1}$)

Noble Gas	k_Q	
He (950 K)	$< 5.5 \times 10^{-15}$	(*)[a]
He (913 K)	2.57×10^{-15}	(42)[b]
Ne (950 K)	$< 3.5 \times 10^{-15}$	(*)[a]
Ne (913 K)	3.33×10^{-15}	(42)[b]
Ar (950 K)	$< 3.9 \times 10^{-15}$	(*)[a]
Ar (913 K)	3.78×10^{-15}	(42)[b]
Kr (950 K)	$< 5.5 \times 10^{-15}$	(*)[a]
Kr (923 K)	3.51×10^{-15}	(42)[b]
Xe (950 K)	$< 3.1 \times 10^{-15}$	(*)[a]
Xe (962 K)	4.83×10^{-15}	(42)[b]

(*) This work

a. Pulse dye-laser excitation + time-resolved atomic fluorescence
    (Signal averaged)

b. Phase shift measurements following dye-laser excitation of
    $Ca(4^3P_J)$ and energy transfer with $Sr(5^1S_0)$.

In chapter 4 similar limits for $Ca(4^3P_J)$ with most of the noble gases have
been presented although quenching by xenon was found to be a factor of at
least ca. 10 faster than the lighter gases and the values for $Sr(5^3P_J)$
estimated here [table (5.2)]. The resulting accord between the limits
obtained here and the absolute magnitudes reported by Malins et al.[42]
should be regarded with caution. The model-dependent nature of the
phase-shift technique can lead to incorrect data. Thus, that method[41] led
to quenching rate constants for $Ca(4^3P_J)$, itself, by neon and argon which
were many orders of magnitude greater than the values clearly established

by Furcinitti et al.[24] who employed time-resolved atomic absorption spectroscopy following pulsed dye-laser excitation in the presence of high pressures (up to ca. 500 Torr) of the noble gases. Similarly, in the present work, only a crude upper limit for the quenching of $Sr(5^3P_J)$ by $Sr(5^1S_0)$, may be estimated from the data given in figure (5.2). This is simply based on the assumption of a linear relationship between k'_{em} and $[Sr(5^1S_0)]$ due to radiation trapping (O) across the narrow range of τ^*/τ_e involved. The 2σ scatter in the resulting data corrected for radiation trapping [●, figure (5.5)] and the range of $[Sr(5^1S_0)]$ investigated thus yields $k[Sr(5^3P_J) + Sr(5^1S_0)] < 2 \times 10^{-13}$ $cm^3molecule^{-1}s^{-1}$ (T = 850 - 1000 K) This rate limit describing electronic to translational energy transfer of ca. 1.8 eV would be expected to be slower than near resonant electronic energy exchange between $Sr(5^3P_J)$ and $Ca(4^1S_0)$.

Clearly to optimise the present technique as a kinetic tool for studying collisional quenching of $Sr(5^3P_J)$ by added gases, the term $\Sigma k_Q[Q]$ in equation (5.1) must be made significant compared with the relatively large term, k'_{em} [eqns. (5.1) and (5.2)], diffusional loss being neglected. Hence, we can write:

$$k' = k'_{em} + k_Q[Q] \qquad (5.4)$$

The collisional quenching of $Sr(5^3P_J)$ by H_2 and D_2 was investigated first in view of their fundamental interest. The isotope effect which occurs in the collisional quenching of $Mg(3^3P_J)$ and $Ca(4^3P_J)$ by H_2 and D_2 has already been demonstrated and one may expect an analogous effect in the case of $Sr(5^3P_J)$. Figure (5.6) shows examples of first-order kinetic plots of the decay of $Sr(5^3P_J)$ in the presence of chosen concentrations of H_2. Similar plots were constructed for the various experiments carried out with D_2. Figure (5.7a) and (5.7b) show the resulting plots of k' against $[H_2]$ and $[D_2]$, respectively, whose slopes, following equation (5.4), yield the following absolute second-order rate constants:

$$k_{H_2} = 3.7 \pm 0.4 \times 10^{-12} \ cm^3molecule^{-1}s^{-1} \ (950 \ K, \ 1\sigma)$$

$$k_{D_2} = 3.0 \pm 0.2 \times 10^{-12} \ cm^3molecule^{-1}s^{-1} \ (950 \ K, \ 1\sigma)$$

these data are incorporated in table (5.3) for the purpose of comparing the results with those for $Mg(3^3P_J)$ and $Ca(4^3P_J)$.
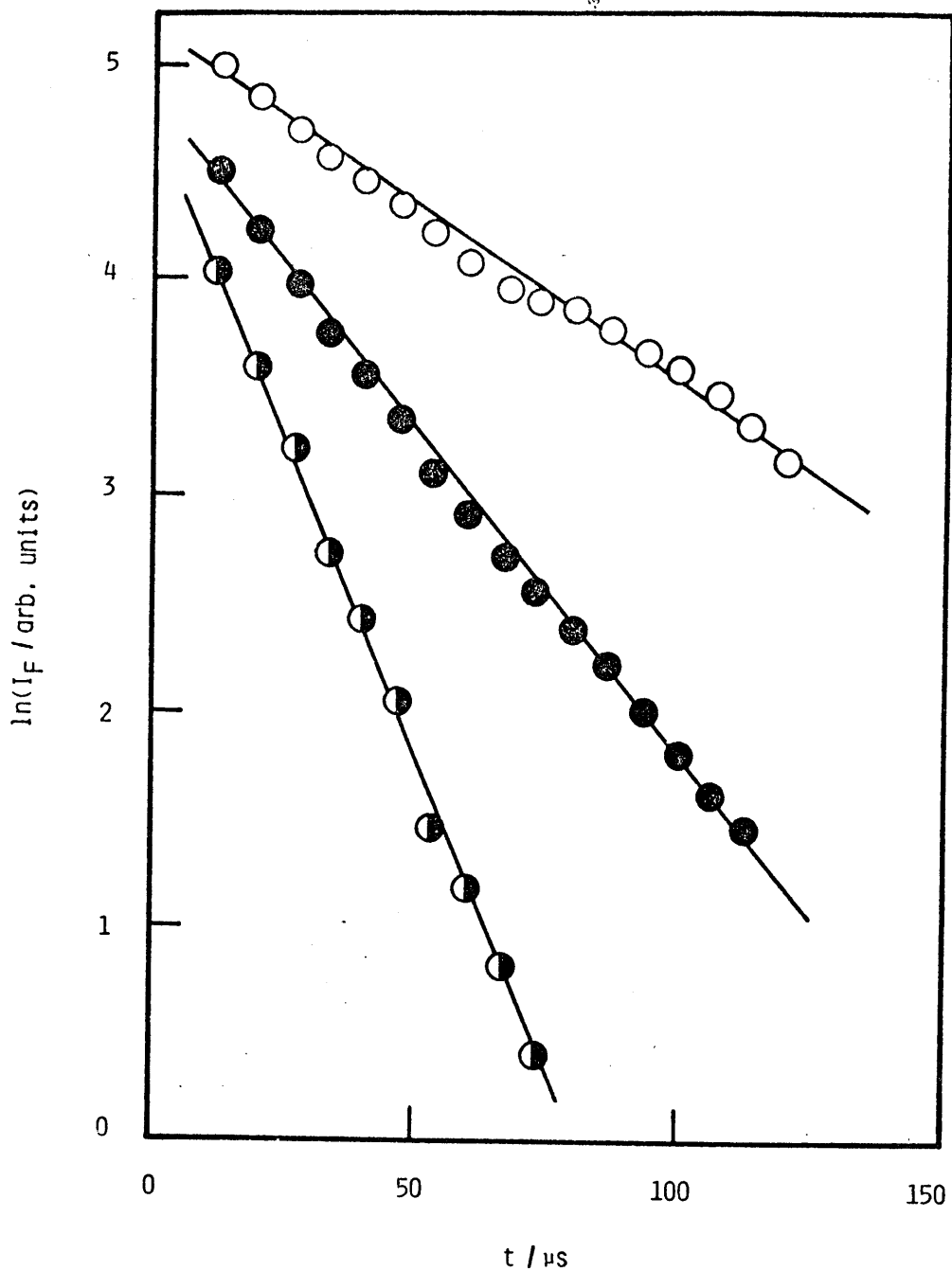
Figure **5.6**

Examples of first-order kinetic plots for the decay of $Sr(5^3P_J)$, derived from the time-resolved atomic emission ($ln(I_F)$ against t) at $\lambda = 689.3$ nm ($Sr(5^3P_1) \longrightarrow Sr(5^1S_0)$) following the pulsd dye-laser excitation of strontium vapour in the presence of molecular hydrogen and helium. (p_{total} with He $= 30$ torr ; T $= 950$ K)

$[H_2] / 10^{15}$ molecules cm^{-3} : ◯ 0.0 ; ● 6.1 ; ◑ 10.7

Figure 5.7

Variation of the pseudo first-order rate coefficient (k') for the decay of $Sr(5^3P_J)$ in the presence of (a) H_2 and (b) D_2. ($p_{total \ with \ He}$ = 30 torr ; T = 950 K)

TABLE 5.3

Absolute second-order rate constants (k_Q, cm^3molecule^{-1}s^{-1}) for the collisional removal of Sr(5^3P_J), Ca(4^3P_J) and Mg(3^3P_J) by H_2 and D_2.

	Sr(5^3P_J)	Ca(4^3P_J)	Mg(3^3P_J)
H_2	$3.7 \pm 0.4 \times 10^{-12}$ (950 K)(*)[a]	$6.0 \pm 0.6 \times 10^{-14}$ (1000 K)(*)[a] $2.26 \pm 0.15 \times 10^{-13}$ (793 K)(91)[b] 3.4×10^{-13} (1073 K)(43)[c]	$7.3 \pm 0.6 \times 10^{-13}$ (800 K)(*)[a] 6.7×10^{-13} (800 K, calc.)(30)[d] $9.1 \pm 1.0 \times 10^{-13}$ (873 K)(25)[b] $1.1 \pm 0.5 \times 10^{-13}$ (room temp.)(27)[e] $9.5 \pm 4.2 \times 10^{-13}$ (800 K, calc.)(32)[d]
D_2	$3.0 \pm 0.2 \times 10^{-12}$ (950 K)(*)[a]	$2.7 \pm 0.3 \times 10^{-14}$ (1000 K)(*)[a]	$1.9 \pm 0.1 \times 10^{-13}$ (800 K)(*)[a] $3.5 \pm 1.7 \times 10^{-13}$ (800 K, calc.)(32)[d]

(*) This work; a. Pulsed dye-laser excitations + time resolved atomic resonance fluorescence with signal averaging; b. Pulsed dye laser excitation + time-resolved atomic resonance absorption spectroscopy c. Dye-laser excitation + phase shift measurements; d. Pulsed dye-laser excitation + time-resolved atomic resonance fluorescence (single-shot); e. Discharge flow + forbidden atomic emission.

All the data for the quenching of $Mg(3^3P_J)$, $Ca(4^3P_J)$ and $Sr(5^3P_J)$ show some isotope effects [table (5.3)], though that for $Sr(5^3P_J)$ is clearly small. Comparison of ratios of k_{H_2}/k_{D_2} are restricted here to investigations in which both quenching rate constants were determined by a given method. Thus, for this ratio, the value obtained is 1.2 ± 0.15 for $Sr(5^3P_J)$ (950 K). This may be compared with the value reported in chapter 4 for $Ca(4^3P_J)$ of 2.2 ± 0.3 at 1000 K. A value of 3.8 ± 0.4 was given in chapter 3 for $Mg(3^3P_J)$ (800 K) which may be compared with the ratio calculated for this same temperature from the data of Breckenridge and Stewart[32] of 2.7 ± 1.8. Whilst these latter authors[32] have demonstrated that vibrational energy in the colliding molecule plays a critical role in influencing the branching ratio between chemical reaction and energy transfer for $Mg(3^3P_J)$, further detailed consideration of the dynamics will be simplified in the case of $Sr(5^3P_J)$. H(D) atom abstraction by $Sr(5^3P_J)$ is highly endothermic[70] and for vibrational energy to play a role in chemical reaction, for H_2, the minimum level involved would be $v'' = 2$. Hence, physical quenching is presumed to be dominant at temperatures accessible in measurements of the present type.

Figure (5.8a) shows an example of the XY-output for the variation of the fluorescence intensity at $\lambda = 689.3$ nm $[Sr(5^3P_1) \rightarrow Sr(5^1S_0) + h\nu]$ following the pulsed dye-laser excitation of atomic strontium in the presence of helium at T = 950 K. Figures (5.8b) and (5.8c) show examples of the effect on the fluorescence intensity decay profiles by the presence of small pressures of molecular nitrogen. First-order kinetic decay plots $[\ln(I_F)$ against t] may readily be constructed from such profiles [figure (5.8)] and these are given in figure (5.9) for the data presented in figure (5.8). The negative of the slopes of these plots [figure (5.8)] yield the first-order decay coefficients (k') for the removal of the "Boltzmannised" $Sr(5^3P_J)$. Following earlier practice, diffusion is neglected and the first-order contribution to the collisional quenching of $Sr(5^3P_J)$ by helium buffer gas would also be constant and relatively small for the fixed pressure of He (ca. 30 Torr) employed in this system. Figure (5.10a) shows the plot of k' against $[N_2]$ on the basis of equation (5.4), the slope of this plot yielding the absolute second-order rate constant, k_{N_2}, for the collisional quenching of $Sr(5^3P_J)$ by N_2. The analogous plot for carbon monoxide is given in figure (5.10b).
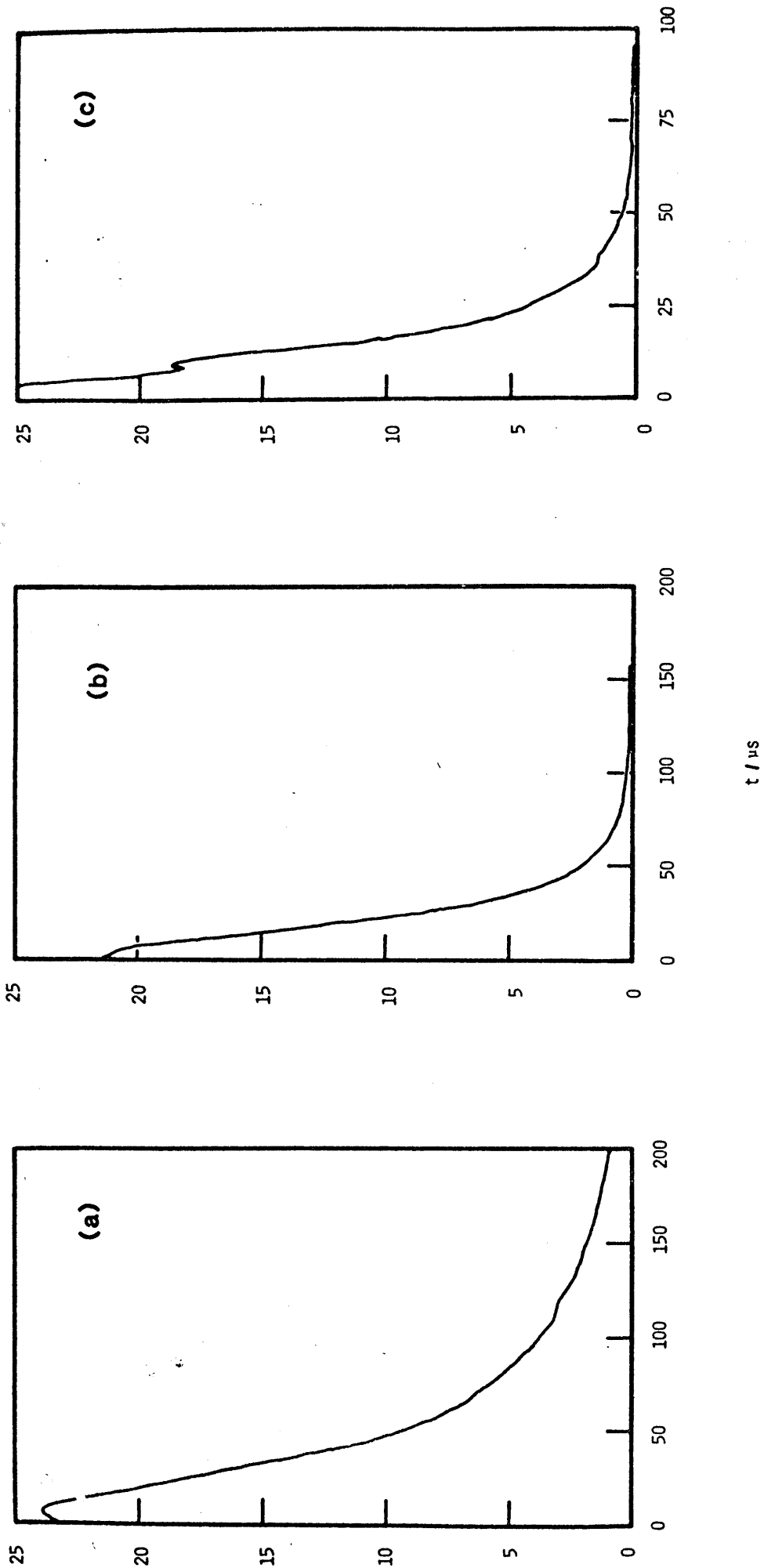
Figure 5.8

Examples of the output of the XY recorder indicating the decay of the time-resolved atomic emission (I_F) at $\lambda = 689.3$ nm ($Sr(5s5p(^3P_1)) \longrightarrow Sr(5s^2(^1S_0))$) following pulsed dye-laser excitation of strontium vapour in the presence of nitrogen.

(p_{total} with He = 30 torr,   T = 950 K)

$[N_2]/10^{15}$ molecules cm^{-3} :   (a)   0.0 ;   (b)   1.2 ;   (c)   2.4
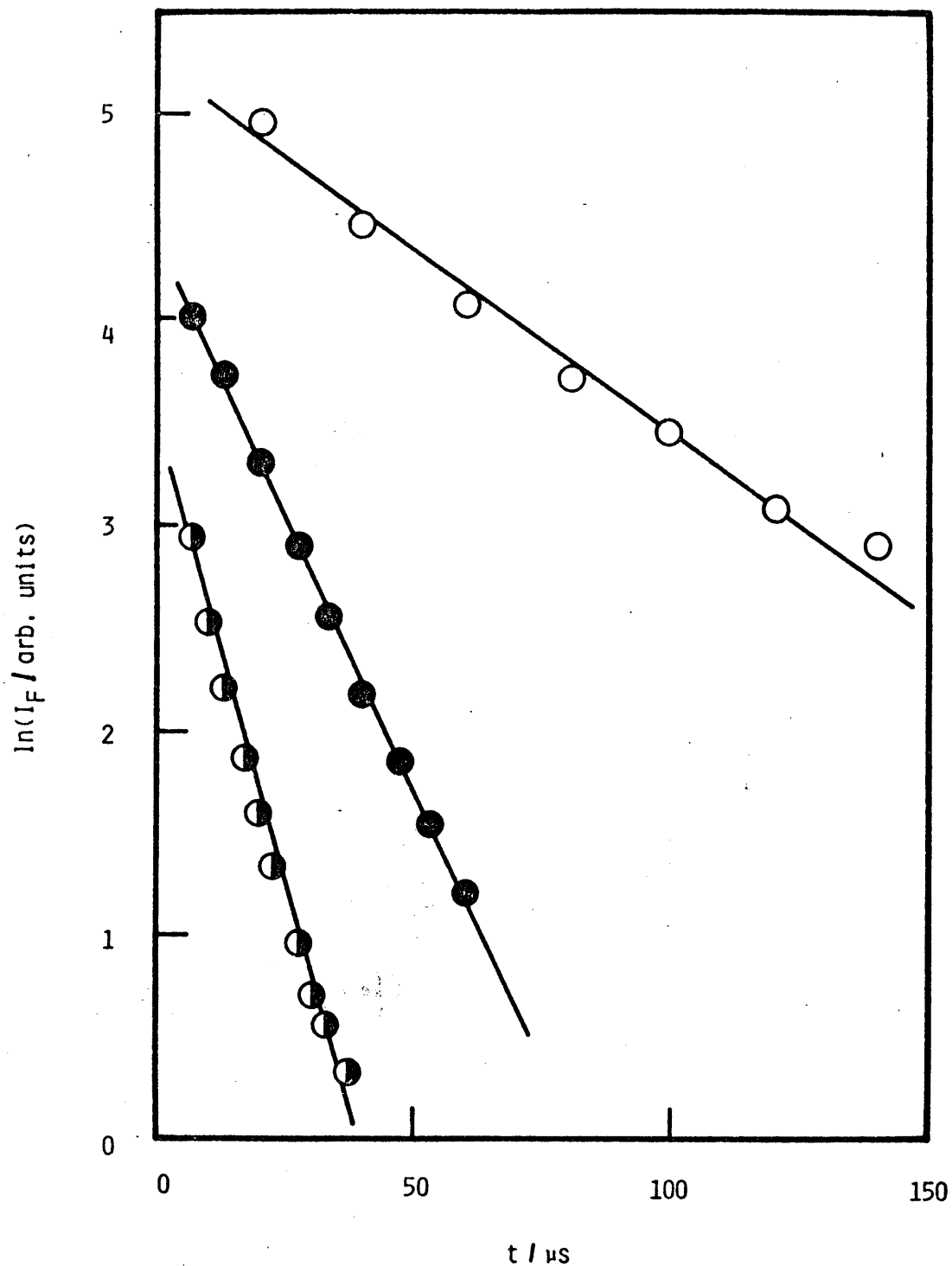
Figure **5.9**

Examples of first-order kinetic plots for the decay of the time-resolved atomic emission ($\ln(I_F)$ against t) at $\lambda = 689.3$ nm ($Sr(5^3P_1) \longrightarrow Sr(5^1S_0)$) following the pulsed dye-laser excitation of strontium vapour in the presence of nitrogen.

(p_{total} with He $= 30$ torr, $T = 950$ K)

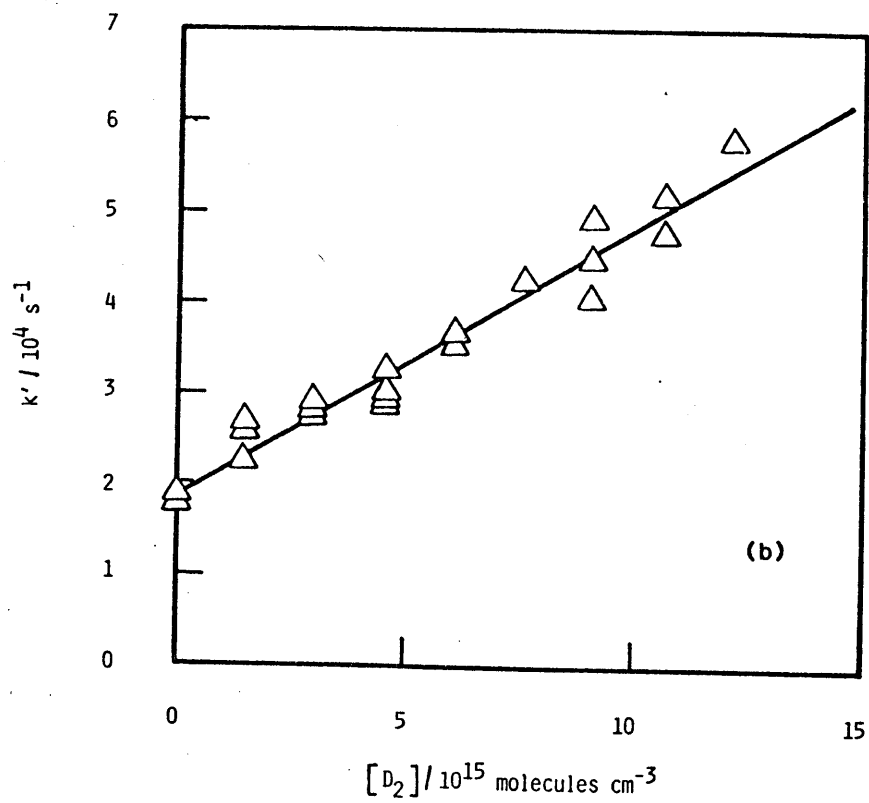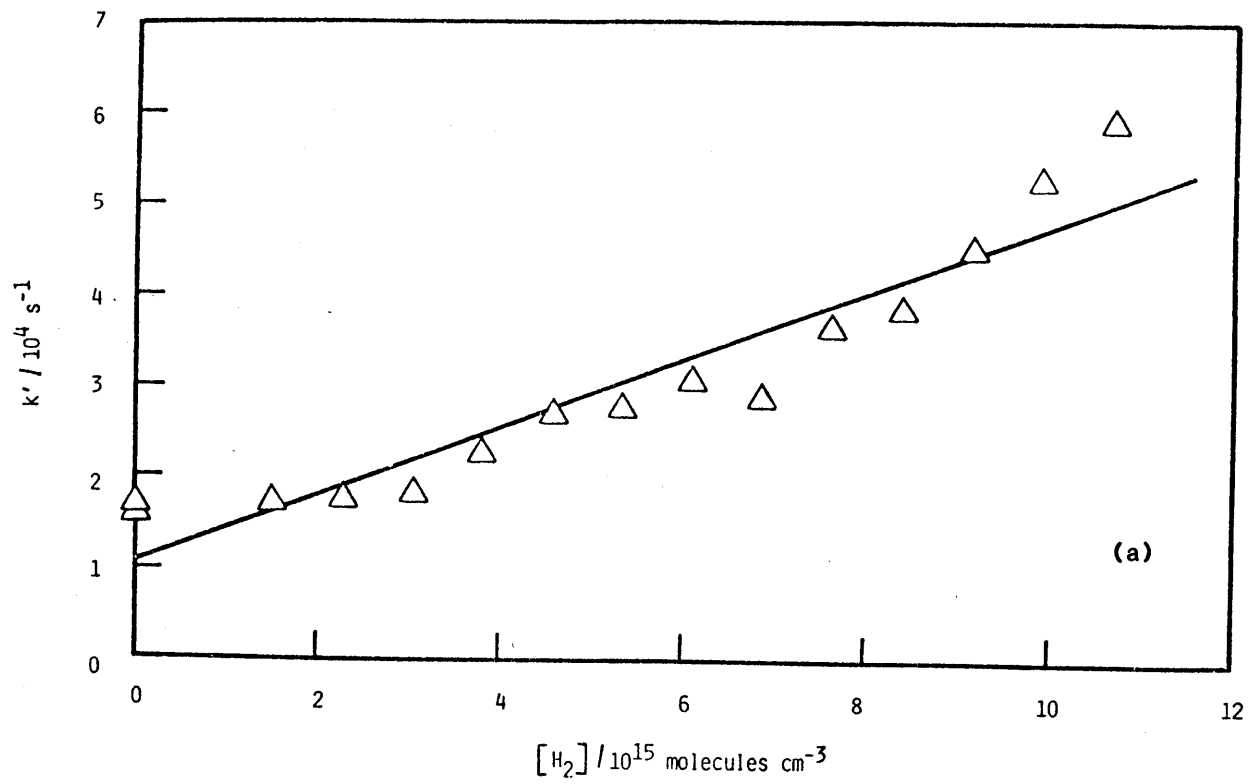$[N_2]/10^{15}$ molecules cm^{-3} : $\bigcirc$ 0.0 ; $\bullet$ 1.2 ; $\leftmoon$ 2.4
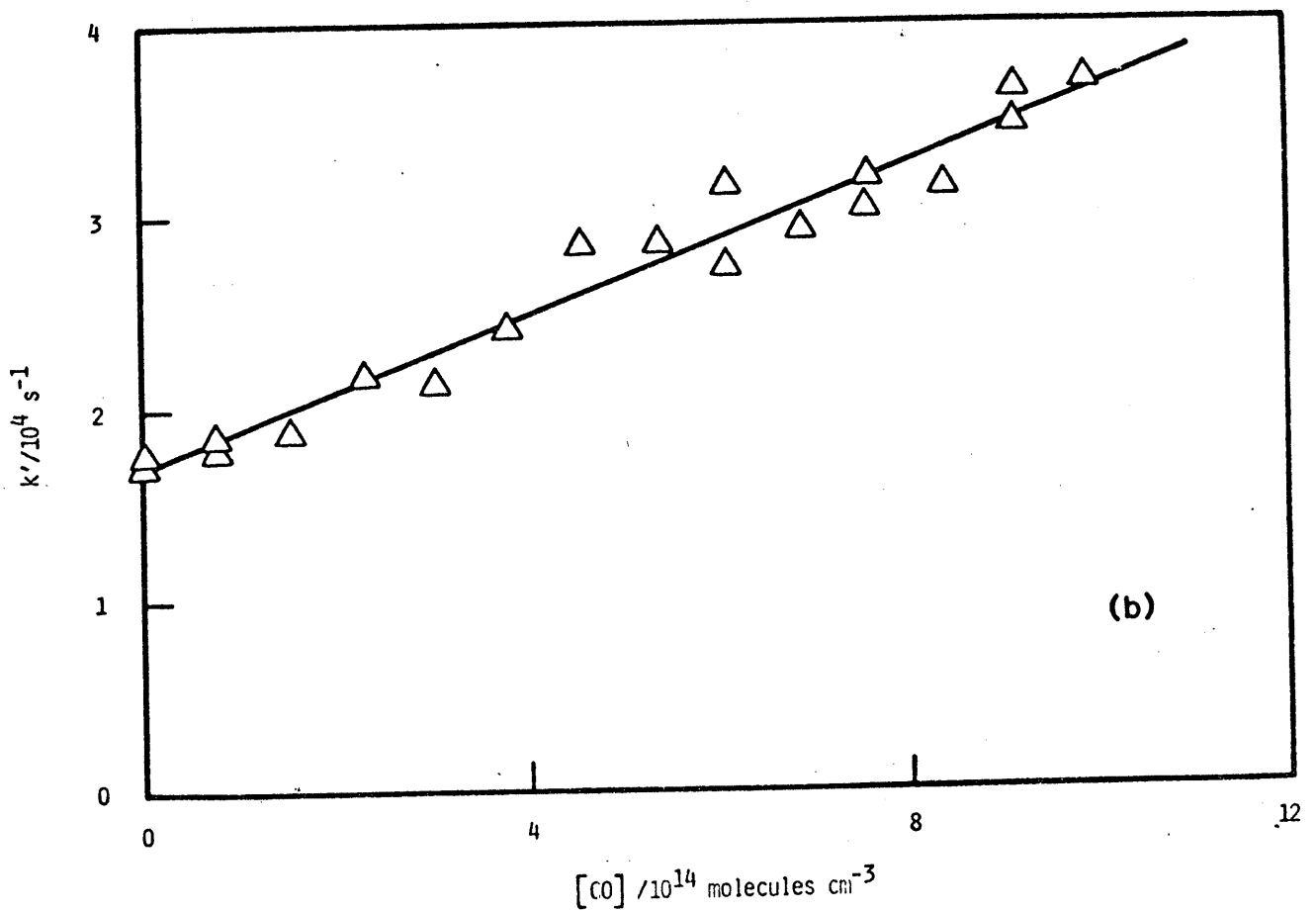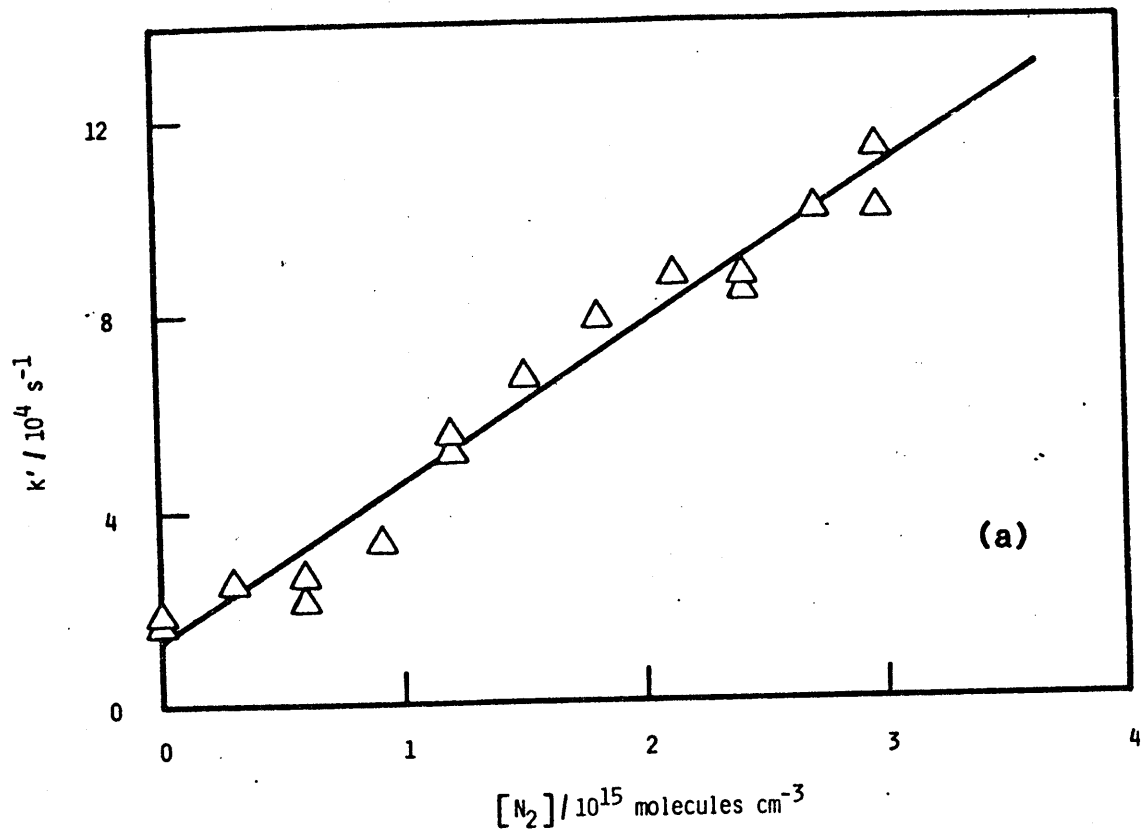
Figure 5.10

Variation of the pseudo first-order rate coefficient (k') for the decay of $Sr(5^3P_J)$ in the presence of (a) N_2 and (b) CO.

$(P_{total}$ with He $= 30$ torr, T $= 950$ K).

Similar measurements to those described above for N_2 and CO were carried out for a wide range of gases (CO_2, N_2O, NH_3, CH_4, CF_4, C_2H_2, C_2H_4 and C_6H_6). However, investigations with those different gases varied considerably in experimental difficulty particularly for oxidising gases, which caused surface oxidation and the subsequent loss of fluorescence signal resulting from a coating of the strontium sample, preventing vaporization of the atoms. Similar effects have been reported for analogous studies on $Mg(3^3P_J)$ and $Ca(4^3P_J)$. This experimental limitation is aggravated here further by the short time scales over which $Sr(5^3P_1)$ is monitored. Figures (5.11) and (5.12) summarise the decay data for these gases in the form of equation (5.4). Any limitations in the range of concentrations employed for these quenching studies [e.g. figures (5.11) and (5.12)] generally result from the effects of surface reaction rather than the upper limit for k' that can be measured. The resulting overall absolute second-order quenching rate constants, k_Q derived from the slopes of the plots k' against $k_Q[Q]$ are given in table (5.4). In the absence of collisional quenching data for this atomic state with which the present results may be directly compared, the data for $Sr(5^3P_J)$ are compared with those for analogous processes involving $Ca(4^3P_J)$ and $Mg(3^3P_J)$ [table (5.4)]. For the range of collisional partners investigated here, the most striking general contrast between the rate data for $Sr(5^3P_J)$ and those for either $Ca(4^3P_J)$ or $Mg(3^3P_J)$ is the considerably greater quenching efficiencies exhibited by most gases towards the heavier $Sr(5^3P_J)$ [table (5.4)]. This is particularly notable considering $Ca(4^3P_J)$, where the electronic energies to be transferred are comparable [1.8 eV for $Sr(5^3P_J)$, 1.88 eV for $Ca(4^3P_J)$][10] and where physical quenching processes as opposed to chemical reaction must clearly take place. For $Sr(5^3P_J)$, this would be the case for N_2, CO, NH_3, CH_4, C_2H_2, C_2H_4 and C_6H_6 from consideration of the bond dissociation energies,[69,70,75] particularly the low bond dissociation energy of SrH $\{D_0^o[SrH(X^2\Sigma^+)] \leqslant 1.66$ eV[70]$\}$ which would make H-atom abstraction by $Sr(5^3P_J)$ endothermic. For the gases C_2H_4 and C_6H_6, no significant difference can be ascribed to the collisional efficiencies for those two molecules [table (5.4)]. On the basis of the reduced masses, quenching of $Sr(5^3P_J)$ by both these molecules can be considered as proceeding at the collision number. In the absence of detailed considerations of donor and acceptor energy levels, discussion is
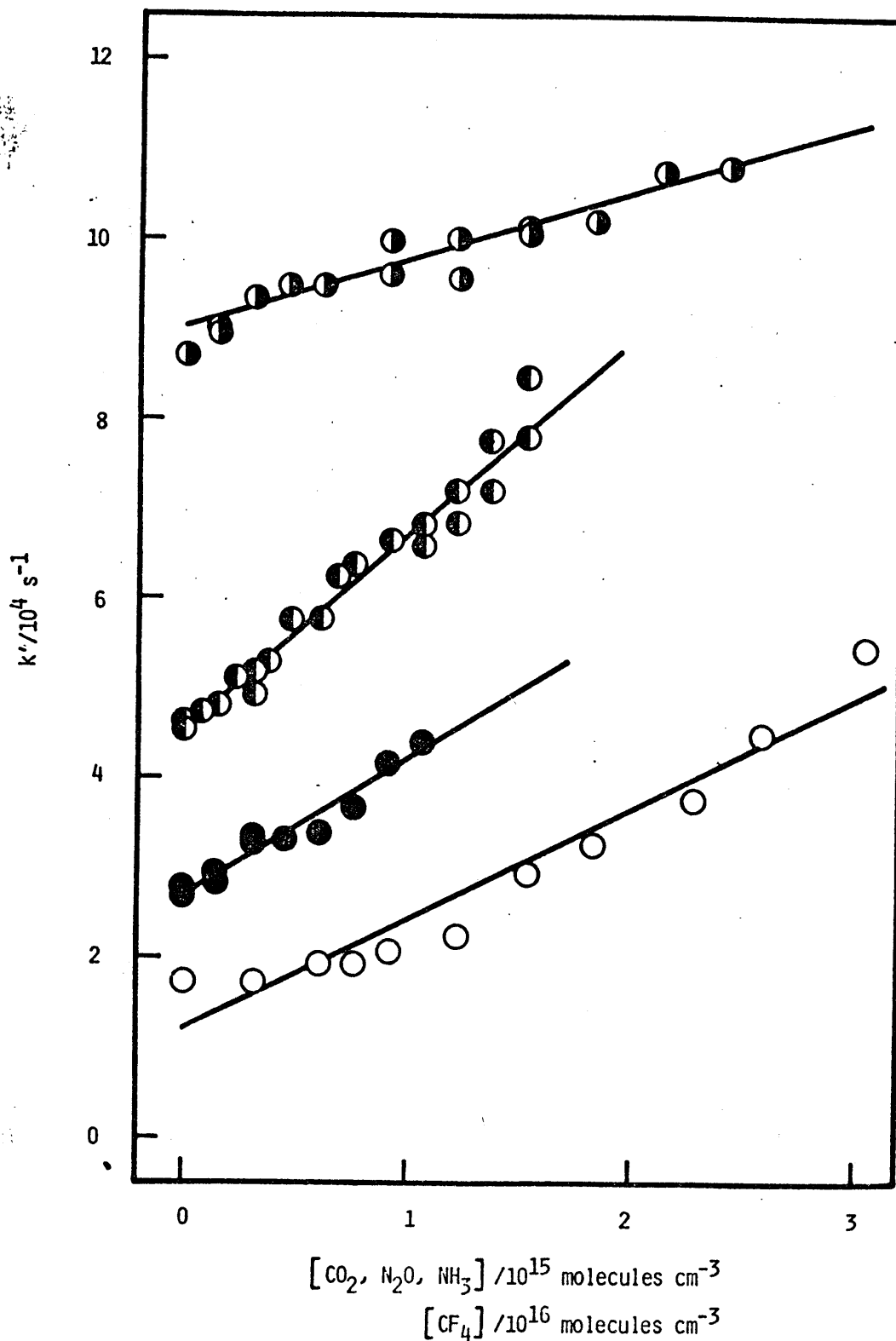
Figure 5.11

Variation of the pseudo first-order rate coefficient (k') for the decay of Sr(5^3P_J) in the presence of CO_2, N_2O, NH_3 and CF_4. (P_{total} with He = 30 torr, T = 950 K)

$\bigcirc$ CO_2 ; $\bullet$ N_2O (k' + 10^4 s^{-1}) ; $\oplus$ NH_3 (k' + 3 x 10^4 s^{-1}) ; $\ominus$ CF_4 (k' + 7 x 10^4 s^{-1})
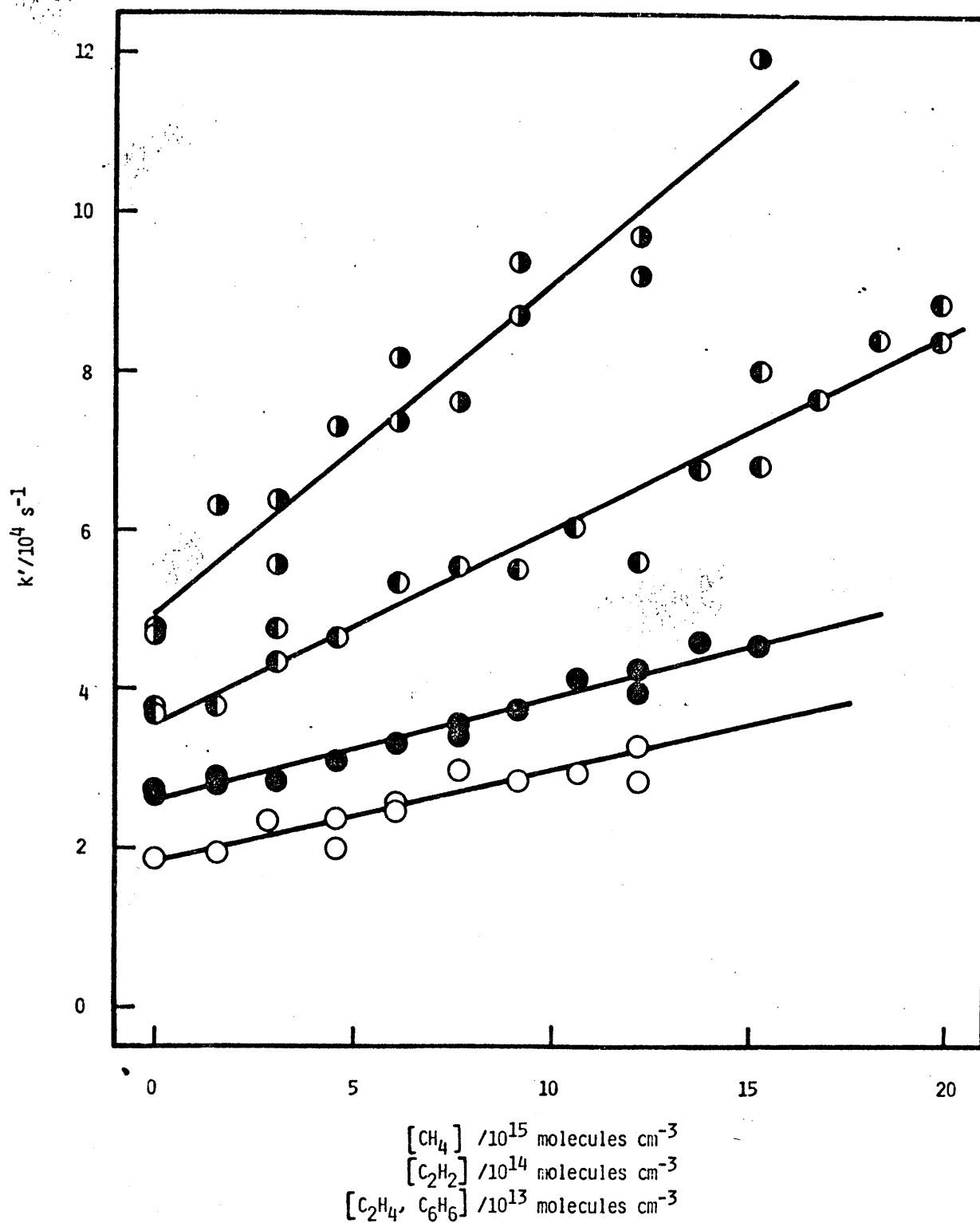
Figure **5.12**

Variation of the pseudo first-order rate coefficient (k') for the decay of $Sr(5^3P_J)$ in the presence of CH_4, C_2H_2, C_2H_4 and C_6H_6. (P_{total} with He = 30 torr, T = 950 K)

○ CH_4 (k') ; ● C_2H_2 (k' + 10^4 s^{-1}) ; ◑ C_6H_6 (k' + 2 x 10^4 s^{-1}) ; ◐ C_2H_4 (k' + 3 x 10^4 s^{-1})

clearly directed towards those quenching gases where atomic abstraction may compete with physical quenching.

Dealing now with the quenching gas CF_4, where orbital symmetry will not be significantly involved for the six atom collisional intermediate, the relative high bond energy of SrF $\{D_0^0[SrF(X^2\Sigma^+)] = 5.58$ eV[70]$\}$ makes chemical reaction thermochemically favourable:

$$Sr + CF_4 \longrightarrow SrF + CF_3 \qquad \Delta H = -0.28 \text{ eV}^{70,75}$$

[D(CF_3-F) = 5.3 eV[75]]. For the 5^3P_J state, the analogous reaction for the excited atom becomes exothermic to the extend of 2.08 eV, and population of the $A^2\Pi$ state of SrF, situated 1.885 eV above the $X^2\Sigma^+$ ground state would still be described by a process which is exothermic overall ($\Delta H = -0.2$ eV).[10,69,75] A further consequence of the absence of significant orbital restriction is the influence of energy on the population of product states resulting from chemical reaction. The detection of chemiluminescence of the electric-dipole allowed A-X emission in the region of $\lambda = 660$ nm should be feasible as a result of the spin allowed, exothermic process resulting from F-atom abstraction process by $Sr(5^3P_J)$. The quenching rates for CH_4 and CF_4, chemical reaction for the former being endothermic, are equal within the 1σ errors [table (5.4)] and physical quenching for CF_4 may dominate removal of $Sr(5^3P_J)$. However, the A-X emission in the time-resolved mode may still be employed both to indicate the reactive channel itself and as a kinetic spectroscopic marker for $Sr(5^3P_J)$ even if the branching fraction for chemical reaction were small.

It would appear that, the reaction of strontium atoms with CO_2 has not been investigated in any detail in molecular beams. For $Sr(5^1S_0)$, the O-atom abstraction reaction is endothermic $\{D[CO2(X^1\Sigma_g^+)] = 5.453$ eV;[69] $D_0^0[SrO(X^1\Sigma^+)] = 4.88$ eV[70]$\}$ though there is correlation between ground state reactants and products:

$$Sr(5^1S_0) + CO_2(X^1\Sigma_g^+) \xrightarrow{^1A'} SrO(X^1\Sigma^+) + CO(X^1\Sigma^+)$$
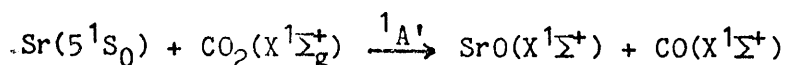
$$\Delta H = +0.573 \text{ eV}^{2,29,30}$$

on the basis of C_s symmetry in the collision complex, coupled with the weak spin-orbit coupling approximation.[17] By contrast there are

symmetry-allowed routes for the chemical removal of $Sr(5^3P_J)$ which are marginally exothermic leading to electronically excited $SrO(a^3\Pi_i)$:

$$Sr(5^3P_J) + CO_2(X^1\Sigma_g^+) \xrightarrow{{}^3A' + {}^3A''} SrO(a^3\Pi_i) + CO(X^1\Sigma^+)$$

$$\Delta H = -0.093 \text{ eV}^{[10,69,70]}$$
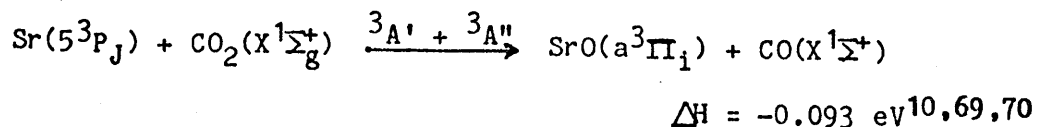
This presumably accounts for the relatively rapid quenching rate, significantly faster than the analogous overall processes for $Ca(4^3P_J)$ and $Mg(3^3P_J)$ [table (5.4)], notwithstanding energy barriers normally observed for O-atom abstraction reactions for such symmetry-allowed channels with this linear 1δ-allowed, closed shell molecule.[4,5] The breakdown of C_s symmetry in the "least symmetrical complex"[17] for this four atom collision complex would still yield a reaction for the 5^3P_J state which was spin disallowed but highly exothermic (-1.893 eV) but even this condition might be significantly relaxed for the heavy strontium atom.

Dagdigian and co-workers[35,99] have reported extensive chemiluminescence from electronically excited SrO following the reaction of $Sr(5^3P_J)$, generated in a low voltage discharge, in a molecular beam with N_2O. The emission is complex, similar to that observed in flames containing $Sr + N_2O + CO$.[26,49,100] and the electronic transitions were not assigned in the beam measurements. Again, employing C_s symmetry in the "least symmetrical complex" for this four atom collisional complex, correlations based on the weak spin orbit coupling approximation[17] indicate symmetry-allowed, exothermic channels to chemical products arising from O-atom abstraction for both the ground state and the low lying electronically excited state of atomic strontium:

$$Sr(5^1S_0) + N_2O(X^1\Sigma_g^+) \xrightarrow{{}^1A'} SrO(X^1\Sigma^+) + N_2(X^1\Sigma_g^+)$$

$$\Delta H = -3.203 \text{ eV}^{[10,69,70]}$$

$$Sr(5^3P_J) + N_2O(X^1\Sigma_g^+) \xrightarrow{{}^3A' + {}^3A''} SrO(a^3\Pi_i) + N_2(X^1\Sigma_g^+)$$

$$\Delta H = -3.118 \text{ eV}^{[10,69,70]}$$
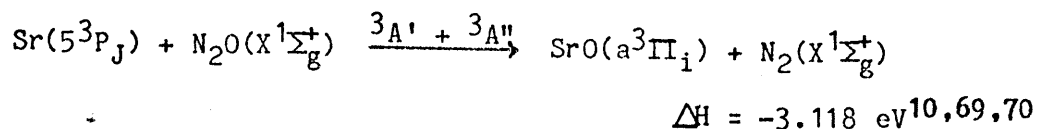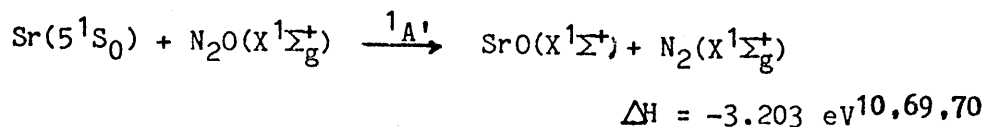
Whilst the observed rapid collisional quenching of $Sr(5^3P_J)$ by N_2O [table (5.4)], corresponding to ca. one in ten collisions, may be presumed as arising from the $^3A' + {}^3A''$ surfaces available for the highly exothermic, symmetry-allowed process, the departure from unit collisional efficiency

is considered to arise from a small energy barrier as with the removal with CO_2.[4,5] Again, as with CO_2, the overall collisional removal of $Sr(5^3P_J)$ by N_2O is considerably more efficient than the analogous processes with either $Ca(4^3P_J)$ or $Mg(3^3P_J)$ [table (5.4)].

TABLE 5.4

Absolute second-order rate constants (k_Q, $cm^3molecule^{-1}s^{-1}$) for the collisional quenching of $Sr(5^3P_J)$, $Ca(4^3P_J)$ and $Mg(3^3P_J)$ by added quenching gases, Q.

Q	$Sr(5^3P_J)$	$Ca(4^3P_J)$	$Mg(3^3P_J)$
He	$< 5.5 \times 10^{-15}$ (950 K) (*)[a]	$< 4 \times 10^{-15}$ (1000 K) (*)[a]	
	2.57×10^{-15} (913 K) (42)[b]	2.13×10^{-15} (ca. 1050 K) (20)[b]	
Ne	$< 3.3 \times 10^{-15}$ (950 K) (*)[a]	$< 4 \times 10^{-15}$ (1000 K) (*)[a]	
	3.33×10^{-15} (913 K) (42)[b]	2.23×10^{-15} (ca. 1050 K) (41)[b]	
		$\sim 8 \times 10^{-21}$ (793 K) (91)[c]	
Ar	$< 3.9 \times 10^{-15}$ (950 K) (*)[a]	$< 4 \times 10^{-15}$ (1000 K) (*)[a]	
	3.78×10^{-15} (913 K) (42)[b]	4.8×10^{-15} (ca. 1050 K) (41)[b]	
		$\sim 8 \times 10^{-21}$ (793 K) (91)[c]	

TABLE 5.4 (continued)

Q	$Sr(5^3P_J)$	$Ca(4^3P_J)$	$Mg(3^3P_J)$
Kr	< 5.5 x 10^{-15} (950 K) (*)[a]	< 4 x 10^{-15} (1000 K) (*)[a]	< 2.3 x 10^{-15} (800 K) (*)[a]
	3.51 x 10^{-15} (913 K) (42)[b]	6.11 x 10^{-15} (ca. 1050 K) (41)[b]	
Xe	< 3.1 x 10^{-15} (950 K) (*)[a]	2.4 ± 0.3 x 10^{-14} (1000 K) (*)[a]	< 1.0 x 10^{-15} (800 K) (*)[a]
	4.83 x 10^{-15} (913 K) (42)[b]	6.70 x 10^{-15} (ca. 1050 K) (41)[b]	
$Sr(5^1S_0)$	< 2 x 10^{-13} (950 K) (*)[a]		
H_2	3.7 ± 0.4 x 10^{-12} (950 K) (*)[a]	6.0 ± 0.6 x 10^{-14} (1000 K) (*)[a]	7.3 ± 0.6 x 10^{-13} (800 K) (*)[a]
		2.26 ± 0.15 x 10^{-13} (793 K) (91)[a]	6.7 x 10^{-13} (800 K, calc.) (30)[d]
		3.4 x 10^{-13} (1073 K) (43)[b]	9.1 ± 1.0 x 10^{-13} (873 K) (25)[c]
			1.1 ± 0.3 x 10^{-13} (ca. 300 K) (27)[e]
			9.5 ± 4.2 x 10^{-13} (800 K, calc.) (32)[d]
D_2	3.0 ± 0.2 x 10^{-12} (950 K) (*)[a]	2.7 ± 0.3 x 10^{-14} (1000 K) (*)[a]	1.9 ± 0.1 x 10^{-13} (800 K) (*)[a]
			3.5 ± 1.7 x 10^{-13} (800 K, calc.) (32)[d]

TABLE 5.4 (continued)

Q	$Sr(5^3P_J)$	$Ca(4^3P_J)$	$Mg(3^3P_J)$
N_2	$3.2 \pm 0.2 \times 10^{-11}$ (950 K) (*)[a]	$8.9 \pm 0.9 \times 10^{-13}$ (1000 K) (*)[a]	$4.9 \pm 0.2 \times 10^{-13}$ (800 K) (*)[a]
		$1.8 \pm 0.39 \times 10^{-13}$ (793 K) (91)[c]	$4.2 \pm 0.2 \times 10^{-13}$ (873 K) (25)[c]
		5.1×10^{-13} (1073 K) (43)[b]	$7.1 \pm 3.3 \times 10^{-13}$ (ca. 300 K) (27)[a]
CO	$2.0 \pm 0.1 \times 10^{-11}$ (950 K) (*)[a]	$3.7 \pm 0.5 \times 10^{-13}$ (1000 K) (*)[a]	$1.4 \pm 0.1 \times 10^{-12}$ (800 K) (*)[a]
		3.2×10^{-13} (1073 K) (43)[b]	$1.0 \pm 0.1 \times 10^{-12}$ (873 K) (25)[c]
			$2.0 \pm 0.7 \times 10^{-12}$ (ca. 300 K) (27)[e]
CO_2	$1.3 \pm 0.1 \times 10^{-11}$ (950 K) (*)[a]	$3.1 \pm 0.3 \times 10^{-13}$ (1000 K) (*)[a]	$1.0 \pm 0.1 \times 10^{-12}$ (800 K) (*)[a]
		1.5×10^{-13} (1073 K) (43)[b]	1.20×10^{-11} (ca. 300 K) (27)[e]
N_2O	$1.5 \pm 0.2 \times 10^{-11}$ (950 K) (*)[a]	$6.5 \pm 0.5 \times 10^{-13}$ (1000 K) (*)[a]	$4.9 \pm 0.3 \times 10^{-13}$ (800 K) (*)[a]
			2.45×10^{-11} (ca. 300 K) (27)[e]
			$2.2 \pm 0.5 \times 10^{-12}$ (ca. 300 K) (37)[e]
			2.1×10^{-10} (900 K) (71)[f]

TABLE 5.4 (continued)

Q	$Sr(5\,^3P_J)$	$Ca(4\,^3P_J)$	$Mg(3\,^3P_J)$
NH_3	$2.2 \pm 0.1 \times 10^{-11}$ (950 K) (*)[a]	$2.5 \pm 0.3 \times 10^{-13}$ (1000 K) (*)[a]	
CH_4	$1.0 \pm 0.2 \times 10^{-12}$ (950 K) (*)[a]	$5.4 \pm 0.4 \times 10^{-13}$ (1000 K) (*)[a] 3.1×10^{-14} (1073 K) (43)[b]	$1.1 \pm 0.2 \times 10^{-14}$ (800 K) (*)[a] $2.8 \pm 0.1 \times 10^{-14}$ (873 K) (25)[c]
CF_4	$7.8 \pm 0.7 \times 10^{-13}$ (950 K) (*)[a]	$1.9 \pm 0.2 \times 10^{-13}$ (1000 K) (*)[a]	$6.5 \pm 0.2 \times 10^{-14}$ (800 K) (*)[a]
C_2H_2	$1.3 \pm 0.1 \times 10^{-11}$ (950 K) (*)[a]	$1.4 \pm 0.2 \times 10^{-13}$ (1000 K) (*)[a]	$3.8 \pm 0.2 \times 10^{-11}$ (800 K) (*)[a] $3.0 \pm 1.7 \times 10^{-11}$ (ca. 300 K) (27)[e]
C_2H_4	$4.2 \pm 0.3 \times 10^{-10}$ (950 K) (*)[a]	$2.3 \pm 0.3 \times 10^{-13}$ (1000 K) (*)[a]	$1.4 \pm 0.1 \times 10^{-10}$ (800 K) (*)[a] $3.4 \pm 0.4 \times 10^{-11}$ (873 K) (25)[c]

TABLE 5.4 (continued)

Q	Sr(5³P$_J$)	Ca(4³P$_J$)	Mg(3³P$_J$)
C_6H_6	$2.4 \pm 0.2 \times 10^{-10}$ (950 K) (*)[a]	$6.0 \pm 0.2 \times 10^{-12}$ (1000 K) (*)[a]	$3.5 \pm 0.1 \times 10^{-10}$ (800 K) (*)[a]
			$1.1 \pm 0.2 \times 10^{-10}$ (873 K) (25)[c]

a – Dye-laser excitation + time-resolved forbidden atomic emission;

b – Modulated dye-laser excitation + phase shift measurements;

c – Dye-laser excitation + time-resolved atomic resonance absorption spectroscopy;

d – Dye-laser excitation + time-resolved atomic forbidden emission (single-shot mode);

e – Discharge-flow + forbidden atomic emission;

f – Chemiluminescence + single-collision conditions;

(*) THIS WORK

6. CONCLUSIONS

The previous chapters have contained an account of the kinetic behaviour of the low-lying ^3P_J electronic states of group IIA elements, namely, Mg, Ca, and Sr, including measurements of the mean radiative lifetimes, diffusion in the noble gases and collisional quenching. The technique of time-resolved resonance fluorescence following dye-laser excitation of the atomic metal in the vapour phase has proved successful in the study of group IIA elements. Particularly important in these experiments is the slow flow system employed, equivalent to a static system, and without which these experiments would not have been feasible. The experiments performed, although similar in technique and objectives, presented a variety of experimental problems which, it is hoped, have quite satisfactorily been overcome by modifying either the techniques or the way the investigations themselves, have been conducted. In spite of their chemical similarity, arising from a common electronic structure, Mg, Ca, and Sr behave in quite a different way in relation to collisional partners. From the experimental viewpoint, this behaviour is important and, to some extent, dictates the experimental conditions and the limitations of the technique employed. Also important is the reactivity of the ground $^1S_0$ states of the group IIA elements, which constitutes an important factor for reactor design as shall be discussed later. The differences in reactivity, allied to the varying metastability of $Mg(3^3P_J)$, $Ca(4^3P_J)$ and $Sr(5^3P_J)$ have been fully discussed in chapters 3, 4 and 5 respectively. The objective of this chapter is not to repeat those discussions, although reference to them is occasionally made, but to consider the behaviour of Mg, Ca, and Sr $(nsnp^3P_J)$ as a whole by comparing results, drawing conclusions and, hopefully, leaving some suggestions for a future work in this important and interesting area.

The use of reactive gases in the experimental set up employed in this work presents some experimental difficulties that will require a different reactor design. As has already been described (see chapter 2), a mixture of carrier gas (helium) and quenching gas passes over the heated

solid metal and carries its vapour into the reaction zone. The advantages of this flow system, kinetically equivalent to a static system, have been fully discussed. However, when the quenching gas passes over the heated metal, reaction may occur leading to surface poisoning. The extent of such a reaction depends of the reactivity of the alkaline earth metal towards the particular quencher employed and is also a function of the concentration of the quenching gas. Considering the reactivities of Mg, Ca and Sr, the latter should be the most difficult to study because of its relatively high reactivity. In this study, however, Ca turned out to be the most difficult element to study due to surface contamination. Several sample changes were necessary during the experiments with Ca, since the fluorescence decay signal, due to surface contamination, became too weak for any practical measurements. On the other hand, the reactivity and concentration of the quenching gas have to be considered, It has been pointed out by Nicks et al.[43] that oxidising gases are more difficult to use in this sort of experiments. This observation has been confirmed and it has been noticed that experiments with reducing gases such as hydrogen and deuterium impose less difficulties than those performed with gases such carbon dioxide, nitrous oxide and other oxigen-containing molecules. The concentration of the quenching gas is an important parameter and has to be carefully chosen at beginning of an experiment. As a result of experimental conditions, that have already been described, the concentration of the quenching gas may be varied from zero up to a maximum determined by the concentration of the mixture quenching gas + buffer gas employed in the flow system (details are given in chapter 2). If that concentration is set too low, the variation of the quenching constant may lay within the experimental error. On the other hand, a concentration too high may result in surface contamination and consequent loss of signal. A successful experiment requires a concentration high enough to give a reasonable variation of the term $k_Q[Q]$, but low enough to prevent loss of signal due to surface reaction between the quenching gas and the metal.

A new reactor design preventing direct contact between the quenching gas and with the hot metal sample, should allow experiments with reactive gases to be performed. Two independent gas inlets would be required in this case; one for the buffer gas which would carry the metal vapour into the reaction vessel and a second one for the mixture of quenching + buffer

gas. These two flows would be mixed before reaching the excitation zone, careful design being required to assure homogeneous composition. In other words, it is suggested that the mixture buffer + (buffer + quenching) be prepared inside the reaction vessel as opposed to being prepared in the flow line as it was done in the present investigation.

The mean radiative lifetime for $Mg(3^3P_J)$, $Ca(4^3P_J)$ and $Sr(5^3P_J)$ has been determined in the presence of all the noble gases and the results are presented in table (6.1). In general, it can be concluded that quenching by the noble gases is too inefficient to compete significantly with spontaneous decay at sensible pressures, with the exceptions of Kr and Xe in the case of $Mg(3^3P_J)$ and Xe for $Ca(4^3P_J)$. The mean radiative lifetimes indicated in table (6.1) as measured in xenon and krypton were found to be consistent with that observed for He when quenching by these heavy noble gases was taken into account.

TABLE 6.1

Mean radiative lifetimes for $Mg(3^3P_J)$ (800 K), $Ca(4^3P_J)$ (1000 K) and $Sr(5^3P_J)$ (950 K) in the presence of the noble gases.

Gas	$Mg(3^3P_J)$	$Ca(4^3P_J)$	$Sr(5^3P_J)$
He	21 ± 0.5 ms	376 ± 27 µs	24 ± 1 µs
Ne	16 ± 1.0 ms	294 ± 22 µs	27 ± 2 µs
Ar	19 ± 1.0 ms	378 ± 31 µs	29 ± 2 µs
Kr	(21 ± 0.5) ms	264 ± 5 µs	28 ± 2 µs
Xe	(21 ± 0.5) ms	(376 ± 27) µs	29 ± 2 µs

The quenching of $Mg(3^3P_J)$ by krypton and xenon, albeit very inefficient, can be accounted for by the greater interaction with these two heavier noble gases as seen empirically using the atomic polarizabilities, making collisional removal more efficient. Alternatively, this can be expressed in spectroscopic terms of the change from Hund's case (a) and (b) for the lighter noble gases to Hund's case (c) for collision between the metal atom and Kr or Xe, facilitating non-adiabatic transitions. The same argument may be used for $Ca(4^3P_J)$ where collisional quenching by xenon was detected. The absence of noticeable quenching of $Ca(4^3P_J)$ by krypton is more difficult to detect

due to the shorter radiative lifetime of $Ca(4^3P_J)$ compared to $Mg(3^3P_J)$. For the same reason, quenching of $Sr(5^3P_J)$ by the noble gases is not expected to be readily observed and certainly would lie within the experimental error in the type of determination employed here.

The quenching constants determined in the present study for $Mg(3^3P_J)$, $Ca(4^3P_J)$ and $Sr(5^3P_J)$ are presented together in table (6.2) in order to compare them. For the sake of simplicity, the experimental errors have not been included. The errors can be found in the relevant chapters and are of the order of 5 to 10% when taken as the standard deviation of the computerised least squares analyses.

TABLE 6.2

Absolute second-order quenching constants, $k_Q(cm^3 molecule^{-1}s^{-1})$, for $Mg(3^3P_J)$ (800 K), $Ca(4^3P_J)$ (1000 K) and $Sr(5^3P_J)$ (950 K) by added quenching gases, Q.

Q	$Mg(3^3P_J)$	$Ca(4^3P_J)$	$Sr(5^3P_J)$
N_2	4.9×10^{-13}	8.9×10^{-13}	3.2×10^{-11}
H_2	7.3×10^{-13}	6.1×10^{-14}	3.7×10^{-12}
D_2	1.9×10^{-13}	2.7×10^{-14}	3.0×10^{-12}
CO	1.4×10^{-12}	3.7×10^{-13}	2.0×10^{-11}
NO		3.2×10^{-13}	
N_2O	4.9×10^{-13}	6.5×10^{-13}	1.5×10^{-11}
CO_2	1.0×10^{-12}	3.1×10^{-13}	1.3×10^{-11}
CF_4	6.5×10^{-14}	1.9×10^{-13}	7.8×10^{-11}
CH_4	1.1×10^{-14}	5.4×10^{-13}	1.0×10^{-12}
C_2H_4	1.4×10^{-10}	2.3×10^{-13}	4.2×10^{-10}
C_2H_2	3.8×10^{-11}	1.4×10^{-13}	1.3×10^{-11}
C_6H_6	3.5×10^{-10}	6.0×10^{-12}	2.4×10^{-10}
NH_3		2.5×10^{-13}	2.2×10^{-11}

Inspection of table (6.2) shows that, for the collisional partners studied, $Ca(4^3P_J)$ presents the lowest quenching constants while $Sr(5^3P_J)$

appears to be the most reactive of the three elements which have been investigated in the present work. Quenching by spherical molecules like CF_4 and CH_4 is very low and may be contrasted with the efficient quenching by hydrocarbons, specially benzene. In each case the collisional quenching may occur via chemical reaction or physical energy transfer. Whether the quenching is chemical or physical, remains to be decided, although several individual cases have been discussed in detail in the previous chapters. A study of the collisional quenching as a function of temperature would help to decide which type of quenching is predominant. A study of the collisional quenching of $Mg(3^3P_J)$ by H_2 and D_2 as a function of temperature was presented by Breckenridge and Stewart[32], but such studies are not yet available for $Ca(4^3P_J)$ or $Sr(5^3P_J)$. Another possibility to be considered is the identification of the final products in cases where chemical quenching appears to be the exit channel. An obvious example of such a situation is the identification of MgO, formed in the reaction of Mg with O_2.

A natural continuation of the present work is the study of quenching constants at different temperatures, in order to determine energy barriers which provide further information on the course of the collisional process. While changing the temperature, of course, one must bear in mind the minimum temperature below which the vapour pressure of the alkaline earth element is too low to allow the atomic densities, required for detection of the resonance fluorescence signal, to be achieved. On the other hand, as demonstrated for $Sr(5^3P_J)$, radiation trapping may occur at elevated atomic densities even for such a forbidden transition. There is a practical limit to the temperature range that may be used in this kind of investigation and this is determined by the vapour pressure on one end and by radiation trapping on the other. Nevertheless, the temperature range over which the experiments can be performed is wide enough to allow a study of the variation of the second-order quenching constants with temperature.

The study of the kinetic behaviour of group IIA elements, even restricted to Mg, Ca and Sr, is a broad field of research which can not be completely covered in a set of studies as discussed in the present investigation. In this work, although limited, the technique of

time-resolved resonance fluorescence following pulsed dye-laser excitation, has been developed and extended. The success of such a technique has resulted in an enlarged body of collisional data for the low-lying electronic states of magnesium, calcium and strontium.

Before commenting finally on this technique, it is useful to examine, briefly, other available techniques for the purpose of considering further work. The beam techniques, although very detailed in its results and allowing studies of energy distribution among reaction products, are limited to those cases where products are susceptible of detection, such as chemiluminescence and laser induced fluorescence. The phase-shift technique is model-dependent and may, as in the case of the noble gases (see chapter 4) lead to results which are wrong by several orders of magnitude. The studies which have employed flames are characterised by being mechanistic by their own nature and the measurements of mean radiative lifetimes and collisional quenching do not constitute their primary goal. The standard time-resolved absorption spectroscopy techniques, following dye-laser excitation make use of a static system which, in turn, presents severe problems of surface contamination of the metal. Furthermore, because the observation zone is very large, compared with the one employed in the experiments that have been described in this work, diffusion can not be studied.

The technique that has been developed here is based on employing a very small reaction zone coupled with the limited light gathering power of a small monochromator attached to the photomultiplier system. Diffusion out of the observation zone, which is that fraction of the reaction zone which the monochromator is able to sample, may then be studied in those cases where its effect is comparable to the spontaneous decay rate. In these cases a noticeable variation in the rate constant k', as defined in the previous chapters, can be recorded.

The flow system employed made possible the investigation of collisional quenching by a variety of collisional partners including; diatomic molecules (H_2, D_2, N_2, CO, NO), triatomic (CO_2, N_2O), tetratomic (NH_3), hydrocarbons (C_2H_2, C_2H_4, C_6H_6) and molecules with spherical symmetry (CH_4, CF_4). The study of O_2 was only possible in the case of

$Mg(3^3P_J)$ where the quenching constant was determined for O_2 as an impurity of argon (see chapter 3).

It is believed that the technique can be extended for the study of collisions with reactive gases, provided some changes are made in the reactor design. The development of the gating system with variable gating time and taking advantage of the pulse generated by the laser unit (see chapter 5), allows very fast quenching constants to be measured. Further improvements in this direction should permit metastable atomic states with even shorter radiative lifetimes to be brought within the range of the present technique. This would include the study of optically metastable atomic barium $[Ba(6^3D_1) \longrightarrow Ba(6^1S_0) + h\nu$, $gA = 7.6 \times 10^6$ $s^{-1}]$.[12]

REFERENCES

(1) - J.G. Calvert and J.N. Pitts, Photochemistry,
(Wiley, N. York, 1966).

(2) - R.J. Donovan and D. Husain, Chem.Rev., (1970) 70, 489.

(3) - D. Husain and R.J. Donovan, Adv.Phot., (1971) 8, 1.

(4) - R.J. Donovan and D. Husain, Annu.Rep.Chem.Soc.,
(1971) A68, 123.

(5) - R.J. Donovan, D. Husain and L.J. Kirsch, Annu.Rep.Chem.Soc.,
(1972) A69, 19.

(6) - D. Husain, Ber.Busenges.Phys.Chem., (1977) 81, 168.

(7) - J.H. Klots and D.W. Setser, in " Reactive Intermediates in the
Gas Phase", Ed. D.W. Setser, (Academic Press, New York, 1979),
Chap. 3, p. 190.

(8) - R.J. Donovan and H.M. Gillespie, in Specialist Periodical
Reports, Reaction Kinetics, Vol. 1, Ed P.G. Ashmore and
R.J. Donovan, (1975), Chapter 1, p. 14.

(9) - W.H. Breckenridge and H. Umemoto, in Dynamics of the Excited
State, Ed. K.P. Lawley, Advances in Chemical Physics, (Wiley,
N. York, 1982), vol L, p 325.

(10) - Atomic Energy Levels, Vols I-III, Ed. C.E. Moore,
(NBSRDS, 35 (U.S. Government Printing Office,
Washington, D.C., 1971).

(11) - C.R. Vidal and J. Cooper, J.Appl.Phys., (1969) 40, 3370.

(12) - C.H. Corliss and W.R. Bozmann, Experimental Transition
Probabilities for Spectral Lines of Seventy Elements,
(Natl.Bur.Stand., Monograph 53, U.S. Department of
Commerce, Washington, D.C., 1962).

(13) - J.J. Wright, J.F. Dawson and L.C. Balling, Phys.Rev.A,
(1974) 9, 83.

(14) - J.A. Davidson, C.M. Sadowski, H.I. Schiff, G.E. Street,
C.J. Howard, D.A. Jennings and A.L. Schmeltekopf,
J.Chem.Phys., (1976) $\underline{64}$, 57.

(15) - Specialist Periodical Reports, Gas Kinetic and Energy Transfer,
Vol. 2, Ed. P.G. Ashmore and R.J. Donovan, (1975)
a - M.F. Golde, Chapter 4, p. 123.
b - M.A.A. Clyne and A.H. Curran, Chapter 6, p 239.

(16) - I.W.M. Smith, Kinetics and Dynamics of Elementary Gas Reactions,
(Butterworths, London, 1980).

(17) - K.E. Shuler, J.Chem.Phys., (1953) $\underline{21}$, 624.

(18) - K. Schoefield, J.Phys.Chem.Ref.Data., (1979) $\underline{8}$, 723.

(19) - J.G. Frayne, Phys.Rev., (1929) $\underline{34}$, 590.

(20) - W. Prokofjew, Z.Phys., (1928) $\underline{50}$, 701.

(21) - C. Loughlin and G.A. Victor, Astrophys.J., (1974) $\underline{192}$, 551.

(22) - R.H. Garstang, J.Opt.Soc.Am., (1962) $\underline{52}$, 845.

(23) - B. Warner, Mon.Not.R.Astron.Soc., (1968) $\underline{140}$, 53.

(24) - P.S. Furcinitti, L.C. Balling and J.J. Wright,
Phys.Letters, (1975) $\underline{53A}$, 75.

(25) - R.P. Blickensderfer, W.H. Breckenridge and D.S. Moore,
J.Chem.Phys., (1975) $\underline{63}$, 3681.

(26) - D.J. Benard, W.D. Slafer and P.H. Lee,
Chem.Phys.Letters, (1976) $\underline{43}$, 69.

(27) - G. Taieb and H.P. Broida, J.Chem.Phys., (1976) $\underline{65}$, 2914.

(28) - D.J. Benard, P.J. Love and W.D. Slafer,
Chem.Phys.Letters, (1977) $\underline{48}$, 321.

(29) - A. Kowalski, Z.Naturforsch., (1979) $\underline{34a}$, 459.

(30) - W.H. Breckenridge and W.L. Nikolai,
J.Chem.Phys., (1980) $\underline{73}$, 2763.

(31) - N. Adams, W.H. Breckenridge and J. Simons,
       Chem.Phys., (1981) 56, 327.

(32) - W.H. Breckenridge and J. Stewart, J.Chem.Phys.,
       (1982) 77, 4469.

(33) - A. Kowalski and M. Menzinger, Chem.Phys.Letters,
       (1981) 78, 461.

(34) - P.J. Dagdigian, J.Chem.Phys., (1982) 76, 5375.

(35) - J.W. Cox and P.J. Dagdigian, J.Chem.Phys., (1982) 86, 3738.

(36) - J.A. Irvin and P.J. Dagdigian, J.Chem.Phys., (1980) 73, 176.

(37) - B. Bourguignon, J. Rostas and G. Taieb,
       J.Chem.Phys., (1982) 77, 2979.

(38) - D.R. Yarkony, J.Chem.Phys., (1983) 78, 6763.

(39) - T.J. McIlrath, Appl.Phys.Letters, (1969) 15, 41.

(40) - T.J. McIlrath and J.L. Carlsten, J.Phys.B, (1973) 6, 697.

(41) - R.J. Malins and D.J. Benard, Chem.Phys.Letters, (1980) 74, 321.

(42) - R.J. Malins, D.A. Logan and D.J. Benard,
       Chem.Phys.Letters, (1981) 83, 605.

(43) - C.M. Nicks, R.J. Malins and D.J. Benard,
       Chem.Phys.Letters, (1982) 89, 523.

(44) - P.G. Whitkop and J.R. Wiesenfeld, Chem.Phys.Letters,
       (1980) 69, 457.

(45) - U. Brinkmann and H. Telle, J.Phys.B, (1977) 10, 133.

(46) - H. Telle and U. Brinkmann, Mol.Phys., (1980) 39, 361.

(47) - U. Brinkmann, V.H. Schimidt and H. Telle,
       Chem.Phys.Letters, (1980) 73, 3.

(48) - L. Pasternack and P.J. Dagdigian, Chem.Phys., (1978) 33, 1.

(49) - D.J. Eckstrom, J.R. Barker, J.G. Hawley and J.P. Reilly,
       Appl.Optics, (1977) 16, 2102.

(50) - D.J. Benard, W.D. Slafer and P.H. Lee,
Appl. Optics, (1977) 16, 2108.

(51) - R.W. Solarz, S.A. Johnson and R.K. Preston,
Chem.Phys.Letters, (1978) 57, 514.

(52) - P.S. Furcinitti, J.J. Wright and L.C. Balling,
Phys.Rev.A., (1975) 12, 1123.

(53) - R. Hultgren, P.D. Desai, D.T. Hawkins, M. Gleisner, K.K. Kelley
and P.D. Wagman, in "Selected Thermodynamics Properties of
Metals", (American Society for Metals, Metals Park, Ohio,
1973).

(54) - D. Husain, L. Krause and N.K.H. Slater,
J.Chem.Soc. Faraday Trans. 2, (1979) 73, 1706.

(55) - A.U. Acuna, D. Husain and J.R. Wiesenfeld,
J.Chem.Phys., (1973) 58, 494.

(56) - W.H. Wing and T.M. Sanders Jr.,
Rev.Sci.Instrum., (1962) 38, 1341.

(57) - J.J. Deakin, D. Husain and J.R. Wiesenfeld,
Chem.Phys.Letters, (1971) 10, 146.

(58) - F.J. Comes and J. Piontek, Chem.Phys.Letters, (1976) 42, 558.

(59) - D. Husain, N.K.H. Slater and J.R. Wiesenfeld,
Chem.Phys.Letters, (1977) 51, 201.

(60) - W.L. Wiese, M.W. Smith and B.M. Miles, Atomic Transitions
Probabilities, (NSRDS-NBS-22) (U.S. Government Printing Office,
Washington, D.C., 1969), vol. II.

(61) - A.B. Callear and J.D. Lambert, in "Comprehensive Chemical
Kinetics", vol. 3, The Formation and Decay of Excited
Species, Ed. C.H. Bamford and C.F.H. Tipper, (Elsevier,
Amsterdam, 1969).

(62) - A.C.G. Mitchell and M.W. Zemansky, Resonance Radiation and
Excited Atoms, (Cambridge University Press, London, 1961),
p. 246.

(63) - M.W. Zemansky, Phys.Rev., (1929) 34, 213.

(64) - G. Boldt, Z.Phys., (1958) 150, 205.

(65) - F. Strumia, P. Minguzzi, G. Giusfredi and M. Tonelli,
4th International Conference on Atomic Physics,
(Heidelberg, 1974).

(66) - C.J. Michell, J.Phys.B, (1975) 8, 25.

(67) - P.J. Dagdigian, Chem.Phys.Letters, (1978) 55, 239.

(68) - R.P. Blickensderfer, K.D. Jordan, N. Adams and
W.H. Breckenridge, J.Phys.Chem., (1982) 86, 1930.

(69) - G. Herzberg, Molecular Spectra and Molecular Structure, III,
Electronic Spectra and Electronic Structure of Polyatomic
Molecules, (Van Nostrand, Reinhold, New York, 1966).

(70) - K.P. Huber and G. Herzberg, Molecular Spectra and Molecular
Structure, IV, Constants of Diatomic Molecules,
(Van Nostrand Reinhold, New York, 1979).

(71) - P.J. Dagdigian, personal communication in B. Bourguignon,
J. Rostas and G. Taieb, J.Chem.Phys., (1982) 77, 2979.

(72) - D.R. Yarkony and C.W. Bauschlicher Jr., personal communication
in B. Bourguignon, J. Rostas and G. Taieb,
J.Chem.Phys., (1982) 77, 2979.

(73) - W.H. Breckenridge and H. Umemoto, J.Chem.Phys., (1981) 73, 698.

(74) - W.H. Breckenridge and H. Umemoto, J.Chem.Phys.,
(1982) 77, 4464.

(75) - V.L. Vedeneyev, L.V. Gurvich, V.N. Kondratiev, V.A. Medvedev
and Ye L. Frankevich, Bond Energies, Ionisation Pontentials
and Electron Affinities, (Edward Arnold, London, 1966).

(76) - C.W. Allen, Mon.Not.Roy.Astronom.Soc., (1957) 117, 622;
Mem.Com.Sol.Canberra, (1934) 1, No. 5 (part 2), p. 67.

(77) - J.W. Schuttavaer, M.J.E. de Bont and Th. Van der Broek,
Physics, (1943) 10, No. 7, p. 544.

(78) - K.H. Olsen, P.M. Routly and R.B. King,
    Astrophys.J., (1959) 130, 688.

(79) - Y.I. Ostrovski and N.P. Penkin, Opt.Spectr., (1961) 10, 219.

(80) - N.P. Penkin, J.Quant.Spectr.Rad.Trans., (1964) 4, 41.

(81) - G. Giusfredi, P. Minguzzi, F. Strumia and M. Tonelli,
    Z.Phys., (1975) A274, 279.

(82) - L. Pasternack, D.M. Silver, D.R. Yarkoni and P.J. Dagdigian,
    J.Phys.B, (1980) 13, 2231.

(83) - G.W. King and J.H. Van Vleck, Phys.Rev., (1939 56, 464.

(84) - L.A. Vainstein and I.A. Poluektov, Opt.Spectr., (1962) 12, 254.

(85) - G. Victor, private communication in P.S. Furcinitti,
    Ph.D. Thesis, (University of New Hampshire, U.S.A., 1975).

(86) - R.N. Diffenderfer, P.J. Dagdigian and D.R. Yarkoni,
    J.Phys.B, (1981) 14, 21.

(87) - E. Lue-Koening, J.Phys.B, (1974) 7, 1052.

(88) - A.N. Nesmiyanov, "Vapour Pressure of the Elements"
    (Academic Press, New York, 1963).

(89) - C. Smithels, "Metals Reference Handbook", 5th Edition,
    (Butterworth, London, 1976).

(90) - J.A.N.A.F., Thermochemical Tables, 2nd Edition, D.R. Stull and
    H. Prophet, Project Directors, (NSRDS-NBS-37, Nat.Bur.Stand.,
    Washington, D.C., 1960).

(91) - P.S. Furcinitti, Ph.D. Thesis, (University of New Hampshire,
    U.S.A., 1975).

(92) - J.A. Irvin and P.J. Dagdigian, J.Chem.Phys., (1981) 74, 6178.

(93) - P.J. Cross and D. Husain, J.Photochem., (1977) 7, 157.

(94) - M.A. Chowdhury and D. Husain, J.Chem.Soc. Faraday Trans 2,
    (1978) 74, 1065.

(95) - P.D. Foo, J.R. Wiesenfeld, M.J. Yuen and D. Husain,
J.Phys.Chem., (1976) 80, 91.

(96) - D. Husain and J.G. Littler, Int.J.Chem.Kinetics,
(1974) VI, 61.

(96) - D. Husain and J.G.F. Littler, Int.J.Chem.Kinetics,
(1974) VI, 61.

(97) - M.D. Havey, L.C. Balling and J.J. Wright,
Phys.Rev., (1976) A13, 1269.

(98) - F. Engelke, Chem.Phys., (1979) 44, 213.

(99) - B.E. Wilcomb and P.J. Dagdigian, J.Chem.Phys.,
(1978) 69, 1779.

(100) - D.J. Benard, W.D. Slafer and J. Hecht,
J.Chem.Phys., (1977) 66, 1012.

(101) - A. Eberhagen, Z.Phys., (1955) 143, 392.

(102) - I-J. Ma, J. Mertens, G.Zu Pullitz and G. Schutte,
Z.Phys., (1968) 208, 266.

(103) - I-J. Ma, G.Zu Pullitz and G. Schutte,
Z.Phys., (1968) 208, 276.

(104) - M. Baumann, M. Holde and H. Vogels, Phys.Vehr., (1964) 4, 41.

(105) - F. Ackermann, M. Baumann and J. Gayler,
Z.Naturforsch., (1966) 21a, 664.

(106) - D. Husain, L. Krause and N.K.H. Slater,
J.Chem.Soc. Faraday Trans. 2, (1977) 73, 1678.

(107) - D. Husain and N.K.H. Slater, J.Chem.Soc. Faraday Trans. 2,
(1978) 74, 1222.

(108) - D. Husain and N.K.H. Slater, J.Chem.Soc. Faraday Trans. 2,
(1978) 74, 1627.

(109) - Specialist Periodical Reports, Gas Kinetics and Energy Transfer,

       Vol. 3, Ed. P.G. Ashmore and R.J. Donovan, (1975),

       a - A.B. Callear, Chapter 3, p. 82.

       b - J.N. Murrel, Chapter 5, p. 200.

APPENDIX

Electric diagrams of the current-to-voltage converter and pre-trigger photomultiplier gating system, including the monostable pulse generator and the gating circuit.

VOLTAGE/CURRENT CONVERTER

FEEDBACK CAPACITOR

10 PF
22 PF
47 PF
100 PF
220 PF
470 PF
1000 PF
2200 PF
5000 PF

FEEDBACK RESISTOR

100K
200K
500K
1M
2M
5M
10M

OUTPUT

47Ω

1K MO

0.02 MFD

+15V

2K HP

SET ZERO

BAL

+V   OUT   -V

E76

+   -

OV

INPUT

-15V

COMPUTING TECHNIQUES

1   2   3   4   12 13 14 15

PU6-2

7   10   6

100MA

ON MAINS

L

N

E

COMPUTING TECHNIQUES

(196)

PULSE GENERATOR FOR P.M. GATING

275

DEPT OF PHYSICAL CHEMISTRY

DESIGNED BY J. GUTTRIDGE
DRAWN BY J. COSTON
DATE 7·4·77

ALL RESISTORS 1W M.O.

-18V

0V

4 WAY PLUG

4

ON

PULSE OUTPUT +4V

100K

0·01MFD D.C.

1 MFD 250V

0·1 MFD 250V

0·01 MFD D.C.

2N2905A

1K

10K

22K

10Ω

0·01MFD D.C.

47K

15K

2N2905A

220Ω

10Ω

0·01 MFD D.C.

4·7MFD 100V WIMA MKS

6 5 4 3 2 1

PULSE WIDTH

0·01 MFD D.C.

4·7 MFD WIMA MKS

47Ω

2N2905A

OA81

2·2K

0·01MFD D.C.

270PF S.M.

10K

100K

+ TRIG MIN +2V MAX +10V

SW POS	PULSE WIDTH μS	CAP P.F. S.M.
1	3·3	220
2	6·0	470
3	12·0	1000
4	24·0	2200
5	48·0	4700
6	105·0	10000

6256B P.M. GATING CIRCUIT MK2

(276)

OV.

OUTPUT

D13
D12
D11
D10
D9
D8
D7
D6
D5
D4
D3
D2
D1

6

5
7
4
8
3
9
2
10
1
11
15
12
14
13

4 X 0·1 MFD 250V

14 X 220K M.Ω.

2·2K M.Ω.

BF 259

330Ω M.Ω.

47K M.Ω.

470ΩM.Ω.

2 X 350PF P.C.

10K M.Ω.

2100PF 1N3070
(6 X 350PF) P.C.

2 X 0·1MFD 3KV

470K M.Ω.

3 X 0·1MFD 3KV

GATE OFF
+ VE INPUT

GATING PULSE SHOULD BE APPROX +4V
AND DURATION SHOULD NOT EXCEED100µS

DEPT OF PHYSICAL CHEMISTRY

DESIGNED BY J.GUTTRIDGE
DRAWN BY J.COSTON
DATE 7·4·77

— E.H.T.